Influence of runout path material on rock and debris avalanche mobility: field evidence and analogue modelling.

A thesis submitted in partial fulfilment
of the requirements for the degree of

Doctor of Philosophy in
Geological Sciences /
Hazard and Disaster Management

Anja Dufresne

University of Canterbury
New Zealand
2009

Another day in the office: sunrise at Hari Hari field station, West Coast, New Zealand.

Acknowledgements

First and foremost, for much good advice and encouragement, I would like to thank my supervisor Tim Davies; who, with great faith and quiet ambition, succeeded in pulling me over to the landslide side of the force. Thank you to my co-supervisor Jim Cole, who kept the professor and me in check and this project on time.

Muchas gracias to Sergio Salinas and Claus Siebe from the Universidad Autónoma Nacional de México, who have endured and encouraged my work at the Jocotitlán debris avalanche just outside Mexico City. I owe my deepest gratitude to Sergio for his unsurpassed patience, field guidance and help, and for procuring coffee in a coffee-less town. For a review of structural geology field work methods and data interpretation I would like to thank Jarg Pettinga.

I am grateful to colleagues around the world who have offered their knowledge and ideas in discussions over glasses of red wine and by electronic thought exchange: Mauri McSaveney, Ken Hewitt, Oliver Korup, Ben van Wyk de Vries, Ben Bernard, Tom Shea, and Jóhann Helgason. Danke auch an Björn Gojdka für seine Einsichten.

Thank you to the incredible technical team: Rob Spiers (who is bursting with creative ideas that inspire by their ingenious simplicity), Vanessa Tappenden, Cathy Higgins, and Jennifer Jackson. My thanks go to Lis Bowman for trusting me with the engineering department's high-speed digital video camera.

The French Connection: Guillaume Chevalier, merci beaucoup pour les moments fantastiques dans les avalanches de roches et pour la compagnie incomparable. Thank you for help in the field to: Anke Zernack, Jon Proctor, Elke Hanenkamp, and Lucille Tatard; for field site access: Nelson Cook and Steve Staples; and for turning the West Coast inside out: un-equalled-in-enthusiasm digger driver Spike Jones.

I would like to extend my gratitude to Lee Siebert at the Washington Smithsonian Institute for supporting a daunting task, and to all the people he persuaded to get involved in the database project: Steve Sparks, Ben Bernard, Jorge Clavero, Shinji Takarada, Sasha Belousov, Marina Belousova, and, by proxy, Natalie Ortiz.

Further afield, I would like to express my humble respect and deepest gratitude to everybody at my nightly sanctuary: the New Zealand Wing Chun / Doce Pares school under otherwordly guidance of Sifu Leigh Jenkins and Sihing Hugh Puttock. Thank you for your dedication in this timeless art. I have learnt incomparable lessons of endurance, letting-go, focus, inner courage, trust, humility, and forces far beyond my perceived physical and mental limits.

This project was funded by a three-year New Zealand International Doctoral Research Scholarship, and field work was supported by the University of Canterbury, Department of Geological Sciences Mason Trust.

Abstract

Rock and debris avalanches result from sudden rock slope failure; they occur in a variety of materials and landscapes, and often have a catastrophic and lasting impact on the society, infrastructure, and landscape of the area. In order to fully understand these events, the factors leading to failure and those influencing the course of the event must be investigated. In recent years, increased attention has been given to numerous aspects of rock/debris avalanche emplacement: among these is the influence of runout path material on the behaviour of snow and ice avalanches, pyroclastic currents, debris flows, volcanic debris avalanches and non-volcanic rock avalanches. The fact that substrates are involved in rock avalanche emplacement has been known since Buss and Heim remarked on it in 1881, but few detailed studies on the effects of this involvement on avalanche emplacement exist. One popular hypothesis which has emerged is that the long runout of large rock avalanches can be explained by the basal friction reduction due to overrunning or failure of saturated substrate material. However, the present study shows that this is not the case. From analysis of nearly 400 rock and debris avalanche deposit descriptions it is evident that:

(1) avalanches inevitably interact with their runout path material;
(2) all large ($> 10^6$ m^3) rock and debris avalanche events have runout distances that exceed simple frictional model predictions regardless of type or degree of substrate interaction;
(3) substrates only add complexities to the 'long-runout' avalanche events similar to topographic interference.

The complexities resulting from substrate interaction include, for example, characteristic deposit surface features such as longitudinal ridges and flowbands, compressional faults and raised margins from rapid deceleration behind e.g. bulldozed substrates; shearing in a basal mixed zone and consequent changes in basal avalanche mechanical properties; volcanic edifice failure on weak underlying sediments with a change in volcano shape; transformation into more mobile debris flows through the entrainment of large quantities of water or water-bearing materials; and many others.

Table of Contents

List of Figures

List of Tables

Introduction

Objectives and Motivation – Thesis outline – Terminology

In the spirit of:

"The basic texture of research consists of dreams into which threads of reasoning, measurements and calculation are woven."

Albert Szent Györgyi

Rock/Debris Avalanche – Substrate Interaction: Introduction and Thesis Outline

INTRODUCTION, OBJECTIVES AND THESIS OUTLINE

Large (>10^6 m^3) catastrophic rockslope and volcano flank failures are infrequent events that nevertheless constitute a significant hazard to population and infrastructure in the area. They are catastrophic in that they occur suddenly, translate great masses of rock and debris at exceptional rates of movement (up to 320 km/h), and bury large areas (tens to hundreds of km^2; with some volcanic debris avalanches covering thousands of km^2) under debris metres to hundreds of metres thick within a very short time (minutes). Vertical displacements, from the top of the failure scarp to the distal deposit edge, exceed 2 km for volcano collapse events, and are typically on the order of 0.5 to 2 km for non-volcanic rock avalanches, with some rare cases exceeding 3 km. Over the past several decades, hundreds of deposits resulting from catastrophic rock slope and volcano flank failures have been indentified. The majority of studies have focused on individual events providing essential data and descriptions of the complexities of these natural events, and thus form the framework for comparative studies. Others deal with theoretical work and modelling efforts. For successful quantification, understanding and modelling of these events, and to assess and predict their hazards, thorough understanding of the processes involved in failure and emplacement, and detailed data are needed as constraints. Any model for avalanche emplacement must further account for and integrate:

- the influence of topography
- deposit morphological features
- internal deposit structures
- runout path conditions

The last of these includes the often-described entrainment of large quantities of water and water-bearing units, sediment mobilization, entrainment of smaller amounts of sedimentary materials, and substrate deformation such as folding and faulting. Few studies to date have explored the interaction of rock/debris avalanches with the materials in their runout paths, though many publications exist in which evidence of their interaction is described from deposits around the world.

The central question of this work addresses these interactions between rock/debris avalanches and the materials in their runout paths. Namely, (how) do snow, ice, water, or sediments (wet or dry) influence the emplacement mechanisms of rock/debris avalanches and do they explain the long runout distances and devastating potentials of large rockslope and volcano flank failure events?

It has previously been shown that the entrainment of sufficient amounts of saturated sediments, snow, ice or surface water into a rock/debris avalanche can cause it to transform into a more mobile debris flow (see Chapter 1 for references). The effects of entrainment of smaller amounts of water-bearing units or of dry, high-friction debris are less well understood: they might change basal mechanical behaviour, lead to bulking of the avalanche, or they may be insubstantial in volume or of a material type that does not influence avalanche behaviour despite their presence as foreign material in the moving mass.

When no entrainment occurs, and avalanche and substrate remain distinct, there are three possibilities: (1) they interact leaving visible traces in the substrate (folds, faults, shear zones, brecciation or other disturbances); (2) they interact without leaving immediately obvious traces (e.g. energy dissipation, pore water leakage, substrate failure at depth, comminution of granular material); or (3) they do not interact significantly. What determines whether or not they interact and how the various types of interaction influence avalanche mobility is a vital question for understanding rock/debris avalanche dynamics, for successful emplacement modelling and hence for hazard zone delineation.

To address this problem a broad and diverse research approach has been adopted. The advantage of such an approach lies in setting out a sound framework for future studies by defining and describing a hitherto vaguely-known phenomenon in its entirety – a perspective on the state-of-the-art. However, it had to be accepted that taking the individual studies to the depth that their potential deserves was not feasible

within the time available. Three major objectives were therefore formulated to concentrate the research of this study:

1. Detailed study of **field examples** with known substrate deformation associated with avalanche emplacement.
2. **Laboratory experiments** to model and directly observe avalanche-substrate interaction.
3. Comprehensive study of the **current state of knowledge** on avalanche-substrate interaction.

The history, objectives and current state of research on the **influence of substrates on rock and debris avalanches** are outlined in **Chapter 1**. Information distilled from the scientific literature is interspersed and complemented by insights and hypotheses developed over the past three years of this project.

This overview is followed by a paper published in *Geomorphology* (**Chapter 2**) on peculiar, yet common morphological features often observed in avalanche deposits, namely **longitudinal ridges** and their expressions as aligned hummocks, flowbands and distal digits. The idea for this paper was sparked by the prominent longitudinal ridges in the Round Top rock avalanche and by descriptions of identical features in other rock avalanche deposits that, like Round Top, also exhibit intense substrate deformation features often associated with the ridges. From the initial assumption that longitudinal surface features and certain substrate conditions were intricately linked, an excursion into phenomena other than rock and debris avalanches (ice and snow avalanches, pyroclastic flows, laboratory experiments on granular flow mechanics) was taken, leading to closer insights into granular flow behaviour and refined assumptions on the degree of the relationship between these two phenomena.

Field studies were carried out to unravel basal avalanche processes and to further investigate previously often invoked but rarely studied avalanche-substrate interaction features in detail. The two **case studies** are presented in the middle part of the thesis: the Round Top rock avalanche in New Zealand (**Chapter 3**) and the Jocotitlán volcanic debris avalanche in Mexico (**Chapter 4**). Field work at Round Top was chosen because of the intense substrate involvement in its emplacement. This event

was compared with rock avalanches that produced deposits of similar volume, but where substrate conditions differed, using data distilled from the literature (see Chapter 6). The central idea that saturated substrates might explain the long runout of large rock avalanches is disputed and the resulting paper is in print in *Earth Surface Processes and Landforms*.

Initially, work on the North Island volcanic debris avalanches at Taranaki and Ruapehu volcanoes was envisioned. However, restricted and poor basal outcrop availability rendered these sites insufficient for the task at hand. That said, findings at Taranaki's distal coastal outcrops provided helpful observations integrated in the general discussion of Chapter 1. For a more detailed study, the Jocotitlán avalanche deposit in México was chosen because of the widespread presence of deformed substrate and excellent outcrop conditions in and around the debris avalanche deposit. Investigations of the deposit's base and adjacent sediment deformation features inevitably lead to broader discoveries of the sequence of events during emplacement of this avalanche and unravelled the history of volcano flank destabilisation and failure; an unexpected expansion of research potential provided by sediment deformation features associated with avalanche deposits. The results are accepted for publication in the *Journal of Volcanology and Geothermal Research Special Issue on Continental Margin Volcanism (Varekamp and Luhr, eds)*.

Laboratory analogue model results briefly touched upon in Chapters 1 and 3 are presented in detail in **Chapter 5**. These experiments were designed to document and illuminate processes acting at the interface of a granular flow/avalanche with various types of substrate/runout path conditions. For example, they tie into findings at the Round Top rock avalanche providing a conceptual framework in the reconstruction of avalanche-substrate interaction processes at this and other deposits.

Before the final discussion and thesis summary, a daunting enterprise that emerged from the initial stages of data collection three years ago is outlined in **Chapter 6**. This is the compilation of a **world-wide database on rock and debris avalanche deposits**. So far, the section on volcanic debris avalanche deposits has grown to close to 300 deposits and it has won international collaboration in the volcanological

community. The list of non-volcanic rock avalanches counts 100 entries to date. Both datasets are still in the constructional phase.

This thesis is the result and summary of a three-year investigation into avalanche-substrate interactions during which data from close to 400 rock and debris avalanche deposits have been collected and compared; supplemented by detailed field studies in New Zealand, Mexico and France… and is far from being complete. The progress made during this project provides new insights into the mechanisms and effects of substrates on rock/debris avalanche emplacement and adds new concepts and complexities to a hitherto little-investigated field of research.

TERMINOLOGY

Researchers in landslide dynamics come from a range of different disciplines and backgrounds such as volcanology, engineering, mathematics, physics, and general geology. Consequently, the range of terms used and the way these terms are defined and interpreted varies; in some cases dramatically. To avoid confusion based on terminology, a brief comment on the main terms and their definitions as used throughout this document is included at this point (in addition, a more detailed glossary of volcanological terms forms part of the database chapter).
'**Avalanche**' and '**flow**' are terms often used interchangeably. In field-scale, natural events 'avalanche' is used to describe unsaturated landslides, rock avalanches, debris avalanches and snow avalanches. 'Flow' on the other hand implies a fluid-like motion of the granular (saturated) material. However, in laboratory studies, researchers tend to use the term to describe any moving granular mass.

A deposit's '**area**' is the land surface covered by avalanche debris. The avalanche area does not include secondary debris flow deposits, sedimentary material disrupted beyond the avalanche margins, 'splash zones' of liquefied debris extruded from beneath the avalanche, areas affected by ejected avalanche boulders, etc.

The term '**coupling**' is used in this work to describe the linking of substrate material with an avalanche, by which it effectively becomes part of the moving mass, but without its particles mixing with the avalanche debris. In the field, use of this term

means that substrate and avalanche are preserved and fully recognizable as two distinct units with a clear contact between them, as opposed to those substrates which have been disrupted and mixed thoroughly into the avalanche (see 'entrainment'). Examples of coupling include: bulldozing, sediment failure at depth and transportation with the avalanche.

'**Debris avalanches**' are rapidly moving masses of unsorted rock, debris and soil mobilized by gravity (after Schuster and Crandell, 1984) commonly triggered by gravitational or seismically induced slope failure or volcanic eruptions. In volcanic settings, the initial source material is typically heterogeneous in type, grain size and strength. Debris is often sourced from the initial slope material, but it can also be entrained from the substrate during runout. Debris avalanches differ from **debris flows** in that they are not water-saturated and in that the load is entirely supported by particle-particle interaction (Vallance and Ballard, 2000). Volcanic debris avalanches described in the literature however include (1) debris avalanches *sensu stricto* that were mainly grain flows as described by Glicken (1998), (2) those that transformed from grain flows into debris flows, and (3) deposits that are entirely those of debris flows (Scott et al., 2001). Debris avalanches are transitional between rock avalanches and debris flows on the continuum to hyperconcentrated flows and further to dilute streamflows (Smith and Lowe, 1991).

'**Dynamics**' treats the action of forces (Oxford English Dictionary (OED)).

'**Entrainment**' refers to the incorporation of substrate material into the moving avalanche debris. The entrained material may remain a distinctly recognizable unit, be sheared, or be crushed and mixed into the avalanche matrix or base.

The '**Fahrbahnböschung**' is a term introduced to the landslide literature by Heim in 1932. It is the connecting line between the highest point of the failure source to the lowest elevation at the distal avalanche deposit toe. *Fahrbahn* is German for the 'path of travel', and *Böschung* means 'slope'. The shorter **Fahrböschung** is normally used in the literature.

'**Fluidisation**' is a state when the sediment strength is lost through moving interstitial fluids or vibration supporting the sediment grains (Maltman and Bolton, 2003).

The term '**lahar**' (Indonesian for 'mudflow') refers to rapidly flowing water-saturated mixtures of rock, debris and water from a volcano (Crandell, 1971; Neall,

1976; Smith and Fritz, 1989). A lahar is an event; it can refer to one or more discrete processes, but does not refer to a deposit (Smith and Fritz, 1989).

'**Landslide**' is a general term used to describe slope failures ranging from those that initiate suddenly with material moving at up to 100 km/h to those which manifest as barely perceptible creep. They can consist of rock, soil, debris or a mixture of all. The source material can be coherent or unconsolidated before failure. The most common trigger for landslides is heavy rainfall, but earthquakes, volcanic eruptions and human activity can also cause them.

'**Liquefaction**' is a state when a sediment effectively behaves as a fluid as a result of strength-loss due to the load being entirely sustained by the pore-fluid and cohesion becoming negligible (after Maltman and Bolton, 2003).

'**Mechanism**' according to the OED is the structure or operation of a machine or other complex system; a theory or approach relating to this. An ordered sequence of events involved in a biological, chemical or physical process.

'**Mobility**' is the ability to move or to be moved; capacity for movement or change of place (OED).

A '**rock avalanche**' results from the sudden failure under gravity of an initially largely intact rock slope. Upon descent and emplacement the rapidly moving mass (up to 320 km/h) breaks up into smaller rock fragments. Rock avalanches are commonly triggered by earthquakes or heavy rainfall; or they can occur with no apparent trigger. Definitions for both 'landslides' and 'rock avalanches' are adapted freely from Luhr (2003); see also Hewitt et al. (2008) for a detailed review.

The **runout** (*L*) of an avalanche is conventionally taken to be the distance from the back of the source scarp to the distal toe of the final avalanche deposit, whereas the value of *L** is the actual length of the deposit itself in longitudinal section (see database glossary in Chapter 6 for an illustrative sketch and references). The prefix '**long runout**' is used in the literature to describe rock avalanches with travel distances that exceed those predicted by simple frictional models; this is sometimes also referred to as 'excess runout distance' (Hsü, 1975).

'**Spreading**' is the extension of avalanche debris over a landscape in the longitudinal and lateral directions with respect to motion direction.

'**Substrate**' is the material present in the path of the advancing rock avalanche mass. In typical rock avalanche settings (mountains) it usually comprises bedrock, valley fill, ice, fluvial and glacial sediments, and soils.

UNIVERSAL FEATURES OF ROCK AND DEBRIS AVALANCHES

Around the world, large (> 10^6 m^3) non-volcanic rock avalanche and volcanic debris avalanche (the latter usually on the order of km^3) deposits share a number of morphological and structural characteristics, including:

- jigsaw fractured clasts,
- increased comminution with travel distance,
- reverse grading,
- remnant stratigraphy,
- lack of mixing between different lithological units,
- hummocky topography, and
- longitudinal and transverse surface features.

They furthermore share the 'long runout' characteristic mentioned in the preceding terminology section. This, like most of the features listed above, is not observed in smaller avalanches (< 10^6 m^3) which commonly behave more similar to simple granular flows and have relatively uniform surface appearance and an internal structure dominated by a less-fractured clast-supported framework (McSaveney et al. 2000).

EMPLACEMENT MECHANISMS – BRIEF REVIEW OF HYPOTHESES

A number of theories and hypotheses have been proposed regarding volcanic debris and non-volcanic rock avalanche emplacement mechanisms. Examples include different flow regimes such as granular flow (Komorowski et al., 1991; Glicken, 1996), Bingham or plug flow (Voight et al., 1983; Takarada et al., 1999) and viscous flow (Sousa and Voight, 1991). Other models concern acoustic fluidisation (Melosh, 1979), mass changes (Cannon and Savage, 1988; Van Gassen and Cruden, 1989; Hungr and Evans, 2004), seismic energy fluidisation (Hazlett et al., 1991), and dynamic rock fragmentation (Davies and McSaveney, 2002, 2006). Many authors,

however, explain the mobility of debris avalanches by processes concentrated in the basal avalanche region; i.e. cushion of trapped air (Shreve, 1968), low-friction sliding on dissociated or melted rock confined along a basal sliding plane (Johnson, 1978; Erismann, 1979; Legros et al., 2000), low-density layer development (Campbell, 1989), presence of a wet basal shear zone (Voight and Sousa, 1994), basal pressure wave propagation (Kobayashi 1994), spreading with constant resistant shear stress (Dade and Huppert, 1998; Kelfoun and Druitt, 2005), lubrication by liquefied saturated sediments (Buss and Heim, 1932; Abele, 1974; Sassa, 1988; Legros, 2002; Hungr, 2006).

Chapter 1:

Avalanche – Substrate Interactions

In the spirit of:

"When you think you understand something,
you have made only the first approach to it."

Miyamoto Musashi

Rock/Debris Avalanche – Substrate Interactions: Problem Statement, Review, and Hypotheses

1.1. PROBLEM STATEMENT

Rock and debris avalanches resulting from catastrophic rock slope or volcano edifice/flank failures are common phenomena. A universal model to explain and predict their behaviour, runout and deposition area must include all variables that influence avalanche dynamics, including failure volume, runout path topography, rock mechanical properties, and substrate interactions; and it must account for all the features observed in these deposits to be successful in hazard management applications.

As will become evident throughout this document, interaction of a moving avalanche with the material present in its runout path is inevitable and has been documented at numerous mass movement deposits world-wide, ranging from snow and ice avalanches, to pyroclastic and block-and-ash flows, to volcanic debris avalanches, non-volcanic rock avalanches, and debris flows. Although a widespread phenomenon, known since Buss and Heim remarked on it in 1881, the influence of substrate material on avalanche motion, dynamics, and morphology is still not fully understood. The quantitative data on avalanches vary notably with investigators from different disciplines and with different research objectives. One of the aims of this project is to compile, discuss and summarize the current knowledge of avalanche-substrate interactions. This chapter deals with the basic mechanical-physical processes of mass movements and from these draws a conceptual framework. Thereafter, examples from the field and laboratory are presented, and hypotheses contrasted.

1.2. THEORETICAL CONSIDERATIONS

Landslide, and rock and debris avalanche deposits are described by the following geometrical relationships (Figure 1.1): drop height (*H*), runout distance (*L*), volume (*V*), area covered with avalanche debris (*A*), and the deposit length (*L**). The 'apparent coefficient of friction' *H/L* is often used as a measure of mobility by numerous authors; low values indicating high mobility. However, the values of rock/debris avalanche deposits (typically 0.1-0.2, but as low as 0.02) are inconsistent with predictions from simple frictional models (0.6), as will be reiterated below. The line connecting the highest point of the source area with the lowest elevation at the distal deposit margin in Figure 1.1 is called the Fahrbahnböschung (more commonly used is the abbreviated word *Fahrböschung*) (Heim, 1932) or travel line, and its angle (β) is another expression of *H/L*:

$$\tan\beta = \frac{H}{L} = \mu_{apparent} \tag{1}$$

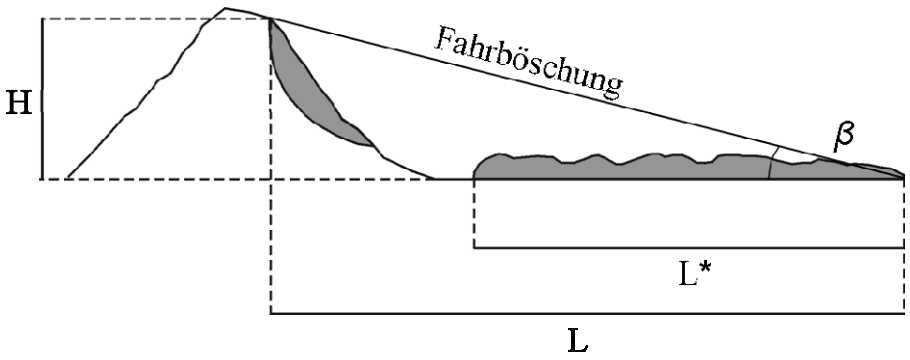

Figure 1.1: Basic avalanche deposit geometries in cross-sectional profile.

In the following section, the emplacement of a geological mass movement is reduced to its very basic and simple processes to outline and analyse the main forces acting on the system. The final velocity of a mass *m* descending an inclined frictionless surface (Figure 1.2b) is identical to its final velocity during free-fall from the same starting height (Figure 1.2a), and can be calculated as a function of displacement:

$$v_f^2 = v_0^2 + 2 \cdot a \cdot d \tag{2}$$

where v_f is the final velocity, v_0 is the initial velocity, a is the acceleration, and d is the displacement distance. In the case presented, $v_0 = 0$, a is the acceleration due to gravity (g), and d translates into the drop height (h). Therefore, the velocity at the bottom of the slope is:

$$v = \sqrt{2 \cdot g \cdot h} \tag{2a}$$

The drop height h can be expressed as $sin\alpha \cdot S$, and equation (2a) can be written as

$$v = \sqrt{2 \cdot g \cdot \sin\alpha \cdot S}\,, \tag{2b}$$

which will become relevant when considering frictional resistance on the failure slope later on.

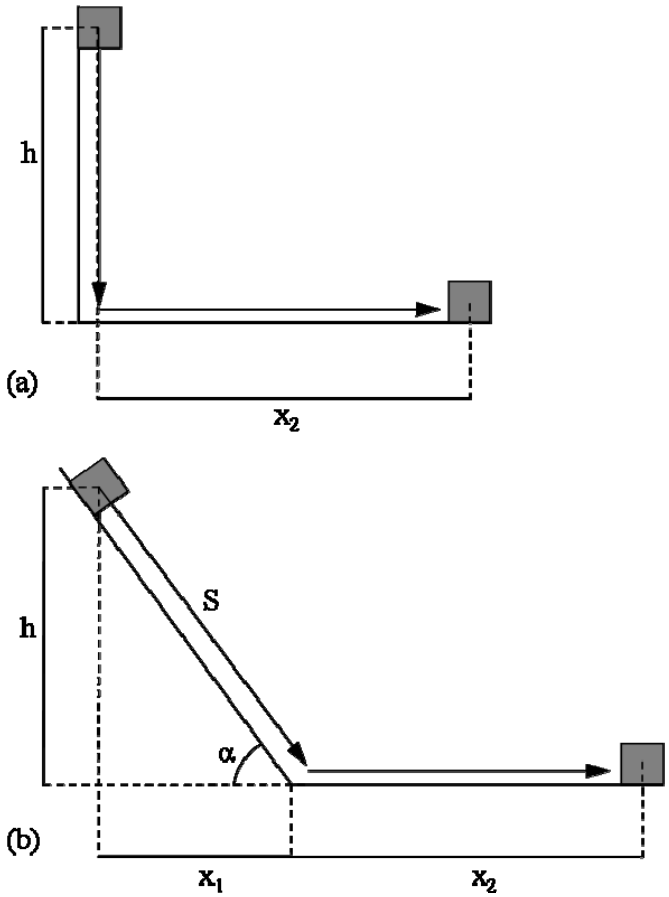

Figure 1.2: Graphics showing the freefall scenario (a) and the frictionless inclined surface (b) discussed in the text above.

The only energy available for further motion across the horizontal runout path (x_2) is the mass' potential energy ($E_{pot} = mg \cdot h$) which is converted into kinetic energy ($E_{kin} = ½\ mv^2$) during descent, and the translation (x_2) of the centre of mass with a deceleration due to friction f ($= \mu \cdot g$) along x_2 can be calculated after re-arranging equation (2a):

$$x_2 = \frac{v^2}{2 \cdot f} = \frac{2 \cdot g \cdot h}{2 \cdot f} = \frac{g \cdot h}{f} = \frac{h}{\mu} \tag{3}$$

The mass comes to rest when its velocity equals zero. In this simplified abstraction of translation of a rigid mass across a 2-dimensional terrain, the basic assumption is that motion occurs through basal sliding with a constant coefficient of friction acting at the interface between the moving block and the surface it travels on. The total translation of the centre of mass (T) for an object descending a hypothetically frictionless inclined surface is the sum of x_1 and x_2:

$$T = \frac{h}{\tan \alpha} + \frac{h}{\mu} \tag{4}$$

In the following, friction on the inclined surface is included. When adding material to the mass in motion (m) on the inclined surface (mass n) or on the horizontal runout path (mass s), the velocity and the total translation of the centre of the combined masses ($m+n+s$) can be calculated via the following equations; which are graphically represented in Figure 1.3:

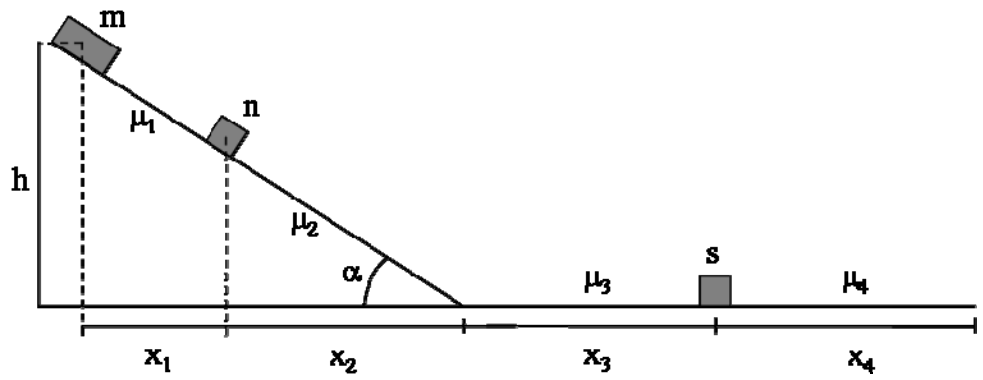

Figure 1.3: Diagram illustrating the setting for equations (5) through (12).

The velocity of mass *m* just before encountering mass *n* is:

$$v_{m1} = \sqrt{\left(\frac{2 \cdot g \cdot x_1}{\cos\alpha}\right) \cdot \left(\sin\alpha - \mu_1 \cdot \cos\alpha\right)}$$

(5)

Momentum is preserved during an inelastic collision between the mass in motion (*m*) and the stationary mass (*n*), and the velocity of the combined masses at this point is:

$$v_{(m+n)1} = \frac{m \cdot v_{m1}}{(m+n)} \tag{6}$$

At the bottom of the slope the velocity of the combined masses $(m+n)_2$ is:

$$v_{(m+n)2} = \sqrt{{v_{(m+n)1}}^2 + \left(\frac{2 \cdot g \cdot x_2}{\cos\alpha}\right) \cdot \left(\sin\alpha - \mu_2 \cdot \cos\alpha\right)} \tag{7}$$

The velocity of mass $(m+n)_3$ just before encountering mass (*s*) is:

$$v_{(m+n)3} = \sqrt{{v_{(m+n)2}}^2 + 2 \cdot g \cdot \left(-\mu_3\right) \cdot x_3} \tag{8}$$

and the velocity of the combined masses $(m+n+s)_3$ at this point is:

$$v_{(m+n=s)3} = \frac{(m+n) \cdot v_{(m+n)3}}{(m+n+s)} \tag{9}$$

Following equation (3), the mass $(m+n+s)_4$ comes to rest when the velocity equals zero:

$$v_{(m+n+s)4} = 0 = {v_{(m+n+s)3}}^2 = 2 \cdot g \cdot \left(-\mu_4\right) \cdot x_4 \tag{10}$$

therefore:

$$x_4 = \frac{v_{(m+n+s)4}^{\ 2}}{2 \cdot g \cdot \mu_4} \tag{11}$$

And the total translation (T) of the centre of mass (m+n+s) is:

$$T = x_1 + x_2 + x_3 + x_4 = \frac{h}{\tan \alpha} + x_3 + x_4 \tag{12}$$

The situation can be adopted for fewer individual masses, and to their varying effects on overall basal friction depending on their composition, by setting n and/or s to zero and varying $\mu_{1\text{-}4}$.

When considering a granular instead of a solid mass there will be spreading of the grains upon emplacement. Adding mass during motion will therefore result in extra spreading. The spreading (= deposit length (L*)) of large granular avalanches is equal to $10 \cdot V^{1/3}$ (Davies, 1982). Estimates of the position of the centre of mass in avalanche deposits proves difficult, and assumptions therefore need to be made when placing the spread deposit length (avalanche tail position) relative to the calculated position of the centre of mass (various possible scenarios are shown in Figure 1.4).

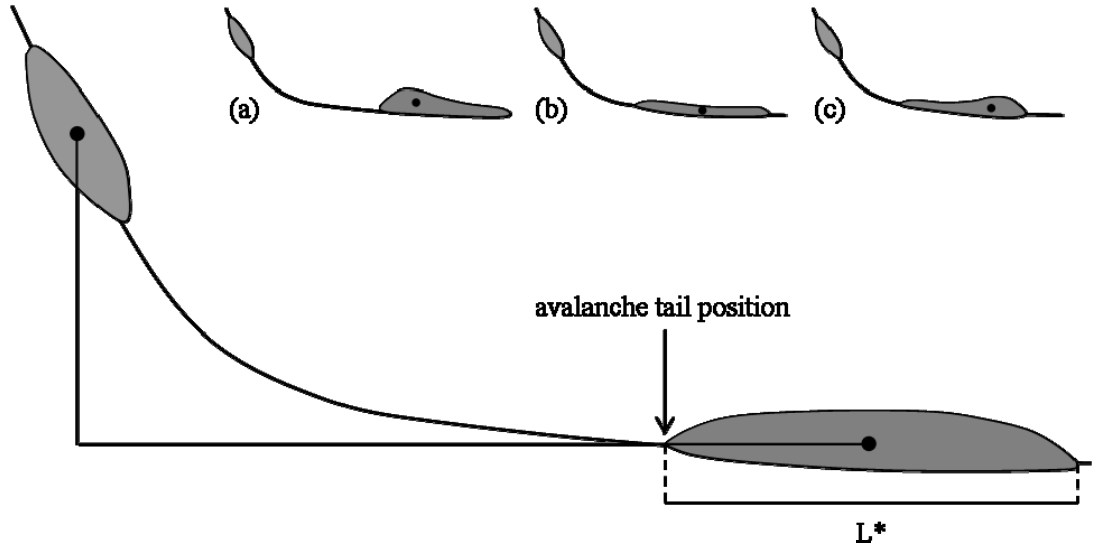

Figure 1.4: Graphic representation of the centre of mass translation and spreading of granular avalanche debris: (a) the avalanche tail moved a long distance from source, leaving a depositional gap in the proximal runout path, and the tail is close to the centre of mass; (b) equal spreading of debris locating the centre of mass in the centre of the final deposit; (c) the centre of mass is close to the deposit distal margin while the avalanche tail came to rest close to source.

In the preceding section, the general scenarios of a granular mass descending a slope and spreading across a horizontal runout path (Figure 1.5a, b) have been calculated using basic geometric relationships and mass energy balances.

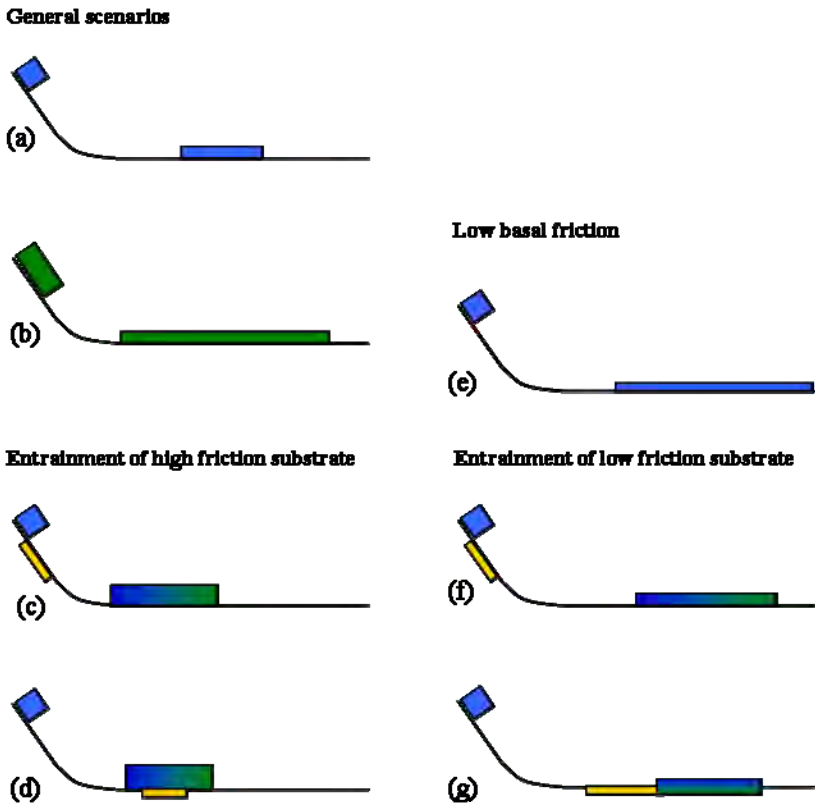

Figure 1.5: Runout distance and deposit thickness relationships to its initial volume and basal conditions: (a) and (b) show the general scaling of runout with volume. In (c) high-friction debris is entrained on the steep failure slopes, whereas in (d) entrainment of the high-friction material occurs on the flatter runout path. Low basal friction scenarios are depicted in (e) in which case basal avalanche friction is lowered by, e.g. emplacement onto glacial ice, (f) where entrainment occurs on the flatter runout path, and (g) where entrainment occurs on the steep failure slopes.

They follow the relationship of longer runout due to spreading with increased failure volume. In scenarios (c) and (d), high-friction debris is added to the moving avalanche. This high-friction debris possesses potential energy available for conversion into E_{kin} in (c), but none in (d). The addition of volume and E_{pot} in (c) is counteracted by an increase in material frictional resistance. No E_{pot} is gained in (d) and the increase in frictional resistance causes more rapid mass deceleration and results in a shorter and thicker deposit relative to the avalanches of comparable volume in (b) and (c). Longer runout can be achieved by drastically decreasing the basal frictional resistance where emplacement occurs over, e.g. glacial ice (e), weak

substrates with low shear-strength or which are prone to liquefaction, emplacement over sediments which, by entrainment, reduce the avalanche's internal friction angle (e.g. Crosta et al., 2006) (g), or the early entrainment of frictional-resistance-decreasing and high-E_{pot} material (f). Thinner deposits can result due to increased lateral spreading or longer runout. High avalanche tail velocities/mobilities result in a depositional gap in the proximal areas (e-g).

A number of forces and processes which govern the motion of large (>10^6 m^3) avalanches are not considered in the above calculations. Generally, all factors that affect avalanche motion can be classed into two categories: (1) those that enhance motion, and (2) those resisting it. Factors of category (1) include the avalanche-intrinsic forces of momentum; potential and kinetic energy; dynamic fragmentation; processes acting at the avalanche base such as reduction in shear and frictional resistance through avalanche processes or substrate interaction; high pore (fluid) pressures and reduced effective stress; debris channelling by topography (Nicoletti and Sorriso-Valvo, 1991); material properties and their dynamic changes during emplacement (e.g. reduced effective stress can be brought about by grain size reduction which leads to higher pore pressures, particularly in weak grains like pumice (Fukuoka et al. 2006)). Category (2) comprises frictional resistance, shear resistance, and inertial resistance (momentum loss) in the avalanche, at its base or within the coupled substrates; topographic obstacles; and encounter of certain types of substrates that impede motion. The mathematical abstractions exercised above furthermore neglect the various processes by which material is incorporated into a moving mass and instead simply work with the addition of mass to mass. It will emerge in this document that the substrate material properties have the most important influence on the effects of material incorporation into a moving avalanche.

1.2.1. Numerical avalanche models implementing substrates

Recently, substrate interactions have been incorporated in numerical models. McDougall et al. (2006) and McDougall and Hungr (2005; 2004) have developed a depth-averaged numerical model based on an existing model, DAN (Hungr, 1995). This model accounts for volume and rheology changes due to material entrainment and is based on a depth-averaged, Lagrangian numerical method (McDougall and Hungr, 2005). This model was used to back-calculate landslide events, such as the

Nomash River (McDougall and Hungr, 2005). Applying a Eulerian-Lagrangian finite element code, Crosta et al. (2008) have developed a 2D-3D model "to simulate the motion of a moving landslide mass on materials with different properties (e.g. hard substrate or erodible soils) and along very rough topographies (e.g. including sharp geometries such as deep and narrow gorges)".

1.2.2. Sediment failure criteria

The important question with regards to substrate influence on avalanche emplacement is when and how a sediment fails; i.e. its erodibility and deformability. In general, a material fails when the applied stress exceeds its strength. Failure can take on a range of styles from brittle to ductile: fracturing, shear failure, liquefaction and fluidisation, slow to instantaneous, and deformation in different rheological regimes.

The simplest expression of the failure criterion, or stress-strain relationship, of a granular material is the Mohr-Coulomb equation whose constituents can be determined in the laboratory by direct shear and triaxial tests (e.g. Savage and Baum, 2005). The Mohr-Coulomb failure criterion describes the shear stress along failure planes at the point of incipient shear failure (Terzaghi, 1943):

$$\tau = c + \sigma \cdot \tan\varphi \tag{13}$$

where τ is the shear strength, c the cohesion, σ the normal stress at failure, and φ the angle of internal friction of the granular material (Figure 1.6).

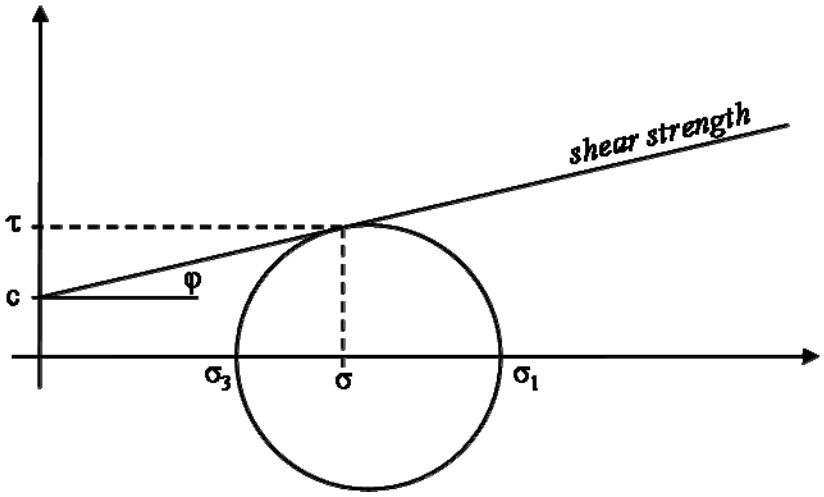

Figure 1.6: Mohr-Coulomb circle defining a material's failure criterion; σ_1 and σ_3 are the major and minor principal stresses in triaxial shear tests, respectively.

The addition of water changes the effective stress by subtracting the pore-water pressure (p) from the total normal stress (Terzaghi, 1943), thus decreasing the shear strength, and the Mohr-Coulomb failure criterion is written as:

$$\tau = c + (\sigma - p) \cdot \tan\varphi \tag{14}$$

The shear strength of geological materials increases linearly with depth below the surface (e.g. Bartetzko and Kopf, 2007). Failure under shear will occur at the intersection of the stress and the strength lines (linear in homogeneous cases (Figure 1.7a) or erratic in inhomogeneous, anisotropic materials (Figure 1.7b).

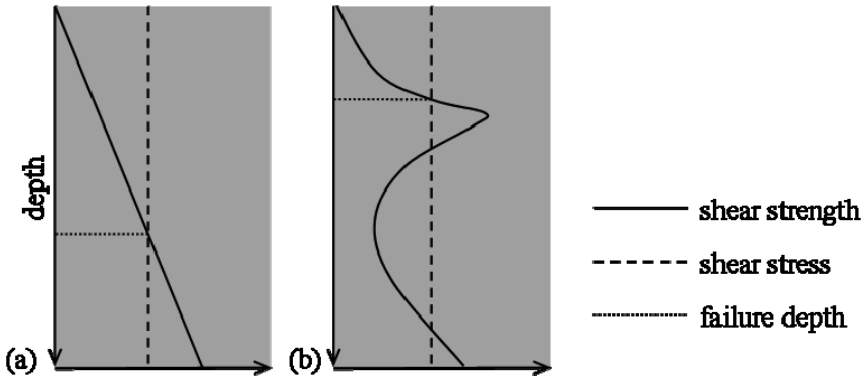

Figure 1.7: Stress and strength relationships with depth.

Material strength increases with higher angles of internal friction or cohesion, and decreases under elevated pore fluid pressure gradients. These are functions of degree of saturation, the granular network (e.g. initial porosity, permeability), dynamic response to stress (e.g. strain hardening or softening, see below), presence or absence of an impermeable layer, etc., and the mechanical properties of a moving granular material are highly heterogeneous in time and space. For a sediment to, e.g. liquefy under rapid loading, the pore pressure and solid grain stress distributions in the dynamic (in motion) state need to be such to reduce the effective stress to zero (frictional, shear and cohesion strength equal zero).

There exists a vast amount of literature on the complex behaviour of heterogeneous and anisotropic sedimentary material. Figure 1.8 serves as an example to illustrate the paths material behaviour can take in the, in this case, porosity-effective stress space.

Reynolds' dilatancy principle observes that dense soils dilate under deformation (pore spaces increase), whereas loose soils contract (pore spaces reduce). A reduction in pore spaces in saturated materials results in an increase in pore pressure gradient and the material looses strength. With respect to debris flow mobilisation, Fleming et al. (1989) and Iverson et al. (2000) observed that contractive soils tend to fully mobilise into debris flows that travel relatively long distances, whereas dilatant soils will either only partially mobilise into debris flows of relatively short runout or remain on the hillside as coherent slide masses.

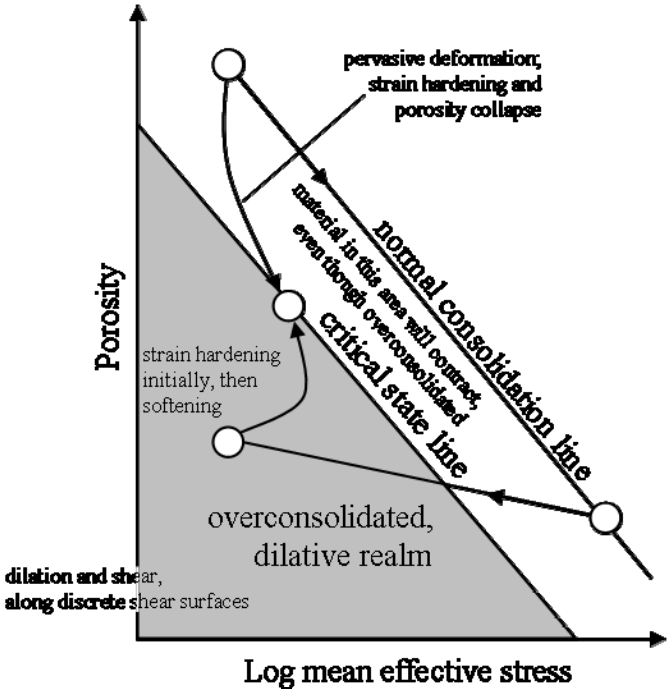

Figure 1.8: Deformation paths in the porosity-effective stress space (Maltman and Bolton, 2003).

This brief excursion into sediment failure and mobilisation criteria only serves to illustrate the complex behaviour of granular materials at the point of and after failure initiation. The shear stress relationship of the Mohr-Coulomb criterion holds true for slowly deforming materials, whereas rapid dynamic changes in properties affect materials under rapid loading by an overriding avalanche which can travel at several 100 kilometres per hour. Details of specific scenarios (e.g. shear failure and frictional resistance) will be discussed in the following sections.

1.3. SUBSTRATE EROSION AND ENTRAINMENT

Studies of substrate erosion and entrainment into a moving avalanche are based, with variable emphases, on field observations, laboratory analogue models, and theoretical considerations, and include the following publications: Crosta et al. (2008; rock and debris avalanche numerical modelling), Sovilla et al. (2006, snow avalanches and numerical modelling), Barbolini et al. (2005; laboratory granular flows), Gauer and Issler (2004; snow avalanches), McDougall et al. (2006) and McDougall and Hungr (2005, 2004; landslide numerical modelling), Hungr and Evans (2004; rock avalanches), Toniolo et al. (2004; laboratory debris flows), Tischer et al. (2001; laboratory granular flows), Sparks et al. (1997; pyroclastic flow field study). Further studies that contain descriptions of erosion and entrainment evidence preserved in the final rock/debris avalanche deposits are listed in Table 1.1. All references for the field study papers mentioned throughout the thesis are listed, by deposit/volcano name, in Appendix A, unless included in the text proper.

Most rock avalanches start life as a relatively coherent (intact or jointed) rock mass on a slope, whereas debris avalanches are sourced in highly heterogeneous materials in terms of grains sizes and mechanical properties. Upon failure, the rock mass descends the slope under gravity and progressively breaks up into smaller fragments during its descent and its travel across the topography. The changes from failure initiation to final deposition include:

- static to dynamic state (rest to motion);
- mechanical properties from static to dynamic;
- volume changes through incremental entrainment and deposition;
- pore space and pressure variations;
- changes in grain size and grain size distribution.

Name	Substrates	Entrainment Style
Adair Park Breccia (VDA)	fluvial deposits	mixed
Allan Hills (RA)	brecciated coal	clasts forming trails in deposit
Almolonga	soil, dry lake bed diatomite	ripped up clasts
Aquabona (RA)	fine marl	mixed
Artillery Peak Megabreccia (RA)	fluvial sands and silts	basal mixed zone
Artillery Peak Breccia Body II (RA)	lacustrine sediments, lithified rootlets, mudstone	injection features
Artillery Peak Breccia Body III (RA)	muddy limestone	clasts
Asama (VDA)	fluvial gravel and fines	clasts, mixed
Aso (VDA)	soil, wood	blocks and fragments
Bandai (VDA)	rounded gravel, wood, soil fragments	erosion
Black Canyon Breccia (RA)	alluvial material	mixed and as clastic dikes
Blackhawk (RA)	arkosic sandstones and mudstones	clastic dikes
Cantal (VDA)	sediments, crystalline basement, volcanics, wood	basal shear zone, rip-up clasts
Casita (RA)	alluvium, tephra, volcaniclastics, surface water	mixed, transformed into debris flow
Cheam (RA)	fine sediments, glacial gravels, sand, wood	diapirs
Chimborazo (VDA)	epiclastic and fluvial sediments	entrained by shearing
Colima, Nevado de (VDA)	volcaniclastics	mixing, transformed into debris flow
Cross Hill Breccia (RA)	sandstone, mudstone	clastic dikes
Derrumbadas, Las (VDA)	limstone, partially consolodated lake sediments	fragments
Eagle Pass (RA)	coarse talus, glacial drift, trees, soil	mixed
El Capitan (RA)	conglomerate	basal mixed zone and clastic dikes
Ghoro, Choh I (RA)	alluvial material	mixed
Gol Ghone (RA)	alluvium, river gravel, fines	no mixing
Huascaran (RA)	ice, morainic material, snow, water, soil, gravel	mixed
Jocotitlán (VDA)	lacustrine sediments, ash, surge layers	clasts
Khait (RA)	saturated loess, river gravel, water	mixed
Leyte (RS-DA)	landslide material, colluvium	mixed
Munday, Mt (RA)	snow	mixed
Nomash River (RS-DA)	liquefied soil, colluvium	mixed
North Long John (RA)	alluvium	possibly remained at avalanche base
Ontake-San (VDA)	river water, saturated sediments	sheared at base?
Parinacota (VDA)	Lauca basin sediments	mixed, entrained as clasts
Pink Mountain (RS-DA)	fine-textured till, colluvium	mixed
Popocatepetl (VDA)	pyroclastic deposits	*not described*
Region Metropolitana (RA)	snow, ice, river sediments	mixed
Roque Nublo (VDA)	ignimbrites, pyroclastic flows, welded ignimbrite, conglomerate, alluvial deposits	sheared, mixed, clasts
Round Top (RA)	river gravel, soil, sand, trees	as clasts in basal zone
Ruapehu (VDA)	saturated mud- and siltstone	mixed, injections, rip-up clasts
Shadow Valley (RA)	soft sediments	basal mixed zone, clastic dikes
Shasta, Mt (VDA)	marine and lacustrine sediments	crushed and mixed into matrix
Sherman Glacier (RA)	glacial ice, soil, till	mixed
Shiveluch (VDA)	soil, pyroclastics, alluvium,wood fragments	basal mixed zone
Socompa (VDA)	gravels, lacustrine, evaporites; (ignimbrite formed basal unit)	clasts
Split Mountain (RA)	alluvial sediments	not described
Taranaki (VDA's)	volcaniclastics, fluvial sediments	flame injections, rip-up clasts, mixed
Tashiro-Dake (Iwasegawa VDA)	tuff breccia	clasts
Tuloca, Nevado de (Pilcaya VDA)	basalt, schist, rhyolite, conglomerate, lacustrine sediments, limestone (proximal to distal order)	mixed, clasts
Tongariro (VDA)	bedded fluvial sands	clasts
Tsing Shan (LS)	colluvium	mixed
Tsok-Dumordo (RA)	silt, sand	diapir-like injections
Val Pola (RA)	landslide debris, lacustrine and fluvial sediments	mixed
Zempoala (VDA)	limestone, chert, sandstone, conglomerate, lacustrine sediments, basalts	clasts
Zymoetz (RS)	snow, soil, fines, till	mixed, till as rip-up clasts

Table 1.1: List of substrate entrainment into rock and debris avalanches; references are provided in Appendix A.

The entrainment of foreign material into the moving avalanche increases its volume and can change the avalanche's bulk or basal composition to such a degree that it affects its mechanical behaviour and changes the evolution of the event (e.g. avalanche runout and spreading, and hence area inundated). The effect depends critically on the substrate type and amount entrained. In typical rock avalanche settings the runout path consists of valley-fill sediments of fluvial, glacial and/or mass wasting nature, and glacial ice, snow, and surface water can be present. In volcanic settings, the runout path topography usually comprises a wide plateau, which may be obstructed by the proximity to other large volcanic edifices, smaller cones and domes, and valleys of fluvial, glacial or tectonic nature. Materials in the runout paths range from volcaniclastics and lava flows, to fluvial and lacustrine deposits, and surface water; in some cases glacial deposits exist.

The following sections (3.1. and 3.2.) discuss the changes of initially dry avalanches that entrained 'sufficient' amounts of substrates to alter the deposit size, shape and behaviour.

1.3.1. Rock slide/avalanche to debris avalanche transformation

Rock slide/avalanche to debris avalanche transformation occurs when debris (e.g. soil, talus, sediments, vegetation, anthropological artefacts, water, etc.) is entrained into the dry mass early in its emplacement. The entrained material is mixed into the moving rock avalanche body as a function of distance travelled and erodible substrate material availability. Hungr et al. (2001) proposed the term rockslide-debris avalanche for events of entrainment ratios greater than 0.25 to emphasize the importance of substrate entrainment in slope failure events. The entrainment ratio (E_R) is defined through: $E_R = V_E / V_R(1+F_F)$; where V_E is the volume of entrained material, V_R is the volume of the initial rockslide, and F_F is the fractional amount of volume expansion due to fragmentation. The amount of material entrained in the examples listed in Table 1.2 is on the order of 20-50 % by volume of the final deposit (after accounting for a ~25 % bulking of the initial rock mass due to comminution), but can be larger for deposits such as the Nevado Huascarán event, where 74 % by volume of the final deposit was entrained ice, snow and moraine material. Eliminating the error that results from assumptions on the volume-increase due to comminution, the amount entrained is contrasted to the original, unfragmented failure volume (Table 1.2). These

numbers show that at least ~ 30 % by volume of the original mass needs to be added by entrainment for the event to be included in the discussed classification. It is important to stress the fact that all of these avalanches entrained material on the steep failure slopes rather than on the flatter runout paths. Therefore, not only was volume added to the avalanche, but also material with a substantial potential energy, which was then available for conversion into kinetic energy during descent and runout. Furthermore, the entrained materials were generally saturated, loose and of weak mechanical properties (water, ice, snow, (liquefied) soil, talus, sand, colluvium, morainic material) which could reduce the frictional resistance to motions, hence allowing greater runout and spreading.

Deposit name	Avalanche Volume [$10^6 m^3$]			Entrained material		
	original	fragmented	total	volume [$10^6 m^3$]	% total	% original
Eagle Pass	0.075	0.094	0.12	0.026	22	35
Nomash River	0.3	0.375	0.735	0.36	49	120
Nevado Huascaran 1962	2.75	3.4	13	9.6	74	349
Ontake 1984	34	42.5	56	13.5	24	40
Rabicano, Cerro*	6	7.5	15	7.5	50	125
Zymoetz	0.72	0.9	1.4	0.5	36	69

Table 1.2: Entrainment of debris into rock avalanches; data from Hungr and Evans (2004). The total avalanche volume is the sum of the fragmented avalanche and the entrained material. Volume-percentages of entrained material are calculated as percent of the total deposit volume, and with respect to the original failure volume; e.g. the Nomash River avalanche started as a failure of 0.3 million m^3 and entrained a volume of material 120 % its original failure volume. **During the Cerro Rabicano event, a later-stage debris flow was produced resulting from landslide dam failure; it is this part of the event that is referred to in Table 1.3, whereas here, only the avalanche section up to the dam location is considered.*

The usefulness of defining such terminology is to focus researchers' and hazard managers' awareness on the potential influences of substrate entrainment on avalanche emplacement dynamics and runout, and the challenges entrainment provide in comparing deposit volumes and runouts of different events to establish empirical relationships between failure volume and maximum distance travelled.

1.3.2. Rock/debris avalanche to debris flow transformation

Rock and debris avalanches can further transform into debris flows by entraining sufficient volumes of water-bearing units or surface water along the runout path. Materials commonly involved in avalanche-to-debris-flow-transformation scenarios include river or lake water, ice, snow, regolith, colluvium, mud, saturated sediments,

soil, and, in the case of a volcanic source, hydrothermally altered rocks from the edifice. The major consequences of avalanche-to-debris-flow-transformation are increased volume and higher mobility, leading to larger areas affected with greater distances from the source included in hazard zone delineation and hazard management considerations. For example, Iverson (1997; and references therein) demonstrated that it is the "interaction of solids and fluids [that] gives debris flows bulk mobilities that commonly exceed those of comparably sized [dry] rock avalanches by 100 %". It is these solid-fluid interactions that also make debris flows highly variable in dynamic flow properties.

Compared to the hummocky rock and debris avalanche surfaces, the deposits of debris flows are typically thinner without substantial morphological variations (e.g. Hungr, 2005). When identifying debris flow deposits in the geologic record, Smith and Lowe (1991) remind that "depositional criteria for recognition of hyperconcentrated flood flows [and debris flows] may not define flow conditions corresponding to empirical definitions (…) or rheological constraints (…)", emphasizing the differences in dynamic and static material properties and appearances. That is, the dynamic porosity and permeability will be variably higher (in time and space) than in the static case due to grain separation by, for example, shearing in the moving mass (the same applies for 'dry' avalanches).

The amount of water necessary to successfully shift the transport mechanisms from that of a granular avalanche to that of a (fully) saturated flow appears to be on the order of 20-50 % by volume. This estimate is based on water contents in debris flows. For example, Iverson (1997) showed that debris flows have a solid-grain volume fraction of about 0.5 – 0.8 in large-scale experiments. Lahars around Mount St. Helens volcano have identical variations in water contents, ranging overall from 22-50 % by volume (Fairchild (1985, 1987), Pierson (1985), Major (1984), as referenced in Glicken (1996)).

In Table 1.3 a number of rock/debris avalanches with associated distal debris flow deposits are listed. In these examples, field observations could discern the parts of the mass movements that behaved as avalanches and those that flowed due to sufficient surficial water or water-bearing material being incorporated into the moving mass. In the case of the Casita event, 35 vol.-% of the final deposit comprises entrained sedimentary material, and 18 vol.-% at Mt. Cayley; values for the other examples

could not be obtained, nor were estimates given on the volume of water (sum of water from source and water gained through entrainment) in the avalanche at the time of deposition.

Example	$L_{avalanche}$ (km)	L_{total} (km)	Reference
Casita	2.5	30.0	Kerle and van Wyk de Vries (2001)
Mt. Cayley	3.5	6.1	Evans et al. (2001)
Nevado de Colima	20.0	120.0	Capra et al. (2002)
Mt. Rainier	2.0	120.0	Vallance and Scott (1997)
Pico de Orizaba	75.0	95.0	Capra et al. (2002)
Cerro Rabicano	17.0	57.0	Hauser (2002)
Nevado de Tuloca	55.0	75.0	Capra and Macias (2000)

Table 1.3: Case studies of rock and debris avalanche deposits with known transition points from avalanche to debris flow.

Apart from flow transformation through entrainment, other mechanisms of debris flow generation by catastrophic slope failure events include sediment mobilization by the advancing avalanche (e.g. Sassa and Wang, 2005), secondary dewatering after or towards the cessation of avalanche motion (e.g. Fairchild, 1987), or following landslide dam failure (e.g. Chen et al., 2004). Initiation and emplacement mechanisms of debris flows form a field of study on their own, and it is beyond the scope of this thesis to go into further details.

1.3.3. Water in the basal avalanche part

In order to affect avalanche dynamics it is not necessary to saturate the entire avalanche body and transform it into a debris flow. Depending on the assumptions made on how the basal conditions control overall avalanche dynamics, and what constitutes the actual base, the influence of water entrainment can be estimated for changes in basal composition and mechanical properties.

To start with, the amount of surface water or water-bearing units in the runout path is one of the factors controlling potential basal saturation. However, their simple presence in the avalanche's path does not predestine entrainment since an avalanche has the capacity to displace rather than entrain; e.g. displacement of the water in Spirit Lake during the catastrophic collapse of Mount St. Helens (MSH) in Washington, USA, May 1980 (Glicken, 1996), and the 1987 Val Pola rock avalanche event in Italy (Crosta et al., 2004); or as evidenced in 'splash zones' of the Elm, Switzerland (Heim,

1932) and Frank, Canada (Cruden and Hungr, 1986) rock avalanches; and flow slides off avalanche lateral margins at the 1964 Hope Slide, and the 1985 North Nahanni Slide in Canada (Mathews and McTaggert (1978), Govi (1989), Evans et al. (1987), as referenced in Hungr and Evans (2004)). What controls whether water *entrainment* or *displacement* occurs; or both as in the MSH case?

Aside from availability of water and erodible, water-bearing material, the porosity and permeability of the basal avalanche part control the amounts and effects of entrainment. When the base consists of large clasts, the pore spaces are large and a high permeability of the moving granular network allows more water to enter the avalanche. At the same time, however, more water per avalanche unit is required to separate the clasts and fully saturate the unit. Finer materials have smaller pore spaces, and can reach saturation at a lower water-to-avalanche volume ratio depending on the grain-size distribution and granular network. Thus, an avalanche with a fine-grained base (as is typically the case in rock and debris avalanches) can reach basal saturation more readily than one with a coarse-grained base. However, permeability is dependant on material composition and grain shapes, and varies highly in actively deforming and in anisotropic sediments (Stephenson et al. (1994), Bolton et al. (1999) as referenced in Maltman and Bolton (2003)). For example, dilation of the mass in motion creates more/larger pore spaces leading to a decrease in the water-to-avalanche volume ratio. At the same time, comminution of avalanche clasts reduces the grain size, thus potentially counter-balancing the effects of dilation.

How much water is necessary to saturate the base during motion to induce an increase in basal pore fluid pressure high enough to effectively reduce the strength, and the shear and frictional resistance of the material, is a complex question and the answer depends on basic assumptions made. Basal saturation is a function of the dynamic avalanche properties, and its feedback on avalanche behaviour will furthermore depend on the avalanche basal area relative to the bulk avalanche three-dimensional geometry. Essentially, we need to define the base in terms of thickness relative to total avalanche thickness and in terms of percent of the avalanche volume. Few studies exist that contain all the necessary parameters of avalanche volume, area covered with debris, avalanche thickness, basal facies description, and basal facies thickness (Table 1.4).

Deposit Name	**Deposit**				**Basal Facies**			
	d_{max} [m]	d_{ave} [m]	V [$10^6 m^3$]	A [km^2]	d [m]	% of $d_{avalanche}$	V [$10^6 m^3$]	% of $V_{avalanche}$
Adair Park Breccia	10-100	nd	nd	nd	3	6.0		
Artillery Peak Megabreccia	nd	80-120	nd	8	2.5	2.5		
Artillery Peak Breccia Body II	35	nd	nd	nd	4	11.4		
Blackhawk	30	10-15	283	14	1	6.7	14	4.9
Cross Hill Breccia	50	nd	20	6	0.75	1.5	4.5	22.5
El Capitan	nd	5-10	40	6	1.5	15.0	9	22.5

Table 1.4: Data of rock avalanche basal units; 'nd' stands for 'not described' in the publication. References of the data sources are listed in Appendix A.

Using the few datapoints presented in Table 1.4, it appears that the basal facies of a rock or debris avalanche deposit can constitute roughly 1-15 % of the deposit thickness, and ~ 5-25 % of the total deposit volume. As these numbers are based on very few, not well constrained datapoints, they are to be regarded as a first approximation in the investigation of basal saturation. As emphasized earlier, the dynamic properties of a moving mixture of solids and fluids are highly variable in time and space during emplacement. The following calculations are very crude and are meant as a thought experiment only. Let's take a typical rock avalanche volume of 40×10^6 m^3 'dry' source material and calculate the amount of water necessary to saturate its base. If the base makes up 5 % by volume (the lowest value in Table 1.4) of the bulk avalanche, then the basal zone volume is 2×10^6 m^3. Assuming further that saturation of this basal material (typically in the fine-to-coarse sand sizes) occurs at ~35 % water-content (based on average debris flow data, see above), then 700,000 m^3 of water are required for saturation. Increasing the basal section of the avalanche to 25 % by volume, and assuming the same volume-fraction of water required to achieve saturation, then the amount of water necessary for basal saturation is 3.5×10^6 m^3. In mountain settings where surface ice, snow and water are readily available, these volumes of water entrainment appear realistic, but will be tested in hypothetical examples following. Rock avalanches of roughly 40×10^6 m^3 can travel approximately 3 to 6 km (see Figure 15 in Chapter 3). Depending on basal-to-avalanche body geometry, the water percolation rates necessary to fully saturate the base will vary (Figure 1.9). A water-volume of 700,000 m^3 can be provided by, e.g. a river 2 m deep, 300 m wide, and 1,200 m long, which are realistic dimensions. To attain 3.5×10^6 m^3 the body of water might have dimensions of 3 m depth, 500 m width and 2,300 m length. This might be a shallow lake or a large, braided river.

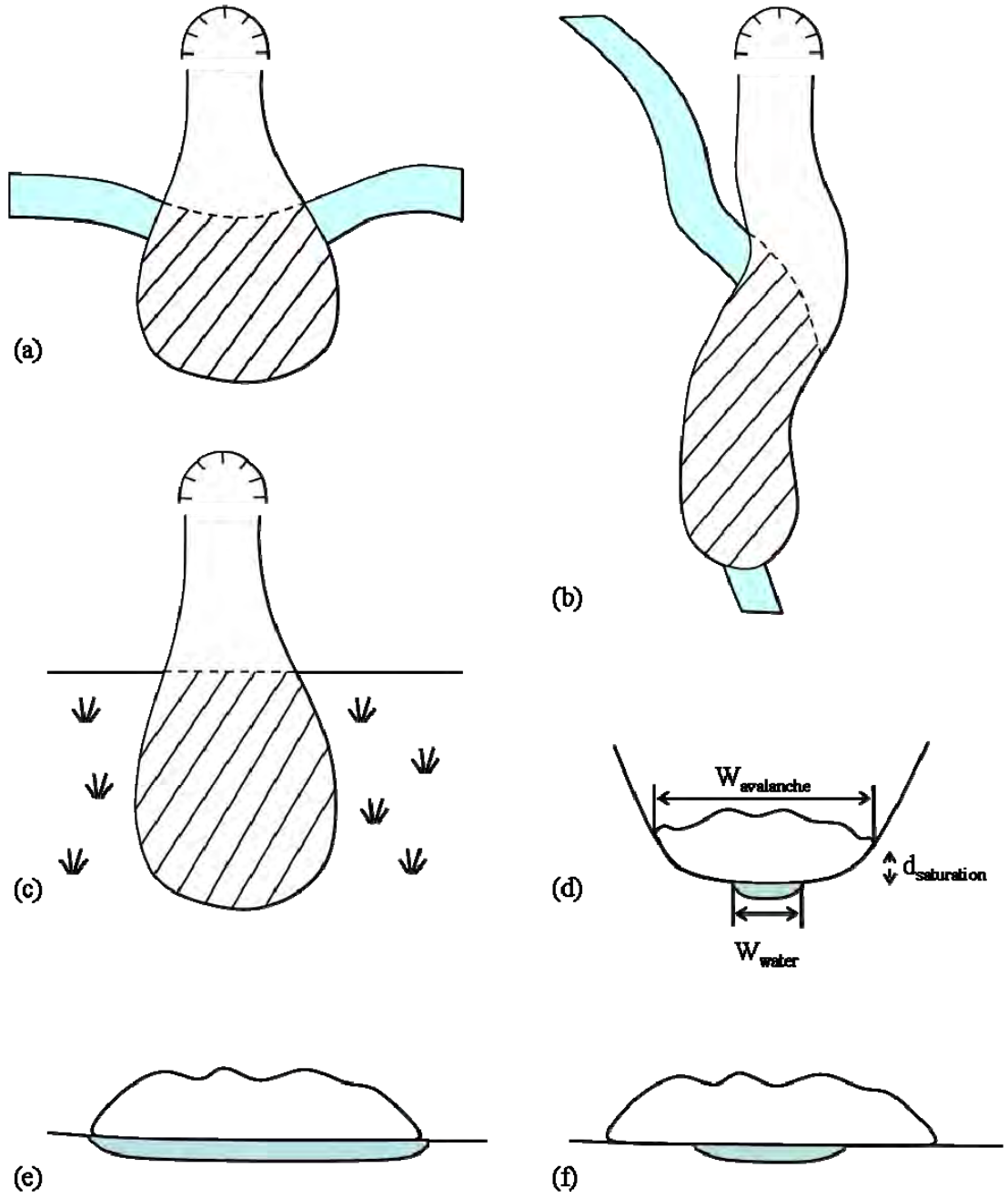

Figure 1.9: Geometric relationships between avalanche and surface water in the runout path; (a) a river or lake spanning the entire avalanche width is crossed and basal saturation is even across avalanche width; (b) topographic confinement changes avalanche to river width relationship; (c) undrained loading over saturated ground (e.g. a swamp); (d) an avalanche emplaced in a river valley is wider than the river and interacts mainly with the dry valley walls, basal saturation might only affect parts of the avalanche; (e) shows a cross-section of scenario (a); and (f) shows a spreading avalanche unconfined by topography encountering a small body of water (i.e. lesser in width than the avalanche).

Other sources of water are the melting of ice and snow, and the presence of saturated sediments. Undrained loading of saturated sediments can create sufficient pore pressure gradients to mobilise interstitial water from the sediment into the rock avalanche, but water volumes entrained per unit time will be less than incorporating free surface water. Alternatively, the loaded substrates can fail at depth and become coupled with the avalanche, thus forming a saturated base under high confining pressures and consequently high pore water pressures. Entrainment and mixing of saturated sediments with avalanche debris, by contrast, will lead to these becoming unsaturated in the moving debris by material dilation due to shearing and as a consequence of mixing with the 'dry' avalanche material. On the other hand, overburden pressure of the avalanche might be sufficient to keep pore water pressures in the basal mixed zone elevated for the time of emplacement duration, essentially turning the event into a composite flow with a basal saturated, mobile facies and a dry (i.e. unsaturated) top layer.

It is evident that the applicability of calculating basal avalanche saturation is crucially dependant on assumptions regarding (1) how much of an avalanche's mobility is controlled by the base, (2) how much of the basal deposit facies identified in outcrops was 'active' during motion, (3) the deposit geometry in cross section (i.e. the relationship between basal-width to deposit dimensions (see also Figure 10 in Chapter 2), (4) the type of interaction (see preceding paragraph), and (5) the composition and dynamic properties of the basal facies material since these govern the amount of water required for saturation at any given point during motion. With improved understanding of avalanche emplacement mechanisms and more detailed data on avalanche basal properties and characteristics, this approach may become a useful tool in avalanche modelling. And with more good data available, statistical analyses can be carried out to test the apparently higher mobility of moist (water-undersaturated) and wet (water-saturated) avalanches compared to dry avalanches of similar volume as postulated by Shaller (1991) and Friedmann (1997); and to also test the relationship between deposit shape and climate put forward by Strom (1996) who suggests that avalanches emplaced in dry conditions preferentially form elongate deposits whereas those in moist/wet conditions are more spread laterally. Examples of elongate deposits in dry/semiarid climates and unobstructed runout paths include the Black Canyon Breccia (US-Arizona, Yarnold and Lombard, 1989), Blackhawk (US-California,

Johnson, 1978), Cross Hill Breccia (US-Arizona, Yarnold and Lombard, 1989), and the Pink Mountain (Canada, Geertsema et al., 2006) rock avalanches.

1.3.4. Entrainment processes and influencing factors

The processes acting during rock and debris avalanche emplacement are impossible to observe directly in the field. However, combining the evidence preserved in outcrops with observations made during laboratory and field-scale granular flow experiments, and with theoretical considerations, provides a good picture of how substrates are mobilised, transported and incorporated by the moving avalanche. The processes of entrainment observed consistently in spite of scale and emplacement mechanism differences are:

1. ploughing,
2. deformation wave / impact erosion,
3. pore pressure changes / fluidisation, and
4. basal abrasion.

1.3.5. Ploughing at the avalanche front

From observations in the laboratory (Barbolini et al., 2005) and in field simulations (Sovilla et al., 2006) it appears that ploughing of the avalanche into the substrate is the most common entrainment mechanism, and likewise the most influential on avalanche dynamics. The main area of avalanche-substrate interaction in these cases is below and ahead of the avalanche front.

Substrate ploughing in small-scale laboratory analogue models generally proceeds as follows (see Figures 3 and 6 in Chapter 5): initial encounter of the advancing avalanche toe erodes the uppermost grain layer(s) of the substrate while compressing the immediately underlying material. With increasing advance, the avalanche begins to plough into the substrate, leading to substrate mobilization ahead and beneath the avalanche front, and failure along shear planes pushes the substrate ahead onto stationary substrate material. Grain bridges are observed to form and fail, and a cyclic expansion and compression of the substrate is observed in the erosion and mobilization process (e.g. Chapter 5; Barbolini et al., 2005; Tischer et al., 2004).

An interesting observation during the emplacement of artificially released snow avalanches by Sovilla et al. (2006) is that a package of substrate snow was entrained

instantaneously. They termed this process ‘step entrainment’ whereby a weak snow layer was sandwiched between harder, stronger snow packs which resisted deformation until the point of sudden failure.

1.3.6. Deformation wave and impact erosion

Impact erosion occurs when isolated avalanche particles ahead if the main body impact on the substrate, compressing or displacing its particles, and is observed prior to ploughing as discussed above. Ahead of the avalanche front in small-scale experiments, Tischer et al. (2004) observed a deformation wave in the granular substrate. As a result of this interaction, the grains at the moving avalanche front loose E_{kin} and the avalanche front velocity decreases. The shockwave through the substrates accelerated particles in the deformable bed and the mobilized particles then moved into the avalanche front where they were accelerated to avalanche velocity.

1.3.7. Basal abrasion and shear

Avalanche particles sliding parallel to and mobilising substrate particles is the process called ‘basal abrasion’ (Gauer and Issler, 2004). Entrainment rates of basal abrasion compared to frontal entrainment through ploughing measured by Sovilla et al. (2006) were of longer duration (1-40 s for abrasion; 0.1-2 s for ploughing) but have a factor of 10 smaller entrainment rates (measured in kg/(m^2s)). In their large-scale snow avalanche experiments, basal abrasion led to comparable amounts of substrate snow entrained as by frontal ploughing, but the material was distributed over a large part of the avalanche from front to tail (as opposed to material concentrated at the avalanche front during ploughing). These authors also observed that basal abrasion predominantly occurred over snow layers with high shear strength, whereas those with low strength (dry, low density, and/or cohesionless snow) were subject to frontal entrainment or step-entrainment.

In the field, basal shearing products are preserved as fine-grained shear (or gouge) zones in the lowermost basal mixed zones of rock and debris avalanches. For example, the basal facies of the Artillery Peak Megabreccia is a 2.5 m thick, contorted-to-structureless mixture of substrate-derived and avalanche materials, but only the lowermost 30 cm are intensely comminuted avalanche fragments and rock flour over a polished and grooved basal contact (Yarnold, 1993); see section 4.3. for more details on substrate shearing.

1.3.8. Pore pressure changes and fluidisation

In the case of substrate fluidisation, the avalanche front generates a pore pressure gradient in the substrate that counteracts the material's cohesive forces and frictional strength (Gauer and Issler, 2004). Pore fluid pressures temporarily reach the point where the incompressible interstitial fluids carry all the applied stresses, leading to loss of shear resistance. Substrates in a fluidised state pose no resistance to avalanche motion, but instead, if coupled with the avalanche, reduce the moving mass' basal frictional resistance, which favours avalanche motion. If the fluidised sediments are not coupled with the avalanche, they might escape and form debris flows or splash zones ahead of the avalanche front (see section 3.3.). The process of 'rapid undrained loading' to facilitate long avalanche runout has been disputed in the literature since Hutchinson and Bhandari proposed this mechanism in 1971. Can a high pore water pressure gradient be maintained for long enough to affect avalanche emplacement? Or is it a process that affects mobility/behaviour of only small parts of the overriding avalanche over a short time? Maintaining high pore pressures is a function of the rate of pore water dissipation. Therefore, an elevated pore water pressure gradient in the sediment's granular network must be maintained for the duration of avalanche emplacement. High emplacement velocities might be sufficient to permit interaction times to be short relative to pore water pressure dissipation rates. An impermeable layer at depth within the sediment could further prevent rapid water escape. On the other hand, hydrofracturing, which can occur in rapidly stressed sediments (Maltman and Bolton, 2003), allows rapid water drainage. Similarly, high sediment permeability over a sufficiently large area/depth can facilitate the loss of a high pore water pressure gradient, or prevent it from developing in the first place. Dilation during shear increases pore spaces and leads to a reduction in pore water pressure.

Sediment behaviour after failure is complex and a function of sediment composition, microstructure, and degree of saturation (see section 2.2.). For example, Osipov et al. (2005) observed in undrained ring shear tests of clayey soils, that the distribution of clay minerals determined the soil resistance to liquefaction (other influencing factors were clay composition and plasticity, and pore water chemistry). Similarly, investigations of liquefaction potential of sands showed that their undrained response in laboratory tests is inherently anisotropic (Vaid and Sivathalayan, 2000).

1.3.9. Erosion depth and rate

The rate of substrate erosion is related to substrate properties (such as shear strength), avalanche velocity (v) and avalanche thickness (loading), and tends to increase with v^2 (Barbolini et al., 2005; Bursik et al., 2005; Takahashi, 2001). A minimum bed shear stress has to be exceeded before erosion commences. The erosion rate furthermore depends on the angle of the slope on which the avalanche is travelling; to which the flow velocity is of course related, but additional complications arise in terms of substrate stability on an incline.

Erosion depths beneath mass movement events deposits range from 0.1 – 8 m in the examples summarized by Hungr et al. (2005).

Some ways of calculating erosion rates (ms^{-1}) are summarized in Barbolini et al. (2005) as simplified expressions from Eglit and Demidov (2005):

- Erosion rate (q) proportional to flow velocity (v): $q = a \cdot v$, in which a is a coefficient that depends on the snow properties and takes into account the density differences between avalanche and substrate.
- Erosion rate (q) proportional to flow depth (d_{av}): $q = b \cdot \left(d_{av} - d_{av}^{*}\right)$, with b (s^{-1}) a coefficient and d_{av}^{*} is the minimum flow depth that produces a load equal to the shear strength of the substrate.
- Erosion rate growing with the square of the flow velocity: $q = c \cdot \left(v^2 - v_{*}^2\right)$, where c (sm^{-1}) is a coefficient and v_* represents a velocity threshold for erosion.

Results by Takahashi (2001) on flume experiments give:

- Velocity-dependent erosion rate: $q = \left(d_{sub} \cdot v\right) / L_{front}$, where d_{sub} is the thickness of the erodible layer, v the avalanche velocity, and L_h the length of the avalanche front.

An erosion rate equation tested against laboratory experiments is cited in Bursik et al. (2005) and it relates the rate of erosion e_s (m^2s^{-1}) to the effective bed shear stress (τ_{eff}):

- $e_s = \alpha \cdot \left(\tau_{eff} / \rho_o\right)^{1/2}$, with α an empirical erosion or entrainment coefficient, and ρ_0 presumably the bulk density of the erodible material.

More work is needed to understand and determine the various coefficients used in the above equations.

Other ways to measure or define entrainment are the dimensionless entrainment ratio (E_R) defined by Hungr et al. (2001; see section 3.2.), and the yield rates (m^3 entrained material per metre travel distance), which can vary orders of magnitude (0-300 in the data summarized by Hungr et al., 2005) for rock/debris avalanches and debris flows.

The rate at which avalanches can erode material from their runout paths is a subject deserving more attention, but detailed field and experimental data are scarce. For numerical avalanche modelling the following parameters are useful to compute the avalanche evolution from initial collapse to deposition:

- source volume,
- volume and depth of erodible material available in the projected path,
- type of sediment materials and its properties (strength, shear and frictional resistance, degree of saturation),
- estimates of amount of material likely to be incorporated into the avalanche,
- constraints on entrainment/interaction style (basal mixing, full-avalanche-depth mixing, bulldozing),
- projected bulking of the avalanche due to (a) fragmentation, and (b) entrainment integrated over the distance travelled,
- avalanche volume lost by deposition at incremental distances from source,
- topographic control on erosion and deposition,
- and the possibility of a threshold-velocity above which erosion ceases.

1.4. SUBSTRATE DEFORMATION

Few studies exist that detail substrate deformation features and processes. Lack of basal outcrops (particularly in the generally thicker volcanic debris avalanche deposits), and differing research foci are probably the main reasons. Table 1.5 is a list of substrate deformation descriptions extracted from the literature.

Basic mechanical-dynamic considerations underline that in any interaction of a moving object with stationary material, energy is transferred ("lost") from the object in motion to the stationary one. Folding, faulting and bulldozing require energy to move or fracture the material. Shearing of substrates at the avalanche base or deeper within the strata likewise requires energy expenditure. Counteracting the decrease of energy available for avalanche motion are, for example, reduced basal friction and the transmission of shear stress into a weak substrate, favouring avalanche spreading/runout. The various processes and potential effects are discussed on the following pages.

Name	Substrates	Interaction
Adair Park Breccia* (RA)	fluvial deposits	folded, contorted
Allan Hills * (RA)	coal, sandstone, siltstone	brecciated, folded, fractures, tilted fragments
Altenau (RA)	lacustrine clays	dipping nearly vertical
Ananievo (RS)	soil, subsoil loam	bulldozed
Artillery Peak* (RA)		folded, contorted
Baga Bogd (LS)	soft material	pushed into 2 km wide chaotic rim
Bashi-Djaya (RA)	subsoil loam	reverse faulting, bulldozing
Black Canyon Breccia* (RA)	silts, gypsiferous clays	folded, overturned
Cantal* (CDA)	weathered granitic basement	sheared, fractured
Cheam* (RA)	1: organic-rich silt and sand; 2: late-glacial outwash units; 3: glaciofluvial gravel; 4: fine sediments	1: contorted, disrupted; 2: tilted, sheared; 3: undulatory contact; 4: liquefied
Chimborazo* (VDA)	1: epiclastic and fluvial sediments; 2: ignimbrite	1: folded, faulted, sheared, undulation; 2: reworked at depth
Cross Hill Breccia* (RA)	gypsiferous claystone	folded, imbricated
Diki'i Greben (VDA)	volcanic deposits	folds along deposit margin
Dulung Bar Darkot	wet sediments	nd
El Capitan* (RA)	playa lake sediments	highly folded, contorted, detached, imbricated
Frank (RA)	alluvium	lateral displacement
Fuego (VDA)	volcaniclastics, unsaturated lacustrine sediments	nd
Ghoro Choh* (RA)	1: alluvial, fluvial and lacustrine sediments; 2: river gravel	1: folded; 2: thrust into arcuate mounds
Gol Ghone* (RA)	carbonates, granite	folded, sheared, pulverised

Table 1.5: Substrate deformation examples; references are listed in Appendix A.

Huscaran* (RA)	glacial moraines	grooved
Inilcheck (RA)	1: alluvium; 2: loam	1: compressed, deformed; 2: cracked
Jocotitlan* (VDA)	volcaniclastic and lacustrine sediments	folded, faulted
Marquartstein (RA)	lacustrine clays, gravel	displaced
Munday, Mt* (RA)	snow	bulldozed at margins
North Long John* (RA)	alluvial fan material	bulldozed
Parinacota* (VDA)	water-saturated sediments	boudinage, folded, faulted, thrust faulted
Pink Mountain* (LA)	sandstone	striation
Round Top* (RA)	saturated peaty soil, river gravel	bulldozed, contorted
Ruapehu* (VDA)	laminated Tertiary sediments	plastic
Satpara Skardu (RA)	alluvial fan material	folding, faulting and intrusion
Shadow Valley* (RA)	soft sediments	folding
Shiveluch* (VDA)	1: soils, tephra; 2:pyroclastic deposits	1: folded, sheared; 2: bulldozed into 1.5 km wide margin
Socompa* (VDA)	1: ignimbrite (basal VDA unit); 2: lacustrine and evaporitic sediments	1: sheared, fragmented; 2: bulldozed, folded, thrust faulted
Taranaki* (VDA)	dune sands, peaty sequences	sheared
Unzen (VDA)	soft soil	soft sediment deformation
Yarbah Tshoh (RA)	alluvium	folded, thrust faulted

Table 1.5: continued

1.4.1. Bulldozing

'Bulldozing' is the detachment of substrate material and pushing of the same into mounds by the moving avalanche. Substrate mounds resulting from large-scale bulldozing at the front of avalanches are referred to as the 'bulldozer facies' (e.g. Belousov et al., 1999). Other bulldozing cases involve (4.1.2.) substrates beneath, i.e. within the avalanche body; and are also reported at their motion-parallel sides (4.1.3.). How does 'bulldozing' differ from 'ploughing'? Both terms essentially describe the same initial process, but result in different outcomes. 'Ploughing' describes any type of substrate pushed by the avalanche and subsequently entrained (i.e. mixed) into the moving debris. 'Bulldozing', on the other hand, refers to pushing (and folding) of substrate units, but with these remaining essentially unmixed with the avalanche debris. The use of these terms in the scientific literature, again, varies from discipline to discipline: 'ploughing' is widely used in the snow and experimental literature, whereas 'bulldozing' has its niche in the rock and debris avalanche literature where it commonly refers to sedimentary units that have been displaced and folded ahead of an avalanche or avalanche hummock/ridge. Substrates involved in bulldozing include volcaniclastics, gravels, soil, sand, loam, snow, alluvium, peaty sequences, lacustrine sediments, and evaporites.

1.4.2. Sediment bulldozing at avalanche terminus

Sediment bulldozing at the terminus of rock and debris avalanches occurred with differing degrees at the following sites: Parinacota volcano (Clavero et al., 2002), Shiveluch volcano 1964 (Belousov et al., 1999), Socompa volcano (van Wyk de Vries et al., 2001), Adair Park Breccia (Yarnold and Lombard, 1989), Ananievo (Abdrakhmatov and Strom, 2006), Baga Bogd (Philip and Ritz, 1999), Blackhawk (Johnson, 1978), and Arvel (Choffat, 1929 as cited in Crosta et al., 2008).

How does substrate bulldozing at the avalanche front affect its runout? And what consequences does it have for the total area affected by the event (i.e. area covered with avalanche debris plus the area of bulldozed substrates outside the avalanche margin, see Figure 1.11).

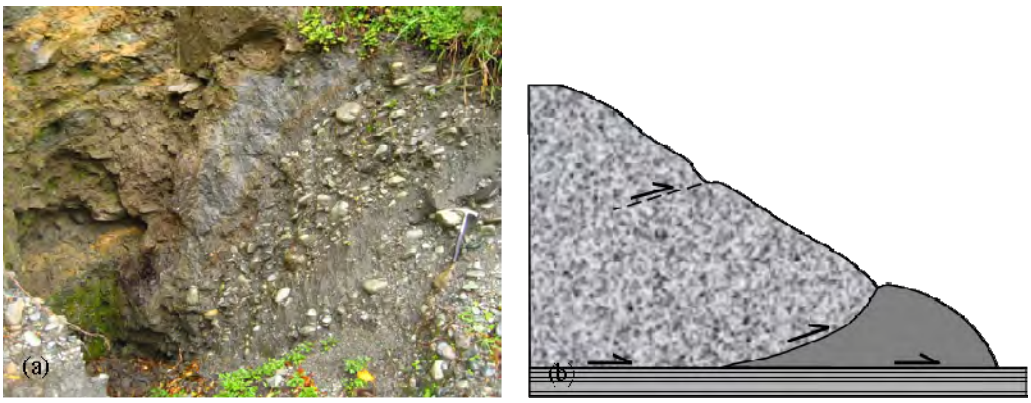

Figure 1.10: (a) Bulldozing of substrate material n front of a hummock within the Round Top rock avalanche, New Zealand (see Chapter 3); (b) sketch of subsoil loam (solid gray) bulldozed over stationary substrate at the Ananievo rock avalanche in Kyrgyzstan (after Abdrakhmatov and Strom, 2006).

Regarding these questions, I would like to put forward two hypotheses: (1) if the avalanche front velocity was low (decelerating rapidly) at the point of commencement of substrate bulldozing, the total area affected is likely to be larger than if the avalanche had come to a stop without mobilizing material ahead of its terminus (see Figure 1.12a). This will usually be the case for substrate encounter in the distal reaches, after the avalanche has decreased in velocity. Within the avalanche front, minor compressional faults are to be expected. (2) If an avalanche front of high velocity mobilizes substrate and bulldozes material, this can in fact become an obstacle in the runout path and rapidly decelerate the avalanche front at the location. The avalanche will come to rest sooner than if it had not bulldozed material (see

Figure 1.12b), and it might have spread beyond the bulldozed facies extent. Here one would expect more intense compressional features within a thickened avalanche front. The effect of this second hypothesis would be larger closer to source (at higher avalanche velocity). Substrate bulldozing can be likened to topographic obstacles; for example, topographic obstacle encountered when the avalanche has travelled a long distance will affect the runout much less than when the same obstacle is close to source.

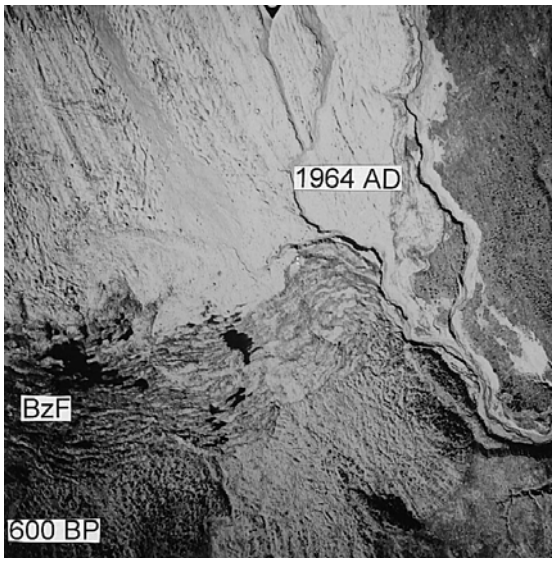

Figure 1.11: Aerial photograph of the distal debris avalanche margin and associated bulldozer facies (BzF; 1.5 km wide and 6 km long) of pyroclastic deposits at Shiveluch volcano, Kamchatka (image from Belousov et al. 1999); 600 BP is an older debris avalanche deposit.

Again, however, the net influence of the substrate on avalanche runout is largely dependant on the substrate properties as demonstrated in numerical models by Crosta et al. (2008), snow avalanche emplacement and erosion observations (Sovilla et al., 2006), and laboratory analogue models (e.g. Chapter 5).

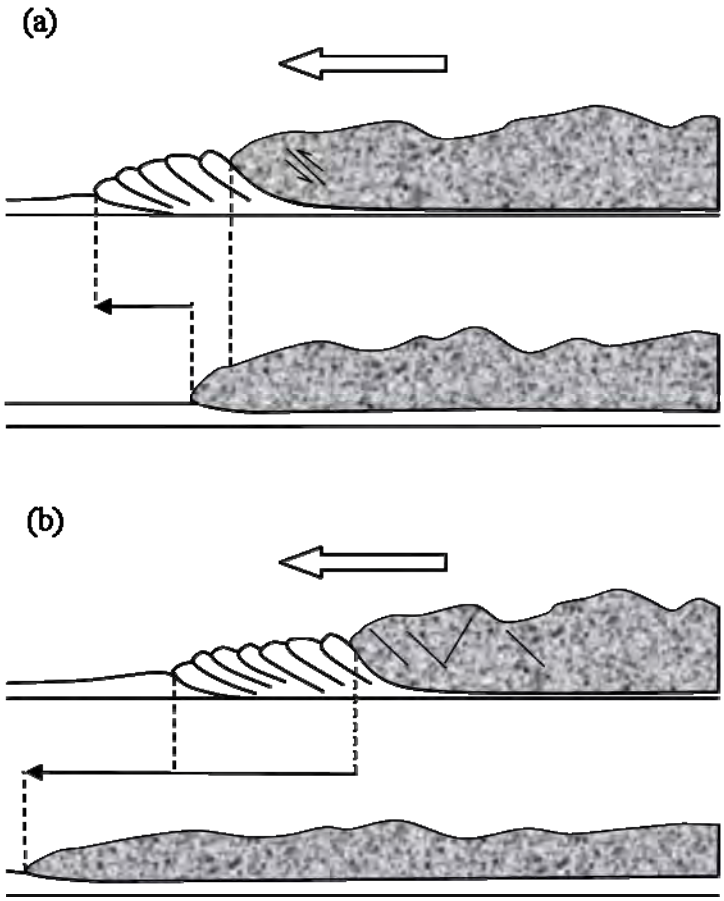

Figure 1.12: Effects of bulldozing at the avalanche front on runout; (a) low-velocity avalanche front bulldozes substrate material and causes greater area inundated by the event than (b) in which the bulldozed substrates slowed down a high-velocity avalanche front efficiently enough to shorten its runout significantly, and possibly less area is effected as a consequence of substrate bulldozing.

1.4.3. Internal bulldozing

Bulldozing of substrates is not restricted to avalanche frontal margins. Indeed, they are found, on a smaller scale, within the interior of deposits where they are typically associated with the location of longitudinal ridge termini; so for example at the Altenau (von Poschinger, 1994), Ghoro Choh I (Hewitt, 2006), Round Top (Chapter 3), and Artillery Peak (Yarnold, 1993) rock avalanches. In these cases, the bulldozed substrates prevented the break-up of longitudinal ridges into smaller hummocks, thus aiding the preservation of these features in the final deposit (see Chapter 2 for more details).

1.4.4. Bulldozing at margins

At the margins of some avalanches, substrates have been displaced and accumulated in long mounds along parts of the deposits such as at Mt Munday (Evans and Clague, 1998), and North Long John (Blair, 1999), for example.

1.4.5. Folding and faulting

Substrate materials involved in folding and faulting associated with avalanche emplacement are listed in Table 1.5 above. During folding and faulting of stationary materials by a moving avalanche mass, energy from the avalanche is transferred into these materials to mobilise and deform them. With respect to avalanche thickness and volume, can substrate deformation (without entrainment) change the avalanche's energy budget sufficiently to alter its behaviour, mobility and runout?

Figure 1.13: Examples of substrate faulting (a) beneath the Jocotitlán volcanic debris avalanche deposit (Krantz compass for scale), and substrate folding (b) associated with the Perrier volcanic debris avalanche deposit (van Wyk de Vries, per. comm.); image is ~ 3 m across, white line traces fold.

One potential example of a change in avalanche behaviour upon the encounter and deformation of weaker substrates is the Ollagüe volcanic debris avalanche in Chile. In the distal reaches of this deposit substrate fold amplitude increased where more ductile substrates were involved in avalanche emplacement (Clavero et al. 2004). Here, isolated hummocks sit atop thickened and folded Salar (unconsolidated saline) sediments (Figure 1.14). The sketched cross section of this area is reminiscent of laboratory experiments of a coal avalanche overriding low-friction substrate material in the form of polystyrene spheres (Chapter 5). Ploughing of the substrate by the overriding avalanche was followed by substrate mobilization into a waveform while

the lower substrate material was compressed and failed at the substrate base (metal plane beneath polystyrene spheres layer). The actively spreading avalanche changed its behaviour once the substrate became mobilized and became a passive layer on top of the moving/sliding substrate wave (avalanche-substrate coupling). No substrate was mobilized at depth ahead of the wave. Coal and polystyrene clasts which deposited beyond the wave reached this location by tumbling down the avalanche front after the cessation of motion. This experiment suggests that momentum transfer from the avalanche into a stationary substrate with low frictional resistance (and or a weak base) can translate the active motion part from the avalanche into the mobilised material below. In more resistant substrates, the transfer of shear stresses into the underlying material impedes rather than enhances avalanche motion (e.g. Gol-Ghone).

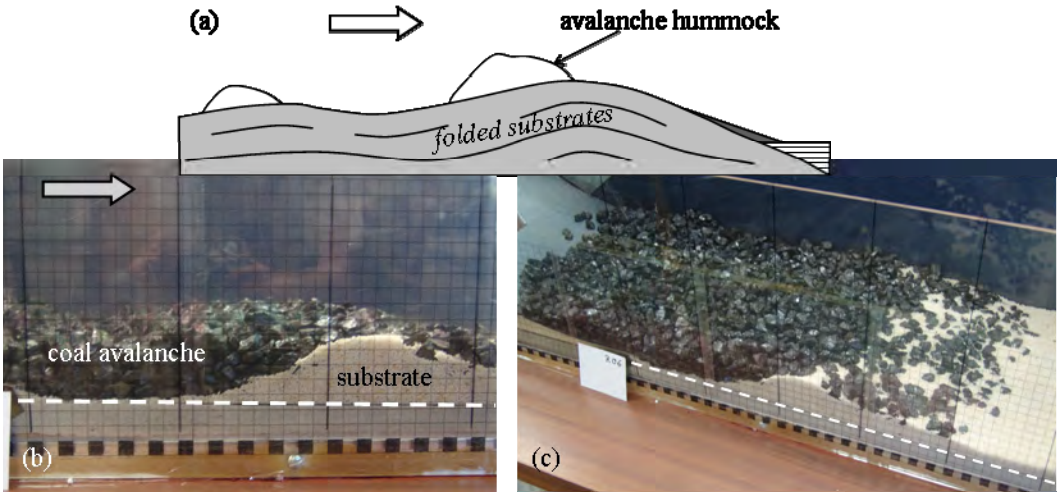

Figure 1.14: Comparison of folding at the distal Ollagüe volcanic debris avalanche ((a), sketch after Clavero et al., 2004) and results from small-scale analogue models (b, c). Dashed lines in laboratory images mark the base (metal plane) of the substrate (polystyrene spheres); grid is in cm.

1.4.6. Basal friction and shear

The influence of basal frictional resistance on a sliding mass has been discussed at the very beginning of this chapter and the results generally apply to real-life granular avalanches with added complexities to the problem.

Basal frictional resistance opposes the forces in motion direction. There are two options for avalanche response: (1) simultaneous and equal deceleration of the full avalanche body, (2) deceleration of the base and shear zone migration up-section with subsequent incremental deposition.

1.4.7. Emplacement onto ice and snow – case of lowered basal friction

Statistically, rock avalanches emplaced onto glaciers are more mobile, consequently resulting in longer runouts and thinner deposits than their counterparts emplaced onto other materials (Evans and Clague, 1998). An increase in avalanche mobility over glacial ice has also been shown in recent numerical models by Sosio et al. (2008). Generally, basal avalanche friction on glaciers is low and thus aids in the free runout of these avalanches.

1.4.8. Shearing

Typically, rock avalanches have a relatively finer-grained base with coarser material towards the top. Volcanic debris avalanches also feature an often finer base, but vary overall due to the highly heterogeneous nature of the source material.
Shearing occurs throughout the avalanche body (e.g. Johnson, 1978; Yarnold and Lombard, 1989; Yarnold, 1993; Davies and McSaveney, 2002) and at three locations near the avalanche base: (1) within the lowermost part of the avalanche itself, (2) at the interface of avalanche and substrates, and (3) within the substrate. The shear locations (avalanche base, plane of contact, substrate) are in continuous contact, and often avalanche and substrate materials mix to produce a basal mixed zone (sometimes referred to as ‘gouge’; a term conventionally used to describe the soft, unconsolidated sediment formed by rock shearing in fault zones; e.g. Bates and Jackson, 1984). Intergranular shear induces comminution of the grains, leading to particle-size reduction as in fault zone gouges. Davies and McSaveney (2008) proposed that dispersive pressure created during shearing and the resultant reduction in intergranular stress within the shear layer (and hence the reduction of frictional resistance to shear) to be an effective explanation for the long runout of large ($> 10^6$ m^3) rock and debris avalanches. Shearing, accompanied by fragmentation and dilatancy is a function of the confining pressure (lithostatic and lateral), and a vertical shearing gradient is expected and observed in the avalanche (e.g. Pollet and Schneider, 2004).

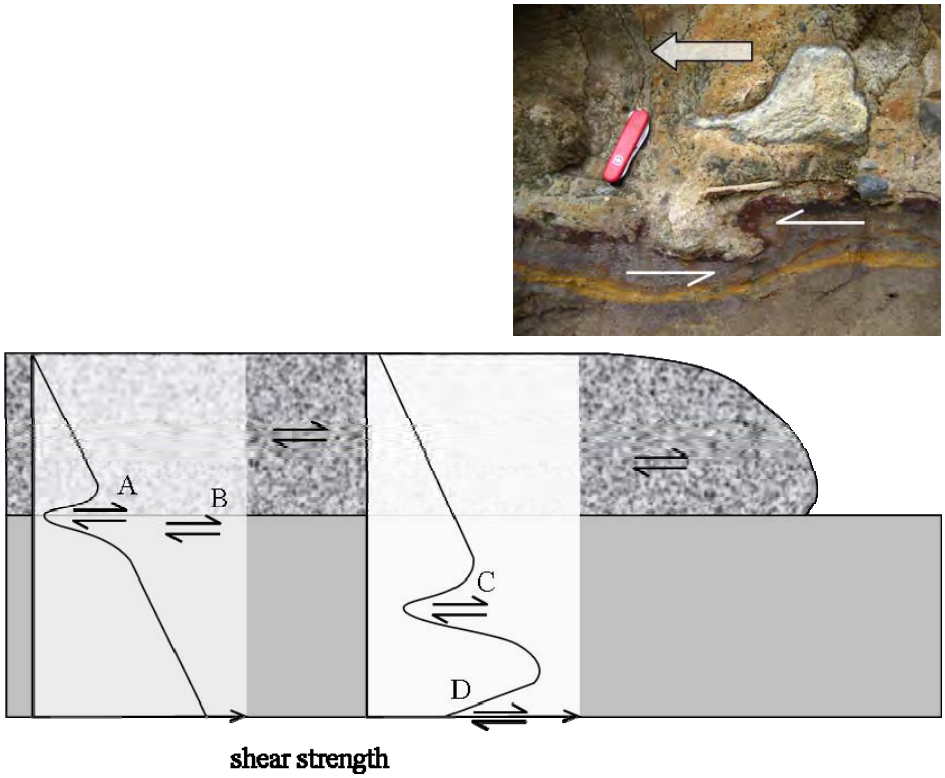

Figure 1.15: The sketch shows the potential locations of shear failure to occur. The shear strength increases with depth. Insert shows shear evidence at the base of the Maitahi debris avalanche, Taranaki volcano, New Zealand; discussed in section 4.7.).

The fact that shear features are preserved in the geologic record suggests a number of possibilities: (1) shearing only took place during the final stages of deposition and is hence a late-stage deceleration feature only, without feedback on avalanche mobility; (2) shearing occurred during full-velocity emplacement and features are preserved because: (2a) shear planes constantly arise and diminish, changing location from moment to moment, and/or (2b) incremental deposition prevents erosion of the features, and/or (2c) lack of spreading due to the lithostatic pressure of the overlying material and lateral confinement by e.g. valley walls (2c inspired by Pollet and Schneider, 2004).

Shear features form beneath rapidly moving rock and debris avalanche as well as slowly advancing glaciers (Piotrowski et al., 1997). However, in high-velocity pyroclastic flows no evidence of substrate shearing has been reported to my knowledge (erosion down to a resistant layer and substrate striation on the other hand are common beneath pyroclastic flow deposits; e.g. Sparks et al. (1997)). What role do emplacement velocity and avalanche material properties play in the production and

transmission of basal shear (from glacial to catastrophic speeds), and is there a threshold velocity above which shearing ceases or alternatively above which all available material is entrained through shear?

Artillery Peak Breccia Body II	lower 4 m, 60-80% matrix, streaked fabric
Artillery Peak Megabreccia	2.5 m thick, contorted to structureless substrate-derived matrix materials and rounded clasts + debris lobe material. Up to 30 cm intensely comminuted breccia fragments and rock flour over polished and grooved basal contact
Aso (VDAD)	coarse-depleted
Black Canyon Breccia	highly sheared, mixed zone: discontinuous, up to 3 m thick, silt- to gravel-sized material. Lowest 5-20 cm highly comminuted rock
Cantal (VDAD)	mixed facies w/ accidental clasts, great amount of fines; ~20 m thick unit, friction structures
Colima, Nevado de (VDAD)	more finely crushed than overlying strata
Cross Hill Breccia	medial: undulatory contact (up to few m relief), comminuted zone 5-10 cm thick (granodiorite). Distal: 75cm thick layer of comminuted
Dulung Bar-Darkot	thoroughly crushed carbonate from avalanche
El Capitan	proximal: 1.5 m structureless sandy conglomerate (rounded substrate clasts, angular avalanche debris). Distal: base highly undulatory w/ relief up to >10 m; 1-4 m mixed zone, containing proximally derived cobbles, clayey slip surfaces. Distal lobes: scoured, undulatory basal surface dipping towards lobe center
Gol-Ghone B	lower 10-15m, clastic dikes, stringers and folds of alluvium
Kokomeren	intensely comminuted alternating sandstone and granite; abrupt boundary to overlying granite 'layer'
Parinacota (VDAD)	Lauca basin sediments lacking primary sedimentary structures; cm-m
Popocatépetl (VDAD)	clay-rich, finegrained, sharp contact
Rogue Nublo (VDAD)	mixed, sheared and homogeneous facies, sharp contact
Shadow Valley	clastic dikes, soft-sed deformation, mixed zone
Socompa (VDAD)	fine-grained, powdery; shear zones and highly fractured area within ignimbrite
Waikaremoana (slide block)	sheared and broken rock, clay gouge w/ slickenside surface

Table 1.6: Selected basal facies descriptions. Deposits without annotation are rock avalanches, those followed by (VDAD) are volcanic debris avalanche deposits; the Waikaremoana slide block is included for comparison; references are listed in Appendix A.

The effects of shearing on the avalanche include: shear stress transfer into the substrate; shear rate in the avalanche is reduced; substrate thickening due to sheared material transported at the avalanche base; material entrainment and consequent change in volume, and a change in basal avalanche composition, grain size and frictional resistance.

At the Cantal volcanic debris avalanche in France, gouge zone material displays evidence of incredible mobility as it is found injected into the weathered granite basement below (Figure 1.16).

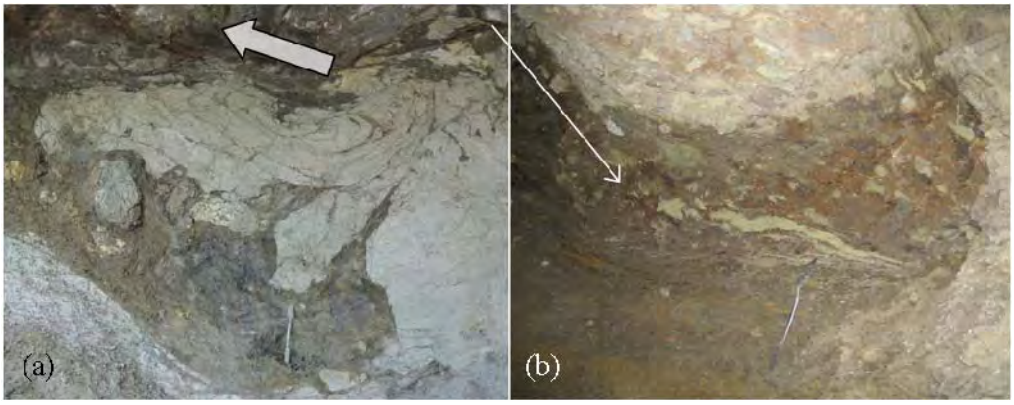

Figure 1.16: Gouge zone material mobility (a): the arrow points into the direction of avalanche travel and sits on the avalanche base as viewed in this cave. The dark material of the gouge zone is injected into the weathered granite substrate (white); 20-cm long tool on gouge zone injection for scale. Exposure of the avalanche base (b) with prominent shear features of gouge, avalanche material and granite.

Decapitated substrate boulders are interesting features at an avalanche base. One way to explain this is simple horizontal shear between the avalanche and the substrate at substrate depth x (the boulder location). Material above the boulder is incrementally or instantaneously incorporated into the avalanche. Substrate compression under the encroaching avalanche leads to the formation of grain-bridges within the substrate. One of the grains in compression (the decapitated boulder) fails, leading to failure of the entire bridge and hence the substrate package at this locality fails instantaneously. The failed substrate is incorporated into the avalanche and/or ploughed ahead, leaving the headless boulder as a marker of the substrate erosion surface.

This demonstrates that shearing beneath advancing avalanches is an effective erosion agent (e.g. Perrier volcanic debris avalanche deposit in France shown in Figure 1.17), as opposed to plucking individual clasts from the substrate similar to rivers extracting material from their beds. An insitu example of grain-bridge failure under an overburden load is preserved in, e.g. subglacial deposits presented by Piotrowski et al. (2004). Emplacement duration (time) and hence velocity therefore appears to be negligible in this process of grain bridge formation and failure (compare glacial to catastrophic avalanche event discussed).

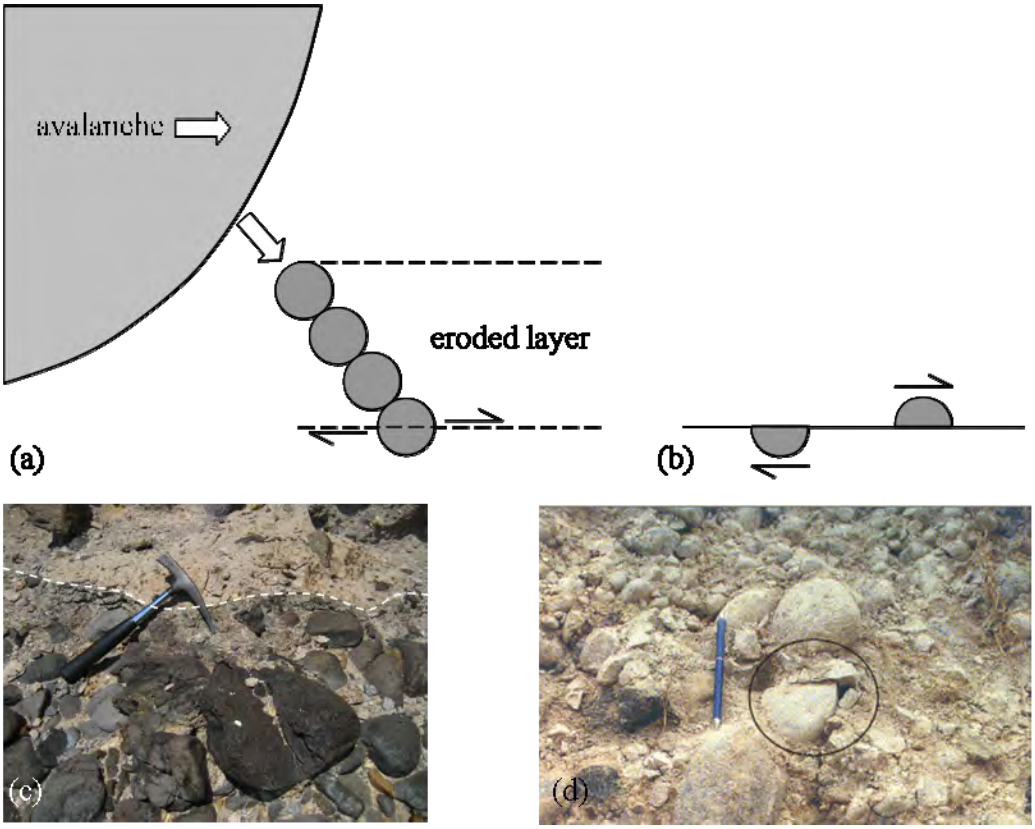

Figure 1.17: Sketch of stress transfer from the advancing avalanche front into the substrate material ahead: (a) grain bridges form in the substrate initially, but fail along a distinct shear zone (b), which is preserved at the deposit base; (c) decapitated and fragmented boulders beneath the Perrier volcanic debris avalanche/flow in France. Hammer for scale; dashed line marks VDAD – substrate contact; (d) cracked and displaced boulder in sediments in the Saadjärve drumlin field, Estonia (image from Piotrowski et al., 1997; w/o permission).

A rare case of basal shear is the preservation of melted material referred to as frictionite or pseudo-tachylite (e.g. Arequipa, material from substrate and landslide in pseudo-tachylyte, Legros et al., 2000; Langtang and the Koefels rock avalanches, Masch, 1985; Spray, 1995). The unusual case of melting at the base of an avalanche was interpreted by Legros et al. (2000) to mark "the transition from non-depositional to depositional environment". These features represent high frictional resistance at the base of the respective avalanches and highly localised heat generation (E-loss) of the moving debris. Furthermore, a thin melt layer at the base of a moving granular flow will impart viscous drag forces (particularly in high-silica materials) and will resist motion at the base of the granular mass.

1.4.9. Substrate failure at depth

Shear or substrate mobilization evidence can be disguised if a substrate package that exceeds outcrop scale has been mobilized beneath the avalanche. In this case, the avalanche-substrate contact appears undisturbed; whereas in fact the failure surface lies well below the avalanche base (e.g. Gol-Ghone B rock avalanche in Pakistan, which sheared substrate to 200 m below the basal avalanche contact; Hewitt 2006). This implies that shear stress transfer from the moving avalanche into the substrate can be effective over great depths and thick sedimentary sequences can become coupled with the moving avalanche (Figure 1.15).

1.4.10. Conditions of the substrate base and influence of substrate thickness

Pre-existing planes of weakness within the substrate (e.g. contact of different units) can influence the response of the substrate package. If, for example, an uppermost strong substrate layer sits atop weak deposits, failure of the substrate is likely to occur along the weak sedimentary contact plane or within the weak underlying sediments (depending on overlying substrate thickness and mechanical strength). On the other hand, a substrate of similar strength and thickness might resist deformation and erosion if its base is strong; examples follow.

1.4.11. Substrate base

In laboratory analogue experiments the presence of a weak substrate base (Figure 1.18a) led to failure and translation of the entire substrate sequence in avalanche motion direction, adding to the translating mass of the material in motion (avalanche plus substrate) while subtracting kinetic energy from the avalanche. In the case of a strong substrate base (Figure 1.18b), this resistance to motion was transferred upwards into the moving avalanche debris, impeding its motion. This resistance to motion not only affected the avalanche front, but was translated all the way to the avalanche tail, which lost mobility behind the slowing avalanche body. The deposit was hence thinner and longer in profile than in the weak substrate base example where the avalanche tail maintained relatively high mobility.

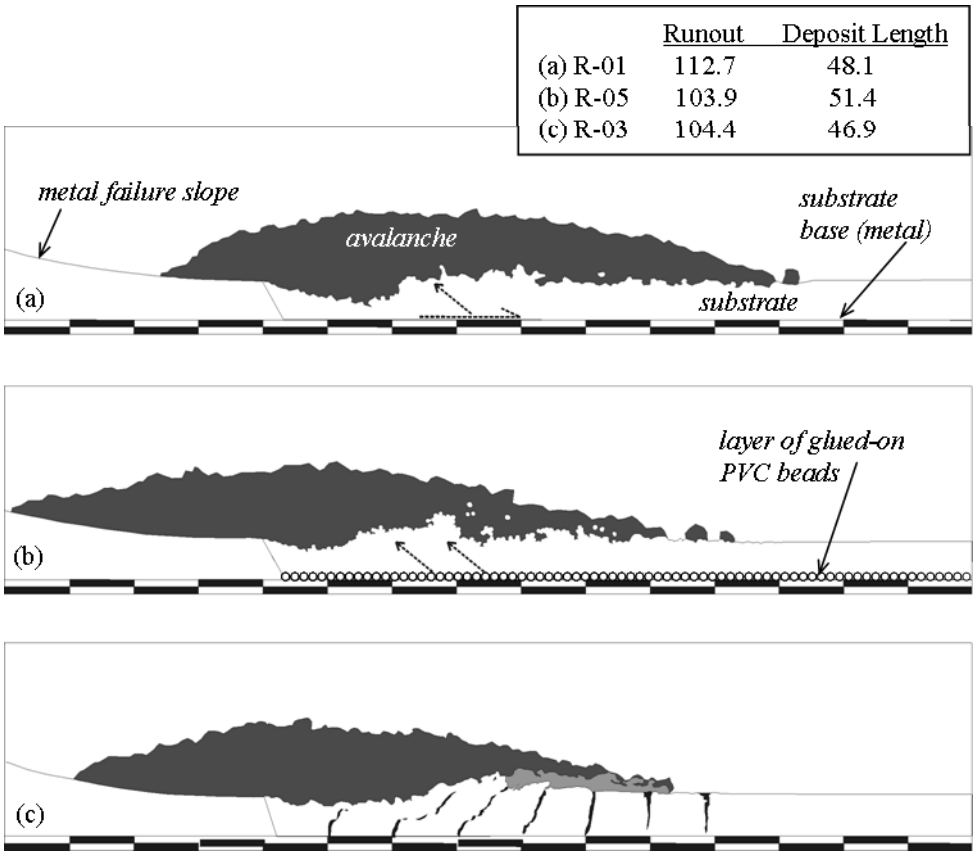

Figure 1.18: Laboratory analogue models of a granular avalanche emplaced over deformable and erodible substrates: (a) dry PVC beads with zero-friction (metal) subsurface; (b) dry PVC beads with resistant subsurface (layer of glued-on PVC beads); (c) dry wheat flour with zero-friction subsurface. Scale is in 5-cm increments.

Runout of the resistant base scenario (b) is shorter than (a), though the lack of sensible scaling calculations leaves this potential trend to be tested in further experiments. A case with deposit profile and avalanche behaviour intermediate between the two cases is emplacement over a stronger, i.e. more cohesive substrate material, in this case wheat flour (Figure 1.18c). Shear stresses imparted into the substrate by the moving avalanche were not translated all the way down to the substrate base (again metal in this experiment analogous to (a)). The uppermost substrate material was readily eroded by the avalanche and transported along its base and front (grey area in Figure 1.18c beneath the avalanche front consists of transported substrate material; its colour is the result of mixing between white and black (marker horizons) wheat flour). Substrate material at depth failed décollement-style and sequential shear planes are preserved in the record by the deformed marker horizons. Below the décollement, substrate material remained unaffected. Compression under avalanche loading most likely increased the internal resistance/strength of the flour and this resistance was

transmitted back into the avalanche, impeding its motion. Runout is comparable to the resistant substrate base case (b), but the avalanche tail retained more of its mobility and came to rest further down the slope than in (b).

1.4.12. Substrate thickness

The thickness of the erodible substrate layer impacts how the substrate base influences avalanche runout. This is a preliminary statement based on too few data points to justify the basis for a testable hypothesis. In laboratory analogue models (Chapter 5) where the substrate failed along a weak plane (metal), the substrate thickness played a minor role (slight reduction in runout at half the substrate thickness; compare R-01 to R-07 in Chapter 5). In the case of a resistant substrate base, the substrate thickness, or number of grains, has a greater effect in the experiment setup conditions in that the thinner substrate favours longer runout than the thicker substrate. Toniolo et al. (2004) related slurry thickness (h) to its yield thickness (h_y) for subaqueous events: $(\rho_s - \rho) \cdot g \cdot h_y \cdot \sin\alpha = \tau_y$, where ρ_s is density of the slurry deposit, ρ the density of the surrounding water, g the acceleration due to gravity, h_y the slurry deposit yield thickness, α the slope angle, and τ_y the slurry yield strength. When $h > h_y$, then remobilization is expected to occur down to a depth at which the yield strength it reached.

1.4.13. Injection features

Upward injection of substrate material into the avalanche body occurs on a range of scales from a few centimetres to many metres in width and length. Their scale, degree of preservation within the deposit and general make-up provides us with good evidence on their occurrence with respect to time in the avalanche emplacement history:

- during full avalanche motion,
- at the final stages of avalanche deceleration and deposition,
- or as a result of post emplacement loading.

In the first case, an opening of space within the granular avalanche network must form either by avalanche dilation or through the forceful injection of over-pressurized substrates. Extension of the avalanche during motion has been proposed as a

mechanism of hummock formation in a horst-and-graben style (e.g. Glicken et al., 1981). Another way to form some of these features during motion is basal shear and the interaction of individual avalanche clasts or units with the substrate. Failure of the uppermost substrate under shear can lead to small portions of it being pushed ahead and sheared into the avalanche base, then transferred higher into the avalanche body where it will exploit contacts between different avalanche units or, if avalanche motion prolongs for some time after entrainment, become incorporated in the form of rip-up clasts, or crushed into the avalanche matrix. In Figure 1.19a, these scenarios are sketched based on field and laboratory experimental evidence. Opening of fractures as the moving avalanche body extends provides space for the loaded substrate material to intrude into, while shearing within the avalanche body destroys the features (Figure 1.19b). Shearing of substrate material into the avalanche body as depicted in (c) will have to occur shortly before cessation of motion for the features to be preserved in the final deposit (field observations show that these injections are often still in association with the substrates they are derived from, and their dislocation and hence disassociation from their origin has to my knowledge not been reported; those cases are rip-up clasts or mixed), or while basal avalanche parts deposited incrementally. Injections are typically bent in the flow direction indicating avalanche travel direction as well as preserving evidence of differential motion at least during the depositional stages of emplacement. However, laboratory tests have also shown that injection features can be bent against the flow direction where individual avalanche clasts (or units) buried themselves into the substrate, so their use as kinetic indicators requires care. Such observations have also been made by Friedmann (1997) at numerous avalanche deposits in the Shadow Valley Basin, US-California. Furthermore, post-emplacement injection of material can produce very similar features as for examples observed in sedimentary deposits under static loading (e.g. Figure 1.19d; Hurst et al., 2003).

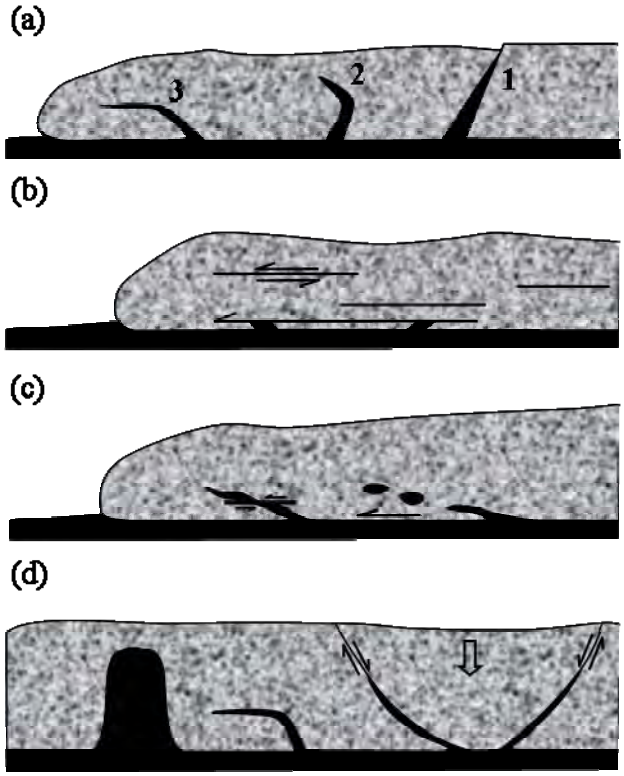

Figure 1.19: (a) injection time sequence from (1) formation of opening in the spreading avalanche and subsequent folding (2) and shearing (3) in avalanche motion direction. (b) differential shear within the avalanche causes injection features to be partially destroyed and the substrate material is mixed into the avalanche matrix. (c) shear at the avalanche base causes material to be entrained into the avalanche as injection features or 'stringers' which may become dissasociated and form trails of clasts in the avalanche; (d) post-emplacement loading features from left to right: vertical injection, injection exploiting zones of weakness, such as shear zones, within the avalanche body, and loading-induced fault generation (after Hurst et al., 2003).

1.4.14. Surface roughness of inerodible runout path conditions in the laboratory

At the laboratory-scale the conditions at the base of a granular flow greatly affect its overall behaviour. Emplacement of an avalanche composed of angular coal clasts over a metal runout surface resulted in a sliding motion of an elsewise interlocked clast network; i.e. the clasts moved together as one relatively coherent body with little grain interactions (i.e. no collisions, rotation, differential movement). Introducing a rough, inerodible surface (glued-on PVC beads, 1 by 3 mm) caused intense grain agitation (termed granular temperature; e.g. Iverson, 1997) and the flow in motion dilated to ~ 325 % (cross-sectional flow thickness) compared to the flow/slide over metal. Grains at the flow base interlocked with the rough runout surface and caused collisions and rotations between overriding clasts. Runout was shortened by 7 % relative to emplacement over metal. A layer of glued-on sand in the runout path also introduced grain agitation, albeit to a lesser extent, and runout was only 2 % shorter

than the metal runout case. Note, however, that these experiments are qualitative, designed to illustrate avalanche-substrate interaction processes, and the total runout values are to be considered with caution.

1.4.15. Undisturbed substrates

Undisrupted substrates beneath avalanche deposits are without doubt the most enigmatic features, yet it is not very common to find entirely unaffected sediments beneath rock and debris avalanches. Where they are described, they present locally restricted phenomena in an event which has eroded and/or deformed underlying material elsewhere along its path. Beneath the Blackhawk rock avalanche in California (USA) sandstone has locally been left undisturbed, whereas erosion, disaggregation, transport, bulldozing and shearing of the same has taken place elsewhere along the avalanche path (Johnson 1978). In the medial reaches of the Cantal debris avalanche in France, conglomerates and sandstones are found intact, whereas sediments, crystalline basement, wood fragments and volcaniclastics were entrained elsewhere (Schneider and Fischer 1998) and weathered granite was subject to deformation and mingling with basal gouge zone material (this study). The El Capitan rock avalanche in Arizona (USA) left proximal conglomerates intact, but comminuted substrates are found in the basal mixed zone and playa lake sediments are highly folded, contorted, detached and imbricated to 5 m depth (Yarnold and Lombard, 1989). At Parinacota volcano, Chile, welded Tertiary ignimbrites escaped unscathed in the distal debris avalanche reaches while elsewhere Lauca basin sediments (fine-grained lacustrine silts, silty to sandy fluvial or deltaic sediments and sandy conglomerates) were mixed into the deposit or entrained as clasts, and underwent folding, boudinage, faulting and thrust faulting in the distal and central parts (Francis and Wells, 1988; Clavero et al., 2002).

In essence, all avalanches interact with their runout path material to some degree, because the occurrence of undisrupted sedimentary material beneath large avalanche deposits is only a localized phenomenon in otherwise erosive and interactive avalanche events. The localized lack of interaction with the substrate is most likely a combination of dynamic changes in avalanche emplacement and the inhomogeneous substrate conditions. Piotrowski et al. (2004) invoked the analogy of sub-glacial sediments consisting of a mosaic of stable and unstable spots, which also applies to

rock and debris avalanche runout paths. Localized 'protection' of the substrates by, e.g. large boulders, tree roots or topographic changes may also play a role. Furthermore, some substrate interactions are not immediately apparent as the failure depth can exceed outcrop scales, in which cases the substrate is strongly coupled with the avalanche in that it has become its basal unit (e.g. Socompa, van Wyk de Vries et al. (2001); Gol-Ghone B, Hewitt (2006)).

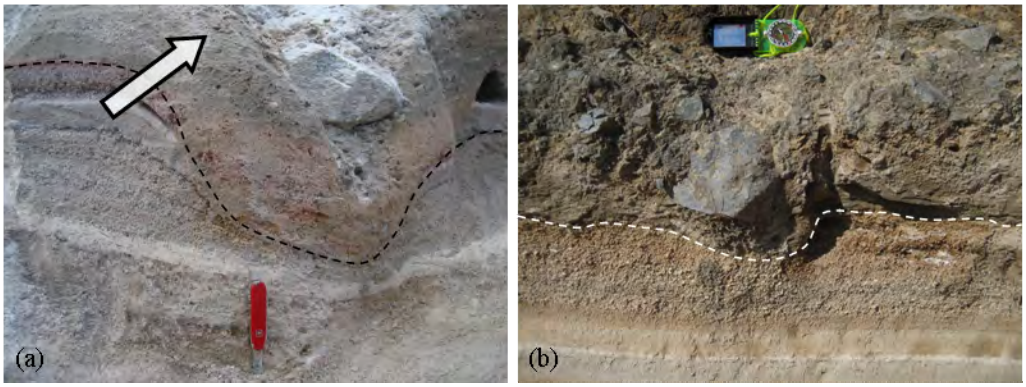

Figure 1.20: (a) Photos of the basal block-and-ash flow section at Tarawera volcano, New Zealand (arrow indicates flow direction; knife for scale). (b) Larger clast at the basal "Las Fuentes" volcanic debris avalanche in Central Mexico (travel direction is unknown in this unmapped deposit; compass for scale). Dashed lines mark the basal contacts.

The basal avalanche composition will also determine the degree of substrate disruption. For example, Shea et al. (2008) postulated that the lubricating basal layers of the Las Isletas and El Crater debris avalanches of Mombacho volcano (Nicaragua) prevented incorporation of significant amounts of substrate. This basal layer is supposed to have prevented the blocky fraction of the avalanche from eroding material. Belousova and Belousov (2008) proposed that a layer of fine-grained, comminuted avalanche "dust" laid down ahead of the coarse avalanche front and body can act as a protective "carpet" with which the coarser avalanche material interacts instead of with the underlying substrate. Beneath the Las Fuentes volcanic debris avalanche in Central México higher substrate disturbance is noted where a larger avalanche boulder impacted the substrate in comparison to interactions beneath finer-grained portions of the deposit (Figure 1.20b, unmapped deposit; observation made by S. Salinas and myself).

At the block-and-ash flow deposit of Tarawera volcano, New Zealand (Figure 1.20a), delicate substrate was preserved beneath the fine-grained portions of the flow, whereas significant disturbance was observed where a larger clast had penetrated through the fine layer and into the substrate below. In this last case, high emplacement velocity might be one of the reasons for the apparent lack of substrate interactions. Likewise, snow-pack in the cirque basin impacted by the Zymoetz River rock avalanche was left in place, albeit with surface striations, where the approximately 34 ms^{-1}, still accelerating debris skirted over it in the outer cirque, whereas erosion of the same snow-cover took place in the main avalanche travel path within the cirque (Boultbee et al., 2006). The potential dependence of basal avalanche grain sizes and its erosive potential is sketch in Figure 1.21:

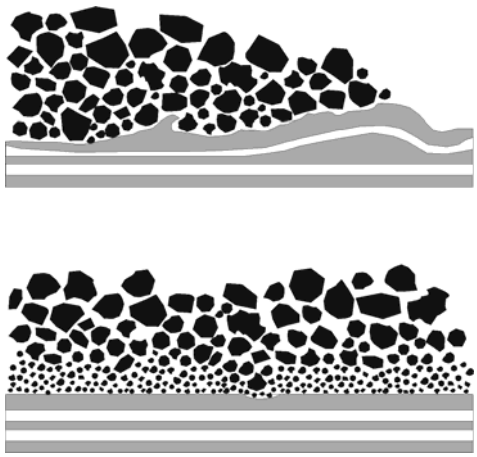

Figure 1.21: Relationship between basal grain-size and avalanche erosion potential.

In some situations of apparently unscathed substrates these simply represent the erosion terminus, an example of which is the distal part of the Maitahi debris avalanche/debris flow of Taranaki volcano, New Zealand (deposit previously mapped and described by Alloway et al., 2005; Stewart et al., 2006).

The Maitahi (Figure 1.22) avalanche incorporated sandy peat, trees and rounded river/beach clasts during its emplacement. The majority of entrained material is concentrated within the lowermost 1-3 m of the deposit, whereas smaller (mm-to-cm-sized) peat (containing pumiceous layers or lenses) and soil fragments are found in the matrix facies, and larger mudstone clasts from the more proximal runout path are incorporated higher in the avalanche. Beneath the ~10 m thick distal section, a 2-3 cm thin layer of locally apparently undisrupted peat is preserved; underlain by dune

sands. In the context of several hundred metres available outcrops (the majority perpendicular to avalanche motion direction) it is evident that this thin layer represents the erosion surface. There exist remnants of shearing at the avalanche substrate interface, flame injections, rip-up clasts, comminuted substrate material mixed into the avalanche matrix, localized absence of the peaty layer (but with discolorations in the remaining sand as observed in sections below the peat layer), and substrate disruptions in the form of small folds (Figure 1.23). One might speculate how such a thin layer of peat could remain beneath a large, erosive avalanche: Bird (2000) observed that "on the west coast of Britain salt marshes are generally firmer than those on the east coast because of the higher proportion of sand in the muddy sediment". Higher sand contents at the interface to the dune sands might also have provided more rapid drainage, providing the sediment with a higher internal angle of friction and hence stability. Where the peat layer is eroded completely, the remaining sediment is overlain by coarser avalanche material than in the portions where peat forms the erosion terminus.

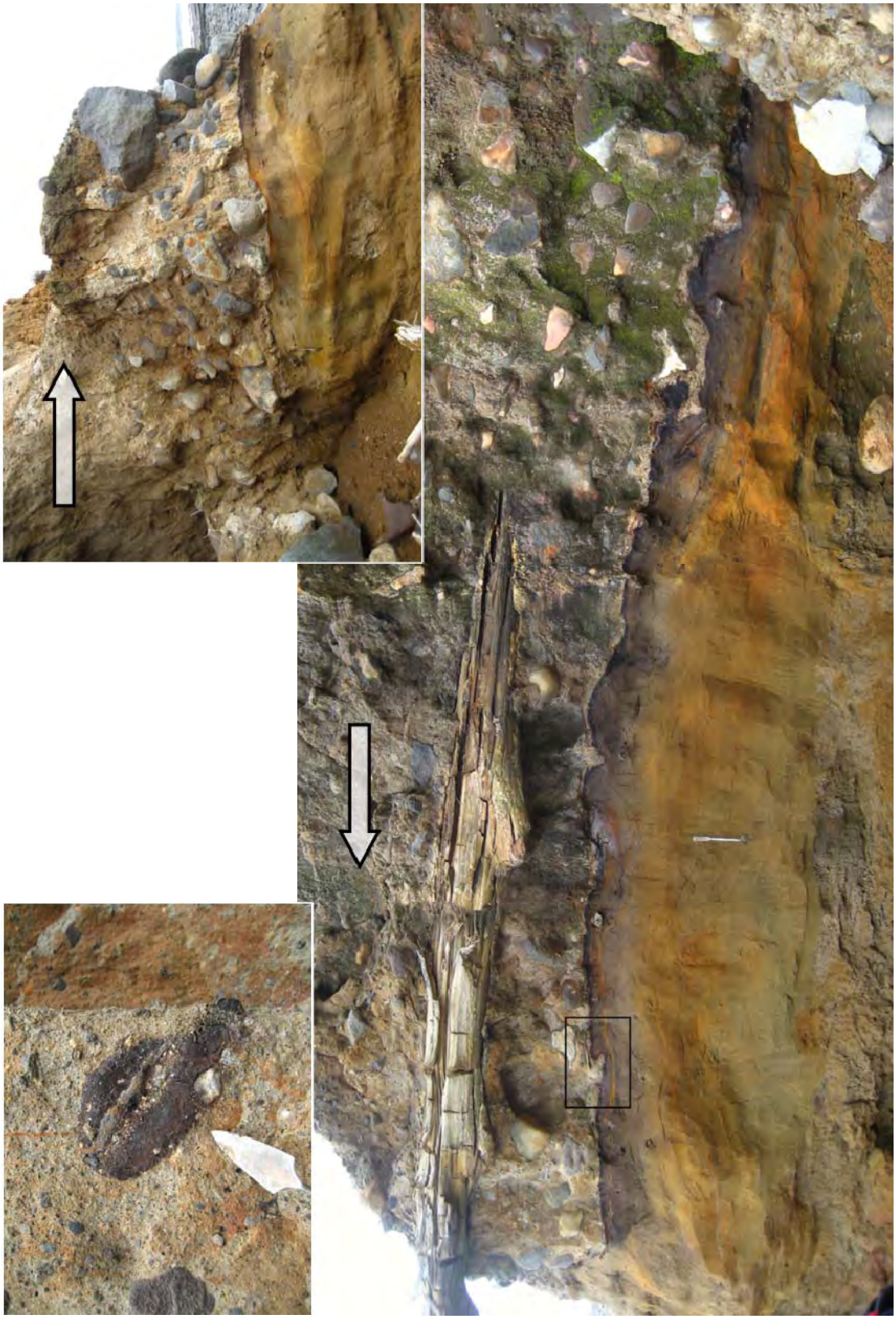

Figure 1.22: Motion-parallel section of the distal (~35 km from source) Maitahi deposit of Taranaki volcano, New Zealand. Tool is 20 cm for scale; small box shows location of image in Figure 1.16; arrows point in avalanche motion direction.

Figure 1.23: (a) motion parallel section showing basal mixed zone and underlying, deformed sands; (b) thin peaty layer underlain by sands, large tree aligned motion-parallel visible in upper right-hand corner of the image; (c) disrupted underlying sands, small erosion channel where larger boulders are concentrated at the avalanche base; section is perpendicular to motion; (d) close-up of avalanche-substrate contact just below the Swiss knife, and small peaty clast entrained in the basal facies just above the knife.

1.4.16. Equifinality, or the elephant in the room

Sediment deformation features associated with avalanche emplacement are not unique to these settings. Other environments yield identical features and range from events of glacial to catastrophic speed, and with scales from microscopic to tectonic. With this fact as no surprise, how can we interpret the formation processes if their environments are so different? This is the underlying question/assumption for interpreting laboratory replications of natural events in which there will always be some factors that are not reproducible, yet in their simplicity, the laboratory models often succeed in imitating real-life complex events, which implies the existence of underlying, simple laws or constraints governing apparently complex field situations. The non-uniqueness of, for example, folds and faults to any specific (geological or laboratory)

setting demonstrates the universality of processes acting in these environments, and that scale effects, overall, are not dominant. In other words, there are limited options for any material to behave in response to stresses, and in essence means that a feature cannot be successfully interpreted without the context it was found in. That said, a set of conjugate faults is always an indication of compressional stresses acting on the material and gives the directions of the stresses it underwent. Therefore, the conjugate fault sets' universality is information about stress directions, regardless of deformation speed or scale of the structures (the latter, of course, scaling with the associated event). Having stated the obvious, for the field of avalanche research this simply underlines the need to discern precisely which features have been caused by the avalanche itself and which must be attributed to other geological or anthropological factors (see study of the Jocotitlán volcanic debris avalanche in México, Chapter 4).

Chapter 2:

Longitudinal Ridges in Mass Movement Deposits

In the spirit of:

"How a system behaves depends on why you are looking at it."

Timothy R. Davies

Longitudinal Ridges in Mass Movement Deposits

A. Dufresne and T.R. Davies

Geomorphology (2008) 105: 171-181

Department of Geological Sciences, Canterbury University, Christchurch, New Zealand

ABSTRACT

Prominent longitudinal features are often reported on the surfaces of mass movement deposits. However, the genesis and implications of these have not hitherto been considered, and herein we present preliminary observations of their occurrence both in the field and in the laboratory. Elongated ridges are often oriented (sub-) parallel to the flow direction and aligned radially from the source due to debris spreading. They are particularly prominent in large ($> 10^6$ m^3) rock avalanches emplaced onto deformable substrates and are also found in the proximal reaches of volcanic debris avalanches. Flowbands, which are longer and thinner expressions of longitudinal ridges, are continuous along the entire flow length and are observed in rock avalanches emplaced onto glaciers, in snow and some ice avalanches, in pyroclastic flows and some block-and-ash flows, in ejecta sheets, in extraterrestrial landslides, and in some volcanic debris avalanches. Other volcanic debris avalanches and the distal areas of rock avalanches often display hummocks that are aligned radially from the source; we propose that these aligned hummocks are remnants of longitudinal ridges. The formation of elongate ridges (and their expressions as flowbands, aligned hummocks, or distal lobes and digits) in qualitatively-similar fashion in both laboratory and field environments suggests they represent an intrinsic tendency of granular flows in a wide range of situations.

2.1. INTRODUCTION

Mass movements occur in a variety of geological materials (rocks, sediments, snow, ice), on different scales (large, > 10^6 m^3, rock and debris avalanches, smaller snow avalanches, sand on dunes, etc), and are found in almost any environment where slopes are present. They can also be produced in the laboratory where the small-scale flows mimic features and behaviours of their field-scale counterparts, providing conceptual models of feature formation and the opportunity to observe flow dynamics up close; however, careful attention to scaling is required.

A lively and continuing discussion in the literature on emplacement mechanisms and dynamics of rock and debris avalanches, pyroclastic and block-and-ash flows, and snow avalanches offers a wide range of models to explain runout, modes of emplacement and deposit characteristics of mass movements. Clearly the basic mechanism of mass movements is that of granular flow, even where large intact blocks (e.g. toreva blocks) are involved.

Herein we focus attention on one prominent and consistent morphological characteristic of the different types of mass movements and granular flows: that of more or less prominent ridging in the flow-parallel direction ("longitudinal ridging") observed on the surfaces of many avalanche deposits (see case studies below). We believe that this reflects processes active during the flow, as well as at the moment the flow comes to rest, and that it may therefore be used to infer aspects of flow dynamics. We offer suggestions on the formation of longitudinal ridges with respect to material properties, emplacement dynamics, and environmental factors such as topography and substrates. While we focus particularly on the occurrence and origin of longitudinal ridges, we also relate them to the occurrence of transverse ridges and hummocks. We begin with a definition of the features observed in the field, and with a brief summary of granular flows and the basic processes of longitudinal ridging.

2.2. LONGITUDINAL RIDGES AND FLOWBANDS: DEFINITIONS

Following the way the terms are generally used in the geological literature (for examples see list of references in Table 2.1) we offer the following general definitions.

Deposit	Hummock	Ridge	Flowband	L [m]	W [m]	H [m]	L/W	L/H	H/W	Comments
Jocotitlan	x			405	330	95	1.2	4.3	0.29	data from topographic map (acrview) using closed contours as base of hummock
	x			443	347	105	1.3	4.2	0.30	
	x			215	180	45	1.2	4.8	0.25	
	x			455	328	115	1.4	4.0	0.35	
Round Top	x	x		100	95	17	1.1	5.9	0.18	height data estimated from field photos . L and W from morphological map.
		x		200	95	17	2.1	11.8	0.18	
		x		380	120	12	3.2	31.7	0.10	
		x		350	110		3.2			
		x		190	80		2.4			
Parinacota	x							4 to 20		from Clavero et al. (2002); L is the average hummock diameter
Altenau		x		377	100		3.8			data extracted from geological map in von Poschinger (1994)
		x		267	100		2.7			
		x		233	78		3.0			
Lastarria			x	2850	145	10	19.7	285.0	0.07	H here is the average deposit thickness estimated; L is estimated from photo in Naranjo & Francis (1987)
Shasta	x			800	630	146	1.3	5.5	0.23	data extracted from topographic map in Crandell et al. (1984)
	x			567	400	73	1.4	7.8	0.18	
		x		2467	800	146	3.1	16.9	0.18	
	x	x		1160	800	146	1.5	7.9	0.18	
	x			600	500	73	1.2	8.2	0.15	
		x		1930	330	85	5.8	22.7	0.26	
Mombacho	x			90	48	9	1.9	10.0	0.19	using averaged graph equations and highest occurrence hummock L from Shea et al. (2008)
Sherman Glacier			x	260	12	3	21.7	86.7		L and W estimated from high-resolution aerial photographs; H here is the average deposit thickness (McSaveney, 1978)
			x	382	16	3	23.9	127.3		
			x	165	6	3	27.5	5.0		
			x	412	24	3	17.2	137.3		

Table 2.1: Data for hummock, ridge and flowband dimensions.

Ridges stand prominently above the rest of the deposit by up to tens of metres and are usually found within the proximal to medial reaches of rock and debris avalanches. Smaller ridges are sometimes found at the distal margins where they grade into frontal lobes. Ridge lengths are typically on the order of hundreds of metres. The terms “ridge” and “elongate ridge” are often used interchangeably. However, the latter is preferentially applied as an emphasis when ridges are especially long, appearing stretched or extended (though no onsistent threshold can yet be determined to

precisely mark the difference) and/or when such long ridges are aligned parallel to the spreading direction.

Flowbands (Figure 2.6A) on the other hand do not stand out high above the rest of the deposit, are usually separated from adjacent parallel bands by narrow "furrows", and generally extend along almost the entire flow length and hence can reach some kilometres in length. Flowbands can split into multiple bands, and in distal reaches they often form digits that sometimes curve in their paths and override other digits obliquely. Flowbands are also sometimes referred to as "striations" because deposits with narrow flowbands often look striated on aerial photographs (e.g. Shiveluch, Belousov et al. 1999; Figure 2.5B). Another variety is a "herringbone" structure on individual flowbands. In this case, the flowbands exhibit V-shaped ridges pointing uphill as described by Naranjo and Francis (1987). These authors used the term "herringbone" to describe the features of the Lastarria debris avalanche deposit (see below and Figure 2.5C) in accordance to its resemblance of structures observed in ejecta sheets found around impact craters, where the term was apparently coined.

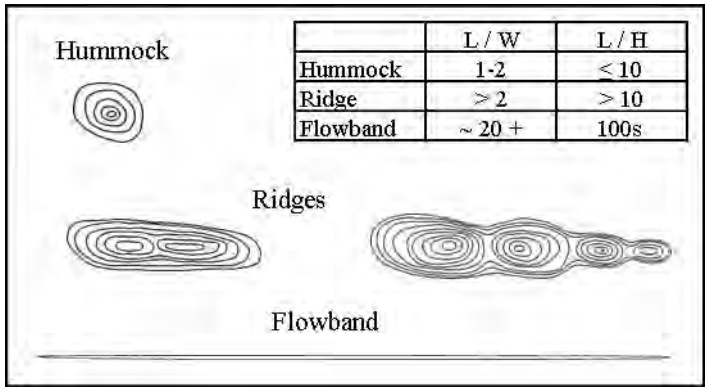

	L / W	L / H
Hummock	1-2	≤ 10
Ridge	> 2	> 10
Flowband	~ 20 +	100s

Figure 2.1: Map-view of hummock, ridge and flowband geometries. Table insert shows the range of values of geometric relationships distilled from descriptions, maps and data presented in the literature.

A continuum of morphologies is apparent from hummocks, through ridges to flowbands. Hummocks have length-to-height (*L/H*) ratios generally less than ~ 10 (Figure 2.1; some field examples are listed in Table 2.1) and length-to-width (*L/W*) ratios of ~ 1-2. These ratios increase to the 100s (*L/H*) and over ~ 20 (*L/W*) for flowbands. Values for ridges lie between the two. These rough definitions are based on available data from the literature and on our own field observations.

2.3. GRANULAR FLOWS – BASICS AND MODELS

Herein we briefly summarise current knowledge of granular flow processes, and outline some published experimental results that suggest that longitudinal striations result from the physics of granular flow, rather than from large-scale environmental peculiarities of debris avalanches alone.

Granular flow is the gravity-driven motion of assemblages of individual solid grains during which the grains interact with each other and with the flow boundaries. Dry granular flow of noncomminuting, noncohesive grains over a rigid base is affected by only two external forces: gravity acting on each grain and friction from the base acting on the basal grains. The intergranular forces are complex; in general they can be anisotropic and heterogeneous. In particular, relative grain motion can be concentrated in narrow layers called “shear bands” (Francois et al., 2002); and shear forces are transmitted across shear bands by quasilinear assemblages of grains in compression, which are called “grain bridges” or “force chains” (Anthony and Marone, 2005); Figure 2.2.

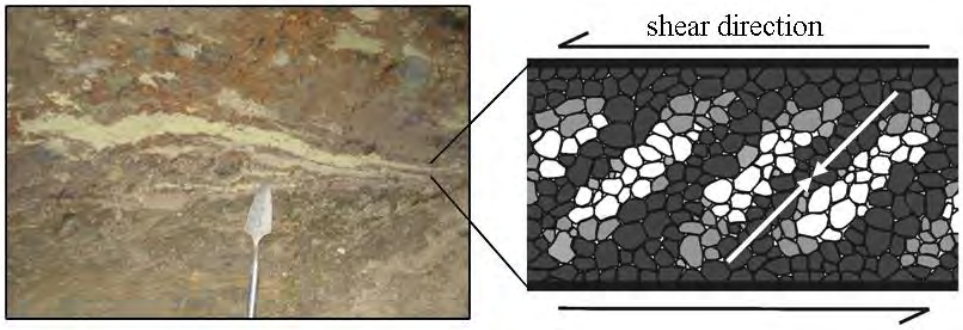

Figure 2.2: Field example of shear bands preserved at the base of the Cantal rock avalanche deposit, France (20 cm long tool for scale). The sketch to the right illustrates the force distribution along grain bridges (arrows) in a granular mass experiencing shear: dark grains within the grain bridges are under higher stresses than the lither coloured ones.

When a grain mass is saturated by water, additional forces arise from pore water pressure distribution and water motion; and the situation becomes still more complex – additionally so if part of the grain mass is unsaturated. Further complications arise when the grains themselves are of a range of sizes and shapes. At present, predicting the three-dimensional flow behaviour of variably sized, shaped, and saturated grain

flows is not possible without substantial empirical input. Hence, although simple in concept, real-life grain flows are complicated in practice. In this context, the appearance of large-scale flow structures (such as ridges in a grain flow) is not a surprise, any more than the appearance of meanders in a river flow is a surprise; neither is predictable from the detail of the preceding steady uniform flow, but both emerge from the smaller-scale dynamics of the "simple" flow of water or grains.

The fact that longitudinal ridging has been reported in very simple and well-constrained laboratory situations (Pouliquen et al., 1997) indicates that this process is a very fundamental phenomenon of granular flow, and is therefore to be expected in more complex grain flows such as field-scale mass movements. In particular, Pouliquen et al. (1997) concluded that the initial instability is related to lateral segregation of grains of different sizes at the front of the flow, because with uniformly sized spherical glass beads they observed no ridging. They introduced larger grains in the form of crushed fruit stones or coarse, irregular beads to generate ridging, which suggests that grain shape and/or density may also have played a role. In a later experiment, Pouliquen and Vallance (1999) found no ridging-type instability in dry flows with mixtures of coarse and fine glass spheres, or in any saturated flows; this suggests that the coarse grains must be angular and that the flow must be less than fully saturated to cause prominent ridging.

All the above experiments took place on rough rigid beds. By contrast, Aranson et al. (2006) studied the theoretical stability of granular avalanches on an erodible bed, using a continuum approach with no grain size specified. They found that lateral instability, which further develops into ridging as a causative factor in the ridging process, occurred if the static and dynamic friction coefficients differed, which is the case for all granular flows, but particularly so for a mixture of small spherical and large angular grains. They also found that ridging would occur under water, with saturated flows. Mallogi et al. (2008) confirmed these results experimentally; in particular, they found that transverse instability occurred whenever the angle of inclination of the substrate was greater than some critical value, and ridging developed as a result of coarsening, although their granular material was narrowly graded. The existence of a threshold angle for transverse instability may suggest that relatively high velocity flows are more liable to ridging.

In our own experiments a small volume (200 ml) of sand was dropped through a 100-cm-long tube onto a metal runout surface, 30 cm wide, just above the slope

transition from 60º to 0º inclination (Figure 2.3A). The sand avalanche developed flow-front irregularities in the form of small undulations (Figure 2.3B), which, however, were short-lived and did not find expression in the final deposit. In a second experiment, a 3-cm-thick layer of flour was introduced into the horizontal runout path. Digitate development of the flow front was more pronounced in this run, which we attribute to enhanced flow perturbation as the sand encountered deformable and erodible substrate conditions (Figure 2.3C). Lobes wider than the original flow front irregularities were preserved in the deposit as a consequence of more material overriding already stationary sand and flow front spray developing. Runout was shorter than in the metal surface case; and substrate erosion, entrainment, and bulldozing were observed. In this qualitative experiment, which simply served to demonstrate the universality of longitudinal flow feature development, no attempt was made to relate the experimental scale to that of field phenomena.

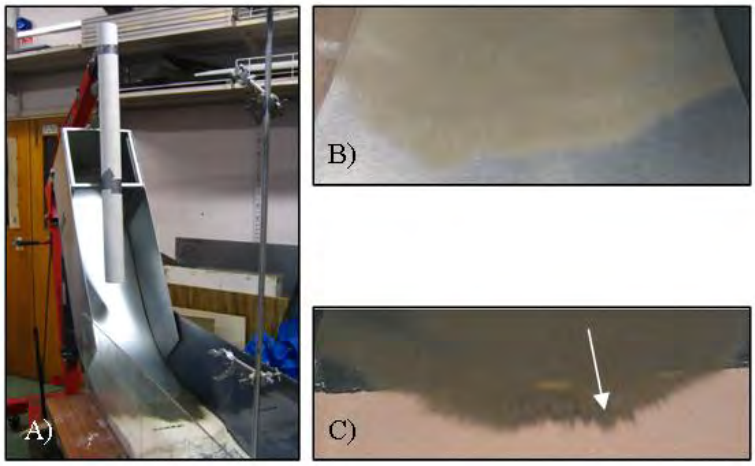

Figure 2.3: (A) experimental setup used in the small scale sand avalanche experiments. The white tube is 1 m long through which the sand was fed unto the metal slope (angle of 60°). This slope gradually decreases in steepness into the horizontal runout plane. In (B) this plane consisted of metal and minute longitudinal features were observed at the avalanche front during flow. In the setup shown in (C) a layer of flour was introduced, simulating rough erodible substrate conditions. These caused enhance flow front perturbations and lead to more pronounced ridging in the flow, which found expression in digitate flow fronts. Flume width is 30 cm.

In summary, all free-surface granular flows apparently have the potential for large-scale longitudinal flow structures that correspond in relative scale and location with ridges. The conditions under which granular flows can be expected to develop prominent longitudinal ridges appear to include:

(i) presence of angular grains and a nonuniform grain size distribution;
(ii) dry or saturated flows;
(iii) rigid or erodible substrate;
(iv) high-velocity flows.

These include all the mass movement situations in which longitudinal ridging has been reported in the field and in the laboratory.

2.4. DATA COLLECTION

During the course of an ongoing investigation of rock and debris avalanche dynamics, a database currently containing close to 400 volcanic and non-volcanic avalanche deposits world-wide is being prepared. Deposit descriptions and statistics are distilled from the literature, such as deposit volume, area, runout, drop height, thickness, etc. Included are the deposit's morphology and texture, data on its source area, pre-avalanche topography, substrate involvement and type of deformation, and many other descriptive features. Within this data array we noticed the repeated mentioning of longitudinal morphological features and we selected the best described deposits with the most complete dataset for hummock, ridge and flowband dimensions for discussion in the next section of this paper. Our research was further extended to snow and ice avalanches, and pyroclastic and block-and-ash flows published in the literature.

2.5. CASE STUDIES

In Table 2.2, a number of well described rock and debris avalanche deposits that feature longitudinal ridges, flowbands, radially aligned hummocks and digitate flow fronts are listed with their respective authors and dates of publication for reference. In the following we briefly describe a select group of these deposits to illustrate their features and give an overview of their general deposit characteristics.

Deposit Name & Location	Deposit Type	Longitudinal Ridges	Flowbands	Aligned Hummocks	Lobate/Digitate Front	Reference
Acheron, New Zealand	RA	x				Smith et al. (2006)
Adair Park Breccia, US-Arizona	RA	x				Yarnold and Lombard (1989)
Altenau, Germany*	RA	x			x	von Poschinger (1994)
Black Rapids Glacier, US-Alaska*	RA		x			Jibson et al. (2006)
Blackhawk, US-California	RA	x		x		Johnson (1978)
Carlson, US-Idaho	RA	x				Shaller (1991)
Dulung Bar-Darkot, Pakistan	RA	x			x	Hewitt (2006)
Fernpass	RA	x				Abele (1964)
Flims, Switzerland	RA	x			x	von Poschinger et al. (2006)
Ganges Chasma, Mars	RA		x			Lucchitta (1978)
Ghoro Choh I, Pakistan*	RA	x			x	Hewitt (2006)
Ghol-Ghone B, Pakistan	RA	x			x	Hewitt (2006)
Marquartstein, Germany	RA	x			x	von Poschinger (1994)
Mink Creek, Canada	RA	x			x	Geertsema et al. (2006)
Mt Munday, Canada	RA		x	x	x	Evans and Clague (1998)
Pink Mountain, Canada	RA	x		x		Geertsema et al. (2006)
Round Top, New Zealand*	RA	x		x	x	Wright (1998); this study
Sherman Glacier, US-Alaska*	RA		x	x	x	McSaveney (1978)
Unnamed Gobi Desert, Mongolia	RA	x				this study
Val Pola, Italy	RA	x	x			Crosta et al. (2004)
Aucancilcha, Chile	VDA	x		x	x	Francis and Wells (1988)
Augustine (Burr Pt), US-Alaska*	VDA			x	x	Siebert et al. (1995)
Chimborazo, Ecuador	VDA	x			x	Siebert (1984); Bernard et al. (2008)
Dikii Greben, Kamchatka	VDA	x				Ponomareva et al. (2006)
El Estribo, Mexico	VDA	x				Capra et al. (2002)
Harimkotan	VDA		x			Belousov et al. (1999)
Jocotitlan, Mexico*	VDA	x		x		Siebe et al. (1992); this study
Lastarria, Chile*	VDA		x	x	x	Naranjo and Francis (1987)
Llullaillaco, Argentina*	VDA	x	x	x	x	Richards and Villeneuve (2001)
MSH, US-Washington*	VDA	x		x		Glicken (1986)
Ollague, Chile/Bolivia	VDA	x				Clavero et al. (2004)
Parinacota, Chile	VDA	x			x	Clavero et al. (2002)
Popcatepetl, Mexico	VDA	x			x	Robin and Boudal (1987)
Shiveluch (1964), Kamchatka	VDA		x			Belousov et al. (1999)
Socompa, Chile	VDA	x				van Wyk de Vries et al. (2001)
Taunshit, Kamchatka	VDA		x			Belousov et al. (1999)
Unzen (1792), Japan	VDA	x		x		Siebert (2002)

Table 2.2: List of subaerial rock and debris avalanche deposit features. Deposits with '*' are discussed in section 2.5 of the text. RA = rock avalanche, VDA = volcanic debris avalanche.

2.5.1. Radially-aligned hummocks in volcanic debris avalanches

Sector collapse of Jocotitlán volcano, México, resulted in the emplacement of a clast-supported debris avalanche with large conical hummocks in the proximal reaches and smaller clusters of hummocks in the distal reaches of the western depositional area (Siebe et al., 1992). These hummocks are all aligned radially with respect to the source (Figure 2.4). The eastern depositional area is block-slide controlled and exhibits a different and partially buried topography. Clast sizes everywhere range

from a few centimetres to several tens of meters in diameter. The deposit lacks fine, weak pyroclastic and hydrothermally altered materials, and was emplaced onto (most likely saturated) lacustrine and volcaniclastic sediments.

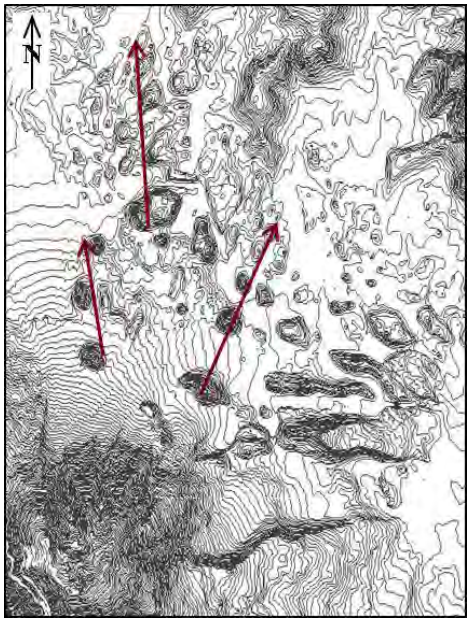

Figure 2.4: Example of hummock alignment in volcanic debris avalanches, Jocotitlán, Mexico. Distance horizontally across image is ~ 9 km.

Hummocks in the 1980 Mount St Helens, Washington, debris avalanche deposit are elongated and oriented dominantly parallel to flow direction (Glicken, 1986). Siebert et al., (1995) observed that at the Burr Point debris avalanche of Augustine volcano, Alaska, proximal hummocks are aligned radial to source, whereas distal hummocks show a transverse orientation where the avalanche has entered the sea. These authors further state that debris avalanches at other volcanoes also display a predominance of radially aligned hummocks.

2.5.2. Prominent elongate ridges in rock avalanches

The Round Top (New Zealand) rock avalanche (Wright, 1998; this study) was sourced in mylonitic schist of the Alpine Fault area. It is mainly clast-supported in the proximal reaches with blocks up to 2-3 m long axis and grades into finer material in the distal reaches with remnant source stratigraphy preserved in the deposit fabric. Large (several hundred metres long and 10-30 m high) elongate ridges are found in the proximal-medial area (Figure 2.5A), whereas smaller hummocks (aligned with

ridge long axes) and digitate emplacement characterise the distal reaches. The avalanche was emplaced onto saturated floodplain gravels, and bulldozed substrata are found at ridge toes.

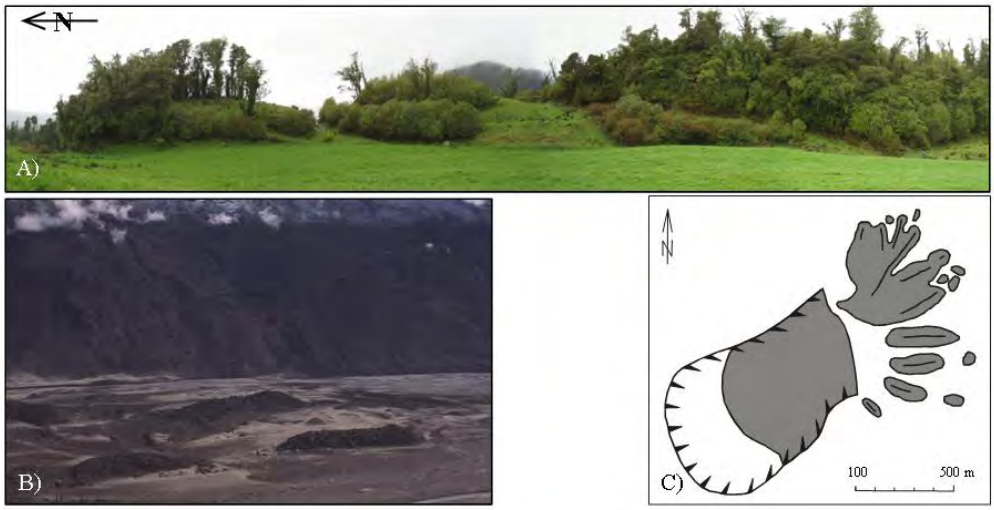

Figure 2.5: (A) One of several elongate ridges aligned radial to source in the Round Top rock avalanche deposit, West Coast, New Zealand (ridge segment shown is ~ 350 m long). (B) Longitudinal ridges (on the order of 35 m in height) in the Ghoro Choh I rock avalanche deposit, Karakoram Himalayas, Pakistan (image courtesy of Ken Hewitt). (C) Simplified mophological map of the Altenau rock avalanche, Germany (modified from von Poschinger 1994) showing ridge elongation and flow direction.

Very similar observations of radial elongate ridge orientation and associated substrate bulldozing at ridge termini have been reported from numerous rock avalanches in the Karakoram Himalaya (Hewitt, 2006; Figure 2.5B), and the Altenau (von Poschinger, 1994; Figure 2.5C) rock avalanches in Germany.

2.5.3. Flowbands in rock avalanches emplaced onto glaciers

The Sherman Glacier rock avalanche, Alaska, has long flowbands and digitate flow fronts (Figure 2.6A, data from McSaveney, 1978 and Nicoletti and Sorriso-Valvo, 1991). It was sourced in sand- and siltstones and entrained snow, ice, soil, and till. Tracing the furrows between the ridges back toward source shows that many contain a large boulder at their "beginning point" (M.J.McSaveney, GNS Science, NZ, personal communications, 2007). Some ridges of rock avalanches emplaced onto glaciers also have large clasts at their distal ends (Evans and Clague, 1998).

A moment magnitude 7.9 earthquake on the Denali Fault, Alaska, in 2002 triggered thousands of small and large landslides (Jibson et al., 2006). The most

spectacular avalanches were emplaced onto the Black Rapids Glacier. They are unusually thin (3 m) for their volume (37 x 10^6 m^3), overtopped a 50-m-high moraine at velocities of over 130 km/h, travelled long distances on a slope of 1-2º, and show sharp margins and long flow-parallel furrows and ridges (flowbands).

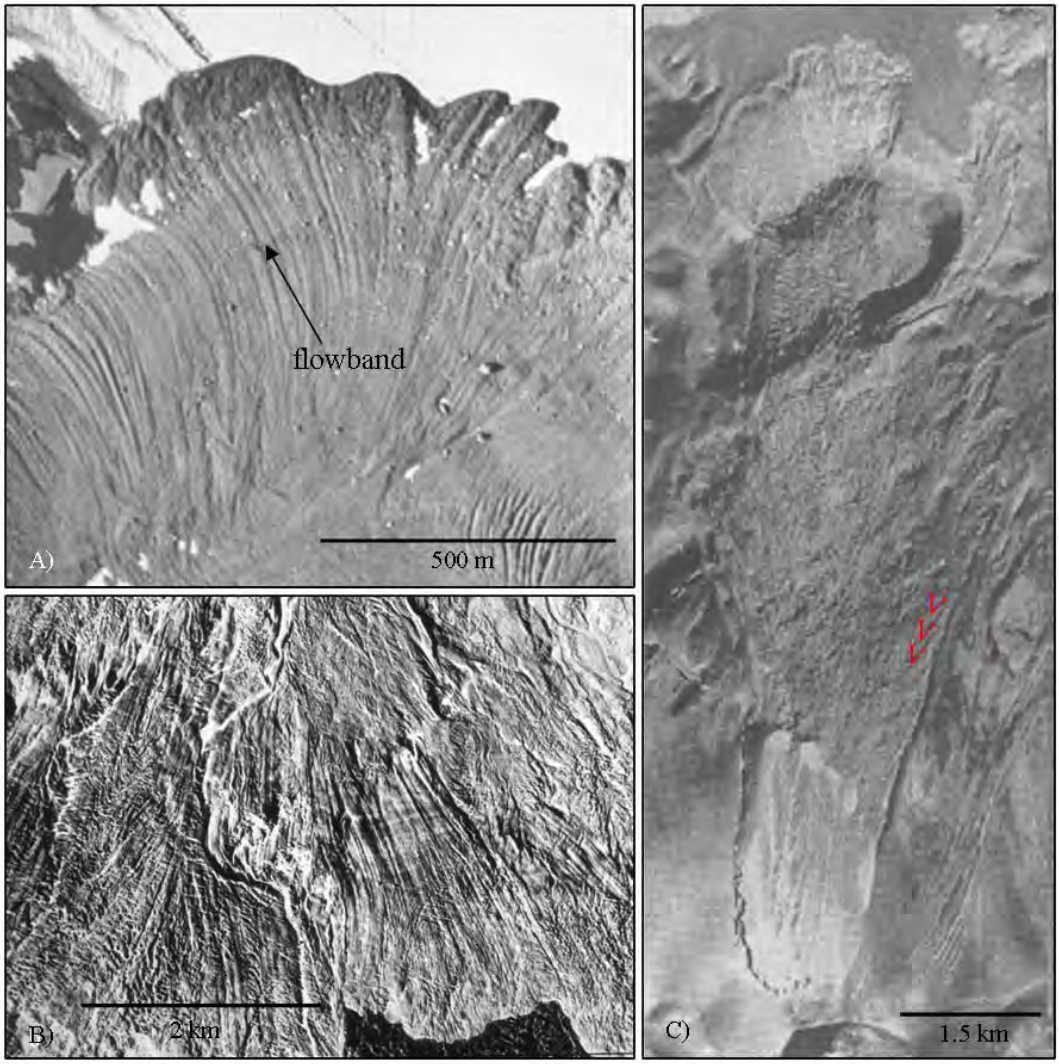

Figure 2.6: Flowbands in rock and debris avalanche deposits. (A) Part of the Sherman Glacier rock avalanche, Alaska (image courtesy of Mauri McSaveney) showing typical flowbands. (B) Striated surface of the 1964 Shiveluch debris avalanche (image courtesy of Alexander Belousov and Marina Belousova). (C) The high-velocity Lastarria volcanic debris avalanche (Naranjo & Francis 1987; image reproduced with permission from publisher) features so-called "herringbone" flowbands.

2.5.4. Flowbands and striations in volcanic debris avalanches

The Lullaillaco volcanic debris avalanche in Argentina (Richards and Villeneuve, 2001) has two major lobes where the flow divided around a cone and travelled down two parallel valleys. It generally lacks larger boulders and was most likely emplaced

hot. The northern lobe is striated and sunk into the distal salt flats. The southern lobe has prominent longitudinal ridges and a distal raised toe where it encountered but did not sink into the salt flats. Striations like the ones on Lullaillaco's northern lobe are also the characteristic feature of the 1964 Shiveluch debris avalanche (Belousov et al., 1999; Figure 2.6B). They extend along the entire flow length and are deformed or disintegrated into a hummocky surface where motion was impeded.

At Lastarria volcano, Chile, the debris avalanche initiated along bedding planes of weak pyroclastic material and created a lobate to digitate deposit that spread only 38º laterally (Naranjo and Francis, 1987). It displays longitudinal ridges with "herringbone" structures similar to those found in ejecta sheets and is entirely composed of mechanically weak pyroclastic material (Figure 2.6C). Its estimated emplacement velocity was 180-300 km/h.

2.5.5. Longitudinal features in submarine debris avalanches

Surface morphologies of submarine debris avalanches are often complicated by secondary turbidites and flow channels in the margin runoff zone, leaving their interpretation for longitudinal features ambiguous. Nevertheless, examples of linear flow structures, elongate blocks aligned parallel to flow direction, and aligned hummocks include, for example, the debris avalanches from Dominica Island, Lesser Antilles Arc (Deplus et al., 2001), offshore Angola (Gee et al., 2006), the Alika 2 off Hawai'i (Moore and Chadwick, 1995), and the La Orotava DA off Tenerife (Huerlimann and Ledesma, 2003).

2.5.6. Flowbands and digitate emplacement of pyroclastic flows and block-and-ash flows

The 1993 eruption of Lascar volcano, Chile, produced a series of pyroclastic flow deposits (e.g., Sparks et al., 1997; Figure 2.7A) with typical finer grained basal layers and coarse clast concentration towards the top and margins. They contain both pumice-rich and lithic-rich facies. The lithic-rich facies is mainly confined to deposit interiors, and lithic-rich deposits were observed on slopes of 6-14º. Pumice-rich facies, on the other hand, typically occur at the margins and distal parts of the pyroclastic flow fans, and pumice-rich deposits were observed only on slopes of < 4º. Curving digitate emplacement is prominent in the flow fans.

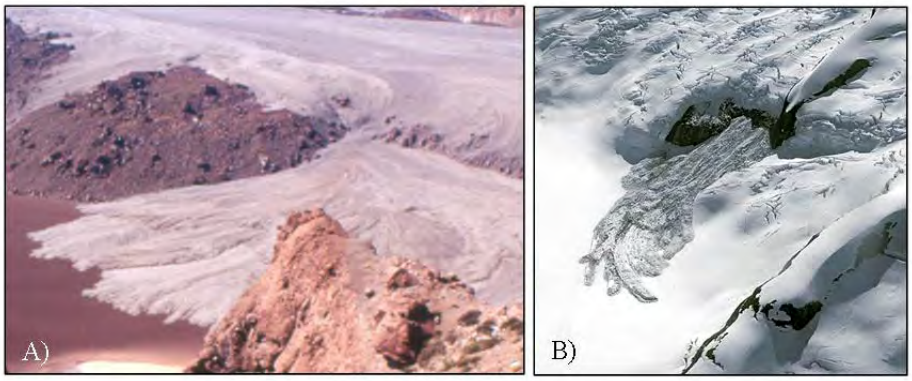

Figure 2.7: Flowbands and digitate deposit shapes in (A) the Lascar pyroclastic flow, Chile (flow fan is approximately 200 m across; image courtesy of Karim Kelfoun) and (B) the Juneau Icefield, Canada (avalanche is about 500 m long; image courtesy of Scott McGee).

Block-and-ash flows from the 1990 to 1995 Unzen (Japan) eruption (Miyabuchi, 1999) exhibit lobate/digitate flow fronts and lateral levees in valley paths. The deposits have unconsolidated ash matrices and blocks up to 10 m in diameter. They were emplaced hot, contain gas escape pipes, and have fine-grained basal and coarse depleted marginal flow units. The estimated total volume (dry rock equivalent) of the block-and-ash flow and talus apron is 1.2×10^8 m^3.

2.5.7. Flowbands and digitate features in snow and ice avalanches

Morphological studies of snow and ice avalanches are far and few between, but several images from the literature and the web show longitudinal ridging and digitate shapes (Figure 2.7B) of many snow and ice avalanche deposits (e.g., Jomelli and Bertran, 2001; McClung and Schaerer, 2006; Pralong and Funk, 2006).

Data collected from dry and damp snow avalanches in the Wasatch Mountains of Utah and from the Chugach Mountains of south-central Alaska during the winters of 1975 through 1979 revealed longitudinal shear planes as the most striking features of many deposits (Mears, 1980). Transverse shear planes were observed in the decelerating parts of the flows. Shear planes in snow avalanches find expression in surficial ridges or, were exposed, as steeply dipping planes like those of faults; they are thought to result from differential motion of the snow pack, and occur in both confined and unconfined runout zones (Mears, 1980).

2.5.8. Ejecta sheets and planetary landslide deposits

Ejecta sheets are often found surrounding Martian and Lunar impact craters. Some are striated, others look more fluid-like with radial digits that seem to have raised toes (e.g., Lunae Planum, Mars; Barnouin-Jha et al., 2005).

Landslides on the extraterrestrial planets resemble their terrestrial counterparts and are sometimes compared to the Sherman Glacier rock avalanche (e.g., Ganges Chasma and Coprates Chasma on Mars; Lucchitta, 1979; Quantin et al., 2004) attesting to their commonly striated/ridged morphology. A particularly interesting feature of a number of Martian deposits is the fact that the divergence angle of the striations increases with distance from source, perhaps indicating a constant divergence velocity as longitudinal velocity decreases. This is also apparent in the pattern of the Sherman Glacier deposit (Figure 2.6A).

2.6. OTHER SURFACE MORPHOLOGIES

Other morphological features of granular flow deposits include transverse ridges and lateral levees (Figure 2.8A, B). These features differ fundamentally from longitudinal ridges, which are extensional, flow-parallel phenomena. Transverse ridges, on the other hand, are usually compressional and are mainly associated with flow deceleration where a change in surrounding or underlying medium increases frictional resistance or absorbs flow momentum, and they appear predominantly in the distal deposit reaches where they also find expression as raised distal margins (Figure 2.8C). Examples include flow into a body of water (e.g., the Unzen 1972 volcanic debris avalanche deposit, with a change from subaerial elongate ridges to submarine transverse ridges; Siebert, 2002); encounters with soft, deformable substrates (e.g., Mombacho (Shea et al., 2008) and Ollagüe (Clavero et al., 2004) volcanic debris avalanche deposits), or decrease in topographic gradient (e.g., Blackhawk rock avalanche; Johnson, 1978). Lateral levees are common features of avalanches emplaced into narrow valleys and result from flow interaction with the dry, sloping valley walls [e.g., the Acheron rock avalanche (Smith et al., 2006) has lateral levees along the valley path but these disappear where the lateral confinement ends]. They occur in snow avalanches because of lateral interaction with stationary snow cover,

and in some flows result from the preferential accumulation of coarse, higher-friction debris at the free surface (Johnson, 1978), which is also common in debris flows.

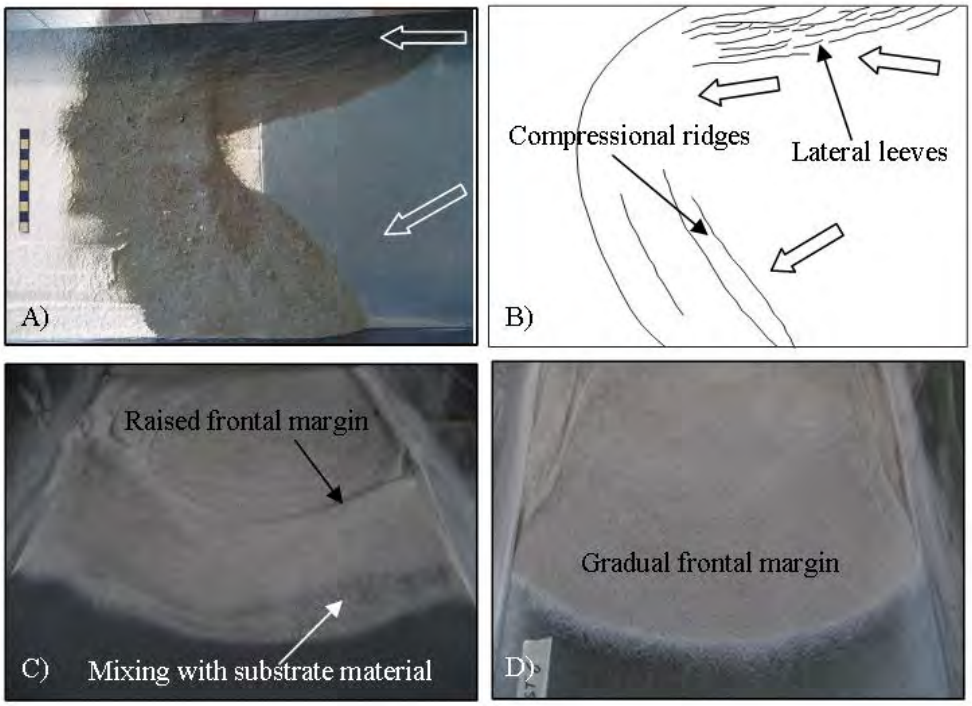

Figure 2.8: (A) Lateral levees developed in a small sand avalanche experiment where flow was parallel to the confining walls (in top part of image), whereas compressional ridges formed in response to deceleration in the lower depositional area. The sand was released down a metal chute and ran out over a 3 cm thick layer of dry flour. (B) Conceptual sketch showing the main flow directions (arrows) and features. (C) Raised flow front of sand avalanche encountering a thin layer of erodible substrate (black sand). (D) Sand avalanche emplaced onto zero friction, undeformable substrate (smooth metal) exhibits gradual flow front thickness decrease. Flume width is 30 cm.

2.7. DISCUSSION

From the preceding presentation of longitudinal morphological features on the surfaces of naturally occurring mass movement deposits, and their small-scale laboratory counterparts, we learned that they can form in a variety of materials, at a range of emplacement velocities and on different scales. The following is a summary relating the observed deposit features with the properties of the materials involved:

(i) High elongate ridges develop in strong, competent, high-friction material, sometimes with a mechanically weak base, i.e., significant substrate involvement such as loose saturated material (rock avalanches on valley fill etc. some volcanic debris avalanches).

(ii) Aligned hummocks in the distal reaches of avalanche deposits appear to develop as a consequence of extensional ridge breakup, when the frontal parts of the ridges have greater velocity/momentum than the rear, which starts depositing earlier or is halted by locally bulldozed substrates.

(iii) Aligned hummocks throughout volcanic debris avalanches form if the source material is strong and competent (i.e. lacks weak pyroclastic or hydrothermally altered material) and the deposit is relatively thick with respect to the width of their basal shear layer (see below).

(iv) Flowbands develop in weak (low density, loose, small clast sizes, highly brittle) source material (snow avalanches, loose volcanic debris avalanches made up of, e.g., pumice or hydrothermally altered fine material, pyroclastic flows) or in fragmented material on a fluidised substrate (rock avalanches on glaciers where basal friction is low), leading to an increase in velocity accompanied by rapid deposit thinning.

(v) In other cases, flowbands are the result of high-velocity emplacement of materials with relatively small clast sizes (some volcanic debris avalanches, pyroclastic flows, ejecta sheets).

Apparently, a relationship involving emplacement velocity, bulk/material density, and frictional behaviour (clast angularity) controls the degree to which prominent longitudinal features form in granular flows from the universal tendency to longitudinal ridging present in all grain flows. Interaction of the mass movement with its substrate furthermore influences avalanche behaviour and ridge/flowband development and preservation.

2.7.1. Emplacement velocity

Flowbands are most prominent in the high-velocity emplacement of, e.g., ejecta sheets (or the unusual Lastarria debris avalanche), in rock avalanches emplaced onto glaciers (e.g. Sherman Glacier, Black Rapids Glacier), and in snow and ice avalanches

(e.g. Juneau Icefield). Where avalanche material moved fastest in the longitudinal flow direction, with material moving much more slowly laterally, ridge and flowband formation is favoured (Figure 2.9A). An example is the Lastarria volcanic debris avalanche with its very directed emplacement (narrow spreading angle of 38°), high emplacement velocity and prominent flowbands in the final deposit. Hungr and Evans (2004) have shown statistically that rock avalanches emplaced onto glaciers travel further distances than those on other materials. These avalanches have the ability to override substantial topographic obstacles at high velocities (e.g. Black Rapids Glacier), are unusually thin and have flowbands as their characteristic surface feature. With more rapid sideways motion (lateral velocity approaches longitudinal velocity), hummocks and ridges tend to break up into clusters (Figure 2.9B). This is the case in the decelerating, spreading distal parts of many rock and debris avalanches. As the lateral velocity increases further with respect to longitudinal velocity, hummocks will become more scattered (Figure 2.9C).

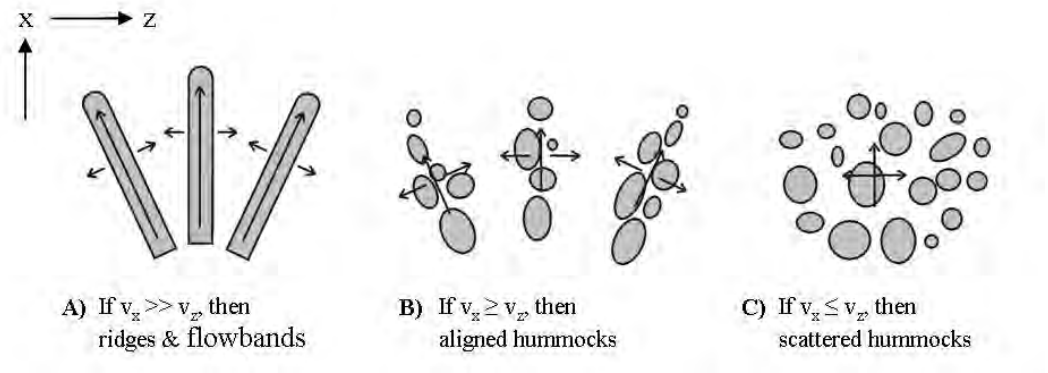

Figure 2.9: Influence of velocity distribution and direction on the formation of elongate ridges versus aligned or scattered hummocks. vx = velocity in flow direction, vz = velocity perpendicular to flow direction. This can apply to the deposit as a whole or to individual areas alone (e.g. lobes, distal versus proximal).

Sudden deceleration (e.g., from an encounter with deformable substrates) will lead to the formation of compressional ridges or raised flow fronts (e.g. Mombacho, Ollagüe). Where flow takes place relative to stationary lateral material, the high-velocity gradient will slow the avalanche material at the sides and lead to the formation of lateral levees (e.g. Acheron).

Small, low-velocity avalanches show compression-dominated surface features. In these cases, avalanche runout distance complies with simple frictional behaviour,

similarly to small sand avalanches emplaced onto rough, unerodible surfaces (e.g., Davies and McSaveney, 1999). In these latter cases, the *tendency* for longitudinal feature formation can be observed on very small scales, but their development is impeded. This means that minute longitudinal features are visible in these simple granular flows in the form of undulating surfaces or irregular frontal margins; but no immediately obvious flowbands, ridges, or digits/lobes have developed in the deposit.

2.7.2. Material properties

The maximum steepness of a static granular pile is controlled by the material's angle of internal friction; this is higher for angular grains than for rounded ones. The ability of a pile to retain steepness while being transported as part of a mass movement depends also on the extent to which flow-induced vibrations affect it. The same applies to the cross-sectional steepness of a ridge or hummock. During runout, therefore, two opposing tendencies are present; the intrinsic tendency of a granular flow to form ridges or hummocks and the tendency of flow motion to flatten them. On this basis we would expect ridges to be relatively less steep-sided in shallower flows because the vibrations from substrate interaction would be greater; this would also be the case in more distal regions. Apparently, mechanically strong, competent, high friction material also should favour the formation of longitudinal ridges and aligned hummocks of substantial sizes (in rock and volcanic debris avalanches 10-100s m height, e.g. Jocotitlán). By contrast, deposits comprising mechanically weak, loose, low-density, lower friction material and smaller clast sizes tend to have long, thin flowbands (e.g. Llullaillaco, Lastarria, Lascar), which, by observation, are less steep than the ridges formed in strong, high friction materials.

Detailed investigation of several hundred hummocks of the 1980 Mount St. Helens debris avalanche showed that block facies hummocks with no matrix facies (type 'A' hummocks) are generally much larger and steeper than those that are made up entirely of matrix facies (type "B"); Glicken, 1986. Furthermore, unusually steep conical hummocks of the proximal Jocotitlán DA lack fine material and consist entirely of large, angular dacite blocks.

2.7.3. The influence of basal geometry on hummock/ridge size

We identify two distinct types of shear in debris avalanches:

(i) Where the shear is concentrated at the base of the avalanche, because of weak substrate or saturated basal material, we call *basally weak*. This appears to be the case in many volcanic debris avalanches and, in general, where the avalanche is wide relative to its depth. In basally weak situations, shear is concentrated in the basal region of the mass movement. If the overlying material is weakly cohesive, as in volcanic debris avalanches, the tendency for the shearing layer to spread longitudinally and laterally will cause the overlying material to fail passively in extension. This will give rise to block-like failures in the extending material, causing ridges and/or hummocks.

(ii) Where the shearing is distributed more or less uniformly through the flow depth, apart from a thin (~ 10 m) carapace of coarse blocky material, we call *basally strong*. This occurs in many dry rock avalanches where the flow is relatively deep and applies to the nonfragmenting carapace (Dunning, 2004) of a basally strong rock avalanche; this is an ~ 10-m-deep layer in which stresses are insufficient to prevent grain bridges from failing by buckling, so little fragmentation occurs and apparent friction is normal. This layer will again fail passively in extension as the fragmenting substrate spreads, giving rise to hummocks or ridges (Davies and McSaveney, 2008).

In both cases, the size of the hummocks or ridges is expected to scale with the depth of the passive layer. Hence, we expect the hummocks on a basally weak avalanche to be relatively larger than those on basally strong avalanches because the depth of the passive layer in the latter is shallower than in the former (Figure 2.10). Field data (e.g., Glicken, 1986; Evans et al., 1994) show that this is indeed the case. Evidence is also available that the size of hummocks decreases with distance from the avalanche source (LeCorvec, 2005), which is to be expected as the depth of the upper nonshearing layer decreases with increased area because of spreading.

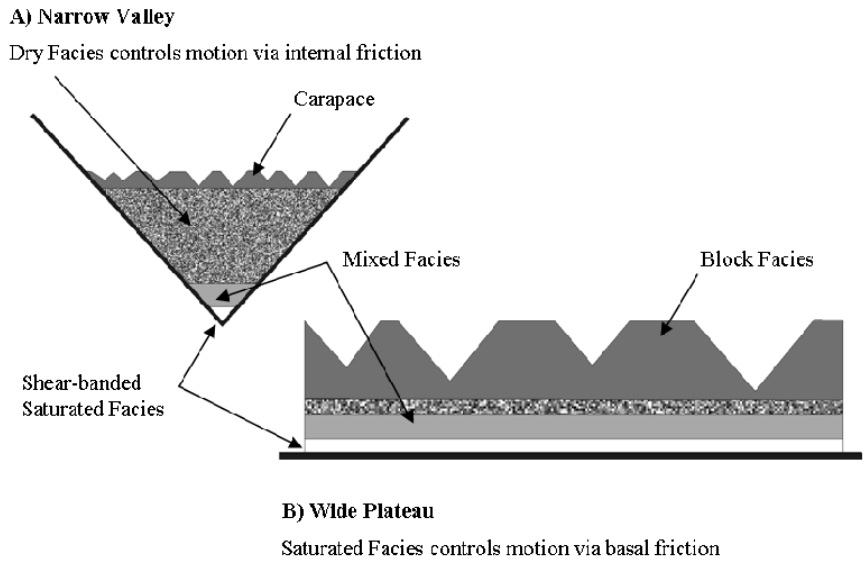

Figure 2.10: Flow cross-sections illustrating hummock size dependence on basal shear zone width. (A) Emplacement into narrow valley in which case the internal avalanche friction has more influence on avalanche motion and morphology development than the relatively narrow basal shear zone (e.g. typical rock avalanche environment). (B) Case of open runout onto wide plains in which case larger hummocks can form in response to the greater influence of the basal shear in controlling avalanche motion.

2.7.4. Substrate influence

When large amounts of saturated substrate material are entrained into a rock/debris avalanche, transformation into more mobile debris flows can occur leaving characteristically thinner and flatter-topped deposits. Smaller amounts of entrainment on the other hand can alter basal compositions and mechanical behaviour, thus influencing overall avalanche emplacement processes. For example, rock avalanches emplaced onto glaciers sometimes appear to be emplaced at high velocity. Snow, ice, and water are mixed into the basal rock avalanche material, fluidizing it and thus reducing its frictional resistance to flow. This could lead to ridges "stretching" into flowbands as there are no obstacles to halt their motion nor are the flows thick enough to generate hummocks.

Flow-front perturbations in any granular flow through an encounter with or entrainment of larger obstacles, overriding of a rough surface, or local deposition of larger avalanche boulders can intensify ridge/lobe/digit development (e.g., Sherman Glacier, Figure 2.6A), or laboratory analogue models (e.g Pouliquen and Vallance, 1999; this study).

An encounter with deformable substrates can locally create hindrances, inhibiting avalanche motion. For example, local bulldozing of substrates beneath an advancing avalanche ridge can impede its advance, leading to compressional features within the ridge and prevention of ridge breakup into hummocks, thus preserving the feature in the deposit (e.g. Round Top, Ghoro Choh I, Altenau). In other cases, the deformable substrate (and also motion into water; e.g. Unzen) can drastically slow the avalanche front leading to the formation of flow-transverse compressional ridges (e.g. Mombacho, Ollagüe).

2.7.5. Feature formation differences in the laboratory and in nature

In the laboratory, ridges and lobes form because of grain size segregation and flow-front perturbations. This leads to accumulation of larger grains in the longitudinal section, while the finer material continues to move downslope; i.e., this segregation of larger clasts at the flow front causes local flow-front perturbation and encourages distinct lobe (ridge) formation. However, uniformly graded, angular material also creates frontal lobes, and we hence do not regard grain size segregation as a necessary process for the initiation of lobes or ridges –particularly since, in the field, such grain size distributions/segregations are rarely observed. Typically, no velocity difference is noted between adjacent ridges, and lithologies extend across them unperturbed from their original location (i.e., no segregation or lateral sorting/rearrangement occurs; e.g., Belousov et al., 1999).

Dufresne (PhD thesis in prep) presents evidence that laboratory subsurface features correspond with those in the field, at least qualitatively; and this supports our suggestion of significant correspondence between field and laboratory surface features.

2.8. CONCLUSIONS

This is an exploratory study of the occurrence and significance of longitudinal surface features in mass movement granular flows. We have identified significant similarities of longitudinal features in mass movement deposits in a very wide range of materials and settings, and we also related the range of feature types (hummocks, ridges, flowbands) to the flow conditions they appear to be largely associated with. We have shown that the formation of longitudinal ridges is an intrinsic process of free-surface granular flows and that the expression of this process as ridges, flowbands, or aligned hummocks at the surface of large-scale mass movement deposits largely depends upon:

(i) the frictional behaviour of the material i.e., its ability to resist internal deformation and the presence of angular clasts with varying grain sizes;
(ii) the emplacement velocity and direction;
(iii) the emplacement geometry and flow cross section; and
(iv) the influence of substrates on the flow dynamics.

Furthermore, processes such as burial or erosion by secondary flows play a crucial role in the preservation of longitudinal features.

Despite the great variety of geological materials forming avalanches and their equally great variety of proposed emplacement dynamics and conditions (rock avalanches, large volcanic debris avalanches, hot pyroclastic flows, snow and ice avalanches, high-velocity ejecta sheets and blast deposits, small-scale laboratory sand avalanches, etc.), the observation that they all share the same family of characteristic surface features indicates that there is considerable potential for further development of this topic, as the longitudinal features provide definite information on flow direction and could provide insights into emplacement processes of granular materials in general.

Chapter 3:

Influence of Runout Path Material on the Emplacement of the Round Top Rock Avalanche, New Zealand

---

In the spirit of:

"When you loose your mind you'll come to your senses."

Dan Millman

Influence of Runout-Path Material on Emplacement of the Round Top Rock Avalanche, New Zealand

A. Dufresne[1], T.R. Davies[1] and M.J. McSaveney[2]

accepted for publication in Earth Surface Processes and Landforms (2009)

[1]Department of Geological Sciences, Canterbury University, Christchurch, New Zealand
[2]GNS Science, Wellington, New Zealand

ABSTRACT

Factors influencing the distance a disintegrating rock mass travels as it spreads across the landscape after detaching from a slope include the volume and mechanical properties of the material, local topography and the materials encountered in the runout path. Here we investigate the influence of runout-path material on the mobility and final morphology of the Round Top rock avalanche deposit, New Zealand. This rock avalanche of mylonitic schist ran out over a planar surface of saturated fluvial gravel. Longitudinal ridges aligned radial to source grade into smaller aligned hummocks and digitate lobes in the distal reach. Soils and river gravels in the runout path are found bulldozed at elongate ridge termini where they formed local obstacles halting avalanche motion at these locations, thus aiding development of prominent elongate ridges on the deposit. Further travel over the disrupted substrate led to avalanche-substrate mixing at the base of the debris mass. Field observations combined with subsurface geophysical investigations and laboratory analogue models illustrate the processes of substrate deformation features at the Round Top rock avalanche.

3.1. INTRODUCTION

The Round Top (RT) rock avalanche deposit is situated on the western rangefront of New Zealand's Southern Alps (Figure 1). It resulted from catastrophic rock-slope failure and has an estimated volume of 45 x 10^6 m^3 (Wright, 1998). Such large (>10^6 m^3) geological mass movements behave distinctly differently than their smaller counterparts in that the latter compare well with laboratory-scale grain flows, whereas the larger ones do not scale with the runout predicted by a simple frictional grain-flow model (McSaveney *et al*., 2000).

Comminution of the rock mass during rock avalanche emplacement has been described by many authors based on thoroughly fragmented source material in the deposit (e.g. Hewitt, 1988; Glicken, 1998) or observation of dust-cloud development in historical events (e.g. Elm; Buss and Heim, 1881; Hewitt et al., 2008). A value of ~25 % volume-increase or bulking from the initial source volume to that of the final deposit is suggested in the literature (e.g. Hungr and Evans, 2004). The process of dynamic rock fragmentation is proposed by Davies and McSaveney (2008 and references therein) to be a mechanism facilitating the long runout of large rock avalanches.

Although failure volume dominates general rock avalanche dynamics (Davies, 1982), their runout is also significantly influenced by the local topography and the surficial materials present in the runout path. Where substantial amounts of saturated substrates and/or surface water, ice or snow are entrained, the rock avalanche will typically transform into a debris flow with a change to a highly mobile flow regime producing a thin and flat deposit. Total travel distances can increase by orders of magnitude by such transformations; e.g. Mt Cayley, Canada (Evans *et al*., 2001; McDougall *et al*., 2006) or Huascarán, Peru (Plafker and Ericksen, 1978). Where the interaction of rock avalanches with saturated substrates takes place without significant entrainment it can lead to complex substrate deformation features (e.g. Hewitt, 2006) and to morphological signatures such as pronounced ridges, flowbands or digitate emplacement (e.g. Dufresne and Davies, 2009), and it may influence flow mobility (see below). In this paper we describe the Round Top rock avalanche deposit, which features elongate radial ridges, aligned hummocks and widespread avalanche-substrate interactions. The description includes deposit morphology and internal

structure, substrate-deformation features, subsurface and trenching investigations of the basal avalanche contact, and laboratory analogue models; it concludes with a general discussion of substrate influences on avalanche emplacement processes.

3.1.1. Terminology

A 'rock avalanche' results from the sudden failure under gravity of an initially intact or fractured/jointed rock slope. Upon descent and emplacement the rapidly moving mass (up to 320 km/h) breaks up into smaller rock fragments (e.g. Luhr (2003); Hewitt *et al.* (2008)).

The prefix 'long runout' has been used in the literature to describe rock avalanches with travel distances that exceed those predicted by simple frictional models; this is sometimes also referred to as 'excess runout distance', as first introduced by Hsü (1975).

3.2. STUDY SITE

The Southern Alps of New Zealand's South Island are the result of oblique collision of the Indo-Australian and Pacific plates. The Pacific Plate is bounded at the western rangefront by the active strike-slip Alpine Fault. From east to west across the Southern Alps, lithology changes from weakly metamorphosed greywacke sandstone to high-grade schists which are juxtaposed to Indo-Australian rocks including granite in the Alpine Fault footwall (Figure 3.1).

Mylonitisation at depth and near-surface cataclastic fracturing along the Alpine Fault Zone is regarded as an important weakening mechanism of the rock mass, preparing it for rock slope failures, which are conspicuous features in the Southern Alps (e.g. Korup, 2004; Whitehouse, 1983). The western rangefront is bounded by steep slopes adjacent to mainly agriculturally developed alluvial plains towards the coast. At the field site of this study, the gouge zone of the Alpine Fault runs along the narrow valley between Mt Harry (deformed granite) and the rangefront (schist and schist-derived mylonite) from which the Round Top rock avalanche originated (e.g. Sibson *et al.*, 1979).

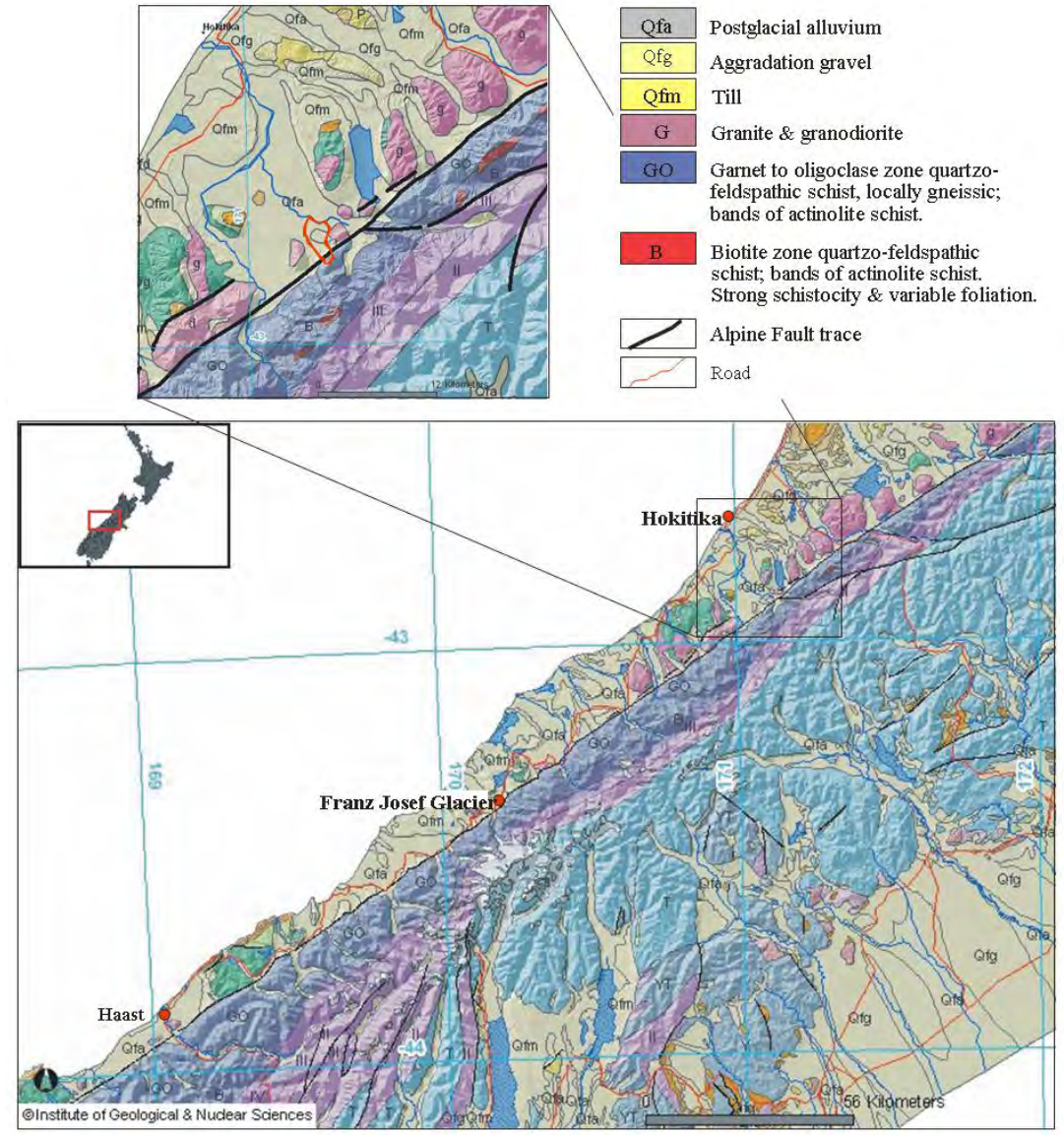

Figure 3.1: Geological map showing lithological changes across the Southern Alps (South Island, New Zealand) and the Alpine Fault trace on the West Coast. On the zoomed image, the location of the Round Top rock avalanche is outlined in red. Image source: online Qmap series of the Institute of Geological and Nuclear Sciences, New Zealand, (http://maps.gns.cri.nz/website/geoatlas/viewer.htm).

Wright (1998) estimated the RT avalanche deposit to cover ~ 5.6 km^2 with a volume of 45 x 10^6 m^3. In addition, the Southern Deposit (SD) of Wright (1998) covers an additional area of 1 km^2 and has a volume of ~ 10 x 10^6 m^3.

Both deposits were emplaced ~ 1,000 years ago (Wright, 1998) onto a wide, saturated alluvial plain not unlike those of the modern West Coast setting. On a runout slope of no more than 1-2 degrees, the RT rock avalanche travelled ~ 3.5 km (L*) as measured from the bottom of the source slope (Figure 3.2), or 4.8 km (L) map distance from the source scarp to the distal edge, with a drop height (H = highest

elevation at source to lowest elevation at the distal edge) of 600 m (Wright, 1998). The Kokatahi River has eroded minor portions of the distal edge of this deposit. The Southern Deposit has a shorter runout of 1.9 km (L) and a drop height of 260 m (H). Both deposits display hummocky topography typical of rock- and debris-avalanche deposits. Herein we focus primarily on the larger Round Top deposit.

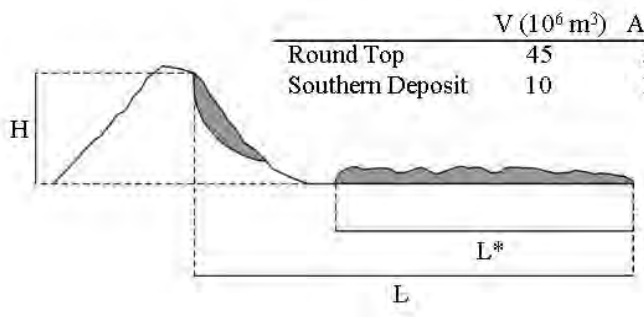

	V (10^6 m^3)	A (km^2)	H (km)	L (km)	L* (km)
Round Top	45	5.6	0.6	4.8	3.5
Southern Deposit	10	1.0	0.3	1.9	1.9

Figure 3.2: Sketch defining rock avalanche deposit dimensions and table of values for the Round Top and Southern Deposit rock avalanches.

3.2.1. Source scarps

The RT rock avalanche source scarp cuts deeply into the northwest-facing flank of the Round Top ridge within the Alpine Fault Zone (Figure 3.3). It is narrow and elongate in the failure direction with a maximum width of 650 m, narrowing to 470 m at the scarp mouth. The total scarp length from headwall to mouth is 1,060 m and its depth from the top of the headwall to the floor of its depression is approximately 320 m. However, these values are liable to error since later fluvial and erosional infill has altered its original shape. Rock avalanches with deep-seated failure scarps have been found to be most likely triggered by seismic shaking, as opposed to slope failures resulting from gradual slope weakening or stress build-up which tend to leave shallow failure surfaces (e.g. Crozier *et al*., 1995); for a detailed discussion on rock-slope failure-scarp dimensions see Turnbull and Davies (2006) and references therein. Following this hypothesis, we surmise that the RT rock avalanche was probably triggered by an earthquake on the Alpine Fault.

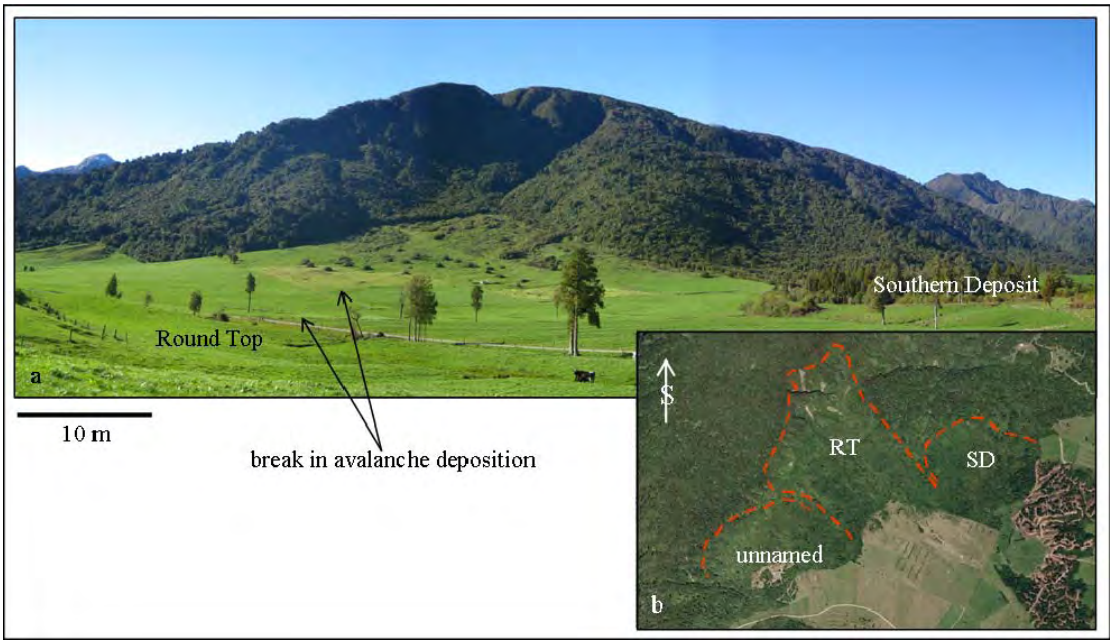

Figure 3.3: Southward view of the source scarps (a), and the vertical aerial view of the area (b). Insert image (b) is 2.3 km across.

Two smaller failure scarps flank the RT scarp on either side (Figure 3.3). The small one to the southwest is the source for the SD rock avalanche, whereas the shallow north-eastern failure surface only has a very small debris fan and small hummocks at its foot. On aerial photographs the three scarps merge almost seamlessly into one another due to younger forest cover than the rest of the ridge. However, they are topographically distinct features.

3.2.2. Deposit age

Radiocarbon dating by Wright (1998) places the RT event at about 930 A.D. (1,100 ± 45 and 1,300 ± 40 ^{14}C yrs B.P.). Our own radiocarbon dating failed to verify this date, instead giving wood log ages of 2,596 ± 39 and 4,815 ± 35 years B.P. for logs incorporated into the avalanche base. These results do not negate Wright's date, but rather demonstrate the difficulty of dating young rock avalanche deposits, particularly where long-lived swamps in fluvial outwash plains accumulated wood of a large range of ages.

3.3. INTERNAL AVALANCHE STRUCTURE

The RT and SD rock avalanche deposits consist of mylonitic schist with varying degrees of foliation. They contain quartzo-feldspathic laminae ranging from sub-millimetre to a few centimetres in thickness. Most outcrops display highly crushed, angular material with remnant source stratigraphy (i.e. darker micaceous laminae alternating with light feldspathic ones; Figure 3.4(a)). Material within the Arthur Road quarry at 4 km map-distance from source still shows the original schistosity, despite its fine grain size and clayey texture (Figure 3.4(b)).

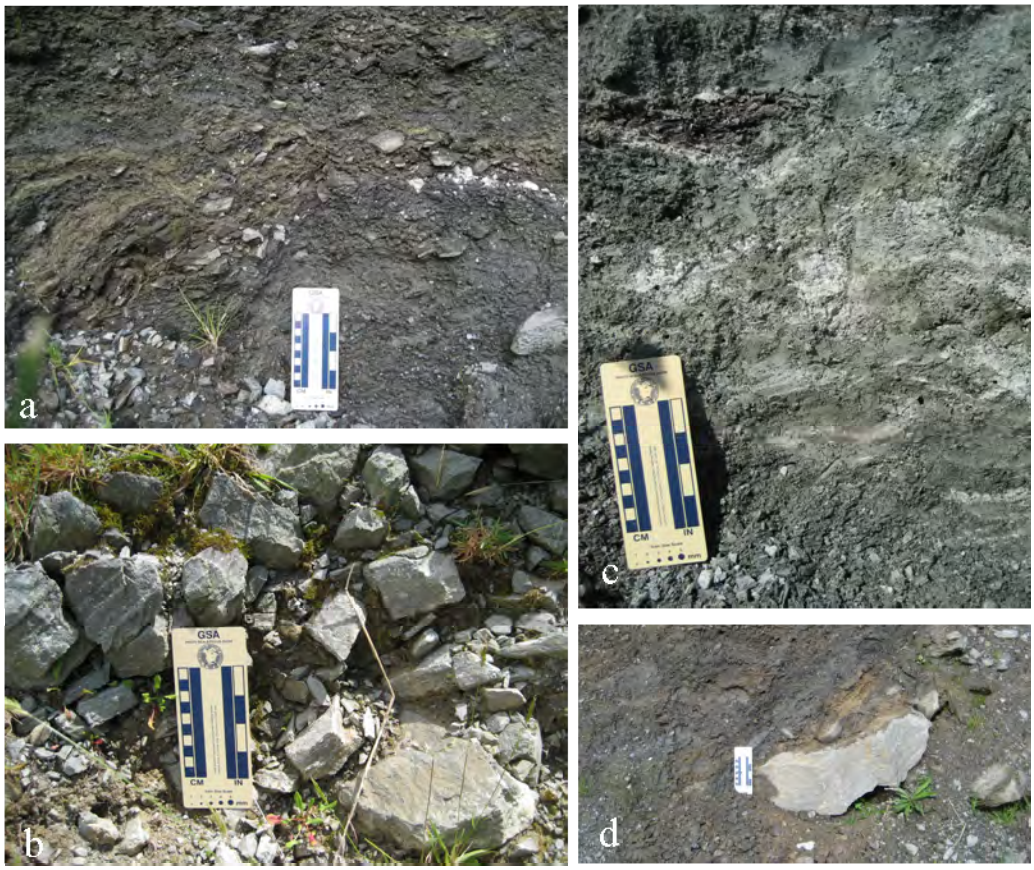

Figure 3.4: Close-up views of internal fabrics of the Round Top rock avalanche deposit: (a) lithological bands survive in crushed and sheared material at approximately 2.5 km from source; (b) common jigsaw-fractured clasts; (c) finely crushed rock avalanche material in the Arthur's Road quarry at ~ 4 km from source (red square in Figure 3.5). The original lithological bands are still preserved despite the fine grain size, clayey texture, and long travel distance; (d) larger clast set within the crushed material shown in (a).

Jigsaw-fractured clasts are common (Figure 3.4(c)); in some areas the deposit is a chaotic mixture of intact angular clasts, ranging from a few centimetres to metres in size, set within a matrix of finely crushed material of the same composition. Large clasts and slabs (2-3 m long axes) have been uncovered from trenches at the edges of hummocks in the medial reaches (Figure 3.4(d) and are also present in distal fields). Isolated pockets of scattered river gravel are found on the lower parts of some medial hummocks within the fields.

3.4. DEPOSIT MORPHOLOGY

Elongate ridges aligned radially to the bottom of the source scar are the most striking morphological feature of the Round Top rock avalanche deposit (Figure 3.5). Swamp- or lake-filled depressions are typical immediately adjacent to disrupted substrates at ridge fronts and at their motion-parallel sides. The largest hummocks are in the medial (and eastern) zone, changing quite abruptly into smaller hummocks in the distal part, which are nevertheless still aligned in an elongate pattern sub-parallel to emplacement direction. The subdued digitate topography of the distal reaches contains swampy depressions with small sand mounds (Figure 3.6). Rock avalanche material is peculiarly absent from these depressions, but is found entirely surrounding them. Most of the proximal zone is buried by a steep debris fan and recent fluvial deposits. However, between the fan and the beginning of the hummocky rock avalanche topography is a gap of depositional evidence.

Like Round Top, the smaller Southern Deposit features elongate ridges, a marked change in topography at distance from source, and digitate emplacement in the distal, and lateral marginal, areas. Proximal ridge axes are aligned oblique to source, trending into flow-parallel ridges in the medial to distal reaches. The spreading angle is less at SD (60º) than at RT (90º). SD material came to rest at the foot of the failure scarp, whereas RT material travelled about 1 km from the bottom of the source scarp before depositing.

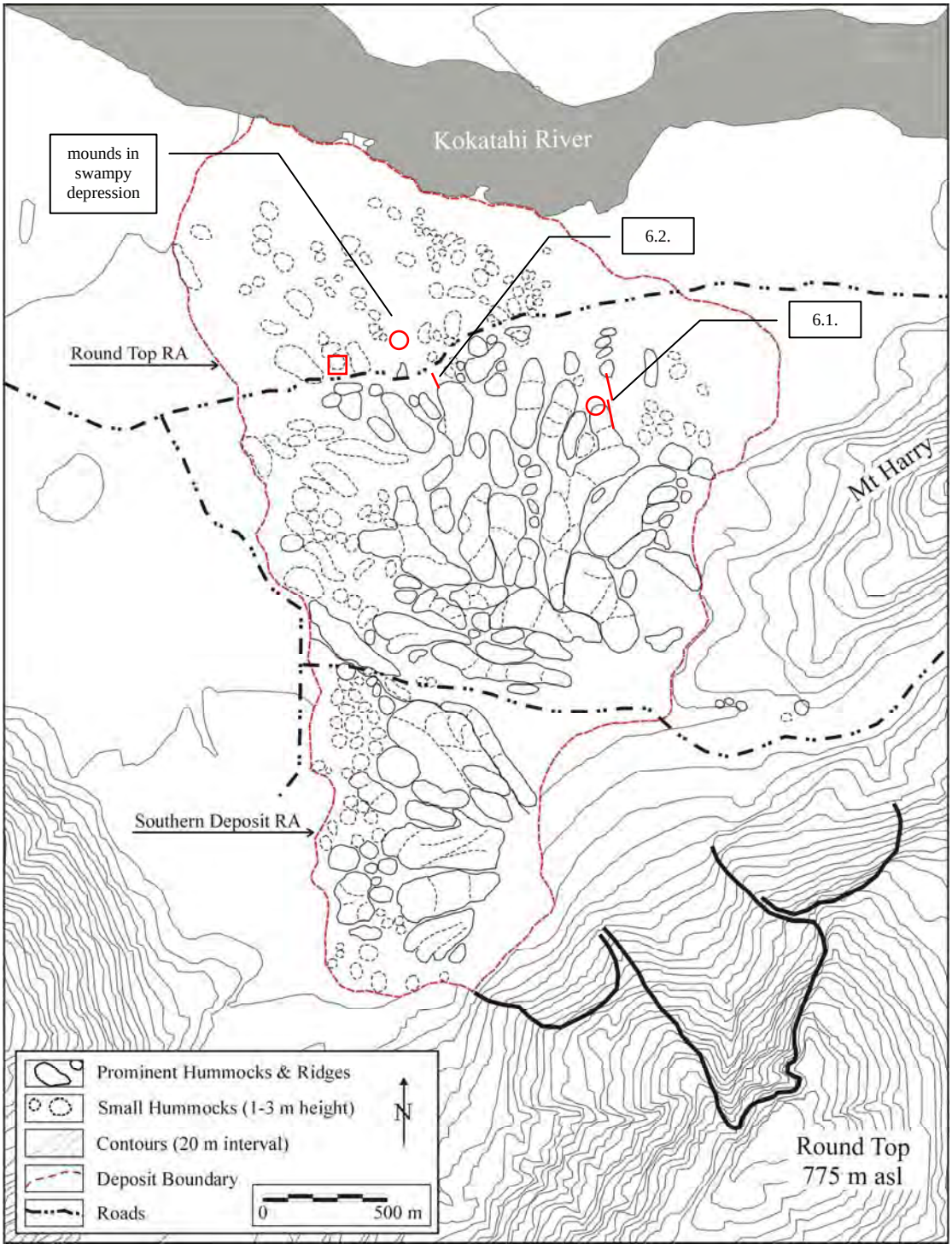

Figure 3.5: Morphological map of Round Top and Southern Deposits. Trench locations are indicated by red circles, GPR lines are shown in red with associated numbers indicating the section of the text they are described in. The red square marks the location of Arthur's Road quarry.

Both deposits show transverse morphological variations: at RT, the largest hummocks and ridges make up the eastern area, whereas at SD the western area has larger hummocks. The boundary between the two deposits is mostly concealed by post-

avalanche fluvial deposits; however, a long relatively flat hummocky ridge separates the two in the very proximal area and is interpreted as a 'lateral levee' of the RT deposit. We speculate that SD was emplaced immediately before or roughly simultaneously with the RT avalanche. Their interaction, similar to topographic interference, during emplacement would also offer an explanation for their transverse morphological variations mentioned above, and for RT's preferred easterly spreading direction.

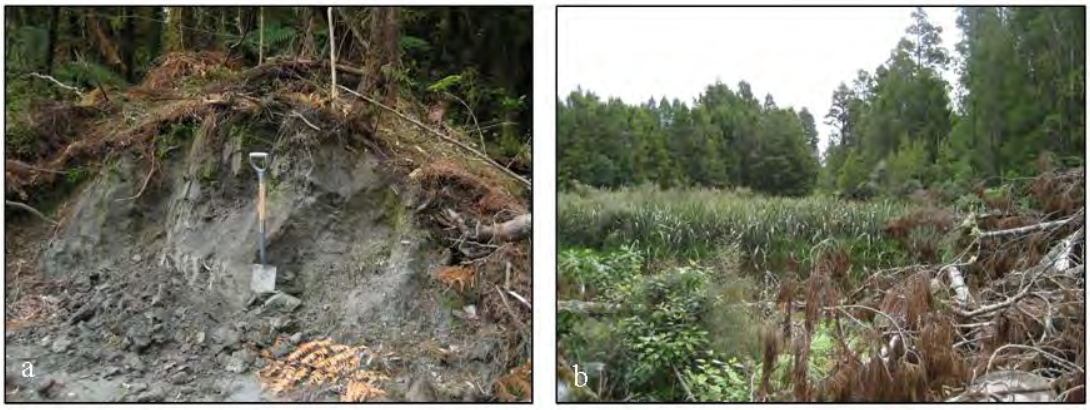

Figure 3.6: Distal deposit area north of Arthur's Road: (a) small mound within swampy depression uncovered by rock avalanche debris; (b) swamp in depression (as marked in Figure 3.5).

3.5. SUBSTRATE TYPES AND SUBSTRATE-AVALANCHE INTERACTION FEATURES

The soil immediately underlying the Round Top rock avalanche deposit is a recent, light grey, silty soil with abundant silt-sized mica. It contains small (mm to a few cm), rounded, multi-lithological clasts, sub-rounded schist fragments and peat. It is schist-derived and formed on fluvial outwash deposits; the high peat content indicates a swampy environment at the time of avalanche emplacement. Preserved soil thickness beneath the rock avalanche varies widely along sections where it has in parts been eroded by the rock avalanche or sheared with thicknesses of around 50 cm remaining. The soil is underlain by 5-8 cm reddish-brown coarse sand, 80 cm poorly sorted river gravel (consisting of layers of rounded clasts up to 20 cm in diameter down to coarse sand), followed by a 15 cm thick layer of coarse sand-to-pebble sized flat river rocks, 10-15 cm coarse sand and finally river gravel in excess of 1 m thickness (limit of

exposure). This section was recorded in front of an elongate ridge in the medial zone where the sequence has been displaced by RT but left intact stratigraphically.

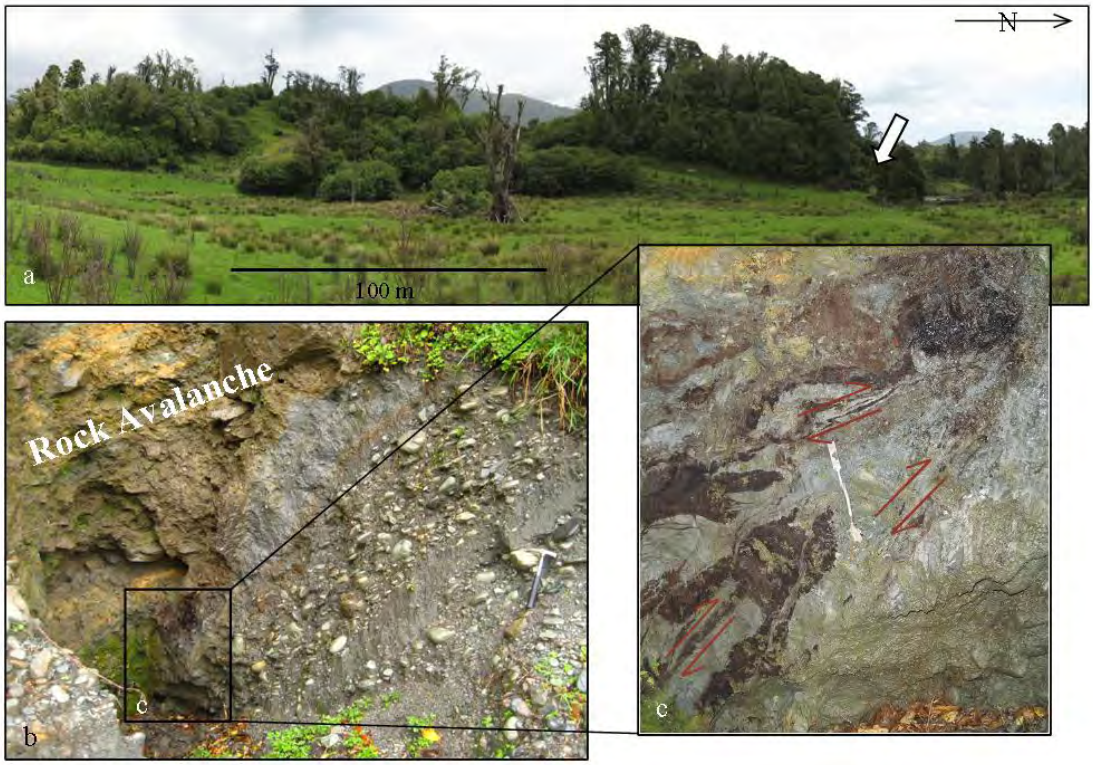

Figure 3.7: Bulldozed substrate sediments in a trench at the end of an elongate ridge: (a) ridge profile south to north; arrow points to trench location; (b) stratigraphically intact soil, sand and river gravel stratum dipping steeply towards the south (against avalanche motion direction), hammer for scale; (c) close-up of sheared peaty soil at the contact to the rock avalanche base, tool for scale is 20 cm long.

In the following section the rock avalanche-substrate interaction features of the Round Top rock avalanche deposit are described from source to distance. There is no exposure in the proximal zone of the deposit which is buried by a large debris fan.

Areas of displaced and deformed fluvial and soil strata in the medial zone are found at the front and sides of hummocks, typically with adjacent swampy depressions and/or lakes. Ductile deformation of soil and peaty soil in contact with the rock avalanche includes shear zones that reflect the sequence of deformation and hence avalanche motion (Figure 3.7). The original soil cover is thinned and, in places, missing. At ridge fronts, the alluvial strata beneath the soil retained its original stratigraphy, with some shear-rearrangement of fluvial gravel, despite being detached and tilted to angles of 45° to 80° in front of the hummock. The basal detachment surface of mobilized substrate lies at a minimum substrate depth of 2.7-3 m based on

the thickness of preserved strata at the ridge terminus. This same soil-gravel stratum, where it has been pushed to the side of the ridge, has been thoroughly disrupted and mixed with avalanche material. This mixing is restricted to the avalanche base (basal mixed zone) which is in sharp contact to the overlying avalanche debris (Figure 3.8a). Elsewhere, other signs of avalanche mixing with substrate include erosion features (highly irregular/undulating contacts; Figure 3.8b) and rare small flame injections (Figure 3.8c). However, the similarities in material (schist-derived soil and schist rock avalanche material) prohibit determining the proportions of entrained and mixed-in soil.

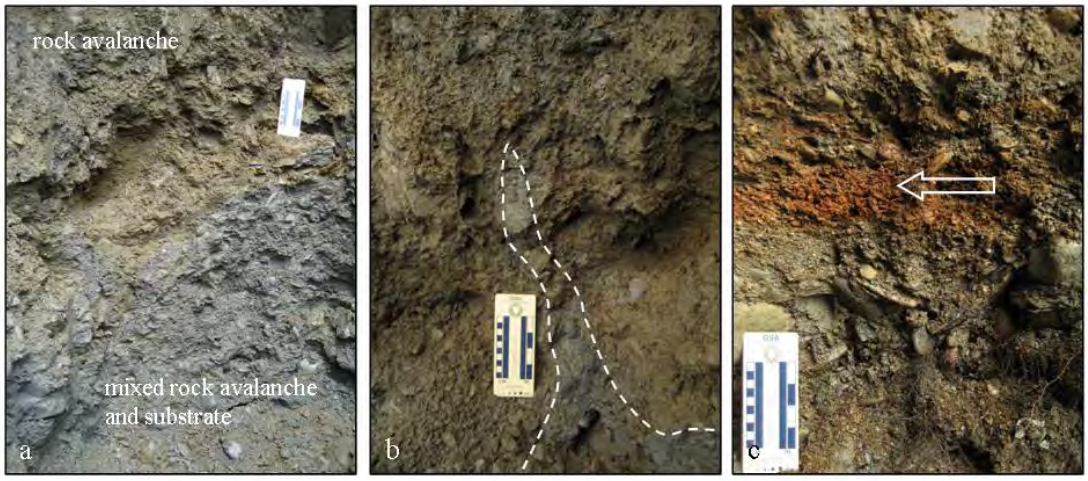

Figure 3.8: Other substrate interaction features: (a) mixing of rock avalanche and substrate material at the motion-parallel side of the ridge shown in Figure 3.7. The transition from rock avalanche to mixed part is just below the cm-scale; (b) small injection feature outlined in white at another trench; (c) erosion of peaty soil down to the underlying sandy layer (arrow points to reddish sand layer at the basal contact of the rock avalanche – reappearance and thickening of the soil layer seen in the trench depicted in Figure 3.7 can be traced along section).

In the medial to distal reaches more chaotic mixing of rock avalanche, soil and gravel is apparent as well as a change in topography to smaller, more subdued hummocks. Small mounds (1.5-2 m high and 5-10 m diameter) made of coarse sand, small rounded gravel and clayey soil are found within swampy depressions that lack rock avalanche cover, but which are entirely surrounded by rock avalanche (see Figure 3.6). Trenching close to the Kokatahi River was restricted by high water tables; however, within a paddock at ~ 4 km distance from source, trenching revealed modern soil and river gravel down to ~ 1.5 m depth. At the edge of a swampy depression ~100 m further north, rock avalanche material exists to a minimum depth

of ~ 2 m. Outcrops in the Southern Deposit are rare since this area has not been modified much for agricultural use (e.g. no farm roads cut into hummocks), nor was trenching attempted in this deposit.

3.6. BASAL AVALANCHE CONTACT AND INTERNAL AVALANCHE STRUCTURES

For sub-surface investigations a Sensors and Software pulseEKKO ground penetrating radar (GPR) system equipped with 100 MHz antennae was used. The system setups were 1 m separation between transmitter and receiver, a step-size of 0.25-0.50 m between data-collection points along the profile, time windows of 200 ns and 600 ns (translating into 10 m and 30 m radar penetration depth, respectively), and a stacking of 32 data traces averaged to create the stored data trace. Topographic GPS surveys were carried out at each GPR site. This study is one of the first few geophysical investigations of rock avalanche deposits: Fernpass rockslide, Austria (Prager et al., 2006); Wanganui rock avalanche, New Zealand (Chevalier, 2008).

3.6.1. Elongate ridge and trench of bulldozed substrate

At the site of trenching and substrate bulldozing shown in Figure 3.7, GPR survey lines were run parallel to ridge elongation direction to provide insights into the extent of substrate deformation, and into the internal features within the ridge. Survey depths along the ridge were 20 m, and 10 m between the ridge and the next hummock. Most of the survey followed a farm road which transits into pasture over the last 30 m of the 270 m long total survey distance. The similarities in physical properties of the coarse avalanche material and the underlying river gravel resulted in indistinguishable signatures on the radar image. With this difficulty in mind, interpretations of reflectors were made in the context of trench and morphological data.

Region (1) in Figure 3.9 marks the transition from one “hummock” to the next within the ridge. Onlapping reflectors dipping to the north can be seen in the upper left corner of Figure 3.10C (marked (1)). Linear cross-cutting reflectors and north-dipping features in area (2) are interpreted as faults. The bulldozed substrates revealed by trenching (Figures 3.7 and 3.9(b)) are clearly recognizable in the GPR transect and

are marked (3) in Figure 3.9. A change in avalanche fabric just to the left of marker (3) is similar to the front of another hummock (Figure 3.10(b)) and suggests compressional structures in accord with deceleration behind an obstacle. Following the subterrain north towards the next hummock, contorted fabric (marked (4) in Figure 3.9(e)) most likely illustrates substrate disruption between the ridge terminus and the next down-motion rock avalanche deposition (hummock onset is marked (5) in Figure 3.9(e)).

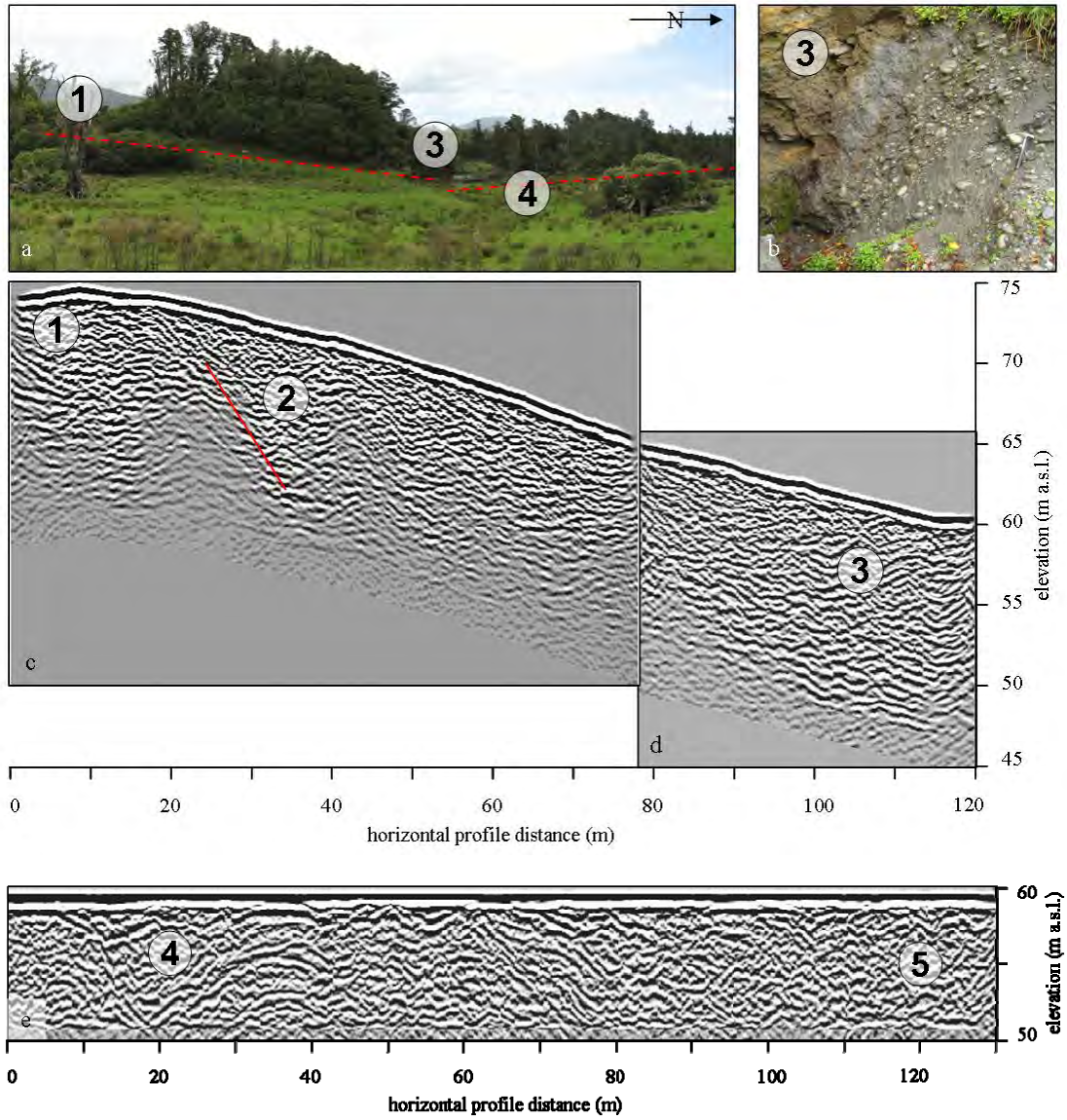

Figure 3.9: Location of GPR lines (a) along the side of the elongate ridge where trenching uncovered bulldozed river gravel at its toe (b). Areas marked with numbers are discussed in the text. The line shown in (c) and (d) runs alongside the ridge following a farm road; the line in (e) connects this area with the next down-motion hummock at 130 m distance. Note profiles are vertically exaggerated.

3.6.2. The distal area

At the transition from high to more subdued smaller hummocky deposit morphology, a short GPR survey was run to image the transition from hummocky to flatter terrain (Figure 3.10). This hummock shows signs of internal compression (reverse faults) as testimony to sudden deceleration.

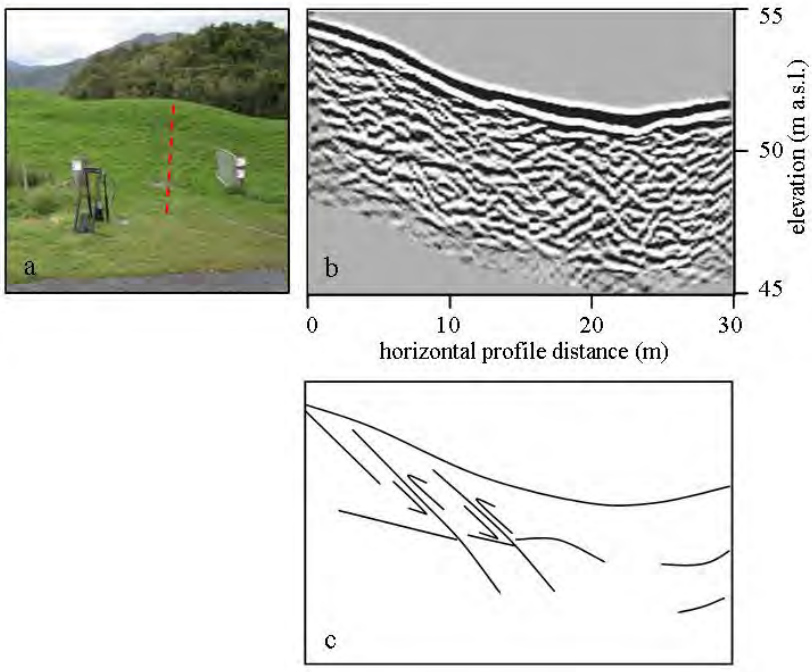

Figure 3.10: Subsurface structure of the transition between the thick medial-distal hummocky topography to the more subdued digitate distal area at Arthur's Road: (a) location of GPR profile (the Round Top ridge and source is visible in the background); (b) GPR profile of hummock front (vertical exaggeration); (c) interpretive sketch of the GPR profile showing lineaments interpreted as reverse faults.

3.7. MODELLING AVALANCHE-SUBSTRATE INTERACTIONS

Field evidence suggests that bulldozing at the front of the RT rock avalanche ridge occurred as follows: the avalanche detached the substrate along a basal décollement at a substrate depth of ≥ 3 m and ploughed it into a mound ahead of the ridge. To simulate the processes involved in and effects of rock avalanche emplacement onto different substrates, small-scale analogue flume experiments using various substrate materials were performed. The horizontal flume bed had a width of 30 cm, flanked by clear plexiglass walls. To accelerate the avalanche material, a 100 cm long metal

slope was attached to the flume via hinges. The slope was equipped with a 30 by 30 cm container with a manual-release door to store the avalanche material at the beginning of each experiment. Angular coarse coal clasts (1-2.5 cm in diameter) simulate the avalanche and finer materials with varying properties were used as substrates. We found that wheat flour provided the most detailed interaction features due to its small grain size, its low density and because it was readily mobilized by the moving coal avalanche clasts. Other materials such as PVC beads showed similar responses to avalanche impact, albeit did not provide the details of deformation due to their larger grain sizes.

Vertical marker horizons (dyed flour) served to document the deformation processes: initially the avalanche toe, when first encountering the deformable substrate, eroded material from its surface (Figure 3.11a) with some spray developing ahead of the flow. With higher loading the substrate surface material was mobilized (b), ploughing/bulldozing commenced (c), and first indicators of subsurface shear failure appeared (d). Further avalanche advance accentuated the shear failure at depth (e) with a décollement developing (f). Mingling of the black marker horizons with white substrate material formed a facies just beneath and ahead of the avalanche front, where it was partially emplaced over stationary substrate material (g). Injection or diapir-like features developed in this zone (h). Ploughing of the avalanche into the soft substrate essentially halted its lower parts, imposing frictional resistance on the uppermost, still mobile avalanche leading to a shorter and thicker deposit compared to emplacement onto less erodible material. The final cross-section in Figure 3.11 documents the depth- and length-extent of substrate failure, the mingled and bulldozed facies at the avalanche front and deposition of this facies onto apparently undisturbed substrate (k). However, this seemingly undisturbed material was minutely mobilized and compressed (arrow in Figure 3.11) and is hence not entirely unaffected by avalanche emplacement.

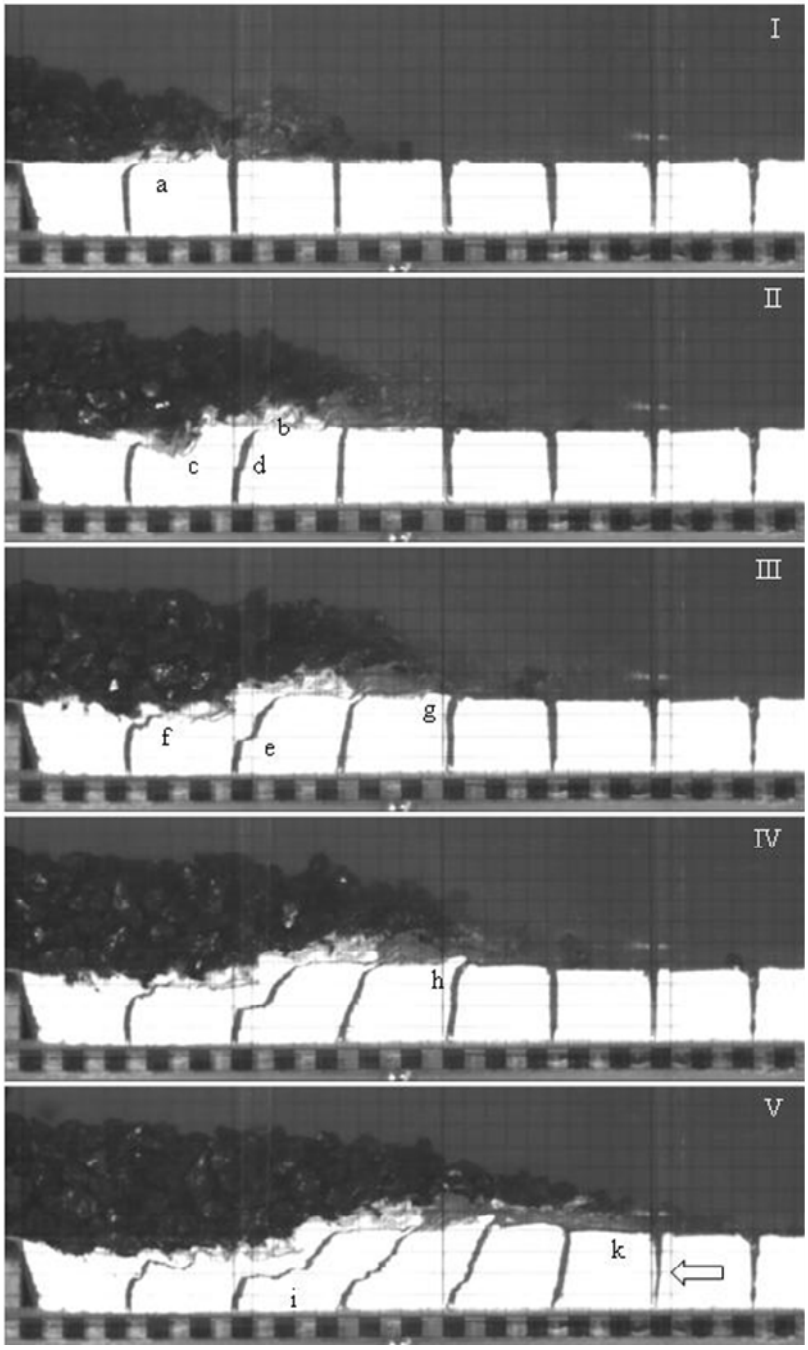

Figure 3.11: Time sequence of small coal avalanche emplaced onto a flour substrate discussed in section 7.2. Vertical marker horizons consist of dyed flour; scale is in centimetres. The images were captured using a high-speed camera recording 900 frames per second; the images show (I) frame 189, (II) frame 259, (III) frame 289, (IV) frame 319, and (V) frame 409.

The simplicity of the experiments described above does not preclude comparison with the complex field avalanche; the striking similarity of features (compare Figure 3.11 with Figure 3.7) produced in the laboratory provides excellent information on the processes of subsurface feature formation found beneath field rock avalanches. It has been shown elsewhere (e.g. Davies *et al.*, 2003; Lajeunesse, in review) that

microscale modelling of natural phenomena such as rivers, can be successful in reproducing processes and tendencies of natural phenomena despite a lack of dynamic similarity. Even though the detailed processes of small-scale water and sediment behaviour differed from those of real-size rivers (e.g. laminar versus turbulent water flow), the authors were successful in predicting river bed response from their experiments. Similarly, the experiments conducted in the context of this research, although not following dynamic similarity, showed processes and features identical to field observations, which demonstrates the universality of such features in spite of arbitrary choice of scale and materials.

3.8. SUMMARY AND DISCUSSION

Deep-seated, most likely co-seismic failure of ~ 45 x 10^6 m^3 of partially fractured mylonitic schist of the Round Top ridge resulted in initially high-velocity emplacement of the Round Top rock avalanche. Deposition of substantial amounts of rock avalanche material did not occur until ~ 1 km from the bottom of the source scarp due to the debris' high momentum upon leaving the source scar. The moving rock mass spread on deformable, saturated fluvial gravels and peaty soil, which it locally mobilised, eroded and bulldozed as revealed by trenches and geophysical surveys. At these localities, the substrate conditions contributed to enhancement of characteristic morphological surface features of prominent longitudinal ridges. Increasing rock avalanche travel distance is accompanied by an apparent increase in basal rock avalanche mixing with substrate material, producing a chaotic facies of angular rock avalanche clasts, river gravel, soil, sand and peat. Digitate emplacement characterises the distal reaches where mobilized substrates (‘sand-mounds’) are found within swampy depressions. A distinct change from large hummocks to more subdued morphology (smaller and flatter hummocks) marks the medial-distal transition. Sudden stopping of the avalanche mass at this transition point is documented as reverse faults within hummock fronts. Transverse morphological variations with larger hummocks in the eastern part of the deposit suggest a preferential eastwards spreading direction of the RT mass. SD on the other hand deposited material close to source and spread preferentially to the northwest due to the interaction of the two rock

avalanches upon emplacement. The lateral spreading angle of the deposit is ~ 90º and might have been greater without the lateral topographic constraints of Mt. Harry to the north and the contemporary Southern Deposit rock avalanche.

From field evidence we deduce aspects of substrate behaviour during the Round Top rock avalanche emplacement: (1) the substrate failed within or just below a sequence of fluvial gravels, ~ 3 m or more below the avalanche base. Despite being displaced and thrust into ramps at ridge termini, the substrate sequence retained its stratigraphy to within 0.5 m of the avalanche base. Here shearing of the top peaty soil and disruption of the thin uppermost sandy gravel occurred. Fluvial gravels lower in the section show signs of shear-rearrangement. (2) Displacement along the sides of ridges thoroughly disrupted the substrate which mixed with rock avalanche material. Points (1) and (2) demonstrate how easily displaced and mobilized the gravel and soil sequences were, and testifies to their low shear strength. Conceptionally, these processes can be envisioned to have taken place as described above in the laboratory experiment (Figure 3.11). (3) The soil failed plastically into sheared peaty layers and lenses. In many places the soil was eroded by the rock avalanche, again reflecting its low shear strength. (4) Further from source, more intense substrate disruption was observed in many swampy depressions accompanied by an apparent increase in chaotic mixing of rock avalanche and substrate with distance; this is most likely the result of liquefaction/disruption and the subsequent avalanche motion over the already ‘compromised’ (i.e. still in the liquefied state) material. (5) Where rock avalanche material is absent between distal digits, sandy mounds are characteristic. These do not show the internal structure often seen in sand- and mud-boils that are the result of a high increase in pore-fluid pressure at depth to the point where interstitial fluids buoy the particles (= fluidization, e.g. Maltman and Bolton, 2003) leading to strength-loss of the material and a stark density contrast with the surrounding material, ultimately resulting in the extrusion of fluidized material to the surface. Instead the mounds are composed of sand to small pebble sized stratified river deposits. There is no clear evidence as to whether the sand mounds formed contemporaneously with avalanche emplacement or if they are loading structures formed at some time after the event.

In summary, the substrate was saturated at the time of the Round Top rock avalanche emplacement, making it mechanically weak and easy to mobilize. Any remaining strength was further compromised by seismic shaking generated by the

triggering earthquake and/or by dynamic loading by approximately 120 million tonnes of material impacting on the fluvial plains. Earthquakes capable of generating deep-seated rock avalanches are tentatively on the order of M > 7.0 e.g. (Keefer, 1994), and seismic signals generated by rock avalanches are comparable to seismo-tectonic events (Weichert *et al*., 1994). For example, the 1965 Hope rock avalanche (V: 47 x 10^6 m^3, H: 730 m) generated a M_S of 3.4 (Weichert *et al*., 1994) and the 1991 Mount Cook rock avalanche generated a M_L 3.9 (McSaveney 2002) for 12 x 10^6 m^3 and a drop height of 2,720 m. However, while far-reaching liquefaction at such low magnitudes is not expected (Wang *et al*., 2006), substrate strength will nevertheless be compromised by the combination of shear stresses and sudden overburden load imposed by the advancing avalanche.

The debate about rock avalanche emplacement mechanisms spans more than a century and has produced a number of hypotheses to explain their conspicuous divergence from simple frictional models. In-depth discussion of the various hypotheses is available in, for example, Legros (2003) or Davies et al. (1999); herein we focus our attention on the effect of substrates on runout. The role of substrates in rock avalanche behaviour is not well understood, and is, in our opinion, critically dependant on the physical properties of the runout path materials (e.g. degree of sediment saturation, thickness, frictional behaviour, etc.). The notion that liquefied substrates play a major role in enhancing avalanche mobility, and hence runout, has been discussed since Buss and Heim first proposed the idea in 1881; Abele (1974, 1997), Sassa (1988), Hungr (1990), Voight and Sousa (1994), and Legros (2002) subsequently followed in the discussion. Hungr and Evans (2004) give considerable credit to liquefied soils for enhancing avalanche mobility. In all the cases presented in their study, an initially dry rock avalanche mobilized and mixed with a substantial volume of substrate material on the steep failure slopes and effectively transformed into a debris avalanche, or even a debris flow, with a consequent change in flow characteristics. Using the data summarized in Hungr and Evans (2004) it appears that ‘substantial’ amounts of substrate entrained constitute somewhere on the order of 20-50 % by volume of the final deposit (Table 3.1), but can be larger for deposits such as the Nevado Huascarán rock avalanche, where 74 % by volume of the final deposit was entrained ice, snow and moraine material. All of these avalanches produced deposits that are longer than they would have been without entraining the substrate

material early in the emplacement because their total volumes increased and they hence had the potential to spread more debris over a greater area; in addition, the entrained saturated material was weak, allowing greater spreading and hence runout.

Deposit name	Avalanche Volume [$10^6 m^3$]			Entrained material [$10^6 m^3$]	
	original	fragmented	final deposit	volume	percent of final deposit
Eagle Pass	0.075	0.094	0.12	0.026	22
Nomash River	0.3	0.375	0.735	0.36	49
Nevado Huascaran	2.75	3.4	13	9.6	74
Cerro Rabicano	6	7.5	15	7.5	50
Ontake 1984	34	42.5	56	13.5	24

Table 3.1: Calculations of rock avalanche volumes into original intact rock mass, volume of the fragmented rock mass, and volume of the final deposit (fragmented rock mass plus entrained substrate materials); data from Hungr and Evans (2004).

Let us now consider cases without substantial substrate entrainment and where substrate encounter was on flatter terrain of the runout path rather than on a steep failure slope. Statistically, rock avalanches emplaced onto glaciers travel longer distances and have thinner deposits than their counterparts emplaced onto other materials (Evans and Clague, 1988). On glacial ice, basal avalanche friction is low, enabling the debris to spread, thin, and travel longer distances. When considering (saturated) substrate sediments, their higher densities and higher surface friction relative to ice and snow change the style of interaction. Material incorporation leads to bulking and a change of at least the basal avalanche composition and mechanical behaviour. Energy is expended when accelerating stationary material to avalanche velocity. 'Sinking' of an avalanche mass into a deformable substrate or bulldozing of same can locally decelerate the base and/or flow front and reduce runout, as for example seen in raised margins of the Ollagüe volcanic debris avalanche, Chile (Clavero *et al.*, 2002) or the Ananievo rock avalanche, Kyrgyzstan (Abdrakhmatov and Strom, 2006), both of which encountered deformable sediments in their distal runout paths. On the other hand, for substrate failure to contribute to lower basal friction and so extend rock avalanche travel distances, sufficient shear needs to be transmitted into a weak substrate. As yet, we do not have a numerical threshold for what constitutes 'sufficient' shear transmission. In addition, any reduction in frictional resistance must also compensate for transfer of kinetic energy to the mobilized substrate, before travel can be extended.

At Round Top, if failure of the saturated soil and low-friction gravel sequence at depth temporarily and over short distances enhanced avalanche mobility, bulldozing of the detached substrates simultaneously opposed this effect by stopping avalanche debris at these (proximal-medial) locations where prominent elongate ridges now stand. At other rock avalanches, a similar interdependence of saturated substrate conditions and pronounced longitudinal ridge formation has been reported. For example, the Altenau and Marquartstein rock avalanches in Germany were both emplaced onto lacustrine clays, display radial longitudinal ridges and, at least at Altenau, substrate was bulldozed ahead of ridges (von Poschinger, 1994). In the Karakoram Himalaya, longitudinal ridges are found in numerous rock avalanche deposits: the Ghoro Choh in particular has very pronounced longitudinal ridges; it was emplaced onto river gravel and other alluvium, and substrate bulldozing features are common at ridge termini (Hewitt, 2006). It has been shown elsewhere (Dufresne and Davies, 2008) that longitudinal ridges are intrinsic properties of granular flows, but that their expression in the deposit depends on the frictional behaviour of the avalanche material, its emplacement velocity, and the substrate conditions.

The Round Top rock avalanche displays prime examples of longitudinal ridges and their distal expressions in digitate deposit shape and aligned hummocks, because (1) the source material consists of mechanically strong, initially relatively coherent rock mass of mylonitic schist. Comminution during runout broke this material into angular clasts providing high-friction material for the formation and preservation of high ridges. (2) Low shear strength runout path material was easily displaced and mobilized beneath and in front of the overriding avalanche, and, as shown above, parts were bulldozed beneath ridges. This created local obstacles to avalanche motion, effectively halting ridge advance and thus preventing its break-up into smaller hummocks at these locations. Even though the bulldozed sediments are now exposed at ridge fronts, their initial position during avalanche motion would have been below the ridge itself (Figure 3.12), slowing the rear while the frontal parts retained their velocity/momentum to continue spreading on the weak substrates, forming smaller hummocks aligned in original ridge motion-direction. As these hummocks detached from the decelerating ridge mass, their continued travel across the terrain disrupted sediments in their path (see GPR profile in Figure 3.9e), while leaving relatively little to no rock avalanche material behind.

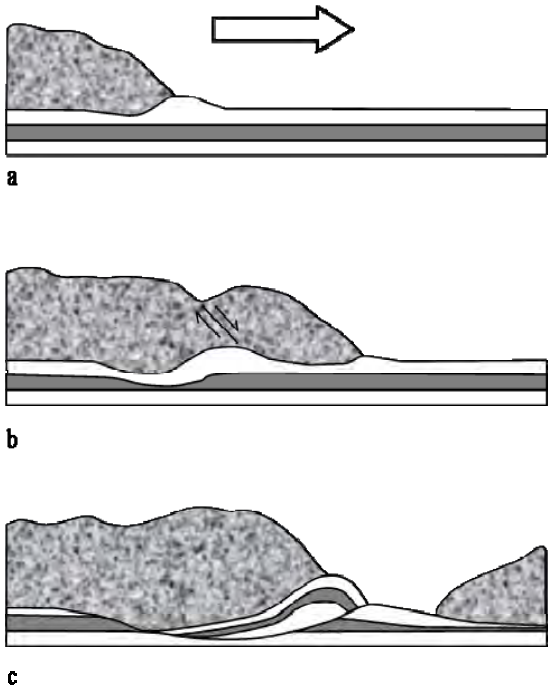

Figure 3.1: Conceptual sketch of substrate bulldozing beneath an advancing rock avalanche ridge: (a) initial encounter of the ridge toe begins to plough into the substrate; (b) as the ridge advances, more substrates are disrupted and are forming a local obstacle beneath part of the avalanche ridge; (c) the rear of the ridge decelerates behind the bulldozed substrates, while the frontal ridge part continues to advance following momentum.

As the thickness of the avalanche reduced with distance travelled, so did its potential for bulldozing sufficient amounts of substrates into local obstacles. Here, accompanied by a change to lower topographic deposit profile, unobstructed runout on a possibly liquefied substrate created digits with smaller, less steep hummocks. Numerous outcrops show that mixing of substrate with avalanche material apparently increases with travel distance compared to the detached, but seldom mixed substrate units in the proximal and medial parts. Sudden deceleration of the avalanche mass at this transition is testified by subsurface investigations revealing reverse faults at a hummock toe (Figure 10).

In essence, whether saturated runout path materials lead to reduced basal friction and longer runout, or whether they reduce avalanche mobility by reducing the available momentum per unit mass depends on the local substrate as well as avalanche conditions and can vary within the same event. In both cases the avalanches reach

travel distances that exceed those of simple frictional model predictions. Therefore, lubrication by liquefied soils and saturated sediment is not a universal explanation for the long runout of large (> 10^6 m^3) rock avalanches; instead the explanation must lie in an avalanche-intrinsic, dynamic process. Substrates then add variations and complexities similarly to topographic interferences (Nicoletti and Sorriso-Valvo, 1991).

The question remains whether emplacement of the same volume and type of material in a similar topographic environment but over a rigid, non-erodible, non-deformable substrate would have led to longer or shorter runout of the Round Top rock avalanche. Unfortunately, no report exists of a rock avalanche which has been emplaced entirely on a non-interactive substrate. Comparing Round Top to a number of rock avalanches of similar deposit volume shows that its runout-to-volume ratio is not unusual (Figure 3.13). It plots, within error, similarly to other rock avalanches with different substrate and topographic runout conditions. It is somewhat less mobile than the El Capitan (US-Arizona) rock avalanche which was emplaced over playa lake sediments (Yarnold and Lombard, 1989), but more mobile than the Val Pola rock avalanche in Italy which entrained high friction landslide debris and impacted onto the Ada River valley trending perpendicular to avalanche travel direction (Crosta et al., 2004); and it was more mobile than the Ananievo rock avalanche in Kyrgyzstan which bulldozed soft sediments at its distal margin (Abdrakhmatov and Strom, 2006). The Marquartstein rock avalanche, Germany, is very similar to Round Top in runout path topography and sediments, and it displays the same surface features of prominent elongate ridges (von Poschinger, 1994). The same applies to the Frank Slide which was emplaced onto a wide alluvial plain, and entrained and transported both water and underlying sediments (Cruden and Hungr, 1986; Cruden and Krahn, 1978). At this stage, we can only tentatively shade in the trends of rock avalanches (in order of increasing apparent mobility) which (1) encountered topographical obstacles, or created hindrances by interacting with soft sediments, (2) entrained high-friction debris, (3) were channelled by topography (Nicoletti and Sorriso-Valvo, 1991), to (4) those with significantly reduced basal friction (e.g. over ice and snow, Evans and Clague, 1988), or which changed in flow dynamics through significant entrainment of saturated material. Further complications probably arise from failure slope geometry and width of the source scarp as suggested by gate-width experiments of Manzella and Labiouse (2008).

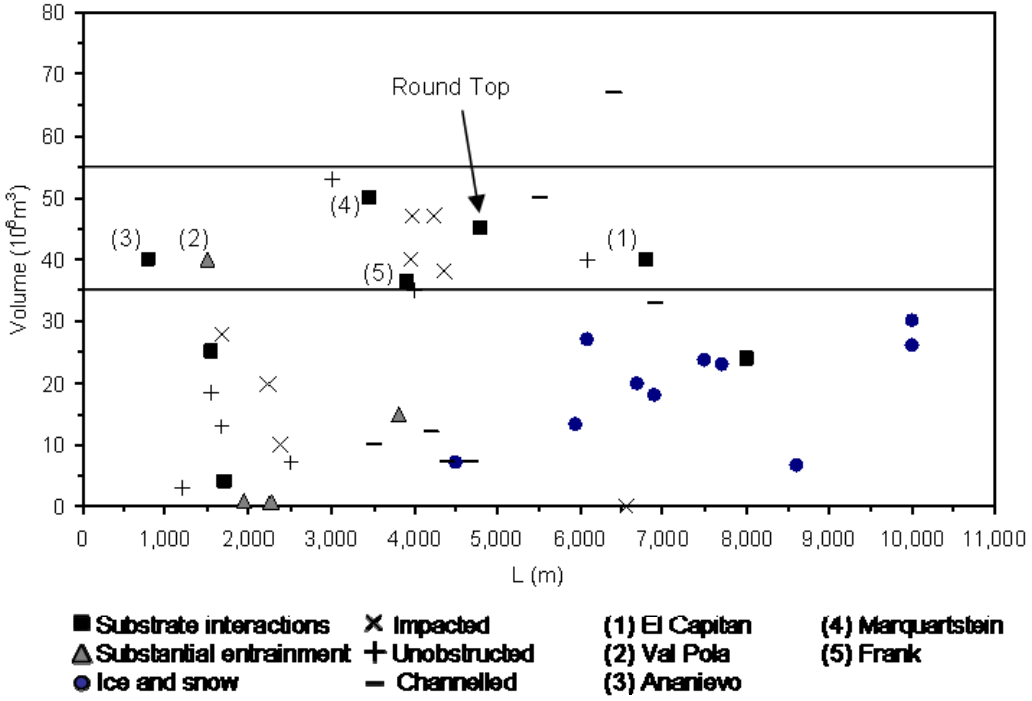

Figure 3.2: Volume – runout relationships of several rock avalanches of similar volume as the Round Top deposit. Squares, triangles and circles represent avalanche deposits with known substrate and interaction types; crosses and dashes are deposits that lack substrate descriptions, and which are instead grouped according topographic conditions. Note that the only group showing a trend are the highly mobile avalanches emplaced onto glacial ice and snow (circles).

3.9. CONCLUSIONS

Whether deformable and erodible substrate conditions increase or hinder avalanche runout is a delicate balance between (1) energy expended to mobilise substrate material, (2) reduced frictional resistance within the failing substrate, (3) the 'efficiency' of substrate mobilisation (i.e. whether it is a continuous process acting at the avalanche front, providing a weak 'sliding plane' for the avalanche at any point in time during emplacement, or whether the substrate is bulldozed into mounds that impede avalanche momentum/motion) and (4) whether the substrate entrainment increases the mobility of the avalanche mass by introducing significant quantities of water.

Acknowledgements

This work formed part of the PhD investigations of AD into substrate influences on rock/debris avalanche dynamics. Nelson Cook and Steve Staples are gratefully thanked for granting access to their properties. Trenches were skilfully and enthusiastically dug by Spike Jones. The fantastic help of Guillaume Chevalier, and assistance of David Nobes and Mike Finnemore with geophysical field work and data processing is gratefully acknowledged. Laboratory experiments would not have been possible without the creative assistance by Rob Spiers. Reviews by Thomas Shea and Johannes T. Weidinger have greatly improved this manuscript. This PhD project was funded by a NZIDR scholarship and financial support for field work was received from the Canterbury University department of geological sciences Mason Trust fund.

3.10. ONLINE SUPPLEMENTARY MATERIAL

3.10.1. Ridge between Round Top and the Southern Deposit

A GPR survey line was run across the ridge separating the two rock avalanche deposits in the proximal area (Figure 3.14). The surface of this ridge had been modified slightly and is in pasture for cattle grazing. Rock avalanche signature in the GPR profile is similar to the signature of the onlapping alluvial fan (shaded area indicated in Figure 3.14), but their contacts are discernable. Sagging or reworking of the upper ridge onto the alluvial fan is seen as a wedge between pasture and fan material. The rock avalanche fabric shows gently inclined reflectors towards the west (border to the Southern Deposit) and steeper dipping reflectors towards the east (Round Top proximal area). The existence of this ridge remains a puzzle that was not conclusively resolved by the geophysical survey. We suggest its origin to lie in the interaction of the Round Top rock avalanche with the previously or contemporaneously emplaced Southern Deposit. For a definite interpretation of its internal structure, comparable GRP investigations of known rock avalanche lateral levees and other ridges would be useful.

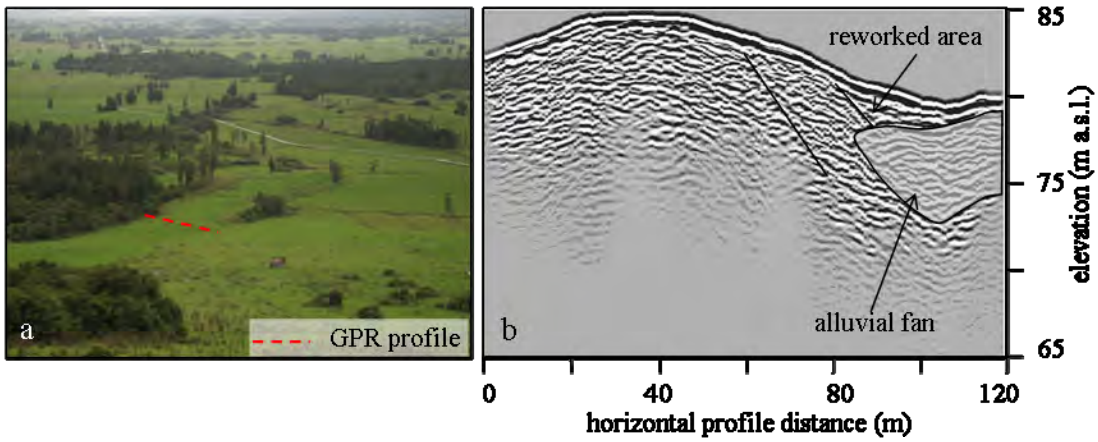

Figure 3.3: GPR profile of the ridge between the RT and SD deposits: (a) location of profile; (b) profile shown east (left) to west (right); note profiles are vertically exaggerated.

3.10.2. Concept model of bulldozed substrate structures

Erosion and other geological and anthropological processes over time work against the preservation of complete records in the field. At the site of substrate bulldozing we hoped to obtain a complete picture of the deformation structures; parts of these were revealed by trenching and geophysical surveys, but parts had been removed by farming or are obscured beneath the local pond. Therefore, we reproduced similar structures in a very simple, colour-stratified sandbox experiment by 'ploughing' a rounded rock (representing the ridge front) through dry sand, resulting in duplex structures within the bulldozed facies giving indications of potential deformation features now missing from RT or not visible in the available sections (Figure 3.15).

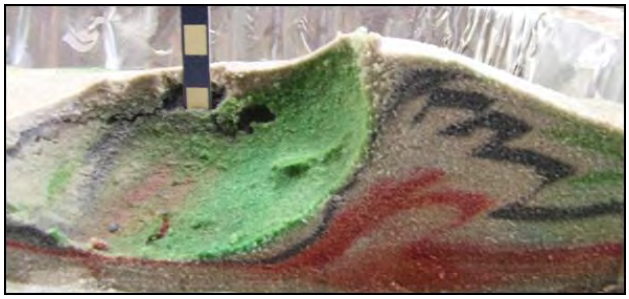

Figure 3.4: Cut parallel to motion through the simple sand bulldozing experiment. The depression with the cm-scale is from where the rock used to simulate a hummock/ridge front has been removed. The originally horizontal colour layers are pushed into a duplex structure ahead of the hummock/rock.

Chapter 4:

Substrate Deformation Features Associated with Emplacement of the Jocotitlán Volcanic Debris Avalanche, Central México

In the spirit of:

"Life comforts the disturbed and disturbs the comfortable."

Dan Millman

Substrate Deformation Features associated with the Emplacement of the Jocotitlán Volcanic Debris Avalanche, Central México

A. Dufresne[1], S. Salinas[2] and C. Siebe[2]

Journal of Volcanology and Geothermal Research (2009), accepted for publication

[1]Department of Geological Sciences, Canterbury University, Christchurch, New Zealand
[2]Departamento de Vulanología, Instituto de Geofísica, Universidad Nacional Autónoma de México, Mexico D.F., México.

ABSTRACT

An impressive debris avalanche deposit is preserved at Jocotitlán volcano in Central Mexico. The northern flank of this edifice collapsed ~ 9,690 years B.P. resulting in a 80 km^2-covering clast-supported deposit that lacks substantial matrix, fine, weak or hydrothermally altered materials. The deposit can be subdivided into three morphologically distinct areas which are each accompanied by specific, and often unique, deformation features in the underlying and adjacent volcaniclastic and lacustrine sediments. From these features, a complex history of pre-and-syn-avalanche events was reconstructed beginning with edifice-spreading on the weak substrate material prior to and in preparation of part of the flank collapse event. The north-eastern flank in particular was strongly coupled with the deforming substrate material as is still evident in its extensional profile and the unique mode of failure during the catastrophic event resulting in the deposition of what resembles non-volcanic blockslide deposits rather than the typical hummocky volcanic debris avalanche morphology. This latter type of failure occurred at the north-western flank of Jocotitlán volcano where few signs of substrate interactions are preserved in a deposit dominated by large conical hummocks. In addition to substrate response, interaction with pre-avalanche topography in the eastern deposit area facilitated the emplacement of a lobe roughly perpendicular to the flank failure direction, at apparent high emplacement velocity, and with longitudinal ridges as its most striking surface expression.

4.1. INTRODUCION

Volcanic sector collapse events are common characteristics of strato- and composite-volcanoes world-wide and have produced voluminous debris avalanche deposits altering the shape of the volcano edifice and their surrounding landscape. The deposits have volumes of up to tens of km^3; and in rare cases hundreds of km^3 have been reported. Areas devastated typically range from a few to 1,000 km^2, with distances from source reaching 10 to 100 km; exceeding 100 km in the cases when avalanches transformed into more mobile debris flows. In Mexico, 48% of the edifice-forming volcanoes are currently known to have produced one or more large debris avalanche deposits (30 deposits recognized at 21 volcanoes; all data from Dufresne et al. 2008). Interaction of these debris avalanches with their runout path material is often reported and substrate relation to avalanche and sector collapse dynamics is the focus of this study.

Jocotitlán volcano is an andesitic-dacitic composite volcano situated circa 60 km WNW of Mexico City. When part of the edifice collapsed to the NNE 9,690 years B.P. (Siebe et al., 1992) it changed the local landscape from a broad volcaniclastic and lacustrine sediment- and lake-filled valley to today's hummocky topography of the clast-supported Jocotitlán debris avalanche deposit.

Deformation features within the sediments underneath and adjacent to debris avalanche deposits are used in the study of avalanche emplacement processes, and help to discern the exact timing of events, i.e. whether deformations occurred (1) before avalanche emplacement due to some local or regional process (e.g. seismic, tectonic, volcano spreading), (2) during avalanche emplacement as a direct consequence of interaction with the moving avalanche material, or whether (3) they are the result of post-emplacement loading by the avalanche mass or some other mechanism unrelated to avalanche emplacement (e.g. tectonic, seismic, etc.). Herein we report the sediment deformation features found in and around the Jocotitlán volcanic debris avalanche deposit and discuss their timing and relation to its emplacement.

4.2. REGIONAL SETTING

The Jocotitlán volcanic edifice is located in the central part of the Trans Mexican Volcanic Belt (TMVB) within the northern Toluca Basin (Ixtapantongo Basin; Figure 4.1). Its current summit reaches a height of 3,950 m above sea level. To the north of Jocotitlán volcano lies the active Acambay Graben, a feature in NNW-SSE extension, roughly perpendicular to the volcanic arc axis (Suter et al., 2001). Its extensional regime reflects the overall tectonic nature of the entire TMVB in recent geological time (Suter, 1991).

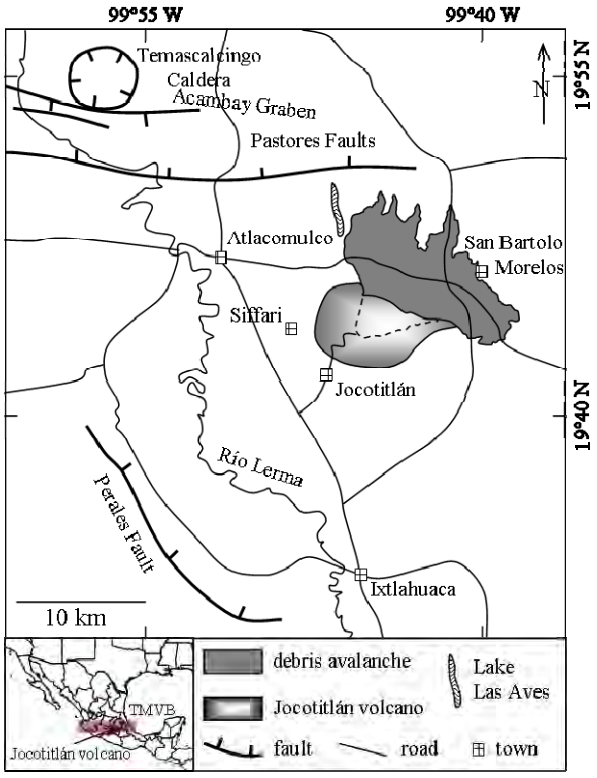

Figure 4.1: Sketch map showing major tectonic features and relevant towns in the vicinity of Jocotitlán volcano.

South of Jocotitlán is the inactive Perales Fault, a normal fault trending roughly NW-SE, and which belongs to a NNW-SSE striking Basin and Range province normal fault system that predates the Acambay Graben system (Suter et al., 2001). A series of basaltic-andesitic scoria cones and few dacitic domes are scattered throughout the Toluca Basin. Jocotitlán last erupted 680 ± 80 years B.P. (Siebe et al., 1992) and is at present in a state of dormancy.

4.2.1. Paleoclimate

From a study at Almoloya Lake south of Jocotitlán, Ludlow-Wiechers et al. (2005) reconstructed the regional Late Pleistocene – Holocene paleoclimate of the central Mexican highlands. Between 11,500 and 8,500 years B.P., the vegetation was very similar to today's moist to sub-humid climate. Cold temperatures before 10,800 years B.P. changed to temperate and warm-temperate conditions that lead to pine forest growth around 10,000 years B.P. A considerable drop in lake level in Central Mexico is inferred from this and other sites to have occurred around 8,400 years B.P. Hence at the time of sector collapse and debris avalanche emplacement, shallow lakes were wide-spread in the central highlands.

4.3. EDIFICE AND DEBRIS AVALANCHE MORPHOLOGY

Steep slopes mark the sides of the Jocotitlán edifice, and its current summit rises 1,300 m above the surrounding landscape which is composed of lava flows, volcaniclastics, and lacustrine sediments. From west to east, morphologically distinct areas of the edifice and debris avalanche deposit can be distinguished (Figures 4.2 and 4.12).

The northern and north-eastern sections of the edifice are scarred following the catastrophic collapse around 9,690 years ago (Siebe et al., 1992). Previously, one single collapse scarp has been outlined by Siebe et al. (1992), within which two distinct source areas can be identified based on edifice morphology and relation to collapse debris distribution. A large, horse-shoe shaped scarp opening to the NNE and extending to the foot of the edifice characterizes the north-western section, whereas collapse of the north-eastern sector produced a long and steep failure surface. Post-collapse volcanic activities in the form of dome extrusions and associated pyroclastic deposits as well as erosional overprinting obscure the original collapse geometry, particularly in the western area.

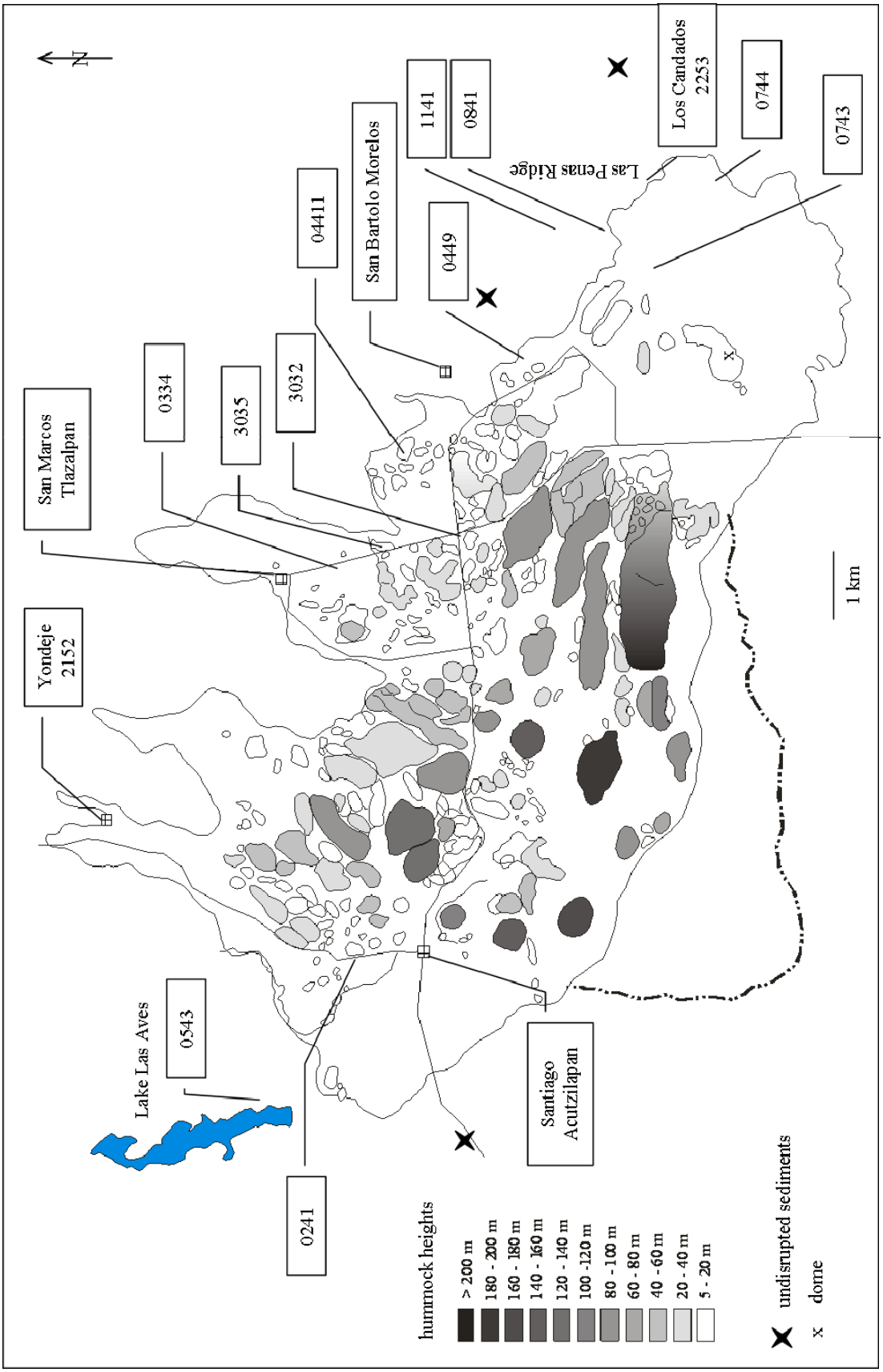

Figure 4.2: Map showing morphological characteristics of the Jocotitlán debris avalanche deposit and outcrops (labeled by numbers as described in the text). Avalanche deposit boundary modified from Siebe et al. (1992).

In its western part, the deposit features strikingly conical hummocks with individual heights of up to 125 m in the proximal zone. With distance from source these grade into smaller hummocks and hummock clusters. The hummocks form alignments radial to source pointing back to the now partially infilled horseshoe-shaped area of the collapse scarp. Debris from here spread over 90°. Near the western margin (Figure 4.4 a) the debris avalanche topography changes abruptly from the thick hummocky deposit to a lower-lying area with few smaller hummocks and ridges visible above the later lake infill. Currently, Lake Las Aves fills part of the north-south trending valley to the northwest of Santiago Acutzilapan; its extent at the time of debris avalanche emplacement remains subject to speculation, but it might have extended to this change in topography at the western margin, offering a potential explanation for its existence. A similar step in topography is seen near San Marcos Tlazalpan accompanied by a change to a flatter, lower-lying distal area with few small, isolated hummocks. Although lacking the topographic step, distal areas of scattered hummocks have also been observed at the Parinacota debris avalanche in Chile (Clavero et al., 2002). Overall, the major volume of the material in the western depositional area was emplaced directly to the north of the collapse scarp and current edifice summit, with less spreading to the north-west and north-east.

On the east side, the edifice is elongated in an E-W orientation and bears a ~ 3.5 km long, steep scarp which extends to the foot of the volcano. The edifice elongation direction and scarp strike coincide with the major fault orientations in the area; however no surface trace of an active fault extending beyond the volcano is recognized. Viewing this ridge from the north lends a step-like impression to its profile, stepping down and extending towards the east (Figure 4.3 a, b).

The long and steep collapse scarp is the source area of the middle and eastern part of the debris avalanche deposit. Boulders in excess of 4-5 metres in diameter make up part the easternmost escarpment of this ridge; however, dense vegetation restricts access to this area. Large landslide ridges or blocks up to 200 m high and 3 km long, with an overall east to west orientation mark the middle part of the deposit. Like a jigsaw-puzzle these ridges can be visually retrofitted into one coherent piece of landscape which fits back into the failure scarp of the Jocotitlán ridge (see Siebe et al., 1992 and reconstruction in Figure 4.3 c).

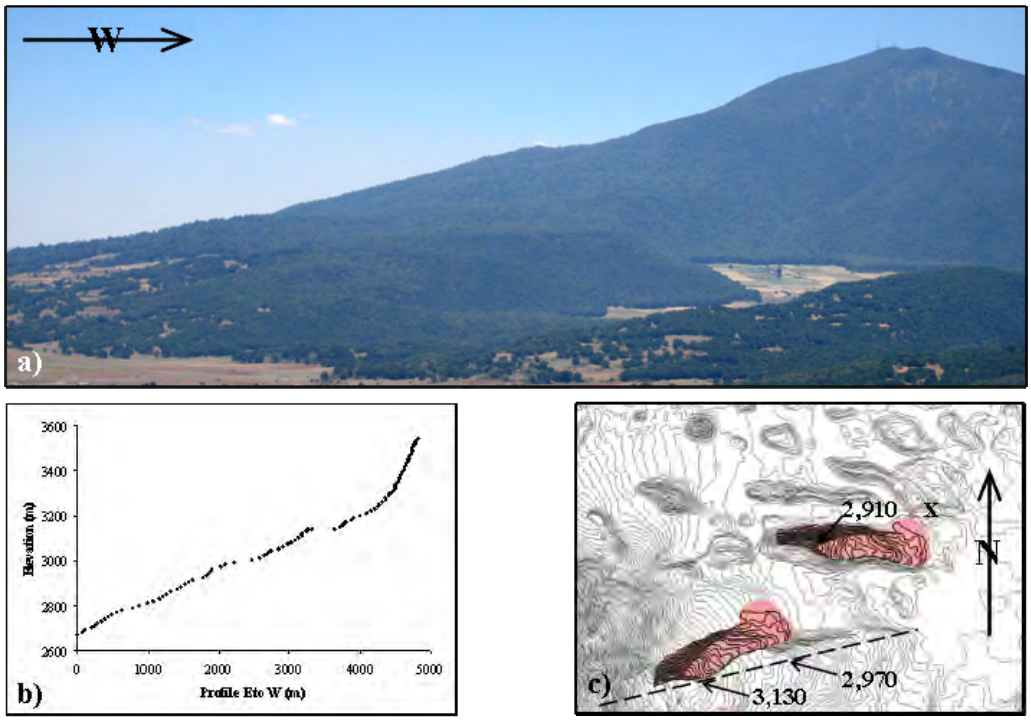

Figure 4.3: Edifice ridge extending to the east from Jocotitlán volcano: b) shows a four-times vertically exaggerated profile (see dashed line in c) from east to west to highlight the topographic steps seen in a). Image c) shows a jigsaw-fit reconstruction of the blockslide component of the debris avalanche resulting in a failure height of 220 m.

The morphological resemblance of this deposit area to blockslides (e.g. Green Lake, New Zealand; Hancox and Perrin, 1994) is striking. Initial failure was directed to the NE , but a change in travel direction occurred almost immediately and is still documented in the rotation of the more distal blocks towards the ENE roughly around point ‘x’ in Figure 4.3 c. The blocks came to rest very close to their source; the toe of Loma Alta was translated roughly 2.3 km, whereas the rest of the initially coherent block disintegrated increasingly with distance travelled, resulting in smaller blocks or hummocks further from source similar to toreva block disintegration at the Socompa debris avalanche (van Wyk de Vries et al., 2001). Similar large blocks at the failure scarp foot are present at other volcanic debris avalanche deposits (e.g. Avachinsky, Ponomareva et al., 2006; Parinacota, Clavero et al., 2002; Socompa, van Wyk de Vries et al., 2001; Shiveluch, Belousov et al., 1999) and several rock avalanche deposits (e.g. Carlson, US-Idaho, Shaller, 1991; Nozzle Slide, Canada, Eisbacher, 1979; Blackhawk, US-California, Johnson, 1978). Traditionally, toreva blocks are defined as a landslide consisting of a single large mass of undisrupted material that underwent backward rotation (Reiche, 1937), but is today mainly used in the volcanic

literature. The non-volcanic landslide literature today usually refers to these as slump blocks. We prefer the term 'blockslide' for the features at Jocotitlán, because they are not 'classical' volcanic toreva blocks in that they are not found at the foot of the horseshoe-shaped scarp and are not in association with the 'typical' debris avalanche part of the deposit. Instead, these hills, with Loma Alta being the most prominent, form their own unit with their own distinct failure scarp and can be retrofitted to one coherent unique part of the edifice, which is not described for toreva blocks elsewhere.

An interesting feature at the eastern side of this blockslide is the sharp line in topography, where we presume a significant difference in elevation existed before edifice failure. Coherent with the travel direction after rotation of the blockslide, material kept moving after or while the blocks came to rest, and further disintegrated when tumbling over the topographic step and spread into the lower-lying landscape, following topography to the southeast (see section 4.4.6 'Eastern lobe' below). A similar change in debris travel direction has been observed at the periphery of toreva blocks at Socompa and Parinacota volcanoes (van Wyk de Vries et al., 2001; Clavero et al., 2002).

Travel direction of this eastern lobe is documented by the orientation of elongate ridges, alignment of small distal hummocks, small-scale substrate deformation features, and trajectories of ejected debris avalanche boulders (see below). As stated above, the source of this lobe is most likely disintegration of the blockslide at the step in pre-avalanche topography since no singular source exists to the WNW, and spreading of debris from the western debris avalanche area prior to blockslide failure is unlikely.

Large portions of the transition area from blockslide to the eastern lobe are flat due to later infill by fluvial deposits that are more than 7 m thick. The kidney shaped dome ('x' in Figure 4.2) within the eastern debris avalanche lobe is of dacitic composition. Its material is glassy, weakly flow-banded and contains few phenocrysts of plagioclase, minor pyroxene and few oxyhornblende. Jocotitlán's lavas are similar in composition but have a distinctly vesicular groundmass with abundant phenocrysts of plagioclase and pyroxene up to 3 cm in size, and lack hornblende.

4.3.1. Morphology summary and emplacement synopsis

Morphological investigations revealed two distinct source areas within the collapse scarp correlating with morphologically distinct debris avalanche deposit areas. The western scarp resembles the typical horseshoe-shape observed at many volcanic edifices which have undergone major sector collapse events in their past, whereas the eastern scarp is very long and steep resembling blockslide failure surfaces as observed in mountainous areas. Furthermore, the step-like profile of the eastern Jocotitlán ridge suggests edifice extension/spreading or slow failure towards the ENE (this possibility is reviewed in the discussion section).

In short, failure of the central north-facing section of Jocotitlán volcano led to emplacement of debris with radially aligned hummocks which decrease in size away from the source. The eastern section of the edifice failed towards the north-east and material remained as larger blocks which deposited relatively close to source. The pre-collapse topography in this area most likely comprised a sharp transition to a lower-lying valley, and interference with this topography caused materials of the large blocks to fail to the ESE and further disintegrate when moving over the topographic step, emplacing a deposit with elongate ridges aligned in flow direction into the lower-lying area.

4.4. SEDIMENT DEFORMATION FEATURES

Substrate deformation features contain valuable information for deciphering processes associated with the emplacement of geological mass movements. At Jocotitlán, each morphologically distinct deposit area is associated with specific substrate features that are dominant in and often unique to the specific morphological domain. Again, features are described from west to east. All values for structural measurements are given according to European convention as dip direction and dip angle (*XXX/YY*), unless otherwise stated.

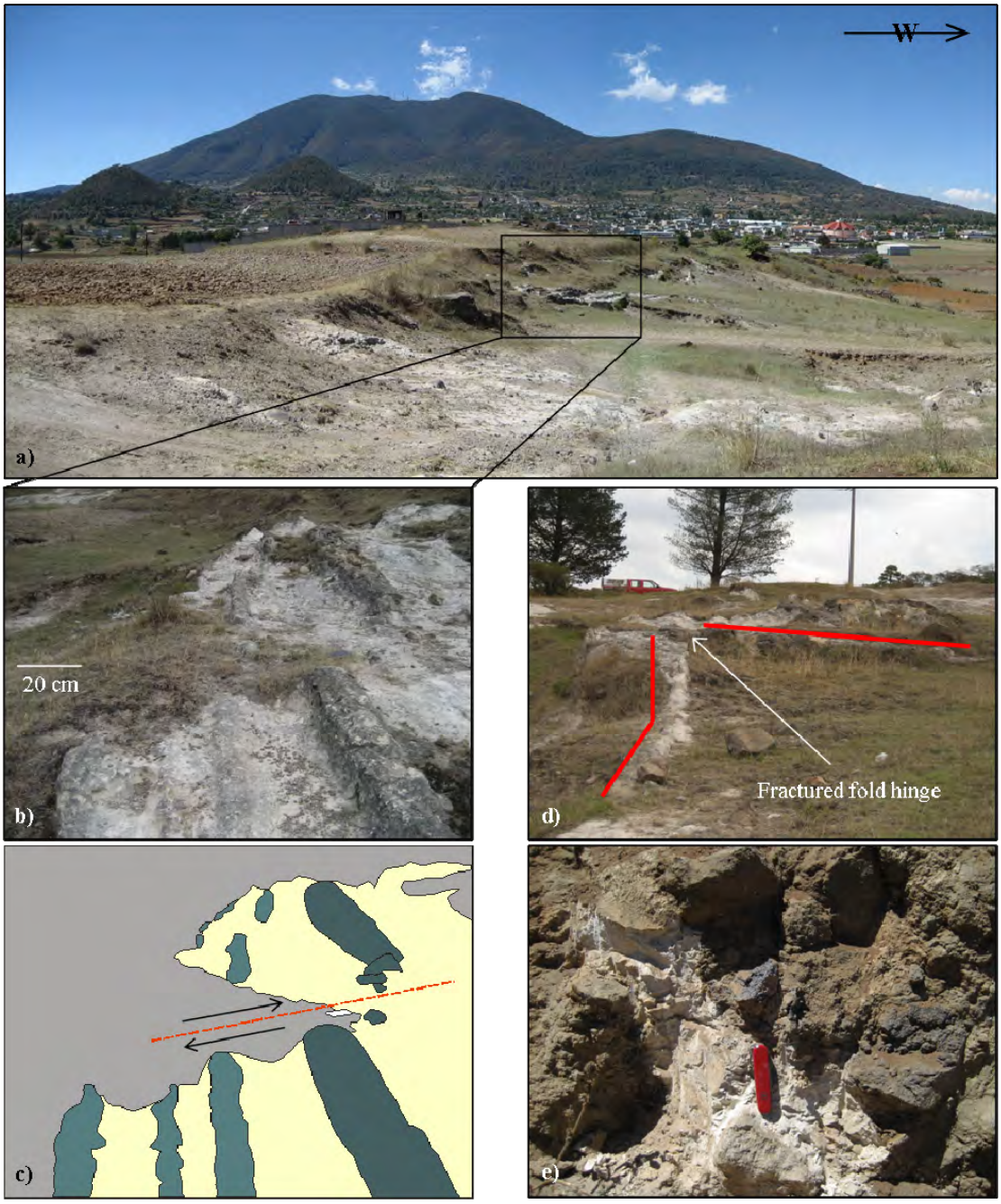

Figure 4.4: Substrate deformation features near western periphery (location 0241). a) View is looking south towards the source area. In the foreground are deformed lacustrine sediments with volcaniclastic beds situated near the western deposit margin at a marked change in topography; b) Close-up photo and interpretive sketch (c) of offset and tilted volcaniclastic beds of ~ 20 cm in thickness; d) Northward continuation of folded and faulted lacustrine beds depicted in c). e) The only evidence of substrate incorporation within the western deposit area was found circa 1 km north from the outcrop shown in d).

4.4.1. The western area

Post-avalanche lake deposits have infilled the lower-lying areas between hummocks and prevent access to the avalanche base. However, at the steeper parts near the western deposit margin disrupted sedimentary units are exposed (0241 in Figure 4.4).

Here, volcaniclastic and lacustrine layers have been upturned, faulted, folded, and offset. From their originally horizontal depositional position they have been tilted to almost 90° with a N-S strike; and it is only in the vicinity of this outcrop (further North, i.e. down-motion; Figure 4.4 e) that evidence of substrate incorporation is found within this western area of the deposit. Elsewhere, the clast-supported debris avalanche is free from entrained material, in addition to being free from fine-grained matrix material.

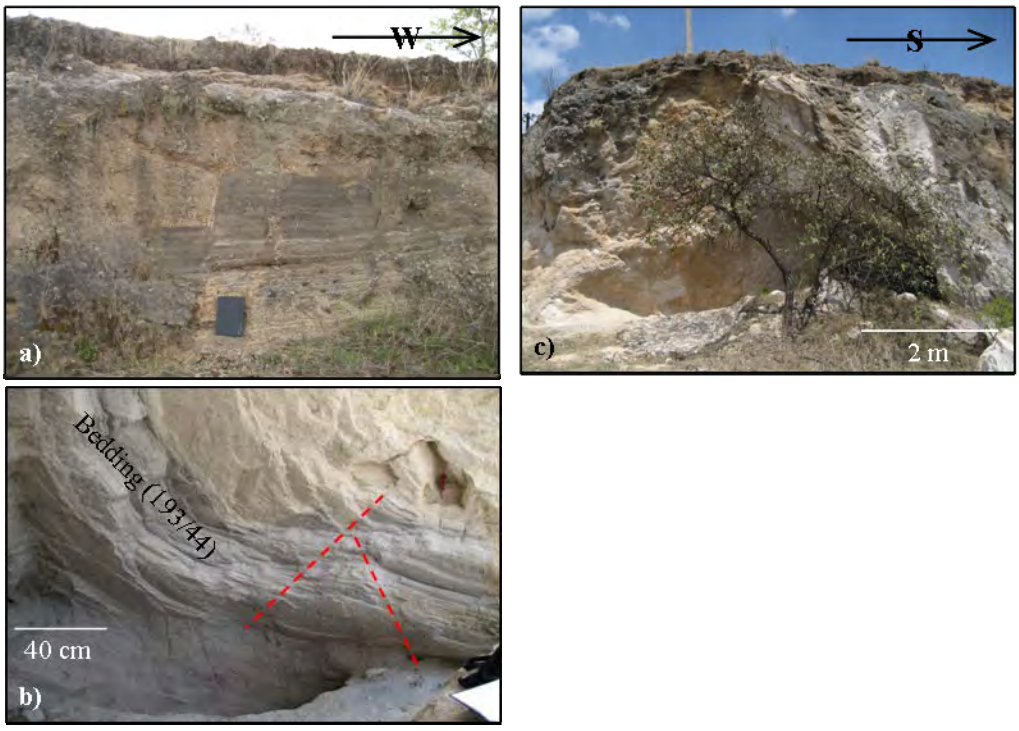

Figure 4.5: Bulldozed sediment deformation features near San Marcos Tlazalpan just north of the prominent step in avalanche topography to the lower-lying area with isolated hummocks: a) Faulted indurated near-horizontal (090/12) pumice units are offset ~30 cm by a normal fault (027/75); b) bulldozed sedimentary units at location 3032: bedding orientation is shown for volcaniclastic layer which is affected by conjugate fault sets in an E-W compressional regime. Overlying these are lacustrine sediments (yellow-white colour); c) down-motion end of hummock. The faulted sediments shown in b) are located behind the tree dipping to the right.

North of 0241, within the town of Yondejé, there is a small exposure of mingled volcaniclastic sediments. Westwards, towards the current shore of Lake Las Aves, tilted, indurated volcaniclastic units are exposed (location 0543 in Figure 4.2).

Near San Marcos Tlazalpan, just north of the step in topography described earlier, layers of lacustrine and volcaniclastic sediments are disrupted and show small-scale

faulting (Figure 4.5 a). Debris avalanche cover is scarce in this lobe and is mainly found as isolated hummocks throughout the valley.

South of this location, and within the hummocky avalanche deposit section, layers of volcaniclastic and lacustrine deposits are found tilted in front of a debris avalanche hummock (location 3032 in Figure 4.2; photos in Figure 4.5 b, c). These units dip south towards the volcano at 40-45°. Conjugate fault sets suggest an E-W compressional regime, whereas small-scale thrust faults concur with avalanche travel and layer tilting direction.

4.4.2. Blockslide

The large ridges of Loma Alta and the rest of the blockslide are predominantly composed of angular to sub-angular dacite clasts, and are, like the western deposit debris, free from fine matrix material or entrained substrates. At its easternmost toe, Loma Alta's base is made up of layered volcaniclastic material, most likely of the original edifice ridge. Basal indurated pumice units and the dacite clasts are in places intricately linked by faults cutting through both. Whether this faulting occurred pre-, syn- or post-avalanche emplacement is unclear.

4.4.3. Mingled sediments (middle and east)

The most striking sediment deformation features are found just north and northeast of the blockslide within the debris avalanche, as well as outside the deposit margin to the north of the eastern lobe (see section 4.4.4. below). The first are mingled sedimentary units found associated with debris avalanche hummocks (bold location numbers in Figure 4.2; photos Figure 4.6). These compacted, yet non-indurated, mingled units are composed of clasts of volcaniclastic sediments (mainly pumice fall) on the order of a few metres in diameter with preserved stratigraphy. They are surrounded by ductily deformed, mingled lacustrine and volcaniclastic sediments; layering is preserved and minor faulting is pervasive. The clasts themselves are rounded, and little 'tilting' from the original layer-orientation occurred despite disruption. The mingled materials surrounding these clasts consist of lacustrine, surge, ash-and-pumice fallout lenses. Some lenses are folded, others stretched and contorted; thrust faults exist. Overall, there is very little mixing of materials from the different units.

Figure 4.6: Mingled sedimentary units associated with hummock locations. The photos show outcrop numbers 0449 (a, b), 0743 (c, d), 0335 (e, f, h) and 04411 (g); A5 field notebook, hammer, compass, spade or excavator for scales.

4.4.4. Location 0841

Outside of the eastern debris avalanche lobe's northern margin, along an over one km-long outcrop at the side of the Las Peñas Ridge, features almost identical to the mingled sediments within the debris avalanche boundary are exposed (Figures 4.7 and 4.8).

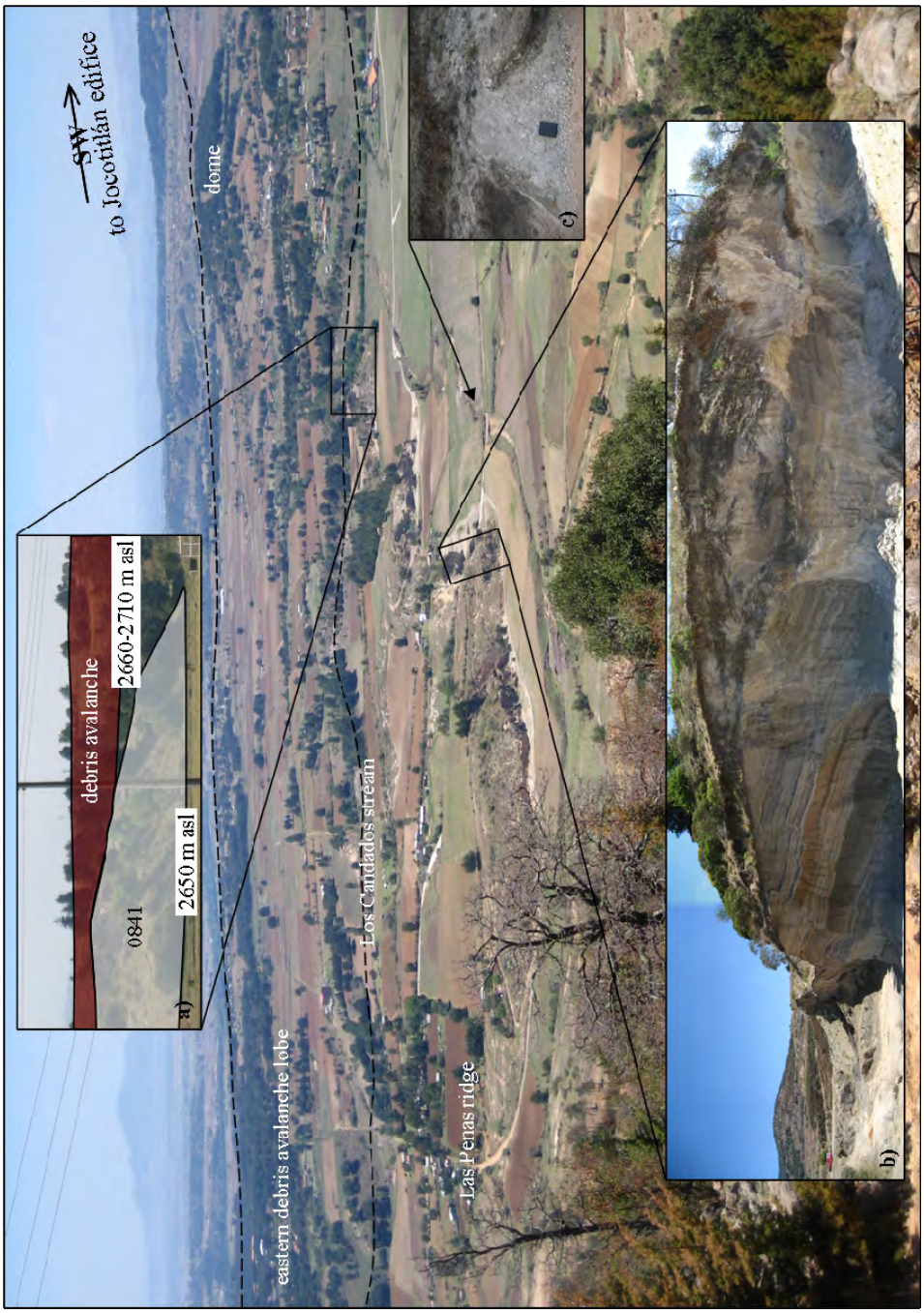

Figure 4.7: View from the Las Peñas ridge down to S. The eastern lobe and the > 1-km long outcrop 0841 are clearly discernible. The eastern lobe boundaries are outlined by dashed lines. Insert a) shows the outcrop in relation to the base of the debris avalanche deposit; b) shows a small quarry along this outcrop displaying the scale of large clasts (the section is about 8 m high) and the nature of the surrounding mingled material. Features along the creek (c) are described in section 4.4.5. of the text.

The major difference to the mingled units inside the deposit is that the clasts here are an order of magnitude larger (up to 10's of metres across). Fresh exposures of lacustrine material show small-scale folding (Figure 4.8 f), attesting to the highly ductile, saturated condition of the material at the time of deformation. Units in the rounded to sub-angular clasts cover all types of volcaniclastic materials (pumice fallout, ash, surges, etc.). Possibly, due to the size of the clasts, more evidence of faulting is well preserved within them than in the smaller clasts within the debris avalanche which bear little remaining evidence of deformation. Measurements of a number of conjugate fault sets, individual thrust faults, and bedding surfaces are represented in Figure 4.8 c. Consistently across the different clasts it is possible to detect a NE-SW compressional deformation regime. Beds dip consistently to the south with few exceptions dipping in the opposite direction.

On top of the southern end of location 0841, adjacent to the debris avalanche margin there is a small outcrop of a thin (< 1 m) unit consisting of sub-angular to sub-rounded lava fragments of dark, glassy appearance with plagioclase and pyroxene phenocrysts (up to 2 mm in size) present in the glassy groundmass. These clasts are surrounded by coarse-to-medium sandy material. The material in this small exposure consists of small rounded clasts set in a fine matrix and resembles debris flow facies. Large clasts (up to 3 m in diameter) of the same composition as the debris flow clasts are found embedded in the sedimentary strata below.

4.4.5. Sedimentary cover adjacent to location 0841

Within the flat landscape outside the DA margin, to the West and adjacent to location 0841, a small creek has cut into the fluvial and volcaniclastic cover (Figure 4.7 c). Disrupted sediments display diapirs, folds and faults of no preferential orientation; bedding dips are mainly to the SSW. At the northward extent of the creek, a small hillock presents sedimentary strata dipping at (226/55) with faults oriented (326/71) and (112/88).

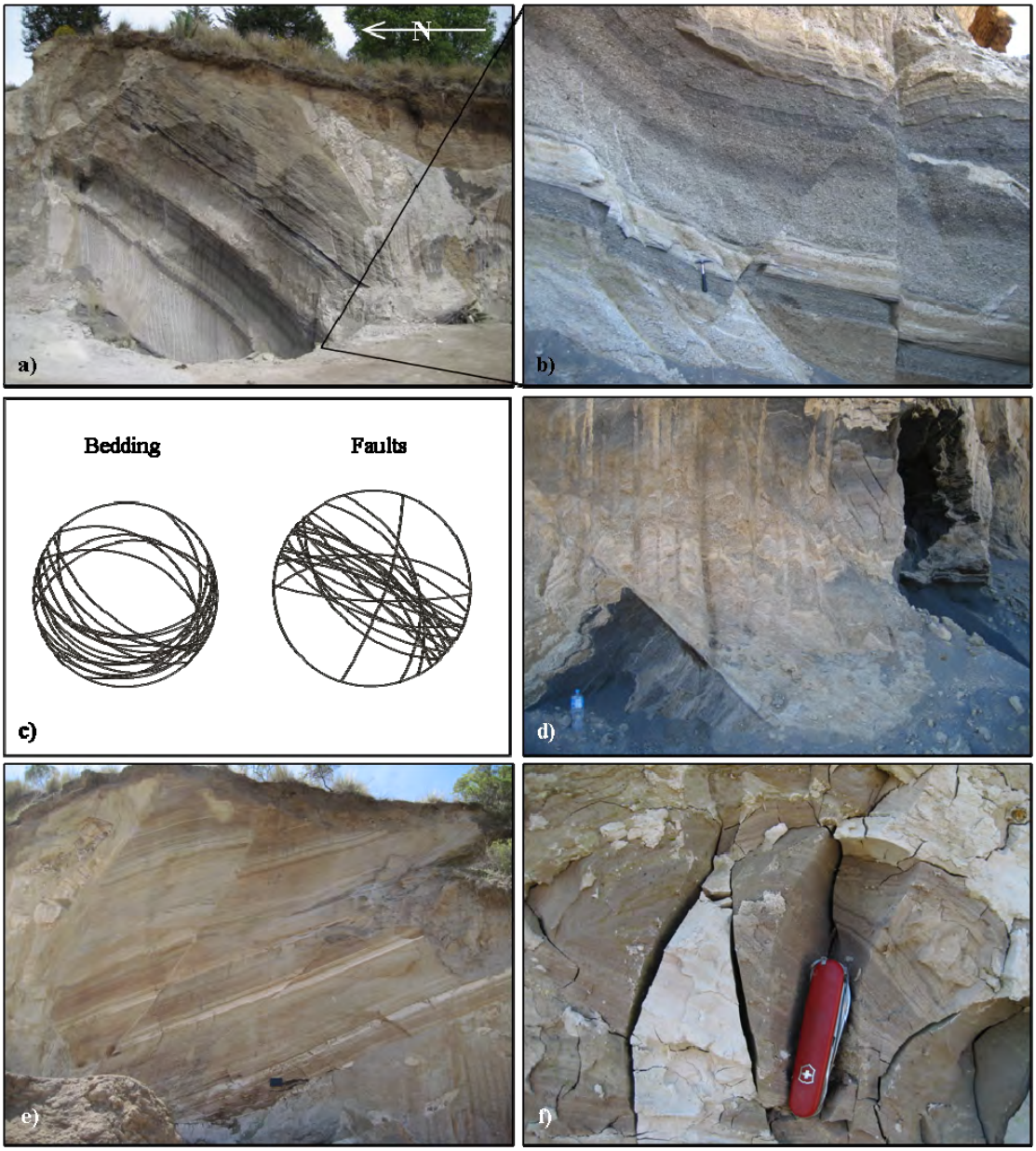

Figure 4.8: Exemplary sections along location 0841: a) pumice fallout and surge layers of the faulted clast (~ 8 m in width) are juxtaposed to lacustrine deposits (wedge to the right of clasts) that contain disrupted lenses of volcaniclastic material; b) Close-up of conjugate fault sets within another clast exposed in the ~ 4 m deep hole in the foreground of a); c) Stereonet projections of fault and bedding orientations; d) Shows a thrust fault (1.5 l water bottle for scale); e) This photo was taken at the same location as seen in the overview in Figure 4.7a); A5 notebook for scale; f) Close-up of intricately folded lacustrine units (the lacustrine units appear whitish where weathered, and light-brown in fresh exposures).

4.4.6. Eastern lobe

Beneath the longitudinal ridges of the eastern lobe, reverse faulting on the cm-scale (Figure 4.9 b) preserves evidence of debris avalanche interaction with the volcaniclastic substrate. Here, along the Los Candados stream is one of the few locations where the actual base of the debris avalanche is exposed. It variably lies

between 2,660 and 2,710 m above sea level, is marked by the occurrence of springs, and is underlain by older volcaniclastic units. Fault orientation (280/79) corresponds to the ridge elongation and travel direction. Small-scale normal faults are also visible in the substrate at the steep margin. These north-and-south-dipping normal faults are the result of material extension beneath the avalanche overburden and lack or removal of lateral support.

The impact fold caused by an ejected boulder from the moving/stopping avalanche debris into soft sediments (Figure 4.9 g) has a fold axis strike of 320°, perpendicular to impact direction. Near the small field of ejected boulders lies an isolated debris avalanche hummock, nestled into the side of the Las Peñas ridge (Figure 4.9 d). Mingled volcaniclastic units are also present within the avalanche body (Figure 4.9 e, f). Post-avalanche emplacement loading features are present in the form of vertical clastic dykes of volcaniclastic material undisturbed by avalanche motion (Figure 4.9 a). The north-eastern margin is steep and a later debris flow facies is present at the other side of Los Candados stream.

The southern margin of the eastern lobe is not well exposed or easily accessible. Close to the edifice, large pieces of indurated volcaniclastic layers and mixed-in pumice units form part of the upper debris avalanche deposit (location 0341). One unit is cut by a fault (340/80). These units are interpreted as rafted material from the blockslide/edifice ridge toe.

Further east, the weathered base of the debris avalanche is exposed at ~ 2,650 m above sea level (location 2058) where light brown pumice fallout forms the substrate. Mixing of substrate and avalanche basal material is evident. The deposit thickness at this location is of the order of ~ 20 m with a steep margin.

The easternmost distal toe of this avalanche lobe thins in places to form a gently sloping margin, whereas in immediately adjacent regions large elongate (> 10 m long axis) hummocks form a steeper debris avalanche perimeter (location 0744). Clusters of individual avalanche boulders (< 1 m in diameter) are found beyond the gently sloping distal avalanche margin. Such spray-zones have been observed, on a larger scale, at Nevado Huascarán (1970 avalanche; Stadelmann, 1983) and, on a smaller scale, beyond isolated hummocks of the distal Parinacota debris avalanche (Clavero et al., 2002).

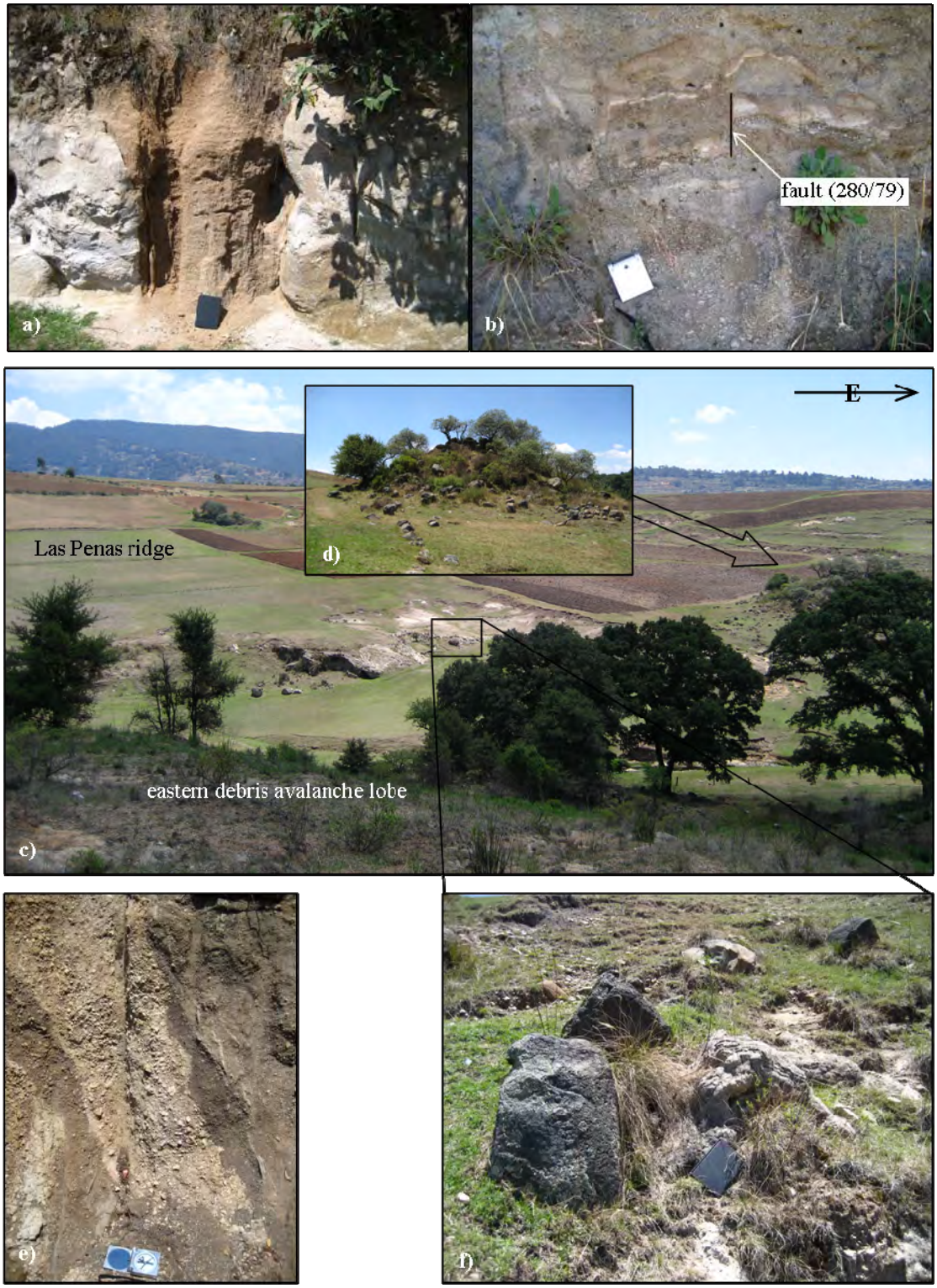

Figure 4.9: Substrate features as found at the base of the eastern lobe (northern margin along Los Candados): a) Vertical injection feature of volcaniclastic material into the lower debris avalanche was produced after the avalanche had come to rest since no flow disruption is recognized in the dike; b) Small-scale faulting in substrate at the basal debris avalanche contact. Both views are to the south.; c) Photo taken from the Las Peñas ridge: at this location an isolated hummock (d) and ejected debris avalanche boulders (f) are present, demonstrating the high mobility of individual debris avalanche components. Mingled volcaniclastic units as described elsewhere within and outside the deposit boundaries are also found in this area (e).

4.4.7. Fractures and undisrupted sediments

Small-scale conjugate fracture sets are widespread in indurated volcaniclastic sediments within and outside the debris avalanche deposit, and are no surprise in a tectonically active region like the Toluca Basin. Strike orientations scatter between 022-060, and 130-170 to the West outside the DA deposit, and have values of 010 and 112 at the SE end of Loma Alta within the DA deposit.

Example locations of undisrupted volcaniclastic sediments in the debris avalanche vicinity are situated west of Santiago Acutzilapan, just outside the margin near San Bartolo Morelos and on the eastern side of the Las Peñas ridge (stars in Figure 4.2).

4.5. DISCUSSION

At the Jocotitlán debris avalanche the different morphological avalanche units correspond with distinct areas of failure within the large source scarp, and each morphological unit is accompanied by characteristic or predominant sediment deformation features. The morphological observations and the distribution of deformed sediments in and around the debris avalanche deposit allow postulating the following hypotheses regarding avalanche emplacement and the conditions leading to edifice collapse:

A. Edifice failure, in the eastern section in particular, was influenced by pre-failure volcano spreading on weak substrate.
B. Volcano spreading accounts for the majority of the observed sediment deformation features.
C. Additional deformation by avalanche emplacement produced overprinting signatures in the underlying sedimentary record.
D. Break-up of the blockslide component and the change in the local pre-avalanche topography resulted in emplacement of the eastern lobe.

4.5.1. The pre-collapse landscape around Jocotitlán volcano

Prior to the catastrophic collapse, the landscape north of the edifice consisted of a broad valley filled with volcaniclastic material, lakes, dried-out lake bed material, and

fluvial runoff from the Acambay ridge and Jocotitlán edifice itself. Estimated average elevation directly to the north of Jocotitlán volcano lay at approximately 2,675 m (avalanche base at San Bartolo Morelos) to 2,700 m (Lake Las Aves) above sea level. At the longitude of San Bartolo Morelos a pre-avalanche topographic step of an estimated 80 m led into a lower valley to the east, which is inferred from the elevation of the distal avalanche base (lowest at 2,620 m a.s.l.) and extrapolations of the topography to the ESE of Jocotitlán volcano where several topographic steps exist. The most prominent step closely follows the 2,620 and 2,610 m contour lines.

4.5.2. The western failure area

Failure of the northern edifice sector, including the ancestral volcano summit, spread debris over an area of 38.3 km^2 with a spreading arc of ~ 90° onto the relatively flat topography of volcaniclastic and lacustrine sediments. This area displays the typical hummocky debris avalanche morphology (Ui, 1983; Siebert, 1984) with hummock size decreasing with distance. The strong and competent source material (large, angular dacite clasts; lack of fine matrix, no weak pyroclastic materials or hydrothermal alterations) and the relatively great thickness of the deposit with respect to its basal shear zone allowed for the formation of large, high angle of repose hummocks in radial alignment with respect to source (see Dufresne and Davies, 2008). In support and contrast, Clavero et al. (2004) and Shea et al. (2008) observed that hummocks at the Ollagüe and Mombacho debris avalanche deposits, respectively, show differences in slope angle according to their construction material: those consisting of single blocks of lava or coarse volcanic breccia have steeper slopes whereas those composed of weaker source and/or runout path material have smoother morphologies.

The main direction of emplacement was straight to the north of the current edifice summit with less material deposited in the distal and marginal areas which are characterized by noticeable changes in avalanche topography to lower-lying areas. These are dotted with isolated hummocks and ridges that have little avalanche material deposited between them. Clavero et al. (2004) and Siebert et al. (1995) have postulated that the encounter of water-rich environments or surface water in the runout path would change avalanche behaviour. Essentially, the encounter of saturated sediments can impede avalanche motion (depending on the degree of sediment saturation, its erodibility and degree of mixing with the avalanche), often

resulting in raised deposit margins. It can be envisioned that the thicker parts of the avalanche (i.e. hummocks and ridges) are able to retain their momentum despite a change in basal resistance and can continue moving beyond the avalanche margin. Where lakes are present one would also expect a dip in topography and avalanche motion into this environment would lead to a lower-lying deposit area and a potential transformation into debris flows through lake water incorporation into the moving avalanche debris. The western avalanche margin, the northern lobe near San Marcos Tlazalpan, as well as location 1141 outside the eastern lobe's margin are good candidates for pre-avalanche lake and river locations, and jumbled sediments are to be expected in an area saturated with water and overrun by individual avalanche fragments (i.e. hummocks). In this context, it is also possible that the impact of the debris avalanche onto the saturated sediments could have caused their disruption at a certain distance from the debris avalanche's edge at the western margin (near Lake Las Aves; location 0543) for two reasons: (1) the deposit's extent beneath the recent lake sediment cover is unknown and it is therefore possible that the distal avalanche toe lies closer to the deformed sediments, and (2) large geological mass movements can generate seismic signals comparable to seismo-tectonic events (Weichert et al., 1994). However, seismic liquefaction from activity unrelated to the sector collapse event is equally possible (coseismic liquefaction and sliding features are reported by Langridge et al. (2000) associated with the 1912 Acambay Fault rupture further to the north).

In this western deposit area, obvious substrate incorporation by the avalanche on the scale as observed in the middle and eastern area was not found; i.e. the substrate does not form parts of hummocks or distal areas. The mingled sediments found in the town of Yondejé (location 2152) are the only exception. The single clear evidence of interaction with runout path material is the displaced sedimentary package at location 0241, signifying the avalanche's ability to plough and push aside weak material; with minor mixing of the substrate material higher into the moving avalanche body as preserved down-motion from this location.

The overall scarcity of basal avalanche outcrops did not allow insights into the potential existence of shear bands at the avalanche base as observed at other volcanoes (e.g. Cantal, Schneider and Fisher, 1998; Roque Nublo, Mehl and Schmincke, 1999; Socompa, van Wyk de Vries et al., 2001) or at non-volcanic rock

avalanches (e.g. Artillery Peak, US-Arizona, Yarnold, 1993 and Black Canyon Breccias, US-Arizona, Johnson, 1978); nor is it possible to recognize whether avalanche and substrate were coupled as suggested for debris avalanches which resulted from volcano spreading on a weak substrate (e.g. Socompa, van Wyk de Vries et al., 2001).

4.5.3. The middle and eastern areas

The overwhelming majority of substrate deformation features is preserved in the middle (blockslide) part and just outside the northern margin of the eastern lobe (location 0841). We propose that pre-avalanche volcano spreading was the cause for the great predominance of substrates in these parts of the debris avalanche deposit. The idea of volcano spreading after van Wyk de Vries and co-workers (2001 and references therein) involves the slow failure of a volcano on weak substrates over which the edifice has constructed itself over time. Under the increasing overburden load, these weak substrates (typically pumiceous, other volcaniclastic sequences and lake sediments) slowly fail and extrude from beneath the volcano, inducing faults and failure planes within the volcano. Van Wyk de Vries et al. (2001) envisioned two different styles in this process: (a) ‘volcano spreading’ in which the volcanic edifice spreads with the substrate, slowly failing under extension, and (b) ‘substrate extrusion’ in which volcano and substrates are decoupled, meaning the substrate material is extruding from beneath the load, while the edifice itself sinks into the ‘gap’, essentially retaining its shape and steep slopes.

Indications of the involvement of weak substrate in edifice failure include the presence of mechanically weak substrate beneath the volcano and large amounts of these forming the basal and distal avalanche parts, a collapse scarp that extends to the foot of the volcano or further, the presence of substrate deformation features in the collapse scarp and near the edifice, and a topographic ring-shaped rise around the edifice from the folding and extrusion of substrates from beneath the volcano (Borgia and van Wyk de Vries, 2003; van Wyk de Vries and Francis, 1997). Volcano spreading-related debris avalanche deposits have been recognized at the Chilean volcanoes Socompa (van Wyk de Vries et al., 2001) and Parinacota (Clavero et al., 2004), and at Mombacho volcano in Nicaragua (Shea et al., 2008; van Wyk de Vries and Francis, 1997).

Here, in the case of Jocotitlán, the concept of volcano spreading will be evaluated against the possibility of (1) substrate bulldozing by the avalanche, which is a viable mechanism for substrate displacement and has been observed at various volcanic and non-volcanic mass movement deposits elsewhere (e.g. Ananievo rock avalanche in Kazakhstan, Abdrakhmatov and Strom, 2006; Socompa volcano in Chile, van Wyk de Vries et al., 2001; Baga Bogd rock avalanche in Mongolia, Philip and Ritz, 1999; Shiveluch volcano in Kamchatka, Belousov et al., 1999), and (2) post-emplacement substrate extrusion from beneath the avalanche body as a result of the sudden increase in overburden load.

4.5.4. Volcano spreading on a weak substrate contrasted with other hypotheses

From an aerial perspective, the distribution of mingled sedimentary units, their overall association with hummock location, and the correlation of blockslide failure direction with the compression direction as deduced from faults and folds within location 0841 sediments might suggest that bulldozing by the debris avalanche could have transported the substrates to their current locations. However, several pieces of evidence argue against this hypothesis.

Evidence (1): the location of mingled sediments at 0841 does not correspond to the specific avalanche travel direction in this area. Even though the blockslide initially failed to the NE, avalanche transport direction changed when it disintegrated over the topographic step to emplace the eastern lobe with a preferential motion direction from the WNW to the ESE; essentially perpendicular to the sediment compression direction.

Evidence (2): the debris avalanche base at this locality lies at least 10-20 m above the mingled sediments of 0841 (Figure 4.7 a; estimates exceed 60 m owing to the lack of exposure of the actual base of the sediment units at 0841) and it seems hence unreasonable that the avalanche ploughed the material ahead or to the side.

Evidence (3): on the W and SW side of Jocotitlán volcano, in an area where no debris avalanche exists, sediment deformation features (Figure 4.10) akin to the ones in discussion are present near the towns of Siffari and Jocotitlán. Features near Siffari (Figure 10 e) are not entirely straightforward in their interpretation as they have the strong appearance of layers deformed (folded with minor faults) as a consequence of or simultaneous event with diapirism as sometimes reported for seismically tectonized sediments (Harp et al., 2003; Tuttle, 2001; Galli, 2000). However, material near the

town of Jocotitlán closely resembles features observed at 0841 and it has undergone N-S compression. This observation is in compliance with loading of the edifice-underlying sediments at this location.

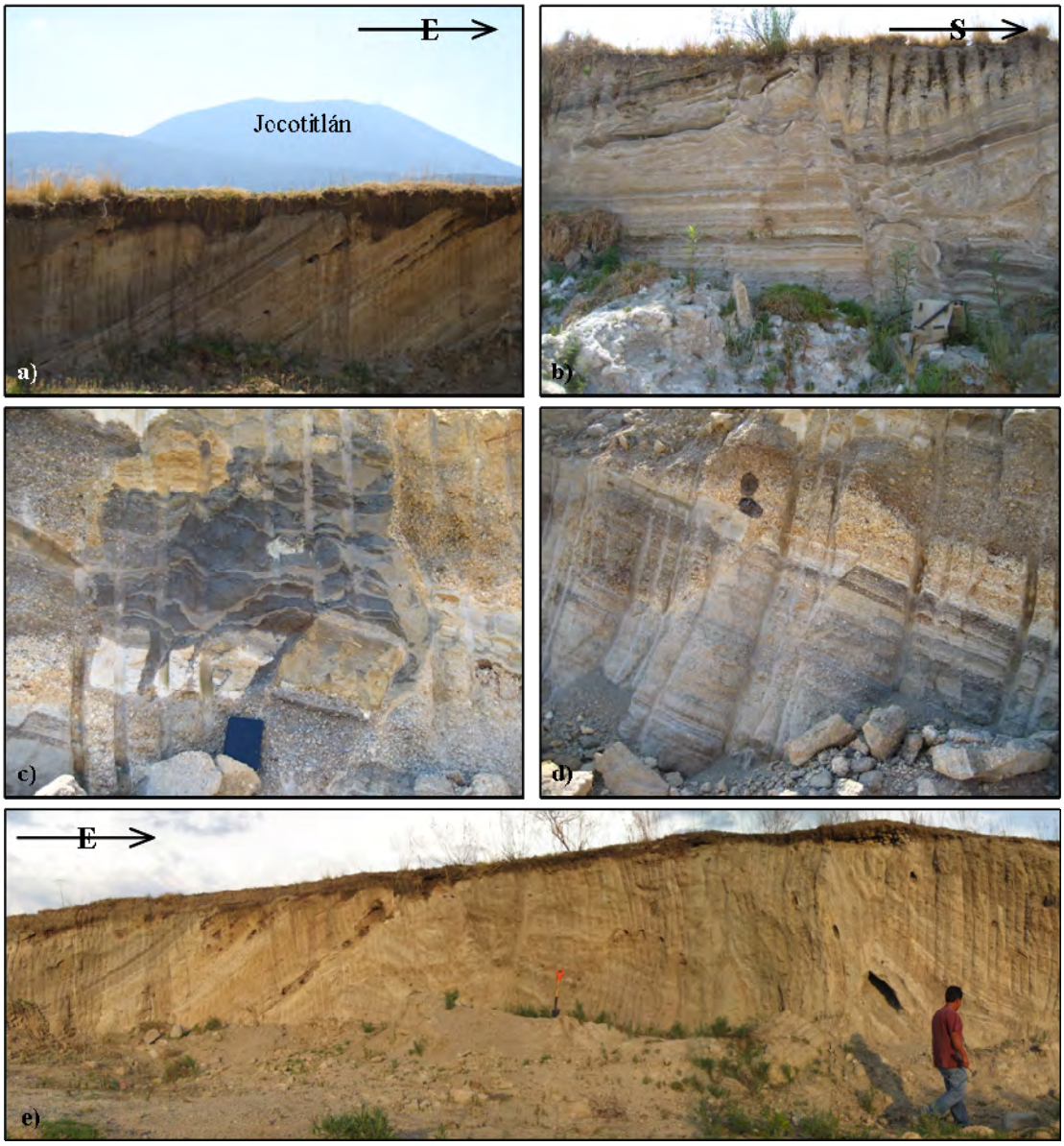

Figure 4.10: Photos a) through d) show deformed volcaniclastic sediments SW of Jocotitlán edifice, near the town of Jocotitlán. Photo e) was taken near the township of Siffari (see Figure 4.1). Sediments here are folded most likely in response to diapirism of either seismic or sediment loading and mobilization origin.

The morphology of Jocotitlán volcano strongly suggests ENE-ward extension of its eastern flank (as discussed in section 4.3, above) which supports a spreading origin of the deformation features: progressive erosion of the adjacent sedimentary support to the east of the edifice, together with pre-existing weaknesses within the edifice

(regional E-W trending normal fault system) favoured slow edifice creep or failure in this area, whereas the northern sector was/is supported by a higher altitude sediment-filled valley abutted by the Acambay ridge to the north.

In Figure 4.11, the bulldozing and volcano spreading hypotheses are contrasted. Images a) and b) illustrate the first two lines of evidence listed above. Image c) illustrates the process of volcano spreading adopted from van Wyk de Vries et al. (2001). In d) a modified version of their spreading concept fitting the particular case of Jocotitlán volcano is depicted. In this case, the entire eastern flank of the edifice is in motion over weak, mobilized, laterally unsupported sediments. Failure of the flank was pre-defined by normal faulting in response to basal edifice extension and faulting orientation coincides with the regional fault pattern.

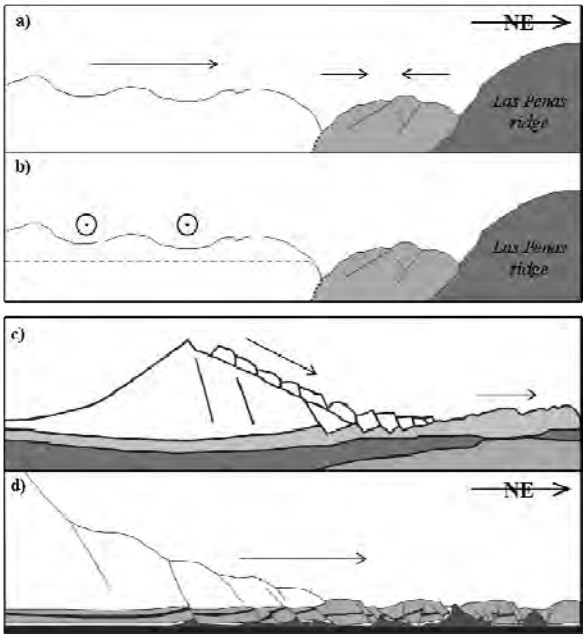

Figure 4.11: (A) Bulldozing scenario sketch contrasted with field relationships (b) that rule out this process as a cause for the features observed in sediments at outcrop number 0841; c) shows the volcano spreading scenario after van Wyk de Vries et al. (2001) and d) an adaptation of this idea to the Jocotitlán case with substrate deformation features reconstructed from field evidence and following analogue models by McClay et al. (2003); see text section 4.5.3.

Behaviour of the spreading substrate follows analogue experiments by McClay et al. (2003) in a study of delta sediments responding to increasing overburden pressure caused by gradual sedimentation. In their model, the sediments fail in extension on a mobile basal layer which is extruded upwards between the failing sediment units or

clasts. Faulting in these cases is normal. Only in the distal regions of the experiment, where the authors had introduced a slight increase in underlying basement slope, did compressional faults (thrusts) form. Although the tectonic setting of a delta region is markedly different from that of volcanic regions, substrate response to an increase in overburden load is a universal process as demonstrated by the similarity of deformation structures produced in the laboratory. The near-edifice substrates at Jocotitlán are not exposed and those found within the debris avalanche carry additional signs of disruption from avalanche emplacement (see below). Features observed in the distal part of the spreading substrate show striking similarities with the models by McClay et al. (2003) where distal faults are compressional due to the interaction with topography.

Further support for a volcano spreading scenario leading to edifice failure and debris avalanche emplacement is the fact that the majority of mingled sediment outcrops lay within the blockslide "shadow-zone" and generally at the northern debris avalanche margin, that is away from the source (and that includes the deformed sediments at Yondejé and at location 2253 in the eastern lobe). Combining the absence of mingled sediments at the eastern or southern margin of the eastern lobe or at the western deposit periphery, with the existence of such mingled material on the opposite side of the volcano suggests that post-emplacement extrusion of material from beneath the avalanche debris is not a viable explanation for their formation either.

4.5.5. Sediment deformation overprinting by avalanche emplacement

Mingled sediment clasts within the debris avalanche boundary are all one order of magnitude smaller than those exposed at location 0841. This and their association with hummock locations can be attributed to 'secondary' deformation during avalanche emplacement of the already compromised (by volcano spreading) sediments. Elsewise, no large-scale mixing of debris avalanche and substrate materials were observed and neither could any evidence be found for avalanche material sinking into weak material as for example observed at the northern lobe of the Llullaillaco debris avalanche in Chile. At Llullaillaco, avalanche material sank into the deposits of the local salt flats (Richards and Villeneuve, 2001). At other cases such as Mombacho (Shea et al., 2008) or Ollagüe (Clavero et al., 2004) sinking avalanche material produced raised margins and transverse ridges. At Jocotitlán, the

lack of substrate incorporation into the debris avalanche can be attributed to the fact that the substrate sediments themselves formed the base of the failing mass as a consequence of volcano spreading. Hence, the avalanche's base consists of a fine-grained layer less capable of erosion than coarser clasts. It is a common observation that volcanic debris and non-volcanic rock avalanche deposits retain their original source stratigraphy (e.g. Dulung Bar-Darkot rock avalanche in Pakistan, Hewitt, 2006; Flims rock avalanche in Switzerland, Pollet and Schneider, 2004; Pacaya volcano, Vallance et al., 1995; Popocatepetl volcano, Siebe et al., 1995; Blackhawk rock avalanche in US-California, Johnson, 1978; Elm rock avalanche in Switzerland, Heim, 1932), and the lack of mixing of the fine basal layer with the coarse upper avalanche unit is therefore no surprise.

4.5.6. The eastern lobe

The eastern debris avalanche lobe is characterized by longitudinal ridges indicating a WNW to ESE travel direction. Longitudinal ridges are an indication of higher spreading velocity in the longitudinal than the lateral direction (Dufresne and Davies, 2009); as would be expected from debris travelling down a valley path. Three observations show the eastern lobe's travel direction: valley orientation, longitudinal ridge strikes, and boulder ejection trajectory. Estimated minimum ejection velocity of this boulder at location 2253 is 60 m/s (216 km/hr). The eastern lobe's source can be narrowed down to three possibilities:

1. Pre-edifice-collapse avalanche deposit of some unknown source.
2. Spreading of western deposit part before blockslide emplacement.
3. Failure of the eastern side of blockslide down/over topographic step.

Evidence for (1): none; no source exists in WNW-ward projection. Evidence for (2): unknown but not impossible. Evidence and arguments for (3) include the blockslide rotation from a NE to an easterly direction roughly around point 'x' in Figure 3 and the pre-avalanche topographic step which would have facilitated failure and disintegration of the blockslide mass down into the NW-SE trending valley. Mingled sedimentary units beneath its northern margin suggest that at least in parts volcaniclastic layers involved in the pre-avalanche volcano spreading form the base of this lobe. Van Wyk de Vries et al. (2001) proposed that the extrusion of substrates

from beneath the Socompa toreva blocks resulted in a mobile avalanche lobe perpendicular to toreva block long-axis orientation in which debris avalanche and local lava flow clasts were rafted on top of the weak substrate. At Parinacota volcano, a debris avalanche lobe of similar orientation with respect to the toreva blocks is described (Clavero et al., 2002). At non-volcanic rock avalanches, “runaway” lobes with an orientation roughly perpendicular to the main emplacement directions are described at several deposits (e.g. U-turn Slide, Eisbacher, 1979; Fernpass, Abele, 1964) and are commonly associated with local steps in topography. These “runaway” lobes are highly mobile and often extend for several kilometres.

4.5.7. Debris avalanche spreading statistics

The Jocotitlán volcanic debris avalanche is an example of a complex emplacement history that can not easily be summarized in single parameters such as volume (V), area (A), drop height (H), runout (L) and deposit length (L*). These parameters are often used to compare rock and debris avalanche events in size and mobility (e.g. Shea and van Wyk de Vries, 2008; Legros, 2002; Dade and Huppert, 1998; Kilburn and Sørensen, 1998; Siebert et al., 1995;). Because of its three distinct morphological units with very different failure and emplacement histories, we propose three separate values for V, A, H, L and L* to represent the deposit in numbers (Figure 4.12).

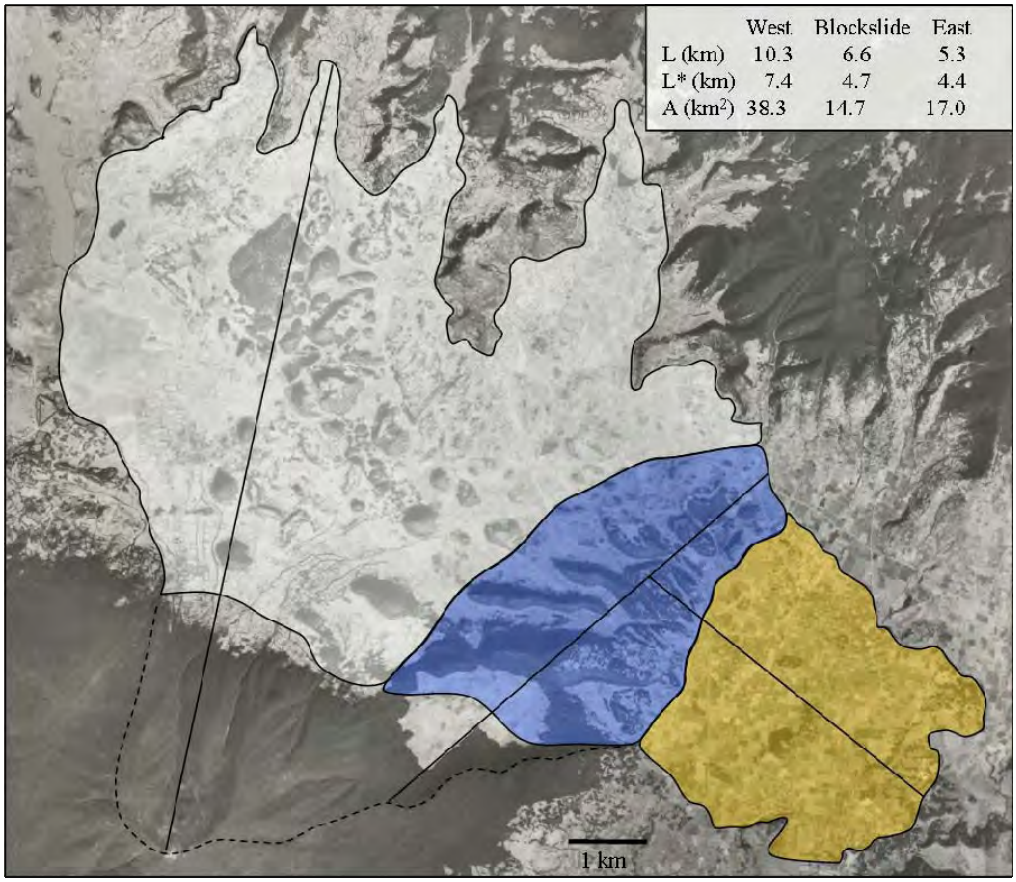

Figure 4.12: The three morphological debris avalanche units are highlighted on this aerial photograph (scale 1:37,000) taken in the year 2000. The runout distances for each individual unit are marked by solid lines and their values together with other deposit statistics are listed in the insert table. See text section 4.5.7. for details.

4.6. SUMMARY

During the catastrophic collapse of the northern flank of Jocotitlán volcano, spreading on weak volcaniclastic and lacustrine sediments facilitated bockslide-style failure of the north-eastern edifice flank, whereas the north-western flank collapse produced a deposit more typical of volcanic debris avalanches. In this western deposit area, large, steep conical hummocks aligned radial to source characterize the deposit morphology, and little interaction with the underlying sedimentary sequences is preserved. Its source scarp has the typical horse-shoe shape of volcanic sector collapse events. Involvement of substrate material is well documented in the blockslide area and the eastern deposit lobe. Here, wide-spread mingled sedimentary units are associated with the location of hummocks, and are also found outside the deposit margin. Relationships of substrate deformation features (fault and fold orientations) and

avalanche travel direction exclude the origin of deformation by avalanche bulldozing. Instead, pre-avalanche spreading of the eastern flank on the unconfined substrate gradually displaced and deformed these and furthermore led to slow flank destabilisation. Secondary 'overprinting' of these pre-avalanche deformation features is evident in outcrops within the deposit boundary, whereas displaced substrates outside the debris avalanche margin retained larger fault and fold structures. Unique to the eastern deposit lobe, the third morphological deposit part, are longitudinal ridges and ejected boulders, both documenting the avalanche travel direction in this area, which is essentially perpendicular to the original edifice collapse direction. This diversion from the travel path can be attributed to a pre-existing step in the local topography over which the blockslide component of the flank collapse disintegrated to emplace the eastern lobe at relatively high velocity.

Acknowlegements

This paper represents part of AD's PhD project on rock and debris avalanche – substrate interaction processes and their feedback on avalanche behaviour. Field work support by the UC Mason Trust Fund and UNAM is greatly appreciated. AD would like to thank Jarg Pettinga for fantastic help with the structural geology aspects, and Tim Davies, Ben van Wyk de Vries and Michael Branney for inspiring discussions. Work by CS and SS was funded by grants Conacyt-50677-F and UNAM-DGAPA IN-101006 to CS. Additionally SS was funded by a scholarship from Posgrado en Ciencias de la Tierra, UNAM (Conacyt-200911).

Chapter 5:

Analogue Model Report:
Dry Granular Avalanche Emplacement over Substrates

In the spirit of:

"I haven't failed; I have found 10,000 ways that don't work."

Thomas Edison

Analogue Model Report: Dry Granular Avalanche Emplacement over Substrates

5.1. OBJECTIVES

In the preceding chapters many avalanche-substrate interaction features have been described and detailed case studies presented. Problems arise in testing avalanche emplacement and substrate-feedback hypotheses because the direct observation of processes acting real rock avalanches is virtually impossible. The aim of the experiments reported herein is to observe and analyse how a granular flow interacts with various erodible and inerodible runout path conditions, how these influence runout and what the step-by-step processes of e.g. substrate erosion, transport and entrainment are.

5.2. SETUP

The 30 cm wide flume consists of plexiglass sidewalls and a 1 m long initial slope whose angle can be varied via a hinge. The initial slope and runout settings have been modified to closer resemble natural slope-to-runout area transitions, and to assure that the avalanche encounters the substrate at a 0º angle (see Figure 5.1). The modified flume bed is supported by 2 glued-on wooden supports to eliminate flexure of the metal sheet. A 30 by 30 cm container at the height of the slope contains unsorted coal (clast sizes 1-2.5 cm) resting at their angle of repose. An avalanche volume of 6 litres has been found be most appropriate for the flume dimensions; i.e. higher volumes lead to deposits thicker than aimed for, whereas smaller volumes do not give the desired runout lengths. The coal is released as an avalanche through a manually operated trap door. Repeated test runs showed no runout length variation when

sudden release is applied; the runout length is only influenced by significantly lower release speeds; which are not applied.

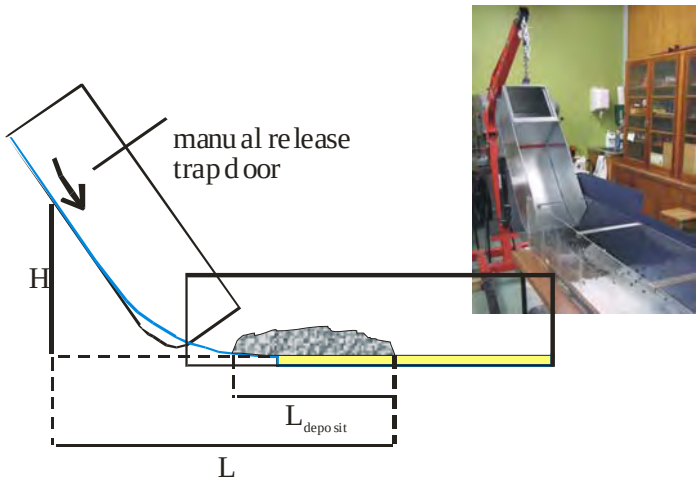

Figure 5.1: Flume setup (blue line = modified setup; yellow fill = substrate; blue fill = Avalanche). L (runout distance from source) and H (drop height) are parameters traditionally used to categorize real-size rock and debris avalanches [ref]. The horizontal distance from the point of release to the beginning of substrate cover is 80 cm.

Each run was documented using a high-speed black-and-white video camera capturing 900 to 1000 frames per second (courtesy of civil engineering department at the University of Canterbury). Using the accompanying MemView software, each run was analysed frame-by-frame.

2.1. Scaling and Material Properties

To model the interactions of granular flows with varying erodible substrate, a very simple geometric model was chosen. Geometric similarity, and to a degree kinematic similarity, is achieved by relating material properties and deposit dimension ratios between the real life cases and the laboratory representations. Dynamic similarity on the other hand is difficult to achieve fully on the small-scale because high shear stresses, grain comminution, etc cannot be modelled in laboratory flows and forces related to the small-scale of laboratory experiments can interfere with the dynamics desired (e.g. water surface tension, cohesion, electrostatic charges). It has been shown elsewhere (e.g. Davies et al., 2003; Lajeunesse, in review) that microscale modelling of natural phenomena such as rivers, can be successful in reproducing processes and tendencies of natural phenomena despite a lack of dynamic similarity. Even though

the detailed processes of small-scale water and sediment behaviour differed from those of real-size rivers (e.g. laminar versus turbulent water flow), the authors were successful in predicting river bed response from their experiments. Similarly, the experiments conducted in the context of this research, although not following dynamic similarity, showed processes and features identical to field observations, which demonstrates the universality of such features in spite of arbitrary choice of scale and materials.

5.3. RUNOUT DEFINITIONS

In the field, rock and debris avalanches conveniently exhibit steep or definite margins leaving little ambiguity concerning their runout distance. Complications only arise if secondary debris flows form gradual transitions with their parent avalanche, if substrates are bulldozed (resolved by defining a bulldozed facies), if the avalanche snout buried itself into runout path material (geophysical investigations could help with this problem), or if post-depositional processes removed (e.g. fluvial erosion) or else altered the distal deposit (nothing one can do in this case but a best guess). Spray zones of freely saltating boulders from the avalanche carapace are features of both real-life and laboratory avalanches and are as such not included in runout estimates, but define a separate feature (here related to L_3, see below).

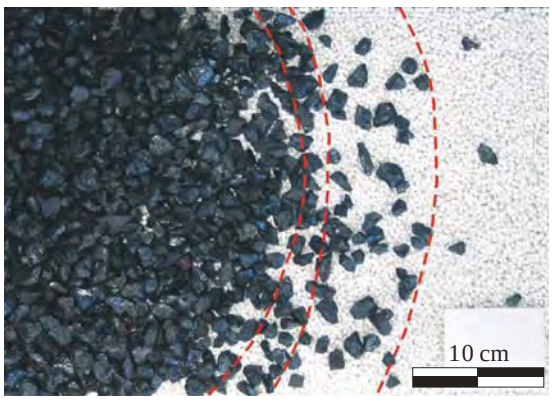

Figure 5.2: Runout definitions from bird's eye perspective. Stipples lines limit (from left to right) L_1, L_2 and L_3.

With the chosen grain-sizes in these experiments, a straight-forward, unique solution to the deposit front definition was complicated. The least ambiguous deposit front definition can be constructed from deposit profiles. Summarized in Figure 5.2 are the contemplations of different deposit front definitions from bird's eye perspective. Seemingly arbitrarily chosen boundaries are based on the most common deposit front features from visual examinations and comparisons of the various runs. These are: extent of 90 % or more clast cover (L_1), extent of 'coherent' clast network (L_2), minimum of 10 % clast cover (L_3), and, were applicable, extent of substrate deformation or bulldozed facies (L_{sub}). Resulting values are compared to the deposit length as distilled from profiles ($L_{profile}$) in Table 5.1. Within an as of yet undefined error margin on each value, most of the L_1 values compare closely to the $L_{profile}$ ones. The only exceptions are R-03 and R-06. In both cases substantial substrate bulldozing resulted in 'passive' transportation of coal clasts on a mobilised substrate and the resulting deposit profiles hence include the 'bulldozed facies' and $L_{profile}$ compares closely to L_2, L_3 and L_{sub}.

Run #	$L_{profile}$	L1	L2	L3	L_{sub}	$L_{deposit}$	$L/L_{deposit}$	Substrate
R-01	112.7	114.3	117.9	125.5	\	48.1	2.34	3 cm dry PVC
R-03	104.4	97.5	104.5	104.5	104.5	46.9	2.23	flour
R-05	103.9	105.2	107.5	107.5	\	51.4	2.02	3 cm dry PVC, rough sub-surface
R-06	115.6	100.0	116.5	116.5	116.5	58.3	1.98	1.5 cm polystyrene spheres
R-07	111.8	112.3	112.3	117.3	\	50.5	2.21	1.5 cm dry PVC
R-08	109.9	111.5	113.0	115.5	\	53.8	2.04	1.5 cm dry PVC, rough sub-surface
R-09	114.6	114.5	116.5	124.5	\	58.5	1.96	3 cm saturated PVC
R-10	106.1	106.5	108.5	111.3	\	60.0	1.77	metal
R-11	104.4	106.0	112.5	122.5	\	55.0	1.90	glued-on sand layer
R-13	99.0	101.0	107.5	113.5	\	51.2	1.90	glued-on PVC layer

Table 5.1: Runout lengths data for the definitions discussed in the text (all values are in cm) For the sake of simplicity and consistency, runout definitions given for each model run described below are those derived from the deposit profiles.

5.4. RESULTS: MODEL RUN DESCRIPTIONS

First test runs were carried out with the above setup, but without substrate. A flume bed was produced with the same dimensions as the modified setup described above, albeit with a continual horizontal runout instead of the substrate depression. Repeated release of 6 litres of coal at a 60º inclined slope resulted in consistent avalanche deposit runouts (R-10).

R-01 (PVC beads)

Avalanche: coarse coal, 6 litres
Slope angle: 60 º
Substrate: 3 cm PVC beads, 1 x 2-3 mm, metal at substrate base
Runout (L): 112.7 cm
Deposit length: 48.1 cm

The initial encounter with the substrate erodes the upper 1-grain-diameter layer and compresses the immediately underlying material (frame 149; Figure 5.3). Subsequently, the avalanche begins to plough deeper into the substrate (frame 229). Once erosion reaches a depth of ~1 cm the non-eroded lower substrate is compressed and moved forward by ~1-grain-diameter at a depth of 2 cm. Shear-failure at shallow inclination in the upper parts of the substrate leads to bulldozing of same onto stationary material beyond the shear planes (frame 249). Upon crossing the ~1 cm depth erosion, failure of the substrate base (metal subsurface) is observed with a simultaneous migration of the substrate failure front ahead of the bulldozed area as a compression front or wave (frame 269). The lower avalanche front slows down behind the increasingly bulldozed substrate, while the avalanche top and front continue moving at relatively higher velocity (frame 289). Towards the end of emplacement, the main avalanche body has stopped while motion of the upper and frontal avalanche parts continues to follow momentum (frame 389).

Substrate mobilisation occurred through shearing (failure planes dipping opposite to avalanche motion direction) and consequent opening of inter-granular spaces, which were immediately reduced again when the mobilised material was compressed and deposited. Thus, a cyclic expansion and compression of the substrate was observed as material was deposited ahead of the erosion front. Small grain bridges formed in the substrate and were destroyed through shear failure or grains slipping past one another.

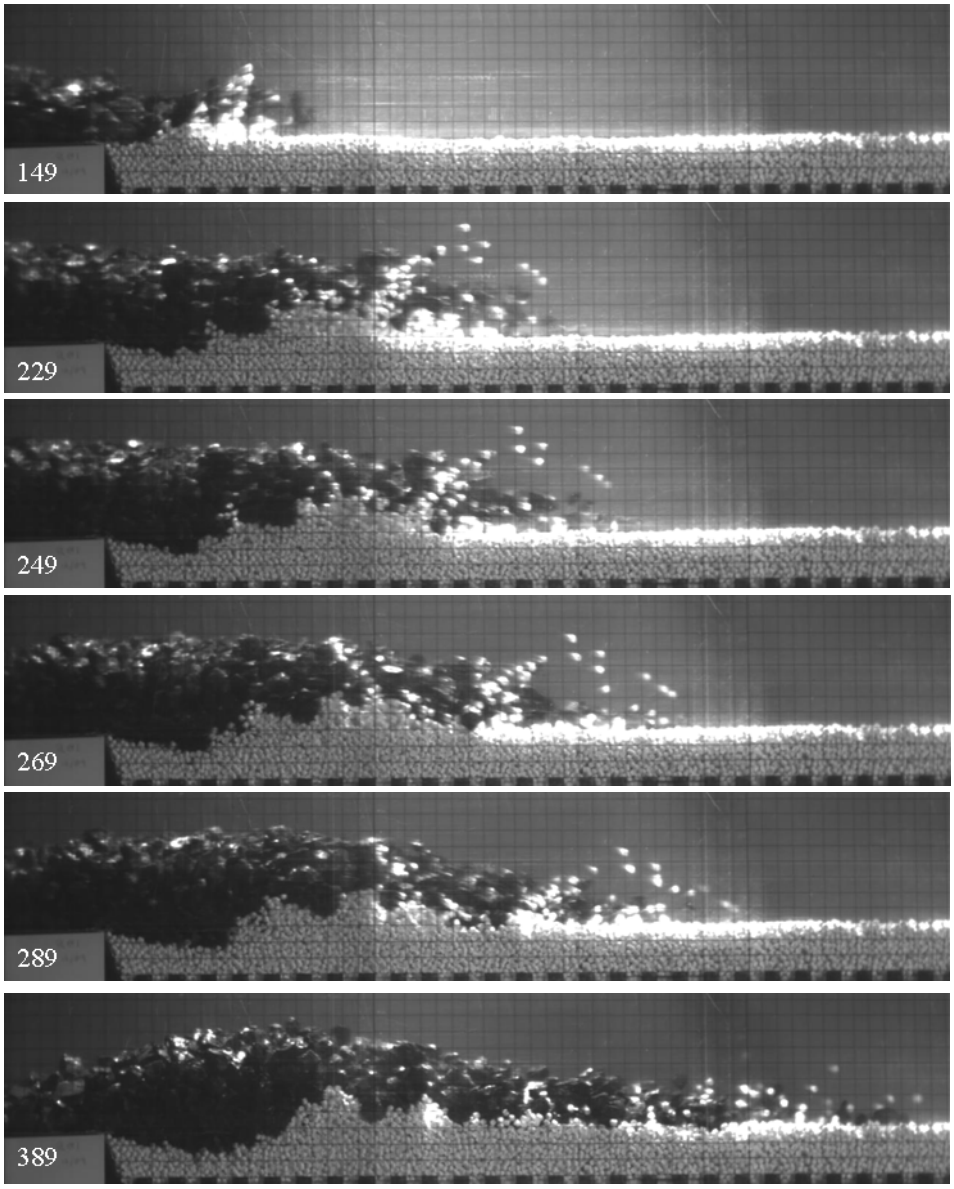

Figure 5.3: Step-by-step analysis of run R-01. Numbers in bottom-left corner refer to frame numbers with a recoding rate of 1000 frames/second.

The flow front overrides the progressively bulldozes substrate like a wave would crash at the shore. Avalanche material behind the bulldozed substrate is compressed as the avalanche rear pushes forward. After the main avalanche body came to rest, the frontal part which overrode the bulldozed substrate continues to move forward with grains rotating past each other and partially sliding along shallow shear planes. Coal clasts at the flow front are agitated by the rough substrate and subsequent collision with each another and they form a spray zone in front of the deposit. The resulting deposit is thickest immediately behind the bulldozed substrate.

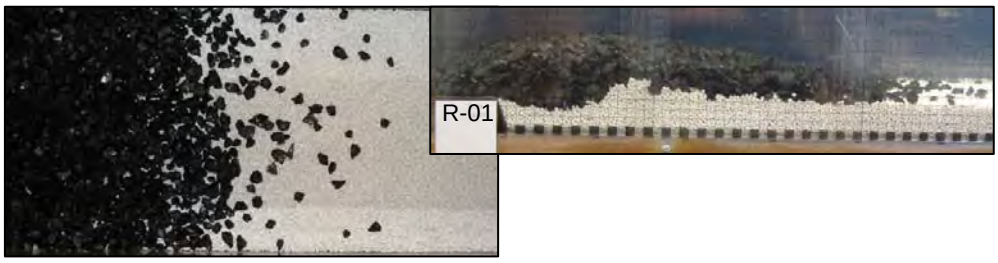

Figure 5.4: Coal emplaced onto dry PVC beads (R-01), bird's eye and final deposit profile views

R-02 (PVC beads)

Avalanche: coarse coal, 6 litres
Slope angle: 50 º
Substrate: 3 cm PVC beads, 1 x 2 mm, metal at substrate base
Runout (L): 106.5 cm
Deposit length: 51 cm

The processes in this run are similar to those in the previous experiment (R01), except that velocity and runout are smaller and substrate bulldozing less dramatic.

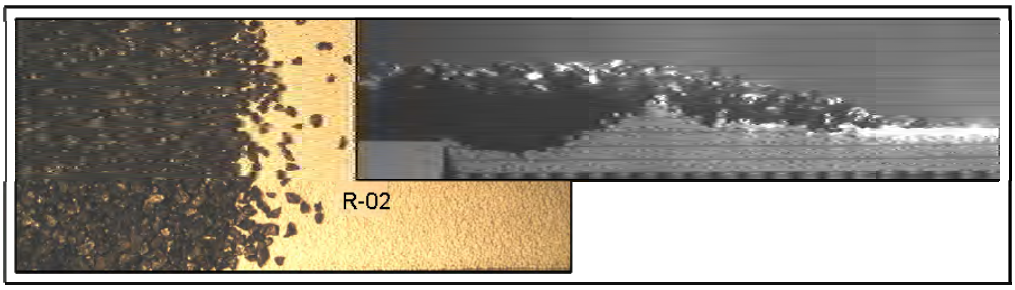

Figure 5.5: Smaller slope angle resulted in shorter deposit and less interaction with the dry PVC substrate (R-02)

R-03, -04 (flour)

Avalanche: coarse coal, 6 litres
Slope angle: 60 º
Substrate: 3 cm plain flour, metal at substrate base
Runout (L): 104.4 cm
Deposit length: 46.9 cm

Identical to run R-01, the initial encounter of the coal avalanche front with the erodible substrate first leads to erosion/mobilisation of the very upper substrate material only (a in Figure 5.7). Marker layer material is mixed and mingled with the

white substrate and bulldozed ahead of and beneath the avalanche front onto stationary substrate (b). The avalanche ploughs into the substrate (c), and shear failure at depth commences (d). With more coal mass loading the substrate, more intense shear failure is observed at different depths (e, f). Compression ahead of the avalanche front can be seen in the upper substrate parts (g), which forms diapir-like features (h). The substrate did not fail along the metal sub-surface, probably due to cohesive forces in the flour, but instead all failure was accommodated by a décollement (i). The arrow marks the extent of internal substrate compression ahead of the avalanche front, which has also lead to substrate thickening (k).
The resulting features show a thick coal avalanche deposit behind a bulldozed substrate facies. Substrate mixing and mingling features with apparent injection features have formed in the bulldozed facies. Substrate failure occurred décollement-style.

Clasts within the advancing avalanche interact through rotations and collisions, whereby spray develops at the front, and the avalanche body itself dilates in respond to clast collisions; initially anyways. Shortly after substrate encounter, the avalanche motion changes from collisional to sliding pretty much passively on the mobilised substrate as if the entire mass (avalanche plus substrate) was merely pushed forward by the avalanche rear with only the upper and frontal avalanche part still acting as a grain flow in which individual clasts rotate past one another.

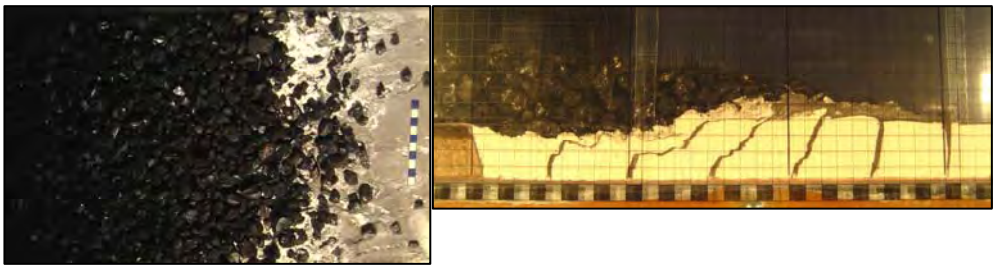

Figure 5.6: Coal emplaced onto flour (R-03), without and with vertical marker layers (dyed flour)

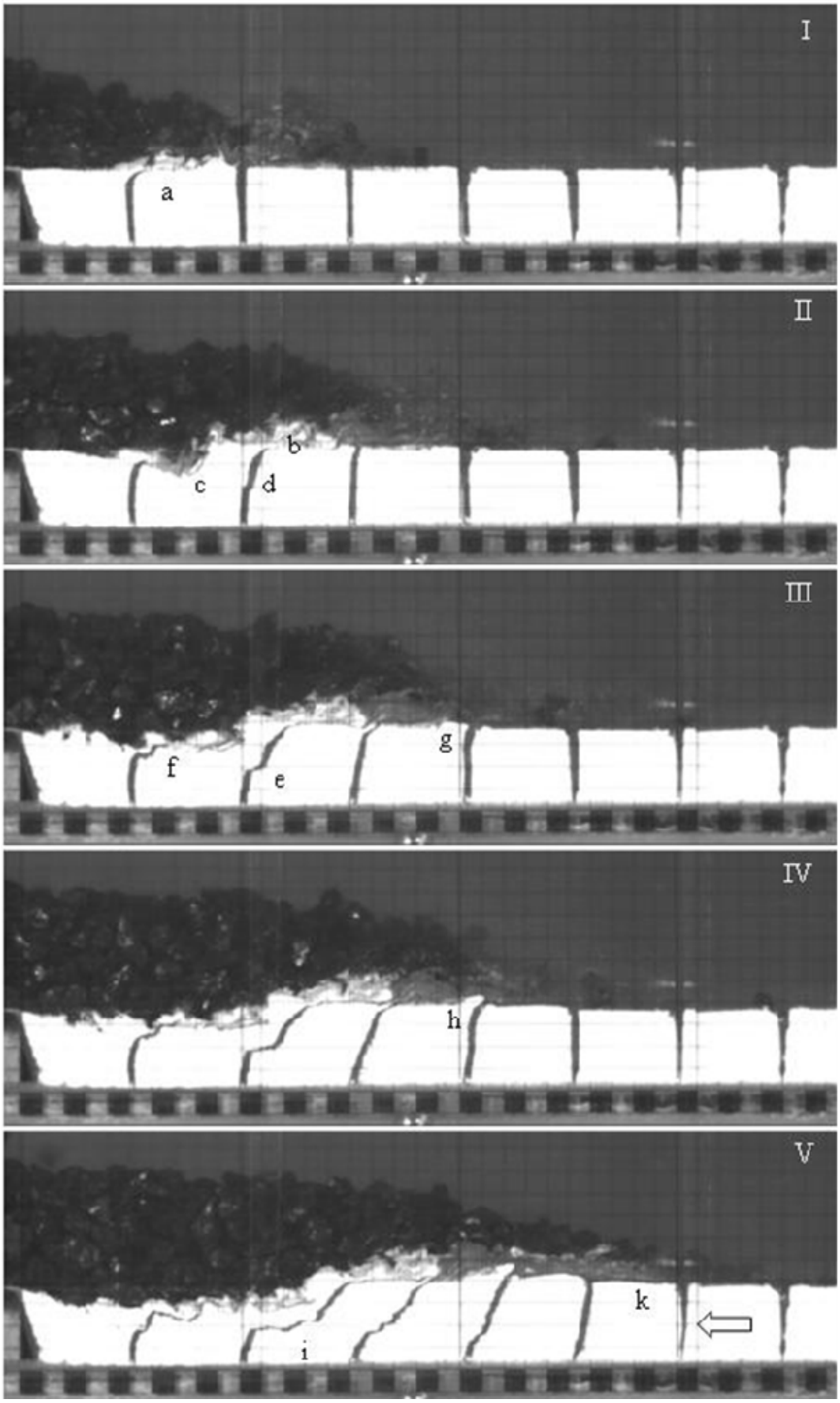

Figure 5.7: Detailed views of coal avalanche – flour substrate interactions (R-03)

R-05 (PVC beads, rough sub-surface)

Avalanche: coarse coal, 6 litres
Slope angle: 60º
Substrate: 3 cm PVC beads w/ roughened (1 layer of PVD beads glued to fabric) sub-surface
Runout (L): 103.9 cm
Deposit length: 51.4 cm

Substrate erosion only affected the upper 1-2 cm. Below that depth no changes in clast arrangement, compression or other disturbances were detected; i.e. no basal failure of the substrate occurred as for example in the runs in which zero-friction metal formed the substrate base.

Figure 5.8: Effects of introducing a roughened sub-surface beneath dry PVC substrate (R-05)

Mobilisation and transport of substrate material was only short distances before it was deposited and overridden by the avalanche. Substrate mobilisation occurred through shearing (failure planes dipping opposite to avalanche motion direction) and consequent opening of inter-granular spaces, which were immediately reduced again when the mobilised material was compressed and deposited. Thus, a cyclic expansion and compression of the substrate was observed as material was deposited ahead of the erosion front. Small grain bridges formed in the substrate, but were again destroyed through shear failure in the upper portions.
Stopping of the coal avalanche body by the compressing substrate was effective, leaving roughly half the avalanche material on the sloping metal runout path. Coal clast behaviour during emplacement was essentially the same as in run R-01 and others.

R-06 (polystyrene spheres)

Avalanche: coarse coal, 6 litres
Slope angle: 60º
Substrate: 1.5 cm polystyrene spheres (1-2 mm diameter), metal sub-surface
Runout (L): 115.6 cm
Deposit length: 58.3 cm

The avalanche overrides and erodes the upper 1-2 grain-diameter thick substrate layer, before ploughing and bulldozing commences. A lot of substrate material is mobilised and becomes airborne at the avalanche front. Substrate bulldozing is accompanied by flame-injections and the substrate forms a 'wave' up to 2 cm above its original surface. This wave is overridden by the avalanche as it forms (like a wave would crash at the beach). Substrate compression and basal failure is beneath the wave front at this stage. Ahead of the wave there is very little compression and failure at depth (particles move by < 1 grain diameter at the most) and substrate failure is mainly restricted to the upper 5 mm. Basal failure (< 0.5 grain diameter horizontal movement) propagates ahead of the wave and up to 120 cm distance (L), to the point when avalanche thickness roughly equals the wave height and when erosion has reached the substrate base. Once basal substrate failure occurs, a change in emplacement dynamics is observed. Before this point the main mode of transport was by sliding on the sloping metal runout path and coal clast agitation above the substrate. Once the substrate was sufficiently mobilised, however, the avalanche body began to ride passively on top of the substrate wave. Towards the end of the run, the wave height above original substrate surface is 3.5 cm. Substrate and coal are mixed ahead of the wave, but remain separate behind the wave (with respect to motion direction). The avalanche front keeps migrating, obeying momentum and gravity at the end of the emplacement. Substrate spray remains active until the end.

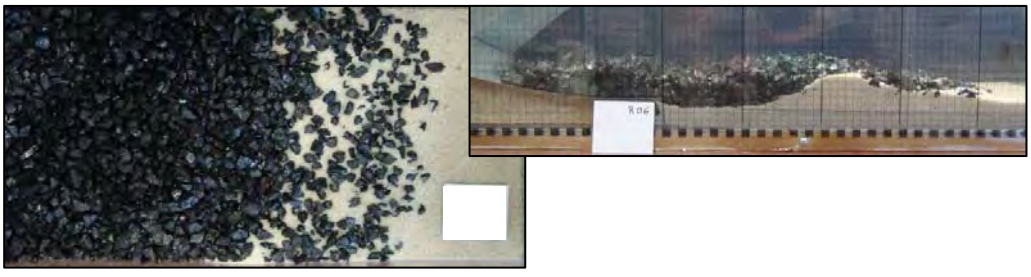

Figure 5.9: Substrate is a thin bed of polystyrene spheres (R-06)

Substrate failure reached 40 cm from the beginning of substrate material in the runout path. The avalanche topography mimics the wave and slope shapes, whereas in other runs there was continual thickening of the avalanche behind the bulldozed substrate.

R-07 (PVC beads)

Avalanche: coarse coal, 6 litres
Slope angle: 60º
Substrate: 1.5 cm PVC beads, metal sub-surface
Runout (L): 111.8 cm
Deposit length: 50.5 cm

Again, initially only the upper grain-diameter thick layer of substrate material is affected. Once erosion has left only a 1-2 grain-diameter thick layer on the metal subsurface, basal failure of an expanding substrate begins, which is immediately accompanied by substrate compression ahead of the erosion front. Here, bulldozing at an angle of 20-25 degrees piles the substrate into a ramp which the coal avalanche partially overrides while being slowed down behind this obstacle.

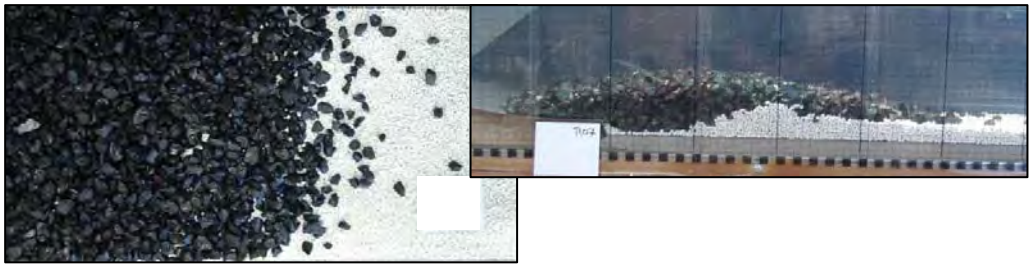

Figure 5.10: Influence of substrate thickness (i.e. depth of failure surface) on avalanche runout (R-07)

During the initial substrate erosion, the avalanche front is under expansion due to clast agitation. This behaviour changes to sliding of the main avalanche mass once substrate bulldozing commences with some clast rotations at the avalanche base and sliding planes detectable within the avalanche body.

R-08 (PVC beads, rough sub-surface)

Avalanche: coarse coal, 6 litres
Slope angle: 60º
Substrate: 1.5 cm PVC beads, rough sub-surface
Runout (L): 109.9 cm
Deposit length: 53.8 cm

The processes in this run are essentially the same as in R-07, except that avalanche stopping behind the bulldozed substrate was more effective, leaving more avalanche material on the sloping runout path, demonstrating the effectiveness of a strong substrate (i.e. lacking weak failure planes) to reduce avalanche mobility. That is, no failure occurred at the substrate base.

Figure 5.11: Roughened sub-surface beneath thin substrate (R-08)

R-09 (saturated PVC beads)

Avalanche: coarse coal, 6 litres
Slope angle: 60º
Substrate: 3 cm saturated (to within upper 1 grain diameter) PVC beads, metal sub-surface
Runout (L): 114.6 cm
Deposit length: 58.5 cm

In this run it is mainly the upper substrate which is affected by avalanche overriding. Migration of substrate deformation to depth only occurs at the location of substrate bulldozing. Grain rotation occurs at the avalanche base, but is not effectively transmitted into the avalanche body, which essentially slides on this basal layer and compresses behind the point of substrate bulldozing. Down-flow of the bulldozed substrate the coal avalanche continues to follow momentum and gravity to form a relatively long and thin deposit front.

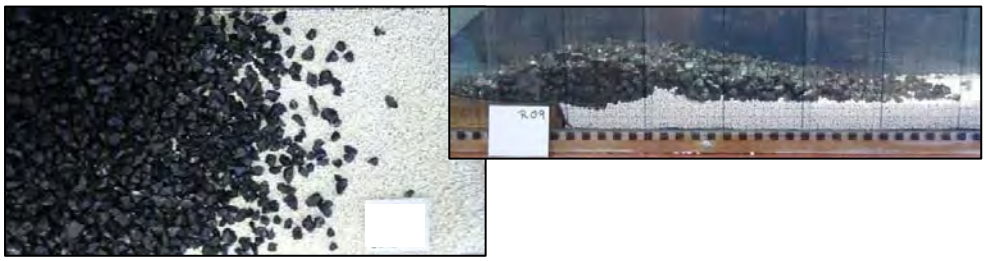

Figure 5.12: Quasi in-erodible substrate effects on runout (R-09)

R-10 (metal)

Avalanche: coarse coal, 6 litres
Slope angle: 60º
Substrate: metal
Runout (L): 106.1 cm
Deposit length: 60 cm

En-masse sliding is the dominant emplacement mechanism in this run. No grain rotation or agitation was observed. The main avalanche body comes to rest at L = 85 to 98 cm (see red arrows in Figure 5.13) while the front keeps extending along internal failure plains dipping at ~25º into motion direction. This deposit front extension is essentially the reason for the tapering deposit front.

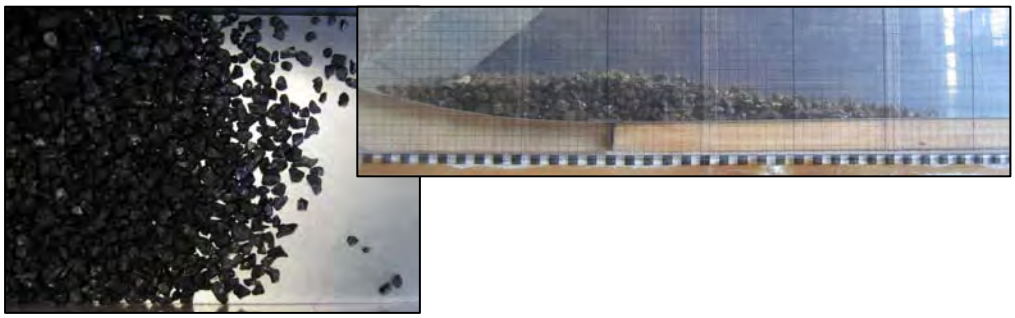

Figure 5.13: Runout of coal avalanche over zero-friction metal surface (R-10)

R-11 (in-erodible sand layer)

Avalanche: coarse coal, 6 litres
Slope angle: 60º
Substrate: thin film of sand glued onto metal runout surface
Runout (L): 104.4 cm
Deposit length: 55 cm

Apparent en-masse sliding was the prevailing emplacement mechanism in this run as well. However, grain agitation at the base once the rough surface was encountered transferred into the main avalanche body in form of clast rotation and subsequent minute flow dilation. The flow came to rest en-masse while the front kept extending a further distance by sliding along shallow internal failure surfaces as in R-10.

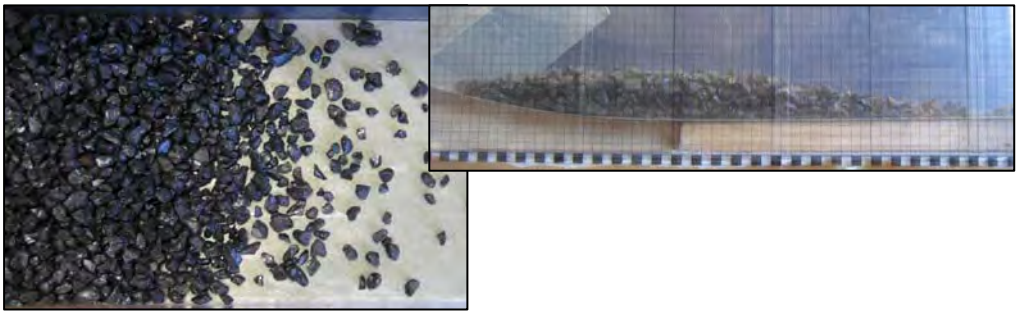

Figure 5.14: Inerodible, undeformable, rough substrate (glued-sand layer, R-11)

R-13 (in-erodible PVC beads)

Avalanche: coarse coal, 6 litres
Slope angle: 60º
Substrate: one-grain-diameter layer of PVC glued onto metal runout surface
Runout (L): 99 cm
Deposit length: 51.2 cm

As soon as the rough PVC substrate is encountered, spray develops at the flow front with vertical flow dilation of up to 13 cm (see Figure 5.16 and compare to in-motion flow front thicknesses of 2-5 cm in other runs). Grains at the base of the thicker main flow body interlock with the rough substrate, essentially halting the advancing flow rear. The dilated flow front collapses to a thin deposit front at the end of motion.

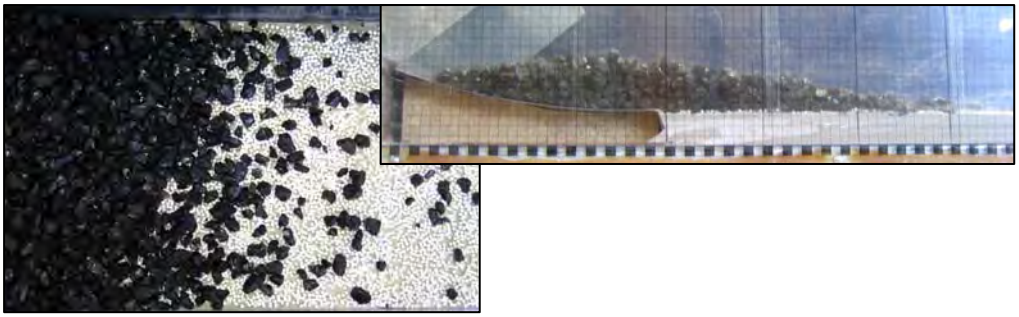

Figure 5.15: Increasing runout surface roughness (glued-on PVC beads, R-13)

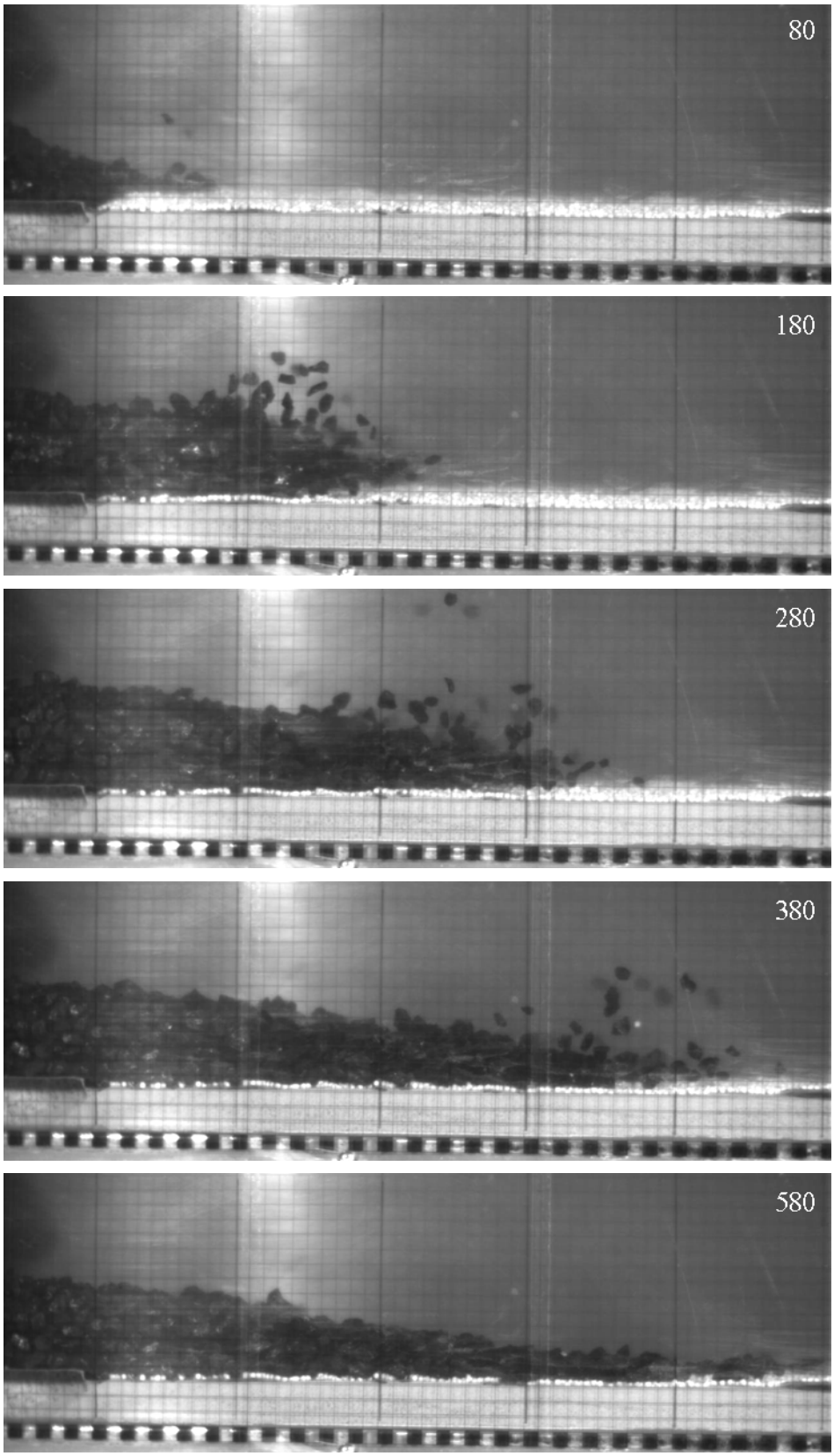

Figure 5.16: Snapshots of run-13 in motion.

5.5. SUMMARY

Though purely qualitative in their design, these analogue models provided helpful conceptual ideas about the formation and evolution of substrate deformation features with some tentative insights into substrate feedback onto avalanche runout and morphology.

5.5.1. Substrate base

In Figure 17, the influence of the base of a deformable and erodible substrate on its response to avalanche emplacement and, in turn, its influence on avalanche behaviour is illustrated. The weak (zero friction) substrate base in experiment R-01 (Figure 5.17a) resulted in the substrate failing in its entirety; i.e. the substrate was mobilized and failed along its weak base. This base in reality could be a pre-existing weakness within the substrate, a shear plane developing as a direct consequence to avalanche impact, or a bedding plane/interface with another layer below.

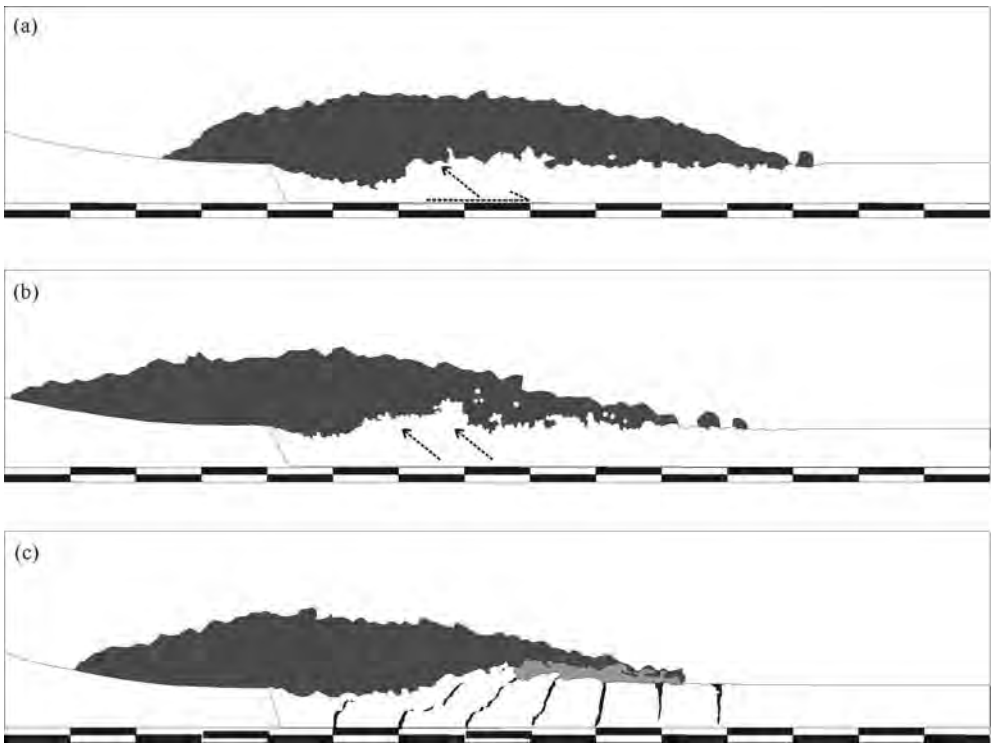

Figure 5.17: (a) runout over dry PVC beads with metal sub-surface (R-01), (b) dry PVC beads on a roughened (layer of glued-on PVC beads) sub-surface (R-05), and (c) runout over flour (R-03). Scales at bottom of images show 5 cm segments.

This case led to longer runout and higher mobility of the avalanche tail than emplacement over the same substrate material with a strong base (Figure 17b). Higher tail mobility had the effect that the deposit is shorter and thicker in profile compared to the strong substrate base case. In this latter case, the strong substrate base caused the entire substrate to be more resistant to deformation, effectively halting the avalanche body and leading to an earlier deceleration of the main avalanche mass with the tail halting behind the slowing avalanche body and depositing early in the runout. Intermediate between the two cases was an avalanche emplaced over a cohesive substrate (wheat flour). The small grain size and high compactability of this material led to failure within the substrate at depth. Material below the failure plane was compressed, but no shear stress was transmitted to its base, which hence remained strong.

5.5.2. Substrate thickness

The same observations of substrate base influence were made with emplacement over thinner substrates of the same material (PVC beads; Figure 18b, c). Interestingly, reducing the thickness of the weak-based substrate resulted in a slightly shorter runout, whereas reducing the thickness of the strong-based substrate resulted in longer runout with respect to the thicker substrate. Runout over low-friction material (polystyrene spheres, Figure 18a) showed the greatest response of avalanche profile shape to substrate conditions. In this run, the avalanche created a substrate ‘wave’ and this mobilized substrate eventually became coupled with the avalanche and formed the active base of the combined granular avalanche. Sufficient momentum and stress was transferred into the substrate for it to fail and ‘carry’ the avalanche, leading to the longest runout observed and deposit morphology that mimics the substrate surface.

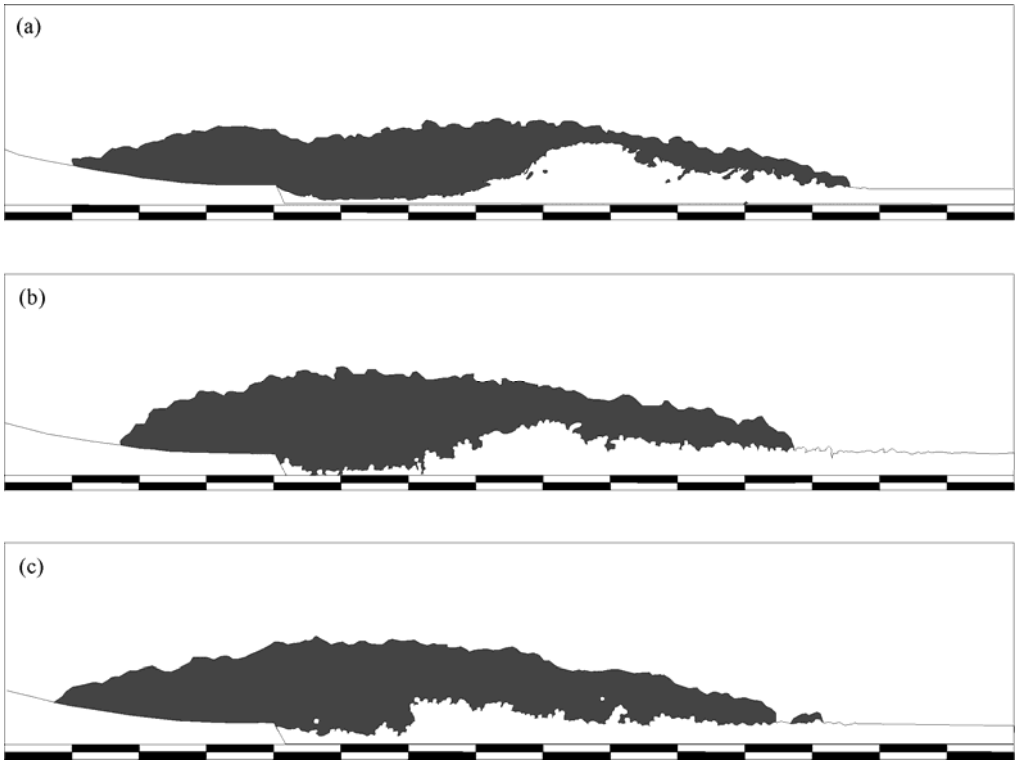

Figure 5.18: Substrate thickness. (a): polystyrene spheres (R-06), (b): PVC beads on metal sub-surface (R-07), (c) PVC on roughened sub-surface (R-08).

5.5.3. Inerodible substrates

Initially, runout over metal was intended to serve as a reference point for relative avalanche runout comparisons. However, a distinct change in avalanche behaviour was observed in the absence of an interacting substrate: sliding of the avalanche body *en masse* was the emplacement mode in the metal runout case, whereas interactive or rough surfaced substrates introduced avalanche grain agitations, and no basal sliding occurred over these materials. Hence, the introduction of inerodible material of varying roughness better served the purpose. Increased surface roughness of these inerodible materials led to shorter runout (bearing in mind that only two data-points exist for this comparison, runs R-11 and R-13), and lower avalanche tail mobilities (i.e. deposition early in the runout path). Interestingly, runout over deformable, yet only slightly erodible material (wet PVC, Figure 5.17d) led to relatively long runout.

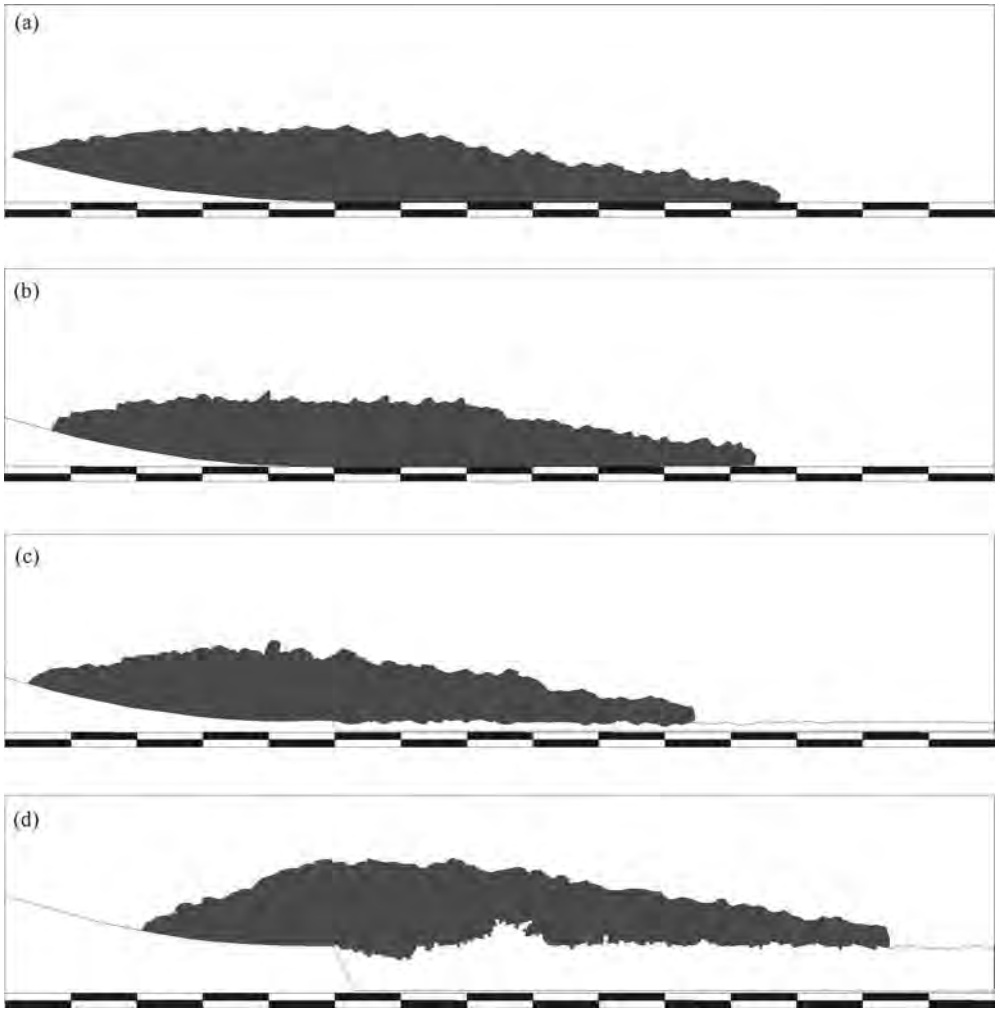

Figure 5.19: (a): sliding on metal (R-10), (b) runout surface roughened by a layer of glued-on sand (R-11), (c) increased runout surface roughness using a layer of PVC beads in the runout path (R-13), and (c) saturated PVC beads (R-09)

5.5.4. Concluding list

Substrate basal conditions affect substrate response and its feedback on avalanche behaviour and morphology:

- A weak substrate base leads to failure along this weak plane; avalanche and substrate become coupled, and the avalanche tail retains mobility.
- A strong substrate base induces substrate resistance to motion, imparting its resistance into the moving avalanche body, leading to avalanche deceleration and early deposition of its tail section.

Substrate thickness influences the substrate's effect on avalanche runout. However, more experiments with careful scaling are required to investigate the observed trends in greater detail and accuracy.

Surface roughness of the runout path can change the emplacement mode of granular flows.

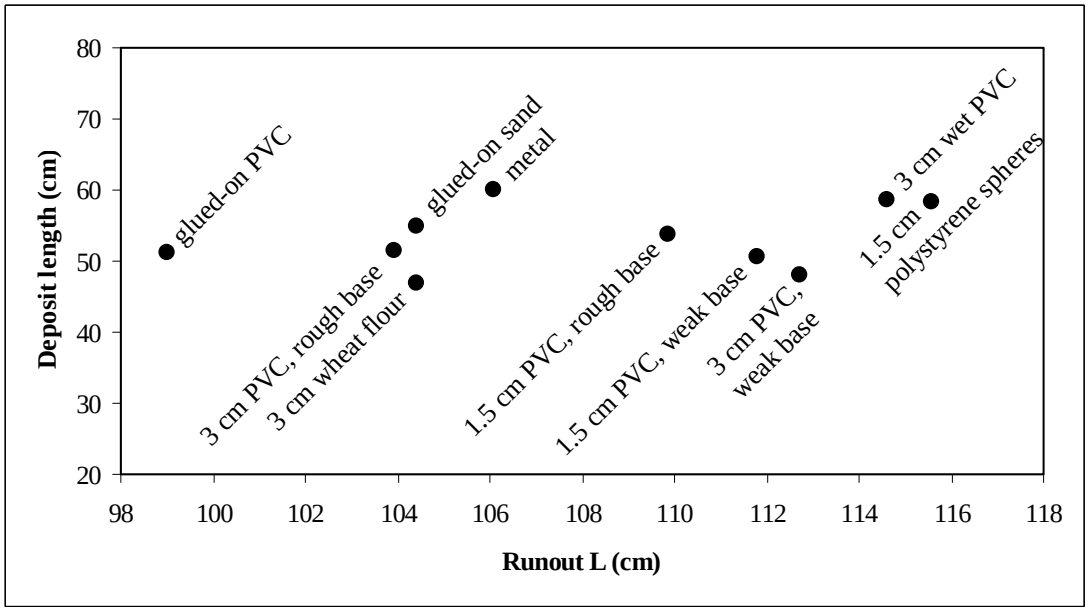

Figure 20: Plot showing deposit length versus avalanche runout in relation to the type and thickness of runout path material.

6. CONCLUSIONS

The experiments herein were successful in reproducing avalanche substrate interaction features observed in rock and debris avalanche deposits. As such, they provide a conceptual framework for ideas exploring the processes acting in real-size avalanches when these encounter and interact with sediments in their runout paths. Furthermore, the experiments provide a basis for further, systematic experimentation on avalanche emplacement dynamics over various substrate. Such future experiments should include scaled substrate properties to simulate real-life sediment frictional behaviours, variations in avalanche grain size to explore its influence on the avalanche's erosion potential, and may consider varying runout path geometries.

Chapter 6:

Compiling a World-Wide
Rock and Debris Avalanche Deposit Database

In the spirit of:

"Sanity is madness put to good uses."

George Santayama

Volcanic Debris Avalanche Deposit Database

A. Dufresne, L. Siebert, B. Bernard, R.S.J. Sparks,
S. Takarada, J. Clavero, A. Belousov and M. Belousova
in preparation for online publication

6.1. OBJECTIVES

The aims of this database project are: (1) to compile the data currently available on volcanic and non-volcanic mass movement deposits, (2) to summarize the state of research in this area, and (3) to make this data available for the scientific community in a format that can be used for a variety of research aims. It will thus provide a useful tool for studies concerning volcanic sector and mountain slope collapse processes, debris and rock avalanche runout mechanisms, numerical modelling and hazard assessments.

A large amount of data on mass movement deposits is available, but comparison between the various datasets is still a challenge due to the differing methods and foci of the studies. Creating comparable datasets is vital for research and hazard management problems.

6.2. VOLCANIC VERSUS NON-VOLCANIC AVALANCHES

Emerging from the distillation of the vast literature on geological mass movements, data compacted into database format revealed that categories for volcanic debris avalanche and non-volcanic rock avalanche deposits are essentially identical, attesting to their overall similarities. However, marked changes had to be made to accommodate the intrinsic differences between the two. To start with, the units for volume, runout and drop height, summarized in Table 6.1 and illustrated in Figure 6.1, had to be adapted to the scale-difference. Most of the non-volcanic avalanche

deposits catalogued in this database are less than 0.1 km^3 in volume, whereas the compilation of volcanic avalanche deposits is currently restricted to those exceeding 0.1 km^3. The lack of data for volcanic avalanche deposits with volumes less than 0.1 km^3 is due to selection criteria at this early stage of data collection, and might generally also be a consequence of frequent transformation into debris flows of the smaller volcanic avalanches, as speculated by Shea and van Wyk de Vries (2008).

	volcanic debris avalanches	non-volcanic rock avalanches
Volume (V)	km^3	$10^6 m^3$
Area (A)	10's to 1,000's km^2	1-100's km^2 (typically 10's)
Runout (L)	> 10 km	< 10 km
Drop height (H)	> 2,000 m	< 2,000 m

Table 6.1: Units and range of values for non-volcanic rock avalanches and volcanic debris avalanches

Furthermore, in terms of deposit characteristics, a column for “molards” was added to the description of non-volcanic avalanche morphologies. This term is primarily found in earlier publications. Horseshoe-shaped collapse scarps and toreva blocks are largely absent from non-volcanic events. The terms “matrix/mixed facies” and “block facies” are not used by landslide researchers. Instead the term “carapace” in rock avalanches matches most closely the volcanic “block facies”. Another complication arises from the differences in focus of the volcanic and the landslide studies. More detail is given to internal fabric and basal outcrop descriptions in the landslide literature, whereas the volcanic literature focuses primarily on morphological and facies features of the deposits, with descriptions of basal features only a recent addition (that said, basal outcrops appear to be less common in volcanic debris avalanches due to the greater deposit thicknesses).

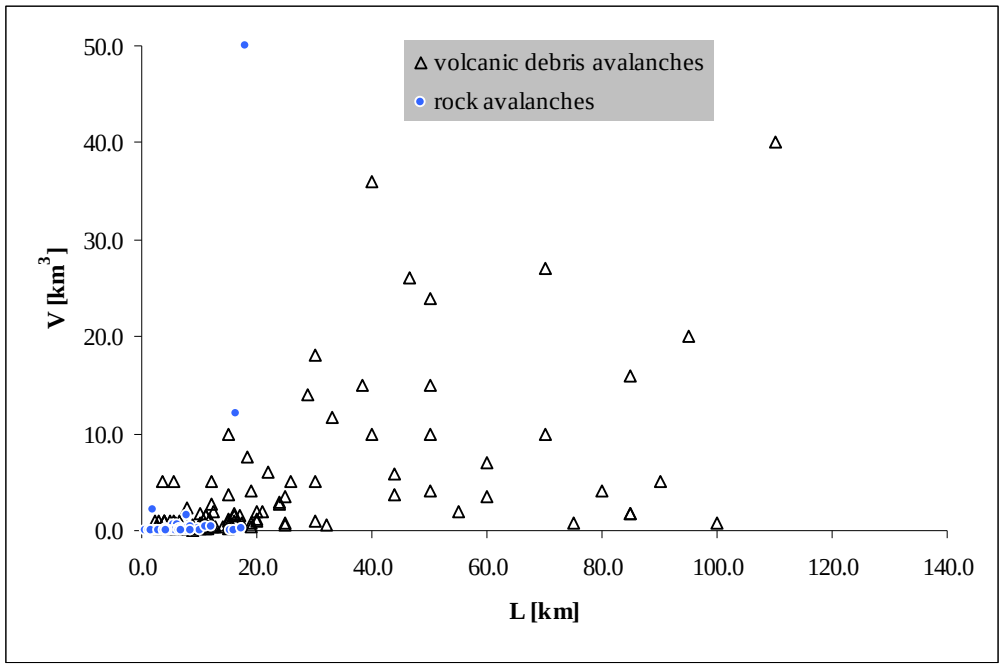

Figure 6.1: Volume versus runout plot illustrating the scale-difference of avalanches sourced in volcanic versus those sourced in non-volcanic materials.

Another marked difference lies in the initial type of material involved. In volcanic collapse events, a mixture of materials (massive lava flow units, unconsolidated ash, pumice and scoria, water) from the volcanic slope is involved, usually with a high voids ratio, and the term “debris avalanche” is used to denominate the resulting phenomenon. For non-volcanic events the initial failure is within a relatively dry, massive, overconsolidated rock mass with low voids ratio, and their movements are typically referred to as “landslides” or “rock avalanches”, both of which may however transform into debris avalanches or debris flows. Whereas the flow of dry cohesionless grains may describe a rock avalanche (strong, partially pre-fractured/jointed source material) reasonably well, volcanic debris avalanches usually contain hydrothermally altered and/or other mechanically weak source materials; clays, ash and other fine-grained, very likely wet or saturated materials (volcanoes are splendid aquifer bearers; e.g. 13 vol.-% of the original edifice failure volume at MSH was water; Glicken, 1996), and possibly hydrothermal fluids. Belousov et al. (1999) observed that debris avalanches composed of hydrothermally altered material were substantially thinner than unaltered ones derived from the same volcanic edifice (Shiveluch in Kamchatka).

With respect to the runout landscape there are also differences in volcanic versus non-volcanic settings. Plateaus and broad inter-edifice valleys filled with volcaniclastic, lacustrine and fluvial sediments dominate the volcanic landscape. Edifices are built on top of these weak materials and these can form part of the initial failure mass (e.g. van Wyk de Vries et al., 2001). In non-volcanic settings on the other hand, bedrock elevated to form mountains with deep-reaching roots are often dissected by narrow valleys, or failures occur onto open plains bounding steep rock-slopes. Sediments in these landscapes are composed of fluvial, glacial and lacustrine materials, talus and other debris, vegetation, and surface water.

6.2.1. Volcanic versus non-volcanic avalanches summary

The main differences between avalanches sourced from volcanic (active or extinct) versus those from non-volcanic slopes are (1) volume (and correspondingly area covered with debris and runout), and (2) the type of source material. Volcanic avalanches are generally larger than non-volcanic ones, and are sourced in weak, heterogeneous materials. Despite the differences discussed above, mountain slope and volcanic edifice failures produce strikingly similar deposits in terms of morphology and basal features.

6.3. DATABASE STRUCTURE

Currently, all data is stored in an *Excel* spreadsheet (see accompanying CD) and is structured as listed in Table 6.2. The volcanic debris avalanche deposit database developed during this study forms part of the Volcano Global Risk Identification and Analysis Project (VOLGRIPA), a global volcanic risk assessment project headed by Steve Sparks, Bristol, England. Eventually, publication of a non-volcanic rock avalanche deposit dataset that is compatible with the volcanic dataset is planned.

The glossary included in the volcanic database is still under review by all members involved to guarantee, as best as possible, a consistent interpretation of the various terms used in the scientific literature. The problems arising from individuals' interpretations of words have been touched upon briefly in the thesis introduction chapter.

(1) Volcano name	Lithological domains
(2) Location	Topographic runup
Country	Faults
Longitude and Latitude	Spreading (º)
Volcano type	Other
(3) Deposit general	**(7) Deposit shape**
Name	Lobate
Type	Digitate
Transformation	Fan-shaped
Deposit age	Elongate/tongue-shaped
Age method used	Round
Age confidence	Other
References	Pre-avalanche topography
Contributions	**(8) Internal deposit structure**
(4) Deposit statistics	Jigsaw-fractured clasts
Volume (V)	Remnan stratigraphy
Volume estimate method	Hydrothermal alteration
Volume confidence	Sorting and grain size
Area (A)	Block facies description
Area estimate method	Mixed facies description
Area confidence	Matrix facies description
$A/V^{2/3}$	Basal facies description
Length (L*)	Basal contact
Runout (L)	**(9) Substrates**
Drop height (H)	Sediments present
H/L	Entrained
Thickness, maximum	Deformed
Thickness, average	Undisturbed
Failure direction	**(10) Geological setting**
Runout slope (º)	Tectonics
Collapse trigger	Climate
Weakening mechanism	**(11) Hazards**
Deposit framework	Associated deposits
(5) Collapse scar data	Associated phenomena
Current state (e.g. filled)	Fatalities
Shape	Major causes of fatalities
Width	Current population in 20 km radius
Length	Current population in 50 km radius
Depth	**(12) Volcano general**
Aperture	Composition
Volume	Edifice volume
(6) Deposit morphology	Diameter and elongation direction
Hummocks	Main type of eruption
Hummock alignment	Last eruption (year)
Longitudinal ridges	Edifice height
Transverse ridges	Summit elevation (asl)
Flat surface	**(13) Additional notes**
Toreva blocks	**(14) Links**
Lateral margin description	Websites, maps, photos,
Frontal margin description	satellite images, online data, etc.
Levees	

Table 6.2: Current organisation of the volcanic debris avalanche deposit part of the database. The non-volcanic rock avalanche deposits section has a similar structure with accommodation of the differences identified above.

To further assist researchers to evaluate the data presented, confidence levels will be assigned to the various numerical values given. This system, which is also still under review, will assign values to e.g. deposit volume estimates depending on the methods used by the respective researchers. For examples, volumes calculated from high-resolution digital elevation models and on the basis of accurate knowledge of the pre-avalanche topography will receive a higher confidence level than those estimated from few deposit thicknesses and area estimates, etc.

6.4. "COMPLETENESS ANALYSIS"

At this early stage of data collection, no single entry (see Table 6.2) is 100 % complete. For example, the plot of volume versus runout (Figure 1) represents 32 % of the entries, and the plot of volume versus area represents only 23 % of all deposits listed in the database. Individual entry 'completeness' ranges from 57 % for known deposit ages, 48 % for drop heights, 25 % for type of collapse trigger, 15 % for collapse scarp descriptions, 14 % for block facies descriptions, 5 % for basal contact descriptions, to approaching 0 % for some fields such as e.g. collapse scarp volume (1 %), pre-failure edifice weakening mechanisms (0.7) or other deposit characteristics rarely discussed in the literature.

6.5. VOLCANIC DEBRIS AVALANCHE DEPOSIT DATABASE GLOSSARY

Basal Facies

Basal part of the debris avalanche that differs from the units above either by mixing of debris avalanche material with material entrained from the runout path (e.g. sediments, organics, etc) or by signs of extensive shearing, structureless appearance, lack of clasts or any other characteristic that clearly distinguishes it from the rest of the deposit. Thickness of this unit can range from a few millimetres to several meters.

Block Facies

The block facies consists of jointed and deformed fragments of volcanic deposits that were derived directly from the source volcano (Ui and Glicken, 1986). A 'block' is a

relatively coherent piece of the source volcano (Ui and Glicken, 1986) and can be of any size, from centimetres to hundreds of metres. They are commonly poorly consolidated, and often preserve the original stratigraphy of the collapsed mountain (Calvari et al. 1998). The term 'clast' is used in Ui and Glicken (1986) to describe individual constituents of the matrix facies to distinguish them from the blocks in the block facies (i.e. a clast can be a derivative of a block or can be foreign material incorporated from the runout path, etc). These definitions of 'block' and 'clast' most closely reflect the common usages of the terms in the literature.

Collapse Scarp

Opened depression, area of the initial destabilization and source of the avalanche.

Collapse Scarp Data (width, length, depth, aperture)

Length (L): distance from the headwall (= wall opposed to the mouth of the depression) to the mouth (=aperture of the sector/flank collapse depression) of the depression (generally the direction of the length corresponds to the direction of the collapse)

Width (W): largest distance between the sidewalls (= walls face-to-face) orthogonal to the length (walls = steep limits of the source)

Actual depth (A_d): height between the summit and the floor (= interior of the depression, generally plane or with a low angle) of the actual depression

Initial depth (I_d): height between the summit of the edifice before the collapse and the floor of the depression before any modifications.

Volume initial of the sector collapse (V_i): volume of the actual depression (calculated with the pre-collapse edifice and the actual edifice).

Direction of the sector collapse: Aperture angle (α); Floor slope (β): slope of the depression floor.

Collapse Scarp Shapes

Shape of the sector collapse scarp in cross section:

- Spoon-like scarp (Mount St. Helens): β gentle, I_d irregular
- Regular scarp (Las Isletas, Mombacho): β high, I_d regular

- Step-like scarp (Socompa): depression floor very irregular, common toreva blocks

Shape of the sector collapse scarp in plan view:

- Horseshoe scar (Mayuyama): W within the depression (commonly α gentle and $L/W > 1$)
- U-shaped scarp (Iriga): W constant from the mouth to the interior of the depression (commonly α gentle and $L/W > 1$)
- Amphitheatre scarp (Shiveluch): W at the mouth of the depression (commonly α high and $L/W < 1$)
- Triangular scarp (Socompa): W at the mouth of the depression (α and L/W variable)

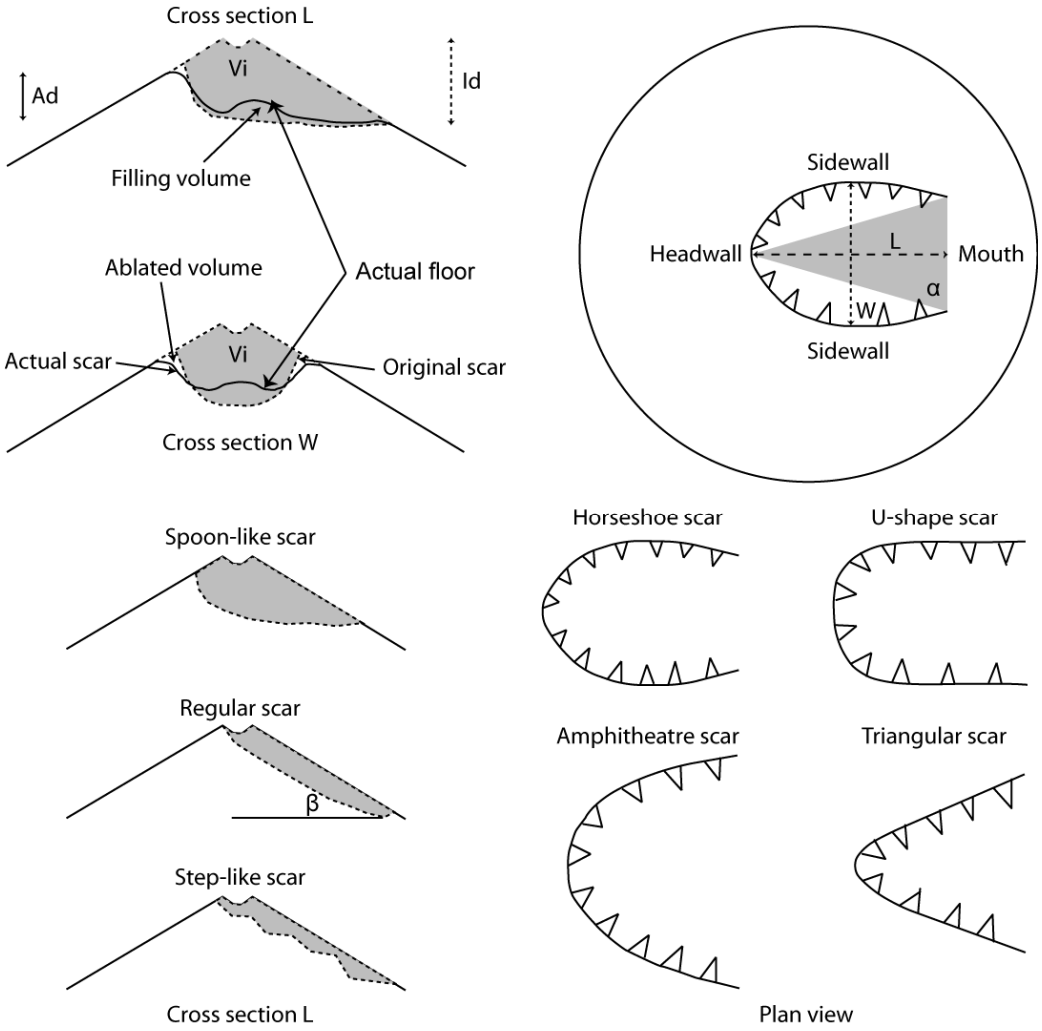

Figure 6.2: Sketches showing the collapse scarp shapes and dimensions; collapse scarp data and shapes courtesy of B.Bernard.

Collapse Trigger

Event which directly triggered edifice/slope collapse, usually an earthquake, eruption or climatic events such as a severe rainstorm.

Complex Volcano

see ‘Compound Volcano’

Compound Volcano

Volcanic massif formed from coalesced products of multiple, closely spaced vents (Davidson and De Silva, 2000)

Debris Avalanche

Debris avalanches are rapidly moving masses of unsorted rock, debris and soil mobilized by gravity (after Schuster and Crandell, 1984) commonly triggered by gravitational or seismically induced slope failure or volcanic eruptions. In volcanic settings, the initial source material is typically heterogeneous in type, grain size and strength. Debris is often sourced from the initial slope material, but it can also be entrained from the substrate during runout. Debris avalanches differ from debris flows in that they are not water-saturated and in that the load is entirely supported by particle-particle interaction (Vallance and Ballard, 2000). Volcanic debris avalanches described in the literature however include (1) debris avalanches sensu stricto that were mainly grain flows as described by Glicken (1998), (2) those that transformed from grain flows into debris flows, and (3) deposits that are entirely those of debris flows (Scott et al., 2001). Debris avalanches are transitional between rock avalanches and debris flows on the continuum to hyperconcentrated flows and further to dilute streamflows (Smith and Lowe, 1991).

Deposit Framework

Description of the overall structure of the deposit, e.g. mainly clast-supported, mainly matrix-supported, structureless, massive, presence of distinct units, mono- or hetero-lithologic, etc)

Deposit Shapes

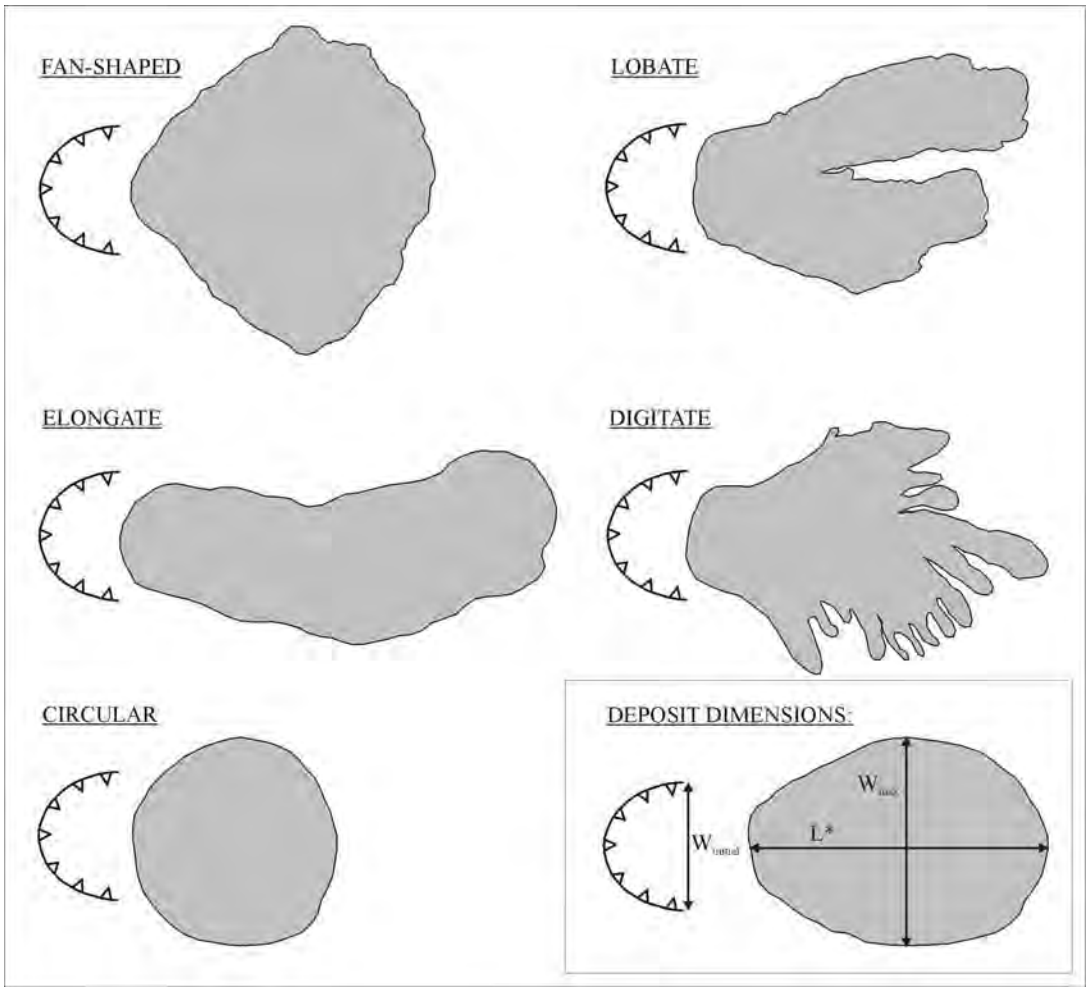

Figure 6.3: Common deposit shapes and definitions of the deposit dimensions.

Drop Height

The drop height (H) refers to the elevation difference from the top of the collapse scar/original summit elevation to the elevation at the distal toe of the deposit. The ratio H/L is commonly used to derive the apparent friction coefficients. (see Figure in 'Length' definition)

Hydrothermal Alteration

Refers to hydrothermal alteration inherited from the source area; excluding post-emplacement in-situ hydrothermal alteration of the deposit where possible

Jigsaw-fractured Block/Clast

Debris avalanche block/clasts that are fractured but not disaggregated (Glicken, 1996)

Landslide

Downslope movement of masses of soil and/or rock (after Bates & Jackson, 1984)

Lava Dome

A steep-sided rounded accumulation of lava extruded from a volcano to form a dome-shaped or bulbous mass on congealed lava above and around the vent (Peterson and Tilling, 2000)

Length

Length 'L' refers to the map distance from the top of the point of origin to the distal end of the deposit (e.g Heim, 1932), whereas length 'L*' refers to the actual length of the deposit (after Davies and McSaveney, 1999) and provides a useful correlation between deposit volume and spreading.

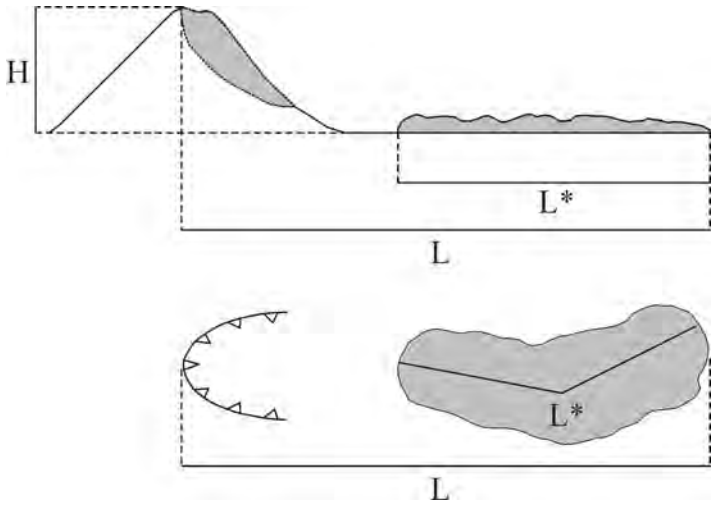

Figure 6.4: Definitions of deposit length (L*), runout (L) and drop height (H).

Lithological Domains

Striking absence of mixing of different lithological units of the source area within the deposit despite intense comminution and long transport distances (also includes entrained material, which is often comminuted as well without mixing with the rest of the deposit material). The position of these lithological domains in the deposit do not necessarily reflect their original position within the source, e.g. initial slope-parallel units may come to rest in the final deposit in this sequence, or the lowest-most unit is

found in the distal deposit area, whereas the originally uppermost units deposited close to source.

Matrix Facies

The fine-grained, crushed material of identical composition as the block facies. Often found in the lower parts of the debris avalanche deposit.

Mixed Facies

The mixed facies is rich in matrix, and often displays various clast lithologies and lacks stratification or grading (Ui, 1983; Crandell et al., 1984; Ui and Glicken, 1986; Glicken, 1991)

Monogenetic Cone

A volcano that erupts only once (Walker, 2000).

Remnant Stratigraphy

Preservation of the original stratigraphy of the source rock, i.e. the lithologies maintain their identity as uniform bands. Textural characteristics of the original rock mass are preserved as the rock is crushed during avalanche emplacement (after Hewitt et al., 2008 and references therein).

Rockslide

The downward and usually rapid movement of newly detached segments of bedrock sliding on a surface of bedding, jointing or faulting. The moving mass usually breaks up into many smaller units. (Bates and Jackson, 1984)

Runout Slope

Slope of the terrain upon which the debris avalanche travelled as estimated prior to avalanche emplacement.

Sector/Flank Collapse:

The sudden destabilization/failure of a major part of a volcanic edifice due to the interaction of two mechanisms: the edifice weakening (hydrothermal alteration,

asymmetric growing…) and a triggering mechanism (eruption, earthquake, heavy rain…).

Shield Volcano

A broad, low-relief volcanic construct made up of relatively fluid lava, typically basalt (Vespermann and Schmincke, 2000)

Stratovolcano

A steep-sided volcano constructed of alternating layers of lava flows and pyroclastic material (after Walker, 2000).

Substrate

Material present in the runout path prior to avalanche emplacement.

Toreva Block

Large coherent segments of the volcano that slid downslope without disaggregation; rotational sliding can produce a reverse dip towards the volcano (modified from Glicken, 1991 and Palmer et al., 1991, as referenced in Siebert, 2002; van Wyk de Vries et al., 2001; Ponomareva et al., 2006).

Volcanic Debris Avalanche Deposit

Volcanic debris avalanche deposits are coarse-grained, poorly sorted, volcanic (partially or entirely) breccias with a grain size from clay to metric blocks (Siebert, 1984). They differ from other volcanic breccias because of their sedimentary architecture such as surface morphology, internal and basal structures, and extent (Glicken, 1991; Ui, 1983).

Weakening Mechanism

Processes prior to edifice/sector collapse that have compromised the stability and integrity of the source material, e.g. hydrothermal alteration, repeated seismic shaking, severe rainfalls and subsequent material alterations, etc.

6.6. ONGOING AND FUTURE WORK

At the time of writing, the database contained descriptions of 299 volcanic debris avalanche deposits from 225 volcanoes and 108 rock avalanche deposits worldwide.

- It is our aim to include submarine volcanic debris avalanche deposits and the smaller, more frequent deposits of less than 0.1 km^3 in volume.
- We hope to encourage data collection to approach a complete (as possible) data set to provide a sound research tool for statistically meaningful analyses and we hope that it offers a platform for previously unpublished data to be made accessible.
- To include a measure of error on data, such as e.g. deposit volume or age, confidence levels will be assigned in accord with the reliability and accuracy of the techniques used to attain said numbers.
- Transfer data into *access*, and format for online publication.
- Furthermore, a compatible database for non-volcanic rock avalanches is envisioned.

Chapter 7:

Summary and Conclusions

In the spirit of:

"A goal is not always meant to be reached,
it often serves simply as something to aim at."

Bruce Lee

Summary – Discussion – Conclusions – Research Outlook

7.1. SUMMARY

Direct observation of rock/debris avalanche emplacement processes is for the most part impossible, and our knowledge of these phenomena is limited to their deposits, to theories of granular flow mechanics, and to laboratory analogues as conceptual models and bridges between theory (dynamic) and field (static) evidence.

The limitations in the study of catastrophic avalanche events were addressed in this work by three major foci:

1. Detailed study of **field examples** with known substrate deformation associated with avalanche emplacement.
2. **Laboratory experiments** to model and directly observe avalanche-substrate interaction.
3. Comprehensive study of the **current state of knowledge** on avalanche-substrate interaction.

1. Well-described and well-exposed rock/debris avalanche deposits with known substrate deformation features associated with the event were chosen to focus attention on basal processes while benefiting from previous work that identified and described avalanche morphology and internal structure.

Observations of basal avalanche/substrate features at Round Top were woven into a comparative study with rock avalanches (a) of similar volume, but differing substrate conditions, and (b) with similar relationships between substrate and morphological features.

(a) It was found that avalanches emplaced over saturated substrates do not travel unusual distances, hence substrate conditions alone cannot explain the long runout of large rock avalanches as has been suggested previously. The explanation for the long runout of large rock/debris avalanches must thus lie in an avalanche-intrinsic process.

(b) While not the explanation for long runout, substrate interactions do introduce complexities and characteristic surface features to avalanche emplacement. Prominent longitudinal ridges are the most characteristic surface features of the Round Top rock avalanche. Here and at other deposits, bulldozed substrate material exists at the ridge termini, initially suggesting a direct link between the morphological expression and the substrate deformation. However, longitudinal surface features are not unique to events with bulldozed substrates and they find their expression in a spectrum of shapes from flowbands to ridges to aligned hummocks, and across a variety of materials and scales. The comprehensive study of substrate features lead to inferences about granular avalanche characteristics reflecting some basic process acting during avalanche emplacement, while the style of longitudinal surface feature development was found to be controlled by a combination of substrate conditions, avalanche velocity and the type of avalanche material.

For a volcanic debris avalanche case study, work on the North Island volcanic debris avalanches at Taranaki and Ruapehu volcanoes was initially envisioned. However, restricted and poor basal outcrop availability rendered these sites insufficient for the task at hand. That said, findings at Taranaki's distal coastal outcrops provided helpful observations integrated in the general discussion of Chapter One. For a more detailed study, the Jocotitlán avalanche deposit in México was chosen because of the widespread presence of deformed substrate and excellent outcrop conditions in and around the debris avalanche deposit. Here the initial assumption was that the large-scale sediment deformation just outside the deposit was a direct result of avalanche emplacement, i.e. bulldozing. It was shown, however, that the deformation features pre-date the collapse event, and that these materials were directly involved in preparing the volcano flank for collapse, supporting the previously formulated volcano-spreading hypothesis through another detailed field analysis. Further intriguing details of avalanche emplacement were deciphered by combining the above findings with other avalanche-related substrate features and morphological evidence to unravel the complex emplacement history of this catastrophic event.

2. The exact process or processes acting at the base of a granular avalanche during travel over deformable and erodible substrate are not completely understood.

A novel approach chosen to illuminate some of the key processes happening well below the surface of the moving avalanche debris was the development of suitable analogue models. With a focus on reproducing the features of field examples and on direct observation of their formation, the results show promising opportunities for further systematic experimentation and more precise quantifications as constraints for numerical modelling.

3. Every model is based on assumptions and requires empirical data from rigorous and detailed case studies. The comprehensive rock- and debris-avalanche deposit database compiled during this work provided an invaluable tool for the detailed study of the selected case examples, for comparison between events, and in providing a thorough overview over the current state of knowledge, areas that lack sufficient input data, and the universality of substrate interaction in large rockslope and volcano flank failure events. Through the careful comparison of data from well-described rock avalanche deposits it was shown through this work that (a) saturated sediments cannot be the explanation for the long runout of large rock and debris avalanches, and (b) that longitudinal surface features are characteristic of rock, debris, ice and snow avalanches.

The breadth of the study produced chapters that are essentially stand-alone projects that complement each other by illuminating a complex topic from different angles, ranging from focusing detailed attention to selected field examples, charting the literature for data and collapsing these into a usable format, by looking at the base of avalanche processes on the small laboratory scale, and by expanding field and laboratory observations with theoretical considerations.

7.2. DISCUSSION

7.2.1. Avalanche Runout

Descriptions of substrate involvement in rock/debris avalanche emplacement and of the avalanche basal facies exist for 12 % of the volcanic deposit entries in the database presented herein, and for 38 % of the non-volcanic deposits. The discrepancy between the two is probably a function of outcrop availability (itself a function of deposit thickness and local erosion rates), and the research foci of the respective researchers in the volcanic and non-volcanic disciplines. Where outcrop situations allow for a closer inspection of the avalanche base, interaction features with the substrate are commonly found – apart from few exceptions (p.57), and spatially restricted examples in otherwise substrate-disrupting avalanche events (p. 56). In short: rock and debris avalanches invariably interact with the materials in their runout paths.

Resulting from the interaction with substrate materials are two extremes of feedback on avalanche mobility: runout enhancement or impediment. The first occurs when:

a) enough water is incorporated to facilitate transformation into more mobile debris flows (p. 27),
b) basal friction is low; e.g. emplacement over glacial ice (p. 46) or by basal saturation (p. 29), or
c) substantial (> 20 % of the final deposit volume) amounts of weak and/or saturated material are entrained on the steep failure slopes (p. 26).

Impediment of avalanche motion, on the other hand, often happens when deforming or yielding substrates are encountered, and is indicated by raised margins and compressional features in the avalanche deposit (p. 79).

In both extremes (runout enhancement and impediment) the avalanches reach travel distances that exceed those of simple frictional model predictions. Therefore, lubrication by liquefied soils and saturated sediment is not a universal explanation for the long runout of large (> 10^6 m^3) rock avalanches (as previously proposed by Buss

and Heim, 1881; Abele, 1974; Sassa, 1988; Legros, 2002; Hungr, 2006); instead the explanation must lie in an avalanche-intrinsic, dynamic process. Substrates then add variations and complexities similarly to topographic interferences (Nicoletti and Sorriso-Valvo, 1991). Further evidence against substrate lubrication as the sole explanation of high avalanche mobility is the observations that avalanches in dry areas also show 'excess' travel distances.

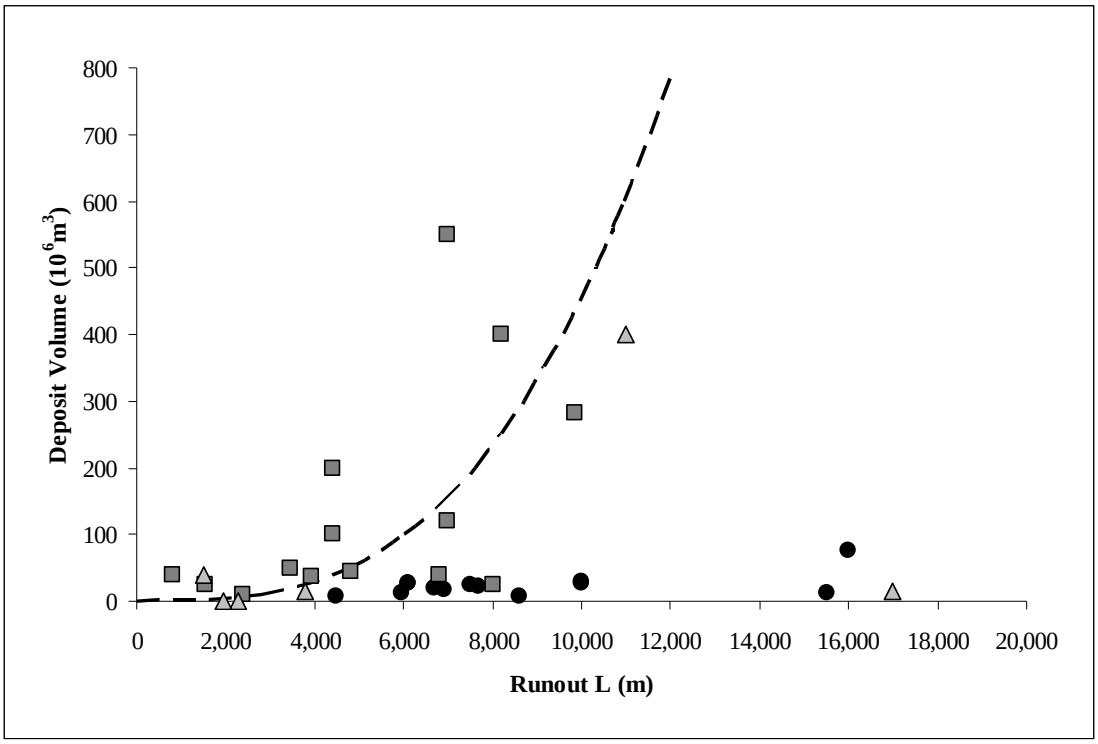

Figure 7.1: Data of rock avalanches emplaced over glacial ice (circles), those which entrained substantial amounts of substrates (triangles), and avalanches that deformed runout path material without entraining larger amounts (squares). The dashed line is an empirical prediction (see text).

Figure 7.1 illustrates the range of avalanche-substrate interaction scenarios and the resultant volume-runout relationships of the avalanche deposits. The only clear trend that can be discerned from this graph is the relatively higher mobility of avalanches emplaced over glacial ice (circles), some of which were also emplaced down narrow valleys. Substantial entrainment (triangles) mainly follows the dashed line of the empirical prediction (except the Cerro Rabicano event which transformed into a debris flow 5 km from source). Substrate deformation cases (squares) show a greater scatter. The dashed line represents runout predictions based on empirical analyses by

Davies (1982) and this study. Davies (1982) found that the spreading (deposit length L^*) of a rock avalanche is related to its total volume (V) by:

$$L^* = 10 \cdot V^{(1/3)} \quad (13)$$

Deposit name	Volume ($10^6 m^3$)	L (m)	L* (m)	L/L*	Reference
Elm	10	2,375	1,820	1.3	Hsü, 1975
Goldau	40	6,100	4,930	1.2	Heim, 1932
Dieblerets	50	5,500	4,920	1.1	Heim, 1932
Poschiavosee	150	4,000	2,800	1.4	Heim, 1932
Kandertal	1,150	10,500	7,900	1.3	Heim, 1932
Flims	1,200	16,500	9,810	1.7	Heim, 1932; Pollet and Schneider, 2004
Round Top	45	4,800	3,500	1.4	Wright, 1998
Mt Cook	24	7,500	6,340	1.2	McSaveney
Acheron	10	3,500	3,030	1.2	Smith et al., 2006
Chaos Jumbles	30	2,910	2,170	1.3	Eppler et al., 1987
average				**1.3**	

Table 7.1: Volume, runout (L) and deposit spreading (L^*) data used to determine the runout-spreading ratio (L/L^*).

Statistically, the average relationship between spreading (L^*) and runout distance (L) is a factor of 1.3 (Table 7.1), therefore:

$$L = 1.3 \cdot L^* \quad (14)$$

Avalanches emplaced on glacial ice are more mobile than this relationship predicts. Those which have entrained large amounts of material follow the predicted trend, whereas avalanches that deformed substrates without entraining substantial amounts scatter and plot on both sides of it. The entrainment cases, even though they travelled longer distances than they would have without entrainment, scale with the prediction because the graph plots the final deposit volumes versus runout.

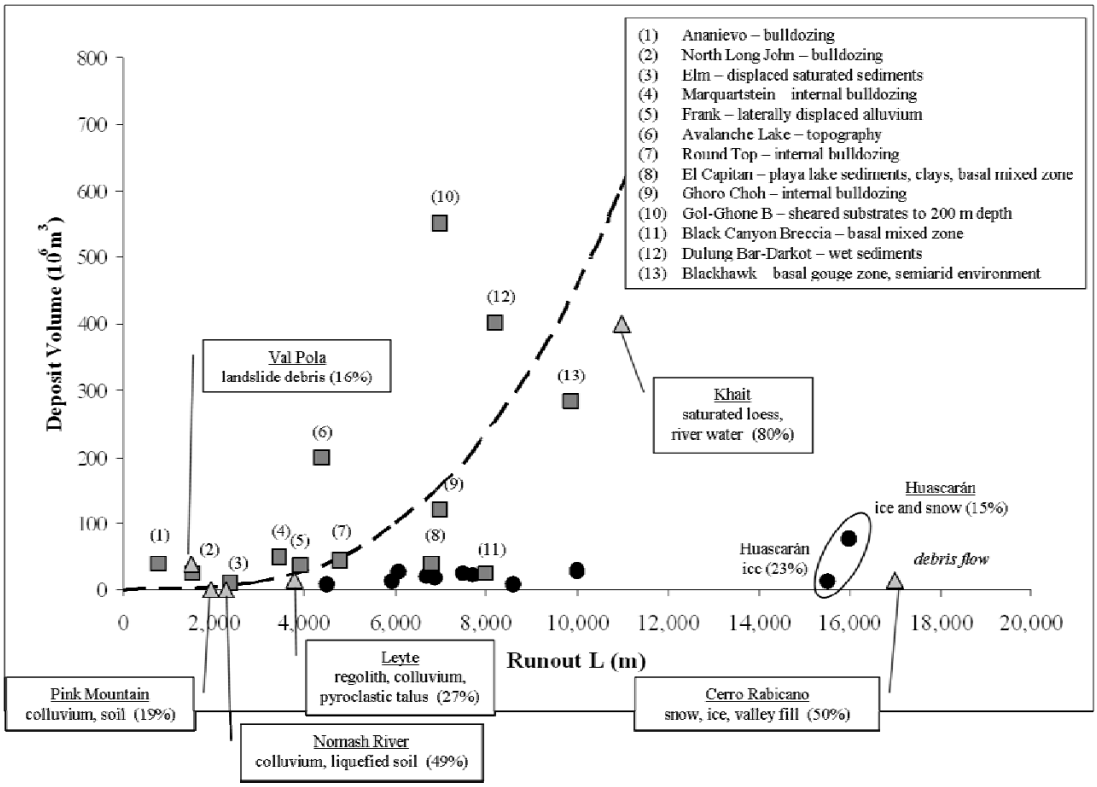

Figure 7.2: Details of substrate interaction types for the data presented in Figure 1. Rock avalanches in boxes have entrained substantial amounts of substrates of the type listed; numbers in parentheses show the amount entrained in percent of the final deposit volumes. Cerro Rabicano transformed into a debris flow at 5 km from source.

These analyses shade in relative trends of the various avalanche-substrate interaction styles detailed in Figure 7.2 and 7.3. At the low end of the trend are substrate bulldozing, topographic interference and energy dissipation by e.g. shear stress transmission into the substrate (p.51). Indications that deformable substrates impede avalanche travel are preserved in the field in the form of raised margins (e.g. North Long John RA), compressional features within the deposit (e.g. Round Top), avalanche material sunk into weak sediments (e.g. Llullaillaco VDA), and bulldozed substrate materials. The volume of substrates deformed by avalanche events can be in the millions to tens of millions of cubic metres (Hewitt, 2006), and the energy needed to deform these is lost from the avalanche kinetic energy, resulting in shorter travel.

At the other end of the substrate-influence trend are processes that increase avalanche runout, such as shearing in a weak basal zone, reduced basal friction and, generally, volume-increase by entrainment (Figure 7.3b). Evidence of high mobility over saturated sediments is preserved in e.g. increased deposit thinning with associated

digitate emplacement or isolated hummocks beyond the deposit margins (e.g. Hewitt et al., 2008).

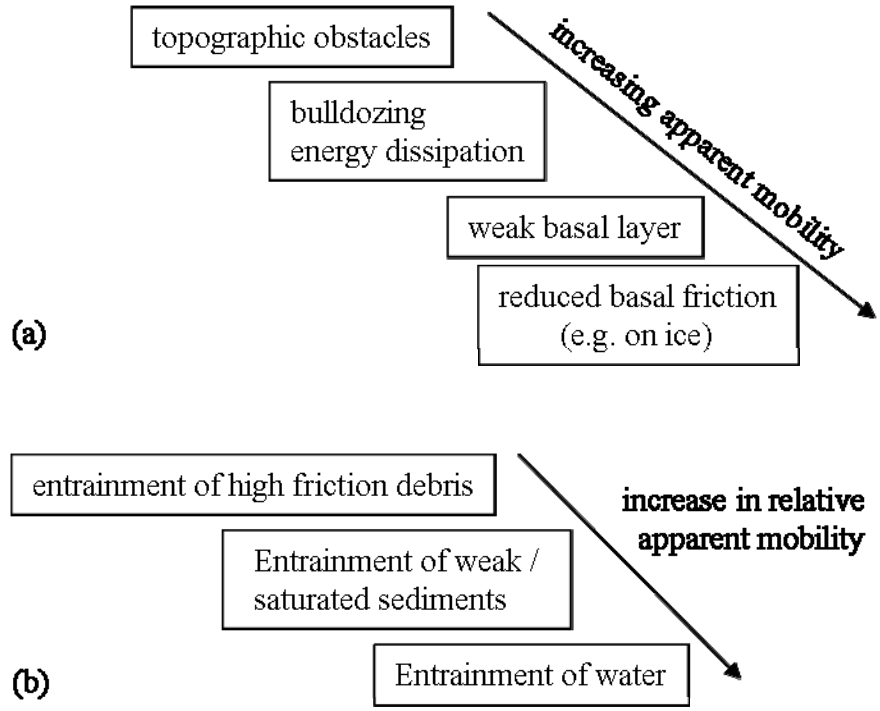

Figure 7.3: Relative avalanche mobility derived from field observations: (a) substrate deformation and (b) substrate entrainment scenarios.

Entrainment of substrate material increases the bulk avalanche volume and hence spreading and runout distance. Common factors involved in the six entrainment examples shown in Figure 7.2 are that entrainment occurred on the steep failure slopes (30-50º), and the events were triggered by high rainfall (Leyte, Val Pola, Pink Mountain, Cerro Rabicano), snow/ice melt (Val Pola, Pink Mountain, Nomash River), or earthquakes (Khait, Huascarán). The runout topography varied from river valleys (Val Pola, Nomash River, Khait, Cerro Rabicano), flat glacial valleys (Pink Mountain) to open plains (Leyte, distal Khait).

The influence of substrate entrainment on avalanche behaviour and runout depends on the substrate material properties and degree of saturation, entrainment style (e.g. ploughing at the avalanche front versus gradual addition of material through basal shear), and the amount entrained. To induce the transformation into more mobile debris flows, about 20-50 % water by volume of the total avalanche

volume is required (p.28). However, saturating the avalanche base alone, instead of the total volume, can lower basal friction and potentially increase mobility (p.29). However, in terms of sedimentary material, the examples shown in Figure 7.2 suggest that the volume of entrained material is less important with respect to influencing avalanche dynamics than the material type, and potentially the style of entrainment. Evidence from the snow avalanche literature indicates that the style of entrainment is related to substrate properties: ploughing is observed in low-friction substrate materials, whereas basal abrasion occurs in high-strength substrates (p.35), which affects the distribution of the entrained material in the avalanche body.

To tie back into the initial theoretical calculations presented in Chapter 1, trends for the scenarios sketched in Figure 1.5 are calculated, which illustrate the effect of basal friction on translation of the centre of mass. Drop height (h), failure slope angle (α) and the total deposit volume are based on representative rock avalanche data from the literature. Assumptions had to be made in terms of positioning the spread deposit around the centre of mass: from field observations it appears most reasonable that about two thirds of the deposit length lie beyond the centre of mass in the down-motion direction (e.g. deposit profile sketches in Heim, 1932).

	h	α	V_m	V_n	V_s	V_{total}	μ_1	μ_2	μ_4	T	L*	L_{max}
(a)	1000	45	40	0	0	40	0.6	0.6	0.6	1667	3420	3947
(b)	1000	45	80	0	0	80	0.6	0.6	0.6	1667	4309	4539
(c)	1000	45	30	10	0	40	0.6	0.9	0.9	1387	3420	3470
(d)	1000	45	30	0	10	40	0.6	0.6	0.9	1345	3420	3548
(e)	1000	45	40	0	0	40	0.6	0.3	0.3	2833	3420	5113
(f)	1000	45	30	10	0	40	0.6	0.3	0.3	2569	3420	4849
(g)	1000	45	30	0	10	40	0.6	0.6	0.3	1804	3420	4084

Table 7.2: Main input parameters for the runout calculations of scenarios (a) through (g), Figure 1.5. Volumes are in 10^6 m^3 and distances for T and L are in metres. The value for x_3 is set to zero to simulate changes in basal friction/entrainment at the bottom of the failure slope; x_1 is set to 500 m. The deposit tail is positioned 1/3 from the centre of mass (T) based on rock avalanche profile sketches in, e.g. Heim (1932).

In these assumptions, no attempt is made to accommodate for (1) basal frictional resistance feedback on avalanche spreading and avalanche tail position even though marked differences in avalanche deposit length and tail mobility have been observed in dependence of basal substrate resistance in small-scale laboratory models (p. 170),

(2) deposit thinning resulting in increased spreading as documented over glacial ice or (3) bulldozing and raised distal margins reducing deposit length. The calculation results are shown in Table 7.2, and Figure 1.5 is reproduced with these values (Figure 7.4).

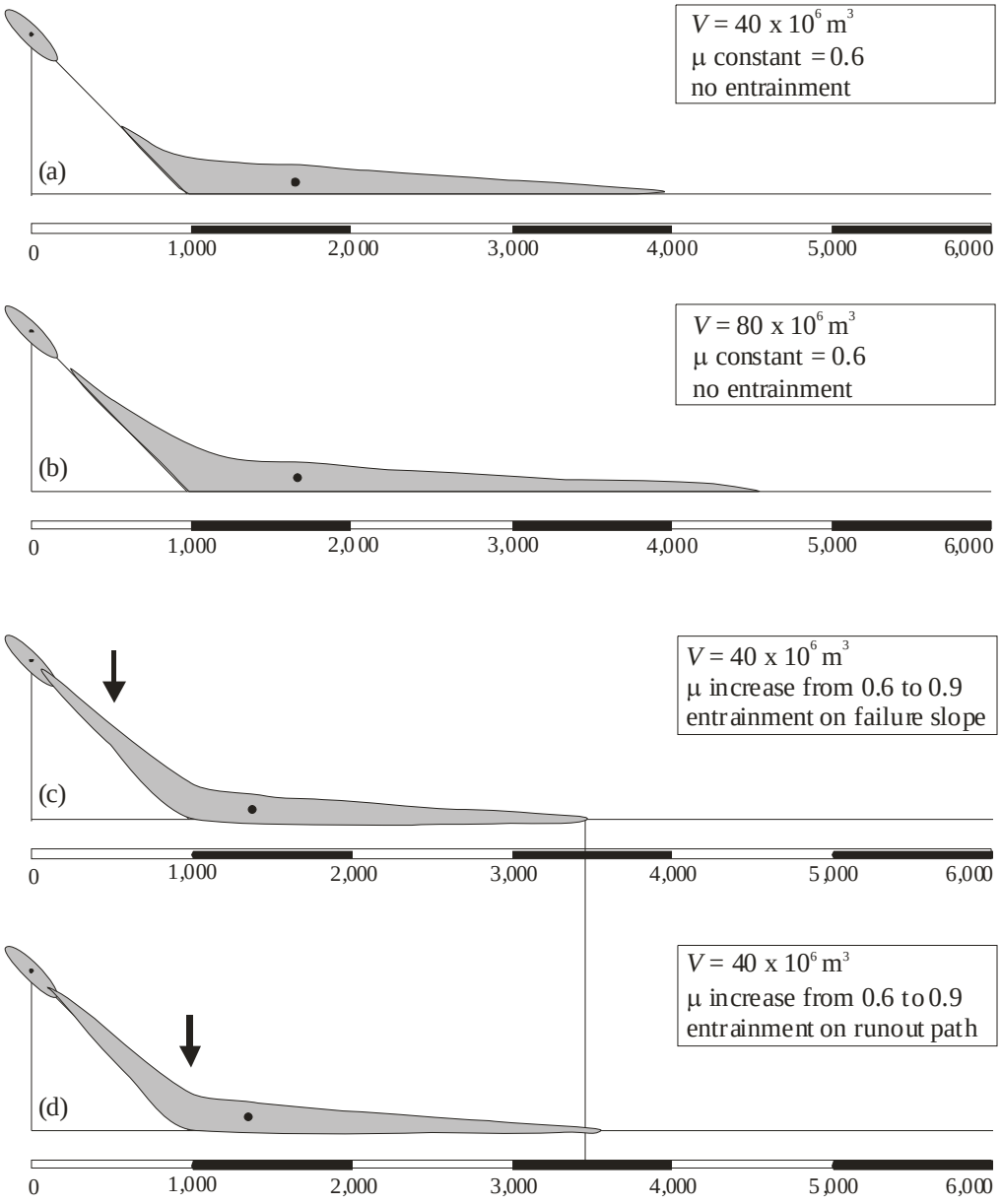

Figure 7.4: Graphical representation of Table 7.2; black dots mark the location of the deposit's centre of mass; arrows point to the location of substrate entrainment. See text for discussion.

For all the case examples shown in Table 7.2 and Figure 7.4, the final deposit volume is 40 x 10^6 m^3 (except for case b). Both cases (a) and (b) have constant basal friction coefficients (μ) of 0.6 and retain constant mass throughout emplacement. Scenarios

(c) and (d) simulate added mass with an increase of μ to 0.9 at the point of entrainment (indicated by arrows in Figure 7.4). Runout lengths are not greatly different and the centre of mass is stopped immediately after leaving the steep failure slope. More realistic analyses would take into account the substrate-induced changes in avalanche deposit spreading and hence morphology (e.g. Crosta et al., 2008); and in fact runout is most likely to be shorter than depicted in the sketches above.

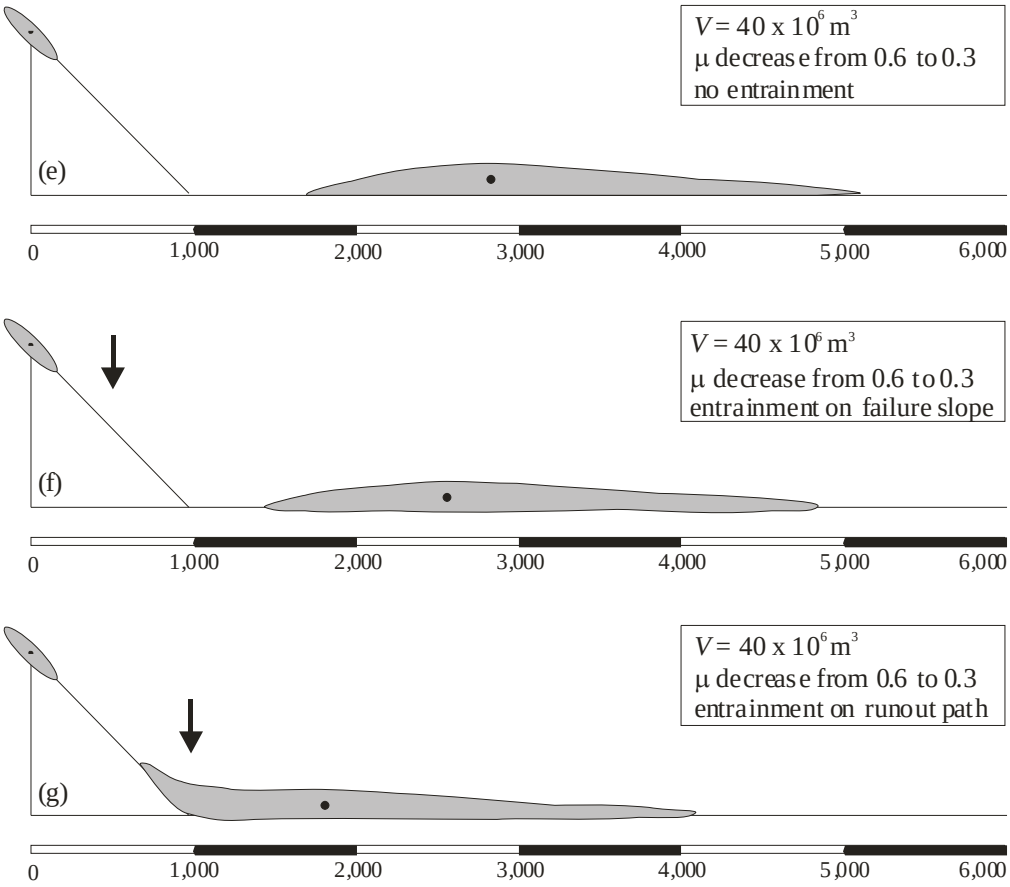

Figure 7.4: continued.

Similarly, for reduced basal friction in scenarios (e) through (g), the simultaneously observed deposit thinning and increased spreading has not been considered in the theoretical considerations, and the trend hence underestimates the increase in runout for these cases. Introducing the same reduction in basal friction and adding mass on the steep failure slopes resulted in slightly lesser runouts (f) than in the glacial ice scenario without entrainment (e) due to momentum loss by adding stationary material to the moving mass in (f). Adding the same volume and lowering the basal friction by the same amount from a point later in the emplacement, i.e. on the flatter runout path

(g), resulted in runout close to case (a) where no entrainment or change in basal friction occurred.

Entraining mass and decreasing basal friction on the steep failure slope has a greater effect on runout than introducing the same changes on the flat runout path because of increased momentum gained during descent. In contrast, adding mass and increasing basal friction shows a greater affect on the flat runout path (Figure 7.5) by inducing more rapid deceleration (compare to the bulldozing hypothesis on page 43).

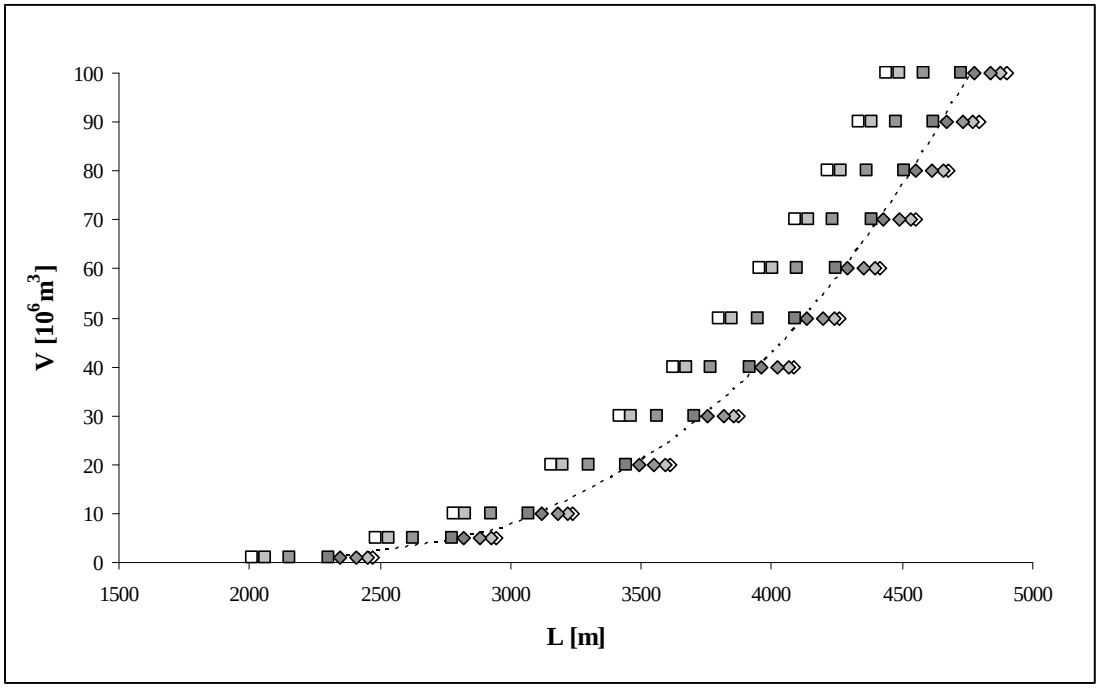

Figure 7.5: Entrainment on the runout path of basal-friction-increasing (squares) and basal-friction-reducing (diamonds) materials is simulated at varying distances from the bottom of the source slope; darker shades are increasing distances (x_3) from 0, 100, 300 to 600 m. The dashed line represents constant mass and basal friction coefficient during runout (scenario (a), Figure 7.4).

Comparing these calculated trends to the empirical prediction discussed above (equation 14) shows that the data overlap (Figure 7.6): the empirical prediction fits closer to the high basal friction data for smaller avalanche volumes, and closer to the low basal friction data for greater avalanche volumes. This can be explained by the effects of volume on basal stresses and fragmentation pressures: greater avalanche volumes will be accompanied by greater avalanche thickness and therefore increased basal stresses and fragmentation pressures, leading to greater avalanche mobility.

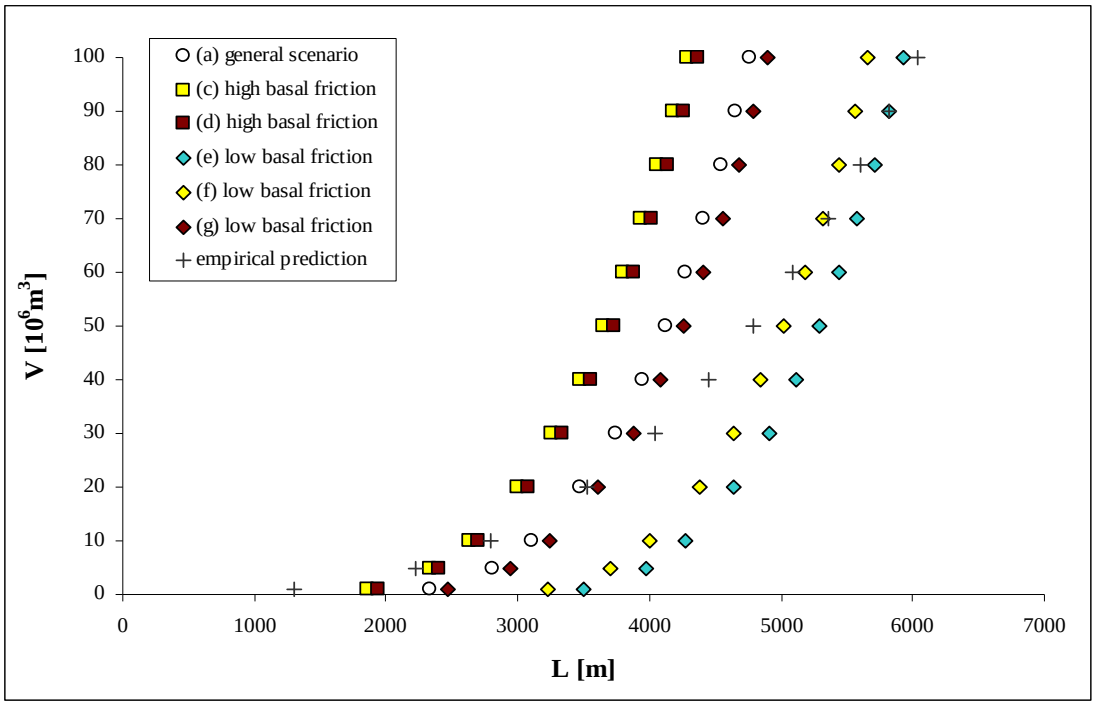

Figure 7.6: Calculations of trends for the various scenarios depicted in Figure 1.5. The empirical prediction is the one discussed above (equation 14).

7.2.2. Volcanic and non-volcanic deposit morphologies

In contrast to non-volcanic rock avalanches, volcanic debris avalanche deposits are generally larger (Figure 7.7), and are sourced in weaker materials, and often involve a weak base composed of fine-grained materials such as edifice-underlying volcaniclastics, the hydrothermally altered core of the edifice, and/or water-saturated material originating on failure planes in edifice aquifers (e.g. van Wyk de Vries et al., 2001; Siebert 2002 and references therein).

The Lastarria avalanche deposit is a good example of weak source material facilitating high-velocity emplacement originating from a low-angle failure plane and producing a deposit with little lateral spreading. Flowbands with herringbone textures similar to those found in crater ejecta, and overriding of a 250 m high cone testify to this event's high velocity.

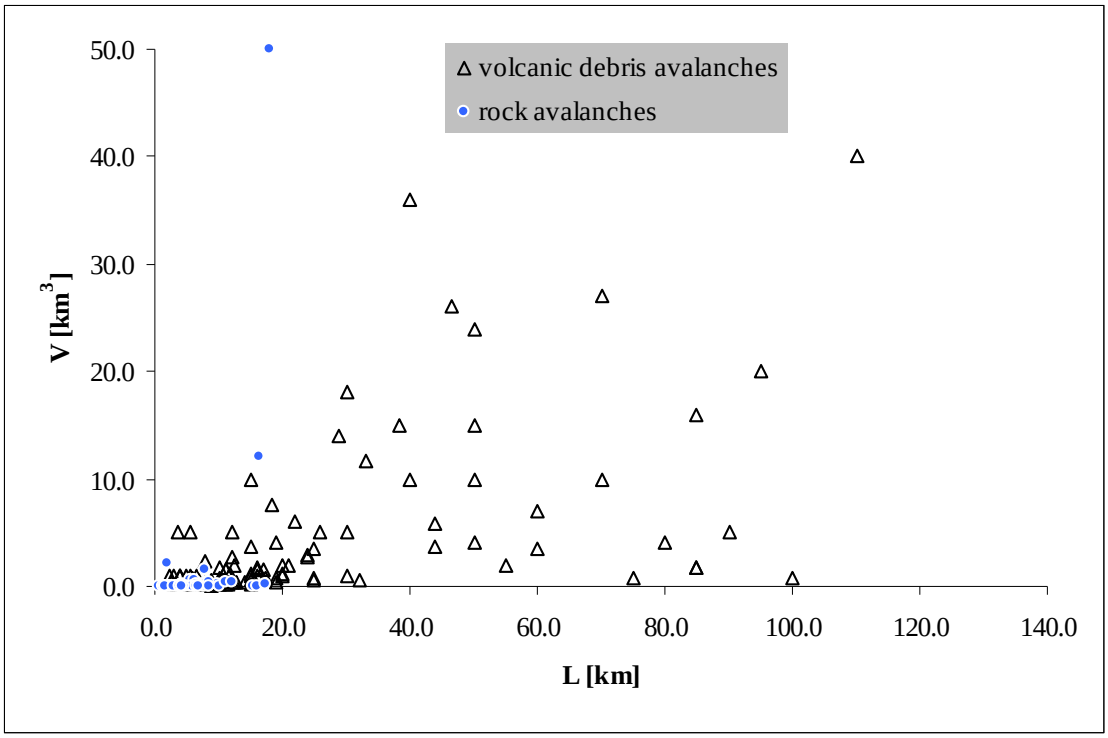

Figure 7.7: Volume-runout relationships of volcanic debris avalanche (triangles) and non-volcanic rock avalanche deposits (circles).

Surface features such as flowbands of both non-volcanic rock and volcanic debris avalanches can be useful for the identification of emplacement dynamics, e.g. in remote investigations, because they provide insights into emplacement velocity, source material properties and basal/substrate conditions (Chapter 2). Numerical classifications of hummocks, ridges and flowbands have been established in this context (p.68).

Longitudinal ridges at the Round Top rock avalanche (Chapter 3) are well preserved examples of how substrate bulldozing influences the formation and preservation of these features in the final deposit by preventing their breakup into smaller hummocks. Even though emplaced onto saturated sediments, the Round Top rock avalanche did not travel an unexpectedly long distance (Figure 3.15, p. 117). Substrate bulldozing might have offset any enhanced mobility, the latter indicated by distal digitate emplacement. An abrupt change in deposit topography is accompanied by compressive features in the hummocks, and signifies sudden stopping of the main avalanche body while the frontal material continued travel to leave a thinner debris cover.

The Jocotitlán debris avalanche (Chapter 4), with its three distinct morphological domains, is a clear example of substrate- and topography-induced complexities in avalanche emplacement. Substrata extruding from beneath the volcano resulted in edifice spreading and ultimately collapse and emplacement of a blockslide deposit. Part of this material toppled over a topographic step and travelled down a broad valley at high velocity leaving large longitudinal ridges. In the western area, where less substrate and topography interaction occurred, the debris avalanche resembles the 'typical' hummocky volcanic debris avalanche morphology. The steepness of these large, unusually conical hummocks is facilitated by the strong avalanche material lacking fines or weak components which would lower the bulk angle of repose (e.g. Chapter 2; Clavero et al., 2002).

In topographically confined runout paths, lateral avalanche spreading is restricted, and the avalanche debris mainly interacts with the dry valley walls, resulting in greater confining pressures and less interaction with substrates to slow the base down through energy absorption (Davies and McSaveney, 2009). Where runout is unconstricted, the deposit planform depends on avalanche velocity, and the underlying sedimentary material. Strom (2006) put forward the hypothesis that in dry climates avalanches have the potential to travel further than those emplaced in wet conditions due to increased lateral spreading of the latter. For lateral spreading to occur, the initial velocity directed linearly away from source must be diverted and momentum dispersed into the flow-perpendicular direction, initiated by e.g. weak basal conditions such as saturated substrates. This will lead to a velocity decrease in the flow-parallel direction and ultimately reduced runout; unless extensive flow thinning occurs simultaneously as observed over ice. Strom's hypothesis could be tested with detailed datasets as envisioned and discussed below.

All the above factors (avalanche source material, runout path topography and substrates) interact to give rise to distinct avalanche surface morphologies and substrate interaction features. On the left hand side of Figure 7.8 are the avalanche properties of basal composition, permeability, and emplacement velocity influencing its erosive capacity, and its source lithology, which plays an important role in e.g. hummock steepness. On the right hand side are the factors that influence the substrate's erodibility and deformability: degree of saturation, porosity and

permeability influencing drainage response, and the sediment thickness and depth to weak layers or interfaces such as layer boundaries. Furthermore, the location of substrate encounter (steep failure slope versus flatter runout path) and the runout path topography (large basal area in contact with substrate on open runout plains versus relatively small basal area in narrow valleys or topographic channelling) play important roles in the feedback of substrates on avalanche dynamics.

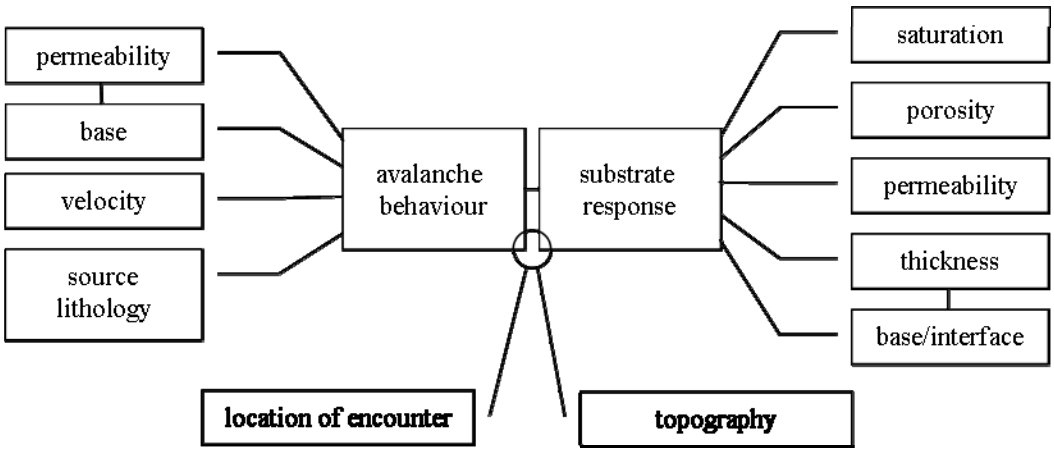

Figure 7.8: Avalanche and substrate properties influencing their interactions. On the left-hand side are the factors controlling the avalanche's erosive capacity, and on the right-hand side are the substrate material properties that govern its erodibility.

It is interesting to observe the similarity of substrate deformation and deposit surface features of mass movement deposits at different scales and with varying details in emplacement dynamics:

- sub-glacial sediment deformation
- high-strength, high-friction rock avalanches
- heterolithological debris avalanches
- volcanic debris avalanches with high proportion of weak materials
- high-velocity pyroclastic flows
- snow and ice avalanches
- small-scale laboratory models

These situations range from very simple laboratory granular flows to large-scale, slow glacial processes, to complex, large-volume, dynamic avalanches occurring in highly different environments and source materials, which indicates that certain features are intrinsic phenomena of all granular materials in motion (see e.g. Chapter 2). Despite the differences in dynamics between the laboratory and real-life avalanche events (Table 7.3) substrate deformation features were successfully recreated in small-scale flume experiments. Though qualitative in nature, the results of small-scale flume experiments conducted during this study have been used to discuss substrate feedback on avalanche runout and deposit length/profile as a first approximation. It has been shown elsewhere (e.g. Davies et al., 2003; Lajeunesse, in review) that microscale modelling of natural phenomena such as rivers, can be successful in reproducing processes and tendencies of natural phenomena despite a significant lack of dynamic similarity. Even though the detailed processes of small-scale water and sediment behaviour differed from those of real-size rivers (e.g. laminar versus turbulent water flow), the authors were successful in predicting river bed response from their experiments. Similarly, the experiments conducted in the context of this research, although not following dynamic similarity, showed processes and features identical to field observations, which demonstrates the universality of such features in spite of arbitrary choice of scale and materials.

Rock Avalanches	Volcanic Debris Avalanches	Laboratory Avalanches
shallow or deep seated failure	deep seated failure	\
\	\	controlled runout
hummocks and ridges	hummocks and ridges	hummocks and ridges
comminution during runout	comminution during runout	\
internal deformation	internal deformation	internal deformation
\	\	homogeneous grain sizes
homogeneous (±) in composition	\	homogeneous in composition
\	hydrothermal material	\
substrate entrainment	substrate entrainment	substrate entrainment
substrate fracturing	substrate fracturing	\
substrate bulldozing	substrate bulldozing	substrate bulldozing
substrate deformation	substrate deformation	substrate deformation
undrained loading	undrained loading	?
\	\	surface tension
\	\	electrostatic charges

Table 7.3: Comparison of laboratory, volcanic debris and non-volcanic rock avalanches

7.2.3. Datasets

In the study of unknown phenomena, general trends are often the first pieces of evidence to be established. The geological sciences in particular deal with complex natural events and are notoriously afflicted with large errors and uncertainties in the data available. Approaches in estimating landslide field data varies between authors and thus introduces a large spectrum of errors creating a dataset with highly variable degrees of accuracy. For example, typical ways of calculating the deposit volume are to multiply the area covered by debris with an estimated average thickness of the deposit, grossly simplifying the deposit geometry and its variations introduced by e.g. topography. Another way is to estimate the initial avalanche volume from geometrical analysis of the failure scar with the addition of an assumed bulking factor of the material due to comminution during failure and runout. More accurate approaches are used when high-precision DEM's (Digital Elevation Models) are constructed from available satellite and aerial photography and by using GIS (Geographic Information System) analyses to increase accuracy in deposit thickness and its variations and spatial distribution.

This field data (deposit volume (*V*), area (*A*) and runout distance data (L)) have been used to outline trends on the behaviour of large rock and debris avalanches. Good correlations between the deposit volume and the area covered by debris, and with the total distance travelled are reported by e.g. Dade and Huppert (1998), Kilburn and Sørensen (1998), Shea and van Wyk de Vries (2008), and Legros (2002) based on log-log plots of selected deposits.

Applying logarithmic plots to the larger dataset of this study does not collapse it into neatly defined trends, but rather suggests a general tendency within largely scattered datapoints. The scatter in Figure 7.9 covers a significant 2-3 orders of magnitude, and is much larger than in the previously published plots. In particular, the rock avalanche deposits data in the *V-A* plot greatly diverges from any straight line, real or inferred. What this shows is that there are unconsidered factors affecting *L* and *A*.

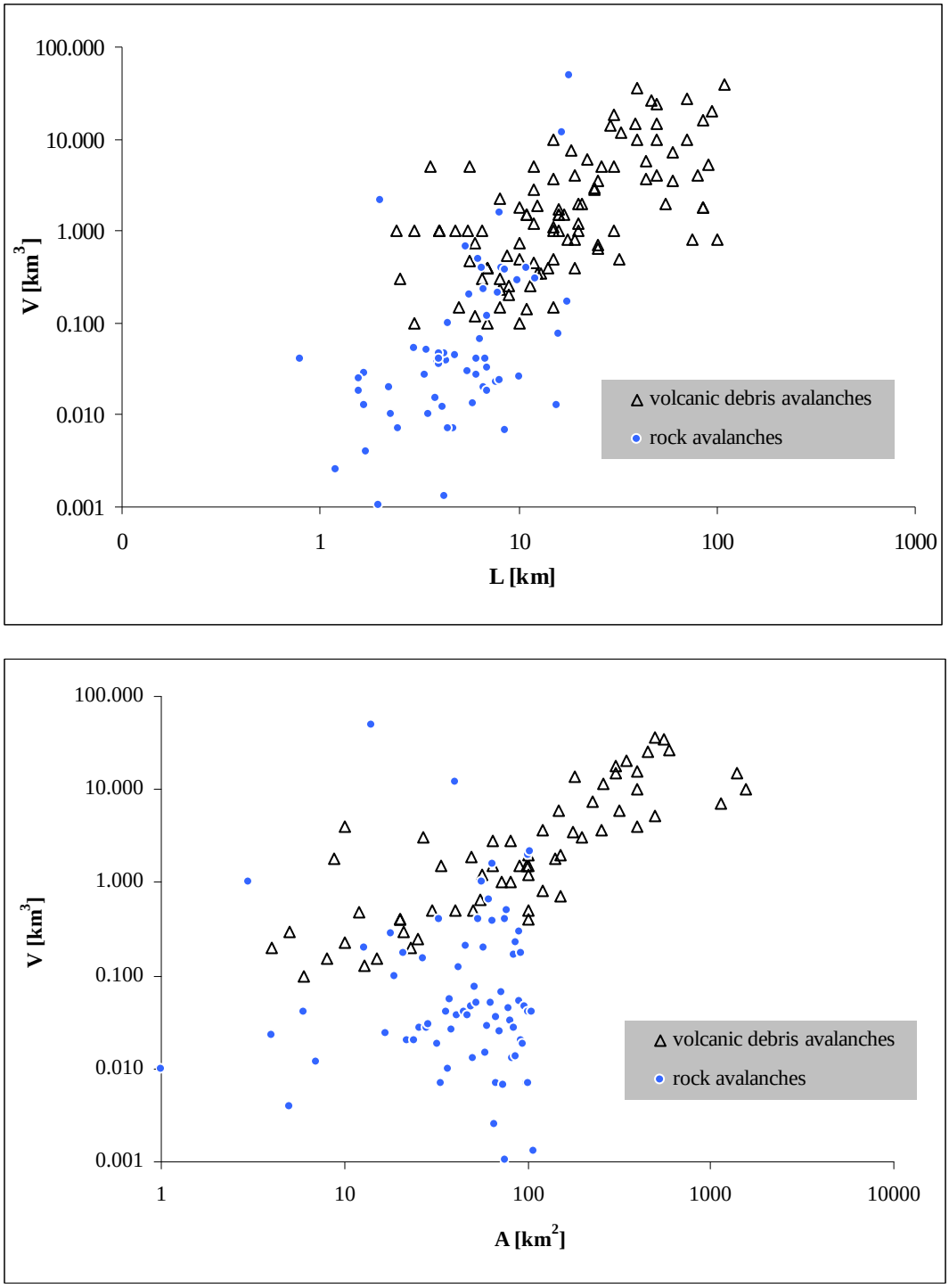

Figure 7.9: Logarithmic plots of volcanic debris and non-volcanic rock avalanche deposits' volume (V) versus runout length (L) and versus deposit area (A).

To correlate the various (known and unknown) factors influencing avalanche behaviour, a unified dataset with quality analyses (confidence levels are currently designed by VOGRIPA to be applied to the volcanic debris avalanche database, which will give a first approximation on the quality of numerical inputs such as *V*, *A*,

L, age, etc; Chapter 6) is needed to provide a sound tool for meaningful statistical analyses. Plotting the data of avalanche deposits according to selected criteria can clarify data plots by explaining "outliers" or by discerning different trends in a largely scattered dataset (e.g. Figure 7.2). Selection criteria might include:

- topographic constrictions and channelling,
- emplacement over specific substrate materials,
- open runout,
- basal conditions,
- source material variations,
- failure slope angle and scarp geometry, and
- combination cases

Some correlations, however, might still only be apparent ones and are only revealed as such when looking at the data from different angles or after gathering more information on the problem. For example, Dade and Huppert (1998) found a correlation between *L/H* and *V*. This correlation was revealed by Kilburn and Sørensen (in the same year) to be no surprise when they found that *H* is, generally, geometrically related to the failure volume because *H* often scales with the failure scar length.

In their recent review of rock slope failure events, Hewitt et al. (2008) point to a shift in research emphasis from the study of single events and regional focus, to a broader, multi-disciplinary and comparative approach, drawing on world-wide datasets to study landslide commonalities. To aid in these research efforts and to test hypotheses with statistical evidence, it is the aim of the database project to compile and unify the volcanic debris avalanche and the non-volcanic rock avalanche data (published and unpublished) and to make it publically available.

7.2.4. Granular flow mechanics

Granular flows are inherently complex and the understanding of their mechanics is often approached through numerical and physical models based on theoretical assumptions and ideal simplifications. Real-life avalanche events in any given geological material and landscape add further complications through variations in

grain material, size and shape, grain size distribution, comminution, degrees of saturation, their interplay with topography and sedimentary material, changes in volume and composition during runout, etc. Field evidence, such as surface morphologies, internal structures and basal contacts, is used to derive information on the behaviour and mechanisms of large rock and debris avalanches. For example, numerous case studies in the past revealed a characteristic feature of rock and debris avalanches from around the world, that of "intensely comminuted debris of the lower/internal parts overlaid by blocky facies" (Abdrakhmatov and Strom, 2006), leading these and other authors previously and since to consider them "universal features, reflecting some basic process acting during rockslide formation and motion". The theory of dynamic rock fragmentation (e.g. Davies and McSaveney 2002, 2006, 2009) to explain the long runout of rock avalanches for example is based on observations like these. During the course of this work, similar characteristic features of granular avalanches across diverse materials and on all physically feasible scales have been discovered in longitudinal surface morphologies (flowbands, ridges and aligned hummocks). Their universality has hitherto not been discussed and their significance as intrinsic outcomes of granular flow mechanics awaits further investigation.

Avalanche-substrate interaction features document processes influenced primarily by two factors: (1) avalanche emplacement mechanisms, and (2) sediment response. Table 7.4 provides a first overview on the types of avalanche-substrate interactions and the insights into avalanche emplacement mechanisms they might suggest.

From this work it is self-evident that an energy transfer between an avalanche and its substrate inevitably takes place. There are no forces that keep the avalanche debris from touching and interacting with the substrate material in its runout path (as for example suggested in the early theory of air-layer lubrication of Shreve, 1968). Undisturbed substrates are localized phenomena only in otherwise erosive and substrate-deforming events. They are found, for example on the lee-side of large boulders or tree trunks, or e.g. in the accelerating part in the runout path curvature were, astoundingly, fragile snow survived unscathed the overriding (without deposition) of rocks and debris travelling at high velocity (Boultbee et al., 2006).

Interaction type	Substrate types typically involved	Insights into avalanche processes	Feedback on avalanche emplacement
Transformation into debris flows	surface water, ice, snow saturated sediments, soil, regolith, colluvium, mud, hydrothermal material	change from 'avalanche' to 'flow'	change in flow regime: longer runout, higher mobility, larger area inundated
Entrainment	anything	erosive capacity	bulking, change in composition, mechanical properties and behaviour depending on type and amount entrained, and entrainment style
Entrainment (> 20 % of final deposit) on steep failure slope	saturated sediments	ease of substrate mobilization on steep slopes	longer runout scales with increase in volume
Low basal friction	snow and ice	importance of basal conditions for the behaviour of the entire avalanche body	longer and thinner deposits; flowband formation
Bulldozing at avalanche front	volcaniclastics, gravels, soil, sand, loam, snow, alluvium, peaty sequences, lacustrine sediments, evaporites	coupling with substrates	(a) decreasing avalanche runout length; (b) increased area inundated. See Figure 1.12.
Bulldozing within avalanche body		coupling with substrates	Preservation of longitudinal ridges by preventing their breakup into hummocks. Hummock shapes.
Folding and faulting	fluvial deposits, coal, sand- and siltstone, silts, gypsiferous clays, lacustrine sediments, alluvium, volcaniclastics, saturated sediments, soils, evaporites	energy transfer	scale dependent, e.g. large-scale folding can lead to bulldozing and loss of kinetic energy to a degree to lead to more rapid deceleration
Shearing and comminution	weathered granite, glacial outwash, carbonate, granite, volcaniclastics, soil, all rock types	shear stress transfer; importance of basal conditions for the behaviour of the entire avalanche body	depends on "sufficiency" of shear stress transfer; weak basal sheared mixed zone and potentially longer runout
Substrate failure at depth	ignimbrite	coupling with substrates, energy transfer	weak basal layer; shear stress and energy 'loss'
Injection features	liquefied soil or clastic sediments	extension and formation of openings during and after emplacement; basal shear; substrate loading	none: feature preservations suggests late-stage event
Truncated clastic dikes	liquefied soil or clastic sediments	differential motion within the avalanche body at least during deceleration stage	none
Undisrupted substrates	conglomerate, sandstone, welded ignimbrite	spatially heterogeneous interaction with substrate; fine-grained basal (boundary) layer in some cases	none

Table 7.4: Summary of substrate interaction styles and their various influences on avalanche emplacement.

The incorporation of substrate material into the moving avalanche mass provides some insights into the heterogeneous nature of the internal avalanche processes as evidence exists for contrasting avalanche behaviour: (a) mixing into the avalanche body, (b) shear and differential motion restricted to the basal portion (basal mixed zone), and (c) shear and differential motion within the avalanche body (e.g. truncated clastic dikes, sheared "stringers" of substrate material in the body). "Avalanche body" here refers to the deposit portion overlying the avalanche base (see Chapter 1 for suggested definitions of what constitutes the avalanche base). The different styles of substrate incorporation demonstrate the ability for a single avalanche event to undergo differing emplacement modes during its history. Mixing suggests some kind of material exchange throughout the avalanche body (contrasting behaviour with cases where the source stratigraphy sequences survived to the distal deposit portions), and possible transition to debris-flow-like behaviour. Concentration of shear at the base and restriction of substrate incorporation into this lower avalanche portion support a plug-flow type of emplacement model in which the main avalanche body experiences a different deformation regime than the base (e.g. Kelfoun and Druitt, 2005), as do undisrupted clastic dikes within the avalanche body. Truncated clastic dikes and stringers within the avalanche body document internal shear stress concentration as for example invoked in the dynamic rock fragmentation model of Davies and McSaveney (2002, 2006, 2009). Evidence for basal frictional resistance is sometimes preserved as striations on the underlying material where this consisted of erosion-resistant material, e.g. bedrock, or where erodible material has been removed by the avalanche front. Striations might suggest some sliding motion at least towards the end of avalanche emplacement.

The degree to which lubrication by liquefied saturated sediments (Buss and Heim, 1932; Abele, 1974; Sassa, 1988; Legros, 2002; Hungr, 2006) influences avalanche travel remains unresolved. As much as they might locally enable a moving rock and debris mass to cover greater distances or spread more laterally, their overall affect on total runout distance remains within the large margin of error in the datasets available to date. Saturated sediments are not a controlling factor in avalanche runout and spreading, but rather add complexities to avalanche runout and behaviour similar to topographic interference (e.g. Nicoletti and Sorriso-Valvo, 1991).

Entrainment ⇨ ploughing motion; shear at base; mixing within avalanche body; inhomogeneous avalanche behaviour; high erosive capacity
Deformation ⇨ energy-transfer
Shear zones ⇨ basal shear; shear-stress transfer
Bulldozing ⇨ coupling with substrates; change in avalanche dynamics upon deceleration; inhomogeneous avalanche behaviour – see two bulldozing hypotheses formulated
Striations ⇨ blocks at base; friction at base; sliding motion
Truncated clastic dikes ⇨ differential movement within avalanche
Undisrupted clastic dikes – plug flow model in which the main body experiences a different deformational regime than the base
No interactions ⇨ most likely substrate controlled; or internal avalanche mechanism prevents transfer of stresses, forces or loading; localized phenomenon (also velocity dependent) – mosaic of substrate conditions and heterogeneous avalanche emplacement dynamics

Table 7.5: List of substrate response to and the inferences made about avalanche emplacement mechanisms.

Evidently the trends identified in this study require a great deal of further work to link them with understanding of avalanche emplacement mechanisms and grain-flow mechanics. To attempt this in the context of the work presented here it would far exceed the current data quality and constraints.

7.2.5. Hazard applications

It has been shown in this work that although entrainment on the steep failure slopes enables an avalanche event to reach greater runout distances than without entrainment, the total deposit volume still scales with runout predictions based on empirical models. The introduction of the term *rockslide-debris avalanche* or *rock avalanche-debris avalanche*, however, remains useful to emphasize the potential of volume and hence runout increase due to incorporation of substrate material into the initial failure volume. It is an important factor to remain aware of for numerical modelling; e.g. back-analyses of avalanche events have proven more realistic when

including substrate entrainment on the steep failure slope than without (e.g. McDougall and Hungr, 2004) and are hence more applicable for hazard analyses. Good information on the following is needed as a framework for such numerical modelling to estimate the final deposit volume, compute avalanche-substrate interaction scenarios, and simulate avalanche runout:

1. location and volume of slope likely to detach
2. erodible substrates in the runout path and their types
3. location of substrate entrainment (slope or (proximal to distal) runout path)
4. surface water in runout path
5. deformable substrate locations
6. topographic constraints on runout

7.3. CONCLUSIONS

The interaction of rock/debris avalanches with the landscape they are emplaced in is inevitable, however

1. saturated sediments in the runout path of rock/debris avalanches are not a universal explanation for the long runout of these events:
    - therefore, the long runout (or 'excess travel distance') must lie in an avalanche-intrinsic, dynamic process.
    - Runout path materials add complexities to the avalanche event similar to topographic influences;
    - one of these complexities is the formation and/or preservation of characteristic surface features of flowbands and longitudinal ridges.

In the two case examples presented:

2. The Round Top rock avalanche preserved evidence for substrates interacting with the advancing avalanche to prevent the break-up of longitudinal ridges:
    - through bulldozing soils and gravels at ridge termini.

- A change in emplacement dynamics is documented in the sudden stopping of the thicker, hummocky medial avalanche part and the thin, digitate distal area where saturated substrates most likely enabled higher mobility and deposit thinning.
- Despite documented substrate involvement, the RT deposit did not travel an unusual distance.

3. Substrate involvement in the failure of the Jocotitlán volcanic edifice caused the blockslide deposit and extended edifice shape in the eastern deposit area. Furthermore,
    - failure of the blockslide over a topographic step resulted in high-velocity emplacement (documented by large longitudinal ridges and ejected boulders) of material down a broad valley.
    - Where less substrate and topographic interactions occurred in the western failure area, the deposit resembles the more typical hummocky debris avalanche morphology, albeit with very steep conical hummocks that can be ascribed to high source material strength and the absence of fine, weak or hydrothermal materials.

4. The influence of substrate material on avalanche runout and behaviour is still a new field in landslide research, and further inquiry into substrate failure conditions, dynamic post-failure behaviour under loading and shearing, interaction with the moving avalanche debris, influence of topography on substrate erodibility, and many other topics, are needed to shed light onto this exciting new field.

5. To aid in the exploration of substrate influence on avalanche dynamics (and other landslide related research interests) a consistent dataset is of vital importance, and is currently under construction for online publication.

7.4. RESEARCH OUTLOOK

- Data compilation and organisation will continue over the next months to prepare the volcanic debris avalanche deposit database for online publication on the VOGRIPA internet platform.
- Time and resources permitting, a similar project in a format compatible with the volcanic database is envisioned for the non-volcanic rock avalanche deposit data.
- A future project should re-create the present analogue models applying careful scaling analyses to facilitate a higher confidence level for the effects of various substrate types on small-scale avalanche runouts.

Appendix A

Table References

Appendix A – Table References

Adair Park Breccia

Yarnold, J.C. and Lombard, J.P. (1989). Facies model for large rock avalanche deposits formed in dry climates. In: Colburn, I. P., Abbott P. L. and Minch J. (Eds.) *Field Trip Guidebook - Pacific Section, Society of Economic Paleontologists and Mineralogists* 62: 9-31.

Allan Hills

Nicoletti, P.G. and Sorriso-Valvo, M. (1991). Geomorphic controls of the shape and mobility of rock avalanches. *Geological Society of America Bulletin* 103(10): 1365-1373.

Almolonga

Vallance, J.W., Siebert, L., Rose, W.I., Giron, J.R. and Banks N.G. (1995). Edifice collapse and related hazards in Guatemala. *Journal of Volcanology and Geothermal Research* 66: 337-355.

Altenau

von Poschinger, A. (1994). Some special aspects of the "impact" of a landslide on the valley floor. *Landslide News* 8: 26-28.

Ananievo

Abdrakhmatov K., Strom A.L.(2006). Dissected Rockslide and Rock Avalanche Deposits; Tien Shan, Kyrgyzstan. In: Evans SG, Scarascia-Mugnozza G, Strom AL, Hermanns RL (eds) Landslides from massive rock slope failure. *Nato Science Series IV, Earth and Environmental Sciences* 49: 551-570.

Artillery Peak Mega Breccia and Breccia Body II

Yarnold, J.C. (1993). Rock-avalanche characteristics in dry climates and the effect of flow into lakes: insights from the mid-Tertiary sedimentary breccias near Artillery Peak, Arizona. *Geological Society of America Bulletin* 105: 245-260.

Asama

Yoshida, H. and Sugai, T. (2006). Magnitude of the sediment transport event due to the Late Pleistocene sector collapse of Asama volcano, central Japan. *Geomorphology* 86(1-2): 61-72.

Aso

Miyabuchi, Y., Watanabe, K. and Okamoto, S. (2003). 14C ages of volcaniclastic deposits discovered on the western slope of Aso central cones, southwestern Japan. *Bulletin of the Volcanological Society of Japan* 48(2): 229-234. (in Japanese with English abstract)

Baga Bogd
Philip, H. and Ritz, J.-F. (1999). Gigantic paleolandslide associated with active faulting along the Bogd fault (Gobi-Altay, Mongolia). *Geology* 27(3): 211-214.

Bandai
Yamamoto, T., Nakamura, Y. and Glicken, H. (1999). Pyroclastic density currents from the 1888 phreatic eruption of Bandai volcano, NE Japan. *Journal of Volcanology and Geothermal Research* 90: 191-207.

Ui, T., Takarada, S. and Yoshimoto, M. (2000). Debris avalanches. In Sigurdsson, H.(ed). Encyclopedia of Volcanoes. Academic Press, San Diego: 617-626.

Siebert, L., Glicken, H. and Ui, T. (1987). Volcanic hazards from Bezymianny- and Bandai-type eruptions. *Bulletin of Volcanology* 49(1): 435-459.

Bashi-Djaya
Hewitt, K. (2006). Rock avalanches with complex run out and emplacement, Karakoram Himalaya, Inner Asia. In: S. G. Evans, G. Scarascia-Mugnozza, A. L. Strom and R. L. Hermanns (Eds.), *Nato Science Series. Series IV, Earth and Environmental Sciences* 49: 521-550.

Black Canyon Breccia
Yarnold, J.C. and Lombard, J.P. (1989). Facies model for large rock avalanche deposits formed in dry climates. In: Colburn, I. P., Abbott P. L. and Minch J. (Eds.) Field Trip Guidebook - Pacific Section, Society of Economic Paleontologists and Mineralogists 62: 9-31.

Blackhawk
Johnson, B. (1978). Blackhawk landslide, California, U.S. Rockslides and avalanches 1, Natural phenomena. Elsevier, Amsterdam, pp. 481-504.

Cantal
Schneider, J.-L. and Fisher, R.V. (1998). Transport and emplacement mechanisms of large volcanic debris avalanches: evidence from the northwest sector of Cantal Volcano (France). *Journal of Volcanology and Geothermal Research* 83: 141-165.

Casita
van Wyk de Vries, B., Kerle, N. And Petley, D. (2000). Sector collapse forming at Casita volcano, Nicaragua. *Geology* 28(2): 167-170.

Cheam
Orwin, J.F., Clague, J.J. and Gerath, R.F. (2004). The Cheam rock avalanche, Fraser Valley, British Columbia, Canada. *Landslides* 4: 289-298.

Chimborazo
Bernard, B., Van Wyk de Vries, B., Barba, D., Leyrit, L., Robin, C., Alcaraz, S. and Samaniego, P. (2008). The Chimborazo sector collapse and debris avalanche: deposit characteristics as evidence of emplacement mechanisms. *Journal of Volcanology and Geothermal Research* 176(1): 36-43.

Colima, Nevado de

Capra, L., Macías, J.L., Scott, K.M., Abrams, M. and Garduño-Monroy, V.H. (2002). Debris avalanches and debris flows transformed from collapses in the Trans-Mexican Volcanic Belt, Mexico - behavior, and implications for hazard assessment. *Journal of Volcanology and Geothermal Research* 113(1-2): 81-110.

Stoopes, G.R. and Sheridan, M.F. (1992). Giant debris avalanches from the Colima Volcanic Complex, Mexico: implications for long-runout landslides (> 100 km) and hazard assessment. *Geology* 20: 299-302.

Robin, C., Mossand, P., Camus, G., Cantagrel, J.M. and Vincent, P. (1987). Eruptive history of the Colima volcanic complex (Mexico). *Journal of Volcanology and Geothermal Research* 31: 99-113.

Cook, Mt.

McSaveney, M.J. (2002). Recent rockfalls and rock avalanches in Mount Cook National Park, New Zealand. In: Evans SG, DeGraff JV (eds). Catastrophic landslides: effects, occurrence, and mechanisms. *Review in Engineering Geology* 14: 35-70.

Cross Hill Breccia

Yarnold, J.C. and Lombard, J.P. (1989). Facies model for large rock avalanche deposits formed in dry climates. In: Colburn, I. P., Abbott P. L. and Minch J. (Eds.) Field Trip Guidebook - Pacific Section, Society of Economic Paleontologists and Mineralogists 62: 9-31.

Derrumbadas, Las

Capra, L., Macías, J.L., Scott, K.M., Abrams, M. and Garduño-Monroy, V.H. (2002). Debris avalanches and debris flows transformed from collapses in the Trans-Mexican Volcanic Belt, Mexico - behavior, and implications for hazard assessment. *Journal of Volcanology and Geothermal Research* 113(1-2): 81-110.

Diki'i Greben

Ponomareva, V.V., Melekestsev, I.V. and Dirksen, O.V. (2006). Sector collapses and large landslides on late Pleistocene-Holocene volcanoes in Kamchatka, Russia. *Journal of Volcanology and Geothermal Research* 158(1-2): 117-138.

Dulung Bar-Darkot

Hewitt, K. (2006). Rock avalanches with complex run out and emplacement, Karakoram Himalaya, Inner Asia. In: S. G. Evans, G. Scarascia-Mugnozza, A. L. Strom and R. L. Hermanns (Eds.), *Nato Science Series. Series IV, Earth and Environmental Sciences* 49: 521-550.

Eagle Pass

Hungr, O. and Evans, S.G. (2004). Entrainment of debris in rock avalanches: an analysis of a long run-out mechanism. *GSA Bulletin* 116(9/10): 1240-1252.

El Capitan

Yarnold, J.C. and Lombard, J.P. (1989). Facies model for large rock avalanche deposits formed in dry climates. In: Colburn, I. P., Abbott P. L. and Minch J. (Eds.) *Field Trip Guidebook - Pacific Section, Society of Economic Paleontologists and Mineralogists* 62: 9-31.

Fuego

Vallance, J.W., Siebert, L., Rose Jr, W.I., Girón, J.R. and Banks, N.G. (1995). Edifice collapse and related hazards in Guatemala. *Journal of Volcanology and Geothermal Research* 66: 337-355.

Ghoro Choh

Hewitt, K. (2006). Rock avalanches with complex run out and emplacement, Karakoram Himalaya, Inner Asia. In: S. G. Evans, G. Scarascia-Mugnozza, A. L. Strom and R. L. Hermanns (Eds.), *Nato Science Series. Series IV, Earth and Environmental Sciences* 49: 521-550.

Gol-Ghone B

Hewitt, K. (2006). Rock avalanches with complex run out and emplacement, Karakoram Himalaya, Inner Asia. In: S. G. Evans, G. Scarascia-Mugnozza, A. L. Strom and R. L. Hermanns (Eds.), *Nato Science Series. Series IV, Earth and Environmental Sciences* 49: 521-550.

Inilcheck

Abdrakhmatov K., Strom A.L.(2006). Dissected Rockslide and Rock Avalanche Deposits; Tien Shan, Kyrgyzstan. In: Evans SG, Scarascia-Mugnozza G, Strom AL, Hermanns RL (eds) Landslides from massive rock slope failure. *Nato Science Series IV, Earth and Environmental Sciences* 49: 551-570.

Iwasegawa (Tashiro-Dake)

Takarada, S., Ui, T. And Yamamoto, Y. (1999). Depositional features and transport mechanism of valley-filling Iwasegawa and Kaida debris avalanches, Japan. *Bulletin of Volcanology* 60(7): 508-522.

Jocotitlán

Dufresne, A., Salina, S. and Siebe, C. (2009). Substrate deformation features associated with the Jocotitlán volcanic debris avalanche, Central Mexico. *Journal of Volcanology and Geothermal Research*: in review.

Siebe, C., Komorowski, J.C. and Sheridan, M.F. (1992). Morphology and emplacement of an unusual debris-avalanche deposit at Jocotitlán Volcano, Central Mexico. *Bulletin of Volcanology* 54(7): 573-589.

Khait

Heuberger, H., Masch, L. Preuss, E. and Schrocker, A. (1982). Quaternary landslides and rock fusion in Central Nepal and in the Tyrolean Alps. *Mountain Research and Development* 4(4): 345-362.

Kokomeren
Abdrakhmatov K., Strom A.L.(2006). Dissected Rockslide and Rock Avalanche Deposits; Tien Shan, Kyrgyzstan. In: Evans SG, Scarascia-Mugnozza G, Strom AL, Hermanns RL (eds) Landslides from massive rock slope failure. *Nato Science Series IV, Earth and Environmental Sciences* 49: 551-570.

Leyte
Evans, S.G., Guthrie, R.H., Roberts, N.J. and Bishop, N.F. (2007). The disastrous 17 February 2006 rockslide-debris avalanche on Leyte Island, Philippines: a catastrophic landslide in tropical mountain terrain. *Natural Hazards and Earth System Science* 7: 89-101.

Marquartstein
von Poschinger, A. (1994). Some special aspects of the "impact" of a landslide on the valley floor. *Landslide News* 8: 26-28.

Mombacho
Shea, T., van Wyk de Vries, B. and Pilato, M. (2008). Emplacement mechanisms of contrasting debris avalanches at Volcán Mombacho (Nicaragua), provided by structural and facies analysis. *Bulletin of Volcanology* 70(8): 899-921.

Munday, Mt.
Evans, S.G. and Clague, J.J. (1998). Rock avalanche from Mount Mundy, Waddington Range, British Columbia, Canada. *Landslide News* 11: 23-25.

Nomash River
Hungr, O. and Evans, S.G. (2004). Entrainment of debris in rock avalanches: an analysis of a long run-out mechanism. *GSA Bulletin* 116(9/10): 1240-1252.

Hungr, O. (2006). Rock avalanche occurrence, process and modelling. In: Evans, S.G., Mugnozza, G.S. and Strom, A. (eds) Landslides from Massive Rock Slope Failure. Springer Verlag: 243-266.

North Long John
Blair, T.C. (1999). Alluvial fan and catchment initiation by rock avalanching, Owens Valley, California. *Geomorphology* 28(3-4): 201-221.

Ontake San (1984)
Hungr, O. and Evans, S.G. (2004). Entrainment of debris in rock avalanches: an analysis of a long run-out mechanism. *Geological Society of America Bulletin* 116(9/10): 1240-1252.

Voight, B. and Sousa, J. (1994). Lessons from Ontake-san: a comparative analysis of debris avalanche dynamics. *Engineering Geology* 38(3-4): 261-297.

Parinacota
Clavero, J., Sparks, R., Huppert, H. and Dade, W. (2002). Geological constraints on the emplacement mechanism of the Parinacota debris avalanche, Northern Chile. *Bulletin of Volcanology* 64(1): 40-54.

Pink Mountain

Geertsema, M., Hungr, O., Schwab, J. W. and Evans, S. G. (2006). A large rockslide-debris avalanche in cohesive soil at Pink Mountain, Northeastern British Columbia, Canada. *Engineering Geology* 83: 64-75.

Popocatépetl

Capra, L., Macías, J.L., Scott, K.M., Abrams, M. and Garduño-Monroy, V.H. (2002). Debris avalanches and debris flows transformed from collapses in the Trans-Mexican Volcanic Belt, Mexico - behavior, and implications for hazard assessment. *Journal of Volcanology and Geothermal Research* 113(1-2): 81-110.

Robin, C. and Boudal, C. (1987). A gigantic Bezymianny-type event at the beginning of modern Volcan Popocatepetl. *Journal of Volcanology and Geothermal Research* 31(1-2): 115-130.

Siebe, C., Abrams, M., Macías, J.L., 1995. Derrumbes gigantes, depósitos de avalancha de escombros y edad del actual cono del Volcán Popocatépetl. In: Comité Científico Asesor UNAM-CENAPRED: Volcán Popocatépetl, estudios realizado drante la crisis 1994-1995. Edición Especial, Secretaría de Gobernación, México, D.F., 195-220.

Rabicano, Cerro

Hauser, A. (2002). Rock avalanche and resulting debris flow in Estero Parraguirre and Río Colorado, Región Metropolitana, Chile. In: Evans, S.G. and DeGraff, J.V. (eds) Catastrophic Landslides. Geological Society of America Reviews in Engineering Geology 25: 135-148.

Region Metropolitana

Hauser, A. (2002). Rock avalanche and resulting debris flow in Estero Parraguirre and Río Colorado, Región Metropolitana, Chile. In: Evans, S.G. and DeGraff, J.V. (eds) Catastrophic Landslides. Geological Society of America Reviews in Engineering Geology 25: 135-148.

Roque Nublo

Mehl, K.M. and Schmincke, H.-U. (1999). Structure and emplacement of the Pliocene Rogue Nublo debris avalanche deposit, Gran Canaria, Spain. *Journal of Volcanology and Geothermal Research* 94: 105-134.

Round Top

Dufresne, A., Davies, T.R. and McSaveney, M.J. (2009). Influence of runout-path material on emplacement of the Round Top rock avalanche, New Zealand. *Earth Surface Processes and Landforms*: in revision.

Wright, C.A. (1998). The Ad 930 long-runout Round Top debris avalanche, Westland, New Zealand. *New Zealand Journal of Geology and Geophysics* 41(4): 493-497.

Ruapehu
Palmer, B.A. and Neall, V.E. (1989). The Murimotu Formation, 9500 year old deposits of a debris avalanche and associated lahars, Mount Ruapehu, New Zealand. *New Zealand Journal of Geology and Geophysics* 32: 477-486.

Satpara Skardu
Hewitt, K. (2006). Rock avalanches with complex run out and emplacement, Karakoram Himalaya, Inner Asia. In: S. G. Evans, G. Scarascia-Mugnozza, A. L. Strom and R. L. Hermanns (Eds.), *Nato Science Series. Series IV, Earth and Environmental Sciences* 49: 521-550.

Shadow Valley
Friedmann, S.J. (1997). Rock-avalanche elements of the Shadow Valley Basin, eastern Mojave Desert, California: processes and problems. *Journal of Sedimentary Research* 67(5): 792-804.

Shasta
Crandell, D.R., Miller, C.D., Glicken, H.X., Christiansen, R.L. and Newhall, C.G. (1984). Catastrophic debris avalanche from ancestral Mount Shasta Volcano, California. *Geology* 12(3): 143-146.

Ui, T., Takarada, S. and Yoshimoto, M. (2000). Debris avalanches. In Sigurdsson, H.(ed). Encyclopedia of Volcanoes. Academic Press, San Diego: 617-626.

Sherman Glacier
McSaveney, M.J. (1978). Sherman Glacier rock avalanche, Alaska, U.S.A. Rockslides and Avalanches. Amsterdam, Elsevier: 197-258.

Shiveluch
Belousov, A., Belousova, M. and Voight, B. (1999). Multiple edifice failures, debris avalanches and associated eruptions in the Holocene history of Shiveluch Volcano, Kamchatka, Russia. *Bulletin of Volcanology* 61(5): 324-342.

Socompa
Van Wyk De Vries, B., Self, S., Francis, P.W. and Keszthelyi, L. (2001). A gravitational spreading origin for the Socompa debris avalanche. *Journal of Volcanology and Geothermal Research* 105(3): 225-247.

Split Mountain
Abbott, P.L., Kerr, D.R., Borron, S.E., Washburn, J.L. and Rightmer, D.A. (2002). Neogene sturzstrom deposits, Split Mountain area, Anza-Borrego Desert State Park, California. In: Evans, S.G. and DeGraff, J.V. (eds) Catastrophic Landslides. Geological Society of America Reviews in Engineering Geology 25: 379-400.

Taranaki
Alloway, B., McComb, P., Neall, V., Vucetich, C., Gibb, J., Sherburn, S. and Stirling, M. (2005). Stratigraphy, age, and correlation of voluminous debris-avalanche events from an ancestral Egmont volcano: implications for coastal plain construction and regional hazard assessment. *Journal of the Royal Society of New Zealand* 35(1-2): 229-267.

Stewart, B., Zernack, A., Procter, J. (2006). Field Trip Guide, GSNZ-NZGS Joint Conference, Massey University, New Zealand.

Toluca, Nevado de

Capra, L. and Macías, J.L. (2000). Pleistocene cohesive debris flows at Nevado de Tuoluca Volcano, central Mexico. *Journal of Volcanology and Geothermal Research* 102: 149-168.

Tsing-Shan

King, J. (1996). Tsing Shan debris flows. *Special Project Report* SPR 9/96: 133. Geotechnical Engineering Office, Hong Kong Government.
– cited in Hungr, O., McDougall, S. and Bovis, M. (2005). Entrainment of material by debris flows. In: Jakob, M. and Hungr, O. (eds) Debris flow hazards and related phenomena. Springer Verlag: 135-158.

Tsok-Dumordo

Hewitt, K. (2006). Rock avalanches with complex run out and emplacement, Karakoram Himalaya, Inner Asia. In: S. G. Evans, G. Scarascia-Mugnozza, A. L. Strom and R. L. Hermanns (eds) Landslides from Massive Rock Slope Failure. *Nato Science Series. Series IV, Earth and Environmental Sciences* 49: 521-550.

Unzen

Siebert, L. (1984). Large volcanic debris avalanches: characteristics of source areas, deposits, and associated eruptions. *Journal of Volcanology and Geothermal Research* 22(3-4): 163-197.

Siebert, L., Glicken, H. and Ui, T. (1987). Volcanic hazards from Bezymianny- and Bandai-type eruptions. *Bulletin of Volcanology* 49(1): 435-459.

Ui, T., Takarada, S. and Yoshimoto, M. (2000). Debris avalanches. In Sigurdsson, H.(ed). Encyclopedia of Volcanoes. Academic Press, San Diego: 617-626.

Val Pola

Crosta, G.B., Chen, H. and Lee, C.F. (2004). Replay of the 1987 Val Pola Landslide, Italian Alps. *Geomorphology* 60(1-2): 127-146.

Waikaremoana

Davies, T.R., McSaveney, M.J. and Beetham, R.D. (2006). Rapid block glides: slide-surface fragmentation in New Zealands's Waikaremoana landslide. *Quarterly Journal of Engineering Geology and Hydrogeology* 39: 115-129.

Yarbah Tshoh

Hewitt, K. (2006). Rock avalanches with complex run out and emplacement, Karakoram Himalaya, Inner Asia. In: S. G. Evans, G. Scarascia-Mugnozza, A. L. Strom and R. L. Hermanns (Eds.), *Nato Science Series. Series IV, Earth and Environmental Sciences* 49: 521-550.

Zempoala

Capra, L., Macías, J.L., Scott, K.M., Abrams, M. and Garduño-Monroy, V.H. (2002). Debris avalanches and debris flows transformed from collapses in the Trans-Mexican Volcanic Belt, Mexico - behavior, and implications for hazard assessment. *Journal of Volcanology and Geothermal Research* 113(1-2): 81-110.

Zymoetz

McDougall, S., Boultbee, N., Hungr, O., Stead, D. and Schwab, J.W. (2006). The Zymoetz River landslide, British Columbia, Canada; description and dynamic analysis of a rock slide-debris flow. *Landslides* 3(3): 195-204.

Appendix B

Process Model Report

Appendix B – Process Model Report

1. OBJECTIVES

The main objectives of these experiments were (1) to test if substrate deformation features beneath an advancing granular mass can be reproduced in the laboratory and (2) which substrate materials work. They formed the basis for the analogue models presented in Chapter 5.

2. METHODS

In a narrow (~50 mm wide) flume, a variety of granular materials (see below) was used as the substrate at a thickness of ~30-35 mm along 1-2 m long segments. Coal was used as the overriding material; it was crushed into angular pieces less than ~17 mm in diameter. The ~70 mm thick coal body was moved using an 800 mm long wooden lath with rows of nails protruding ~30 mm to grip the coal. The lath has a block-plane design to move the coal as steadily as possible. Slightly more pressure was applied at the rear for ease of initiation and motion. Using gravel instead of coal did not yield different results but caused significant damage to the plexi-glass walls of the flume and was hence dismissed.

Note: the overriding material is herein referred to as “coal body” or sometimes as “flow”, and the underlying granular material layer as the “substrate”. Direction of coal body movement is occasionally referred to as “flow”-direction.

A first set of 21 runs was conducted to test the set-up and do-ability, documented with still photographs and observations made while handling the lath. These runs were followed by a set of 31 runs filmed with a high-speed video camera taking 200 frames per second as well as still photography in most cases. The numbering for this last set was changed from "run-xy" to "M-xy" for "movie".

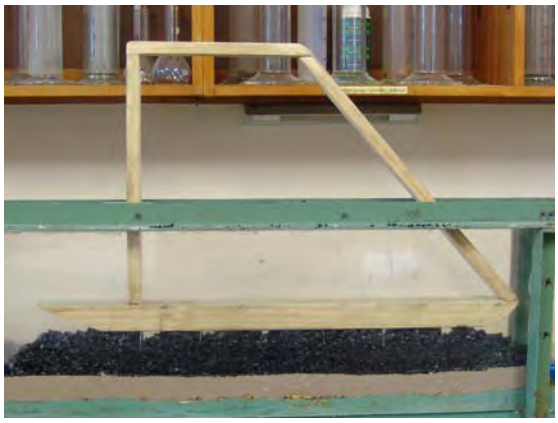

Figure 1: Set-up of process model apparatus: motion is from right to left.

Angular coal clasts were used to simulate the avalanche body, ranging in clast size from 5-15 mm in most runs. Materials used as substrates were mainly in the silt to medium sand size range, apart from vermiculite, PVC and polystyrene spheres in the granule range, soil in the coarse sand to granule range, and the 'high-viscosity-water' wallpaper paste.

<u>Substrates</u>

Silty to fine sand (dry / wet / saturated)
Fine to medium sand (dry / wet / saturated)
PVC granules (~2 mm diameter & ~3 mm long, dry)
potting soil (moist / saturated)
pulverized dolomite (dry)
vermiculite (dry)
wallpaper paste (thick, "gooey" consistency)
polystyrene spheres (~1 mm diameter) in dry, silty to fine sand layer

3. RESULTS

Regardless of material used or degree of saturation, substrate undulation, dragging along the coal body base and injection into the overriding coal was observed in almost all runs. The only exception was wet sand, which was merely eroded at the very surface with “rip-up” clasts entrained into the coal. Substrate thickening due to basal drag reached 10-25 mm locally on top of an initially 30-35 mm thick substrate. Disturbances reached depths of up to 15 mm. Injection of substrate material into the coal body was up to 20 mm high. Most pronounced disturbances occurred beneath the lath rear where most pressure was applied.

3.1. Most Common Deformation Features

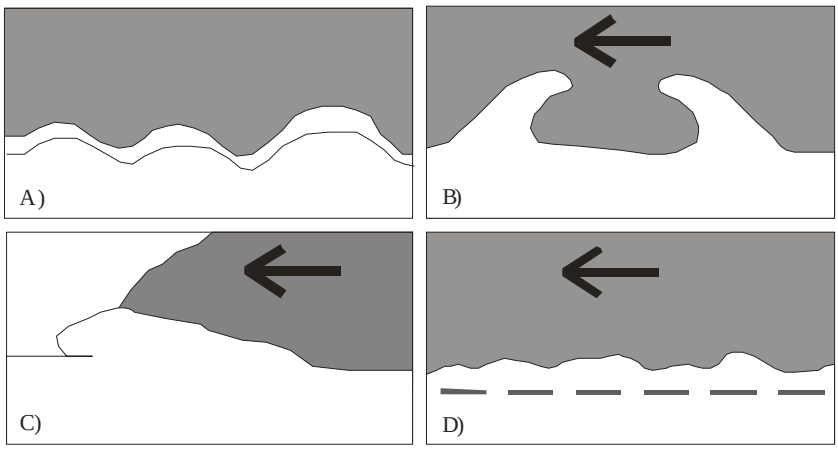

Figure 2: Sketches of the most commonly observed experimental substrate deformation features. (A) Substrate undulation; dashed line marks original substrate surface. (B) Substrate injection into the moving coal clast body, occasionally accompanied by shearing of the injected material. (C) Substrate bulldozing ahead of the moving coal body and deposition onto undisrupted substrate material. (D) Dragging and consequent thickening of substrate.

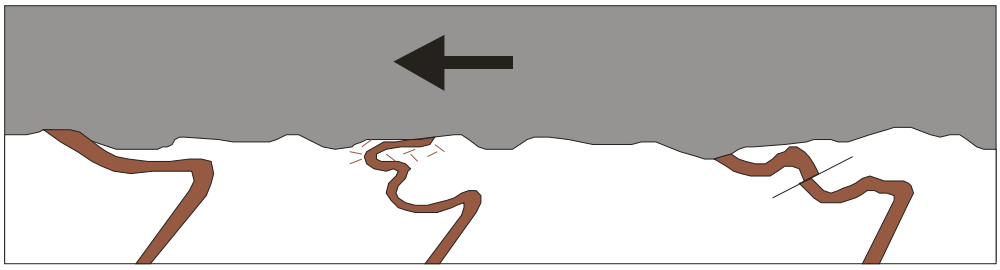

Figure 3: Marker layer disruptions (overturning, folding, mixing, and faulting)

3.2. Saturated Sand

(runs 1, 3, 5-11; M-09, M-10, M-24, M-25)

Bulldozing, disturbance and erosion/dragging of the substrate were, to a degree, observed in every run. Highly saturated sand mainly undulated beneath the coal with little to no entrainment. Undulations were relatively small and were partially smoothed out as more material progressed over them. Less saturated sand was bulldozed at the flow front but exhibited less dragging beneath the coal body. Some of the resulting 'mounds' survived, whereas others were ripped up and incorporated into the deposit. Coal clasts were buried into the sand in both cases, but appear to be more pronounced in the highly saturated case.

Two grain size classes (one <7mm; one >7mm) in a stratified coal 'flow' (run 9; coarse on top) led to preferential accumulation of the coarse material at the flow front. Undulation and dragging appeared to occur mainly beneath the coarse clasts at the front. The small clasts formed a relatively coherent wet mass and were preferentially buried compared to the coarser clasts.

Increasing shearing speed was tried with the small clast sizes (run 9b) and led to the formation of a coherent sand-coal basal layer upon which the coal was much easier to shear than on sand alone. Similarly in runs M-09 and M-10 coal clasts "got stuck" in the sand and formed a sand-coal basal layer. Very minor substrate dragging and injection occurred in these cases. Introducing coloured sand layers revealed more intense deformation (mixing and mutual injection of the sand layers) in the upper 10-15 mm than could be observed in uni-coloured sand. The coal feels harder to shear across saturated sand than across dry sand.

3.3. Unsaturated Wet Sand

(runs 2, 12, 13; M-26-28)

Erosion and minor dragging of the top sand layer (~5 mm) and small "rip-up" clasts incorporation into the overriding deposit was observed. A sand chunk ~2 cm long, 1 cm deep was detached from the substrate in run 12 but remained in its initial location.

3.4. Dry Sand

(runs 14-18; M-01-08, M-18-21)

Using dry, loose sand resulted in similar deformation features as seen in the highly saturated cases. Sand was temporarily injected flame-like into the deposit, and was

sometimes sheared in and opposite to flow direction before sieving back to the bottom. Sand was eroded and dragged with the coal body at its base, and bulldozed at the front. Entrainment in "chunks" and/or mixing of sand and coal within the coal body base was common (the temporary coal-sand layer was up to 20-25 mm thick). Varying the speed did not result in different deformation features, apart from more dramatic sand accumulation by drag and more spray at the coal body front in the fast run.

Using coloured marker layers dipping at ~20 degrees into flow direction showed folding, overturning and faulting of these layers in flow direction and partial mixing with the white sand where eroded and moved with the deposit. Up to 15 mm substrate material was redeposited. Horizontal marker layers undulated, thinned and thickened before being folded. Some local mixing of marker and white substrate occurred where the overburden pressure was high enough to mobilise the substrate at depth.

Using horizontal coloured marker layers with polystyrene beads in the second layer resulted in the uppermost blue layer undulating, thickening and injecting with spray at the flow front. The white polystyrene-sand layer was easily mobilised, undulated, thickened and injected into the upper blue layer in both directions (forward and backwards). Some disturbance of the third (green) layer (forward injections into and mixing with white layer above) was noted. In parts the blue layer was completely eroded, in other parts thickened to ~ 12 mm. The upper white layer also injected into the coal. It was very easy to shear the coal across this substrate.

3.5. Granular PVC

(run 19; M-30, M-31)

Substrate thickening at the deposit front and thinning below the deposit body was very pronounced ("wave" in front of coal of up to 60-70 mm). Spray occurred at the front. Single PVC grains were incorporated up to almost 30 mm high into the coal. PVC injected wavelike into the coal in and opposite to movement direction. Coal clasts were buried into the substrate, which "gave" easily to the overriding coal (ease of shearing).

3.6. Moist Potting Soil

(M-22)

Very little spray occurred at the front. The sand (thin marker layer on top of soil for colour contrast) undulated, thickened and injected into coal (both directions). Likewise soil injected up into the sand and sand injected downwards into the soil (up to 5 mm deep). The entire substrate "gave" easily to the overriding coal with the rear of the lath consequently sinking down.

3.7. Saturated Potting Soil

(M-23)

The top sand marker and the soil undulated almost uniformly in the beginning. Sand injected backwards into the coal and also began undulating independently of the soil. Lath was sub-parallel until it got stuck, thereafter it was tipped: mixing of sand and soil and more complex and intense injection occurred at that stage. It was easy in both cases, moist and saturated soil, to shear the coal. The soil instantly mobilised well ahead of the coal body at the very onset of coal loading.

3.8. Wallpaper Paste

(M-29)

The substrate was immediately pushed into a great mound or "wave" (~ 60-70 mm) in front of the coal. The coal did not override the mound but made it to the crest. It was very easy to shear the coal which sank into the substrate immediately, almost to the flume floor. Some coals clasts remained stationary within the substrate depth while the remaining deposit continued to move. Some substrate stringers developed within the mixed coal-substrate zone (up to 25 mm high), elongated, folded, detached, and formed back into a 'blob'.

3.9. Pulverized Dolomite

(M-14-17)

Similar substrate behaviour as in the dry sand runs was observed. Some spray at the saltating coal body front occurred. Undulation, injection into and opposite to flow direction, substrate thickening and erosion, mixing of marker layers with white substrate, marker layer thickening and thinning were common features of all four

runs. The dolomite displaces readily, corresponding to shearing with immediate mobilisation (substrate dragging and consequent thickening).

3.10. Vermiculite

(M-11-13)

Bulldozing at the flow front occurred to some degree. Substrate compaction and dragging occurred below the main flow body and substrate injections and undulations were common. Individual vermiculite pieces injected into the coal and coal clasts were buried. Individual coal clasts got stuck in the substrate, and then rotated and remobilised as more clasts moved and rotated over them. Up to ~ 10 mm substrate thickening was observed.

4. DISCUSSION

The experiments show that a number of substrate deformation features can be produced by simply shearing granular materials. The laboratory features resemble those observed in outcrops of sub-avalanche and sub-glacial settings as well as some of those observed beneath advancing dunes and within liquefied loaded sediments. All these real life cases involve an overlying mass moving/shearing across a failing substrate. The experiments provide the opportunity to study the formation of such features.

4.1. Laboratory Problems

- Pressure on the granular mass is highly variable during motion as the lath is human operated and coal clasts occasionally jam the lath between the plexiglass walls.
- Wet sand adheres to the coal and may result in ‘false’ entrainment.
- Water surface tension.
- Surface electrical charges on particles and flume walls, particularly for vermiculite.

4.2. Observation Summary

Substrate disturbance in the model occurred beneath almost the entire coal body length, but preferentially and most intensely beneath the lath rear were most pressure was applied. Bulldozing occurred at the body front where eroded and transported substrate material was pushed, sometimes onto undisturbed substrate (note: very little pressure exists at the front and coal clasts tumbled almost freely with saltating clasts ahead of the body). Mounds were also pushed up beneath the length of the coal body (substrate dragging). Rip-up clasts were predominant in unsaturated sand, but occurred in other materials as well (saturated and dry sand, dry dolomite, soil; individual PVC grain incorporation). Deformation fronts were observed to migrate down into the substrate with extensive shearing, folding, mixing and faulting of marker layers. Interestingly, injections into the coal body not only occurred into "flow"-direction but also opposite to it with the injected substrate material sometimes being sheared in both directions simultaneously. This apparent 'counter-flow' injection is mainly caused by differential movement/shearing of coal clasts (see 'Kinetic Indicators' below). In the cases where coal and sand formed a coherent basal layer, the remainder of the coal body became easier to move on this new surface. Soil, wallpaper paste and granular PVC "gave" easily to the overriding coal body, and posed very little resistance to motion. Similarly, polystyrene spheres mixed into a dry sand layer assisted the "ease of shearing". It felt harder to move the lath when unsaturated and saturated sand was used as the substrate (water surface tension?).

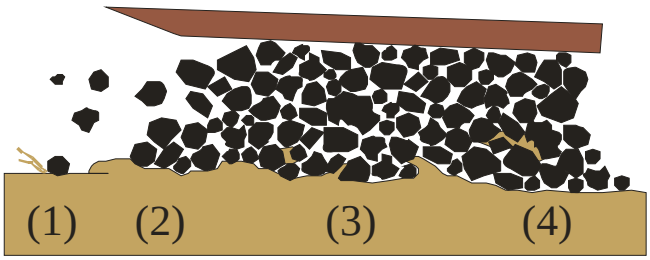

Figure 4: Illustration of the different features observed during coal shearing across a deformable substrate

The main features resulting from coal shearing across a deformable substrate (Figure 4) can be summarized as follows:

- saltating clast impact on undisturbed substrate causing spray
- bulldozing at 'flow' front, sometimes onto undisturbed substrate surface
- substrate dragging & injecting, 'rip-up' clasts, marker layer deformation
- substrate erosion, injection, shearing within coal, more intense marker layer deformation

4.3. Feature Formation

Erosion (result of substrate mobilisation and dragging)

bulldozing: substrate material is pushed into small mounds by the coal body and by individual clasts at the 'flow' front at any overburden pressure. Mobilisation is in parts caused by falling clast impact.

dragging: mobilisation and transport of substrate material at the flow base by clasts pushing down and forwards.

Inclined marker layer disturbance

folding: substrate mobilisation shears the upper portions of the substrate leading to an apparent overturning (stretching in 'flow' direction) of the marker layers. Coal clast burial or local substrate compression by individual clast pressure pushes the marker layer down and forwards at depth, causing more folding. This can affect the entire upper part of the marker layer or only a small breadth at depth leaving the very top and the bottom part stationary and unaffected (temporarily)

faulting: effect of substrate shearing at depth or coal clasts pushing into the substrates at an angle (compressing or mobilising the substrate locally leading to inclined shear surfaces).

mixing: substrate mobilisation, particularly where overburden pressure is high.

Horizontal marker layer disturbance

folding: shear and downward pressure is transferred to depth, compressing local areas. The marker layer is pushed downwards in an arc and/or pushed forward into

stationary substrate hence leading to thickening and thinning and fold-structure formation.
mixing: substrate mobilisation, particularly where overburden pressure is high.

Entrainment (incorporation of substrate material into the flow body)
injection: the substrate is locally pushed into mounds (dragging) and pushed upwards into the coal, and over and around coal clasts. Coal clast rotation and differential movement of individual clasts or entire coal body segments produce shearing or stringer formation within the coal body.
rip-up clasts: less easily mobilised substrates are eroded by abrasion/scouring with chunks being pushed or rotated up into the moving coal.
mixing: as injection. Beneath the lath rear more coal is pushed into the substrate and substrate is hence squeezed upwards and mixed with the coal.

4.4. Intensity of deformation

No control or measure of shear stress or pressure was possible in these experiments. However, the intensity of deformation increased with increasing overburden pressure and, to a lesser extend, increasing shear velocity.

4.5. Preservation stage and avalanche dynamics

Early preservation = deformation during late stage(s) of emplacement; intense mixing etc. = continuous disturbance throughout emplacement and body length; overprinted deformation = repeated disturbance. Structural measurements in the field should be compared to ‘undisturbed/pristine pre-avalanche’ substrate features.

4.6. Kinetic Indicators

The deformation features obtained are relatively straightforward kinetic indicators. Inclined marker layers are overturned into flow direction. Recumbent folds are the result of a deformation front at depth where the very upper substrate is stationary and only a thin band is mobilised, i.e. compressed by clast burial or shear transferral to that horizon. Horizontal marker layers are pushed into folds with the thinned leg up-flow and thickening in dune shape. However, some injections into the overriding coal or into horizontal marker layers have an apparent kinetic direction opposite to flow-direction. This is in part due to the interaction with moving and rotating coal clasts

and in part due to pressure variations within the coal body locally pushing the deformation front downwards.

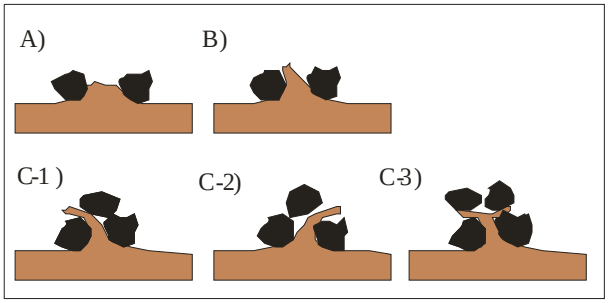

Figure 5: Examples of different 'entrainment directions'. Coal avalanche motion is from right to left. (A) and (B) small amounts of substrate material are mobilized into the coal avalanche without further transport of shearing. (C-1) Injected substrate material is sheared in avalanche motion direction. (C-2) the injected material is apparently sheared against avalanche motion direction by an avalanche clast burying itself into the substrate. (C-3) A combination of C-1 and C-2.

4.7. Structures and Substrate Type

	Injection	stringers	undulation	rip-up clasts	dragging	buried clasts	spray	bulldozing	shearing 'ease'	marker layers:	folded	faulted	mixed
dry sand	x	x	x	(x)	x	x	x	x	\	x	x	x	x
unsaturated sand	(x)	\	(\)	x	x	\	\	\	\	n\a	n\a	n\a	n\a
saturated sand	x	x	x	x	x	x	\	x	\	(x)	(x)	\	x
Soil	x	\	x	\	x	x	(x)	x	x	n\a	n\a	n\a	n\a
pulverized dolomite	x	\	x	x	x	x	x	x	\	x	x	\	x
PVC	x	x	x	x	x	x	(x)	x	x	n\a	n\a	n\a	n\a
wallpaper paste	x	x	x	\	x	x	\	x	x	n\a	n\a	n\a	n\a
Vermiculite	x	\	x	x	x	x	\	(x)	\	n\a	n\a	n\a	n\a
polystyrene spheres	x	x	x	(x)	x	x	x	x	x	x	x	(x)	x

Table 1: Summary of substrate deformation features related to substrate type

References

A-Z

References

Abele, G. (1964). Die Fernpasstalung und ihre morphologischen Probleme. *Tubiner Geograpgische Studien* 12: 123 pp.

Abele, G. (1974). Bergstürze in den Alpen. *Wissenschaftliche Vereinshefte* 25: 230 p.

Abele, G. (1997). Rockslide movement supported by the mobilization of groundwater-saturated valley floor sediments. *Zeitschrift der Geomorphologie* 41(1): 1-20.

Abdrakhmatov K., Strom A.L. (2006). Dissected Rockslide and Rock Avalanche Deposits; Tien Shan, Kyrgyzstan. In: Evans SG, Scarascia-Mugnozza G, Strom AL, Hermanns RL (eds) Landslides from massive rock slope failure. Nato Science Series IV, Earth and Environmental Sciences 49: 551-570.

Alloway, B., McComb, P., Neall, V., Vucetich, C., Gibb, J., Sherburn, S. and Stirling, M. (2005). Stratigraphy, age, and correlation of voluminous debris-avalanche events from an ancestral Egmont volcano: implications for coastal plain construction and regional hazard assessment. *Journal of the Royal Society of New Zealand* 35(1-2): 229-267.

Anthony, J.L. and Marone, C. (2005). Influence of particle characteristics on granular friction. *Journal of Geophysical Research B: Solid Earth* 110(8): 1-14.

Aranson, I.S., Malloggi, F. and Clément, E. (2006). Transverse instability of avalanches in granular flows down an incline. *Physical Review E - Statistical, Nonlinear, and Soft Matter Physics* 73(5): 4 pp.

Barbolini, M., Biancardi, A., Cappabianca, F., Natale, L. and Pagliardi, M. (2005). Laboratory study of erosion processes in snow avalanches. *Cold Regions Science and Technology* 43: 1-9.

Barnouin-Jha, O.S., Baloga, S. and Glaze, L. (2005). Comparing landslides to fluidized crater ejecta on Mars. *Journal of Geophysical Research E: Planets* 110(4): 1-22.

Bartetzko, A. and Kopf, A.J. (2007). The relationship of undrained shear strength and porosity with depth in shallow (<50 m) marine sediments. *Sedimentary Geology* 196: 235-249.

Bates, R.L. and Jackson, J.A., eds (1984). Dictionary of Geological Terms, 3rd Edition, Anchor Books.

Belousov, A., Belousova, M. and Voight, B. (1999). Multiple edifice failures, debris avalanches and associated eruptions in the Holocene history of Shiveluch Volcano, Kamchatka, Russia. *Bulletin of Volcanology* 61(5): 324-342.

Belousova, M. and Belousov, A. (2008). Mechanism of long runout of volcanic debris avalanches: what we can learn from basal contacts of their deposits. *Abstract*, IAVCEI General Assembly, Reykjavík, Iceland.

Bernard, B., Van Wyk de Vries, B., Barba, D., Leyrit, L., Robin, C., Alcaraz, S. and Samaniego, P. (2008). The Chimborazo sector collapse and debris avalanche: deposit characteristics as evidence of emplacement mechanisms. *Journal of Volcanology and Geothermal Research* 176(1): 36-43.

Bird, E. (2000). Coastal Geomorphology: an Introduction. Wiley, Chichester: 206.

Blair, T.C. (1999). Form, Facies, and depositional history of the North Long John rock avalanche, Owens Valley, California. *Canadian Journal of Earth Science* 36: 855-870.

Bolton, A.J., Clennell, M.B. and Maltman, A.J. (1999). Nonlinear stress dependences of permeability: a mechanism for episodic fluid flow in accretionary wedges. *Geology* 27: 239-242.

Borgia, A. van Wyk de Vries, B. (2003). The volcano-tectonic evolution of Concepción, Nicaragua. *Bulletin of Volcanology* 65(4): 248-266.

Boultbee, N., Stead, D., Schwab, J. and Geertsema, M. (2006). The Zymoetz River rock avalanche, June 2002, British Columbia, Canada. *Engineering Geology* 83: 76-93.

Bursik, M., Patra, A., Pitman, E.B., Nichita, C., Macias, J.L., Saucedo, R. and Girina, O. (2005). Advances in studies of dense volcanic granular flows. *Reports on Progress in Physics* 68: 271-301.

Buss E. and Heim A. (1881). Der Bergsturz von Elm. Zürich, Worster.

Calvari, S., Tanner, L.H. and Groppelli, G. (1998). Debris-avalanche deposits of the Milo Lahar sequence and the opening of the Valle del Bove on Etna volcano (Italy). *Journal of Volcanology and Geothermal Research* 87(1-4): 193-209.

Campbell, C.S. (1989). Self-lubrication for long runout landslides. *Journal of Geology* 97(6): 653-665.

Cannon, S.H. and Savage, W.Z. (1988). A mass-change model for the estimation of debris-flow runout. *Journal of Geology* 96(2): 221-227.

Capra, L. and Macias, J.L. (2000). Pleistocene cohesive debris flows at Nevado de Toluca Volcano, central Mexico. *Journal of Volcanology and Geothermal Research* 102: 149-168.

Capra, L., Macías, J.L., Scott, K.M., Abrams, M. and Garduño-Monroy, V.H. (2002). Debris avalanches and debris flows transformed from collapses in the Trans-Mexican Volcanic Belt, Mexico - behavior, and implications for hazard assessment. *Journal of Volcanology and Geothermal Research* 113(1-2): 81-110.

Chen, C.-Y., Chen, T.-C., Yu, F.-C. and Hung, F.-Y. (2004). A landslide dam breach induced debris flow – a case study on downstream hazard areas delineation. *Environmental Geology* 47: 91-101.

Choffat, P. (1929). L'ecroulement d'Arvel (Villeneuve) de 1922. *Bulletin de la Societè Vaudoise des Sciences Naturelles* 57(1): 5-28.

Clavero, J., Sparks, R., Huppert, H. and Dade, W. (2002). Geological constraints on the emplacement mechanism of the Parinacota debris avalanche, Northern Chile. *Bulletin of Volcanology* 64(1): 40-54.

Clavero, J., Polanco, E., Godoy, E., Aguilar, G., Sparks, R.S.J., van Wyk de Vries, B., de Arce, C.P. and Matthews, S. (2004). Substrata influence in the transport and emplacement mechanism of the Ollagüe debris avalanche (Northern Chile). *Acta Vulcanologica* 16(1-2): 59-76.

Crandell, D.R. (1971). Postglacial lahars from Mount Rainier volcano, Washington. *U.S. Geological Survey Professional Paper* 677: 75 pp.

Crandell, D.R., Miller, C.D., Glicken, H.X., Christiansen, R.L. and Newhall, C.G. (1984). Catastrophic debris avalanche from ancestral Mount Shasta Volcano, California. *Geology* 12(3): 143-146.

Crosta, G.B., Chen, H. and Lee, C.F. (2004). Replay of the 1987 Val Pola Landslide, Italian Alps. *Geomorphology* 60(1-2): 127-146.

Crosta, G.B., Imposimato, S. and Roddeman, D. (2006). Continuum numerical modeling of flow-like landslides. In: S. G. Evans, G. Scarascia-Mugnozza, A. L. Strom and R. L. Hermanns (eds), *Nato Science Series. Series IV, Earth and Environmental Sciences* 49: 211-232.

Crosta, G.B., Imposimato, S. and Roddeman, D. (2008). Numerical modelling of entrainment/deposition in rock and debris-avalanches. *Engineering Geology*: (in press) 10.1016/j.enggeo.2008.10.004.

Crozier, M.J., Deimel, M.S. and Simon, J.S. (1995). Investigation of earthquake triggering for deep-seated landslides, Taranaki, New Zealand. *Quaternary International* 25: 65-73.

Cruden, D.M. and Hungr, O. (1986). The debris of the Frank Slide and theories of rockslide-avalanche mobility. *Canadian Journal of Earth Sciences* 23: 425-432.

Cruden, D.M. and Krahn, J. (1978). Frank rockslide, Alberta, Canada. In: Voight B (ed) Rockslides and Avalanches: 1. Natural Phenomena. Elsevier, New York: 97-112.

Dade, W.B. and Huppert, H.E. (1998). Long-runout rockfalls. *Geology* 26(9): 803-806.

Davidson, J. and De Silva, S. (2000). Composite Volcanoes. In Sigurdsson, H., Houghton, B.F., McNutt, S.R., Rymer, H. and Stix, J. (eds) Encyclopedia of Volcanoes, Academic Press: 663-681.

Davies, T.R. (1982). Spreading of rock avalanche debris by mechanical fluidization. *Rock Mechanics* 15: 9-24.

Davies, T.R., McSaveney, M.J. and Hodgson, K.A. (1999). A fragmentation-spreading model for long-runout rock avalanches. *Canadian Geotechnical Journal* 36(6): 1096-1110.

Davies, T. R. and McSaveney, M. J. (1999). Runout of dry granular avalanches. *Canadian Geotechnical Journal* 36(2), 313-320.

Davies, T.R. and McSaveney, M.J. (2002). Dynamic simulation of the motion of fragmenting rock avalanches. *Canadian Geotechnical Journal* 39(4): 789-798.

Davies, T.R.H., McSaveney, M.J. and Clarkson, P.J. (2003). Anthropic aggradation of the Waiho River, Westland, New Zealand: microscale modelling. *Earth Surface Processes and Landforms* 28: 209-218.

Davies, T. R. and McSaveney, M. J. (2009). The role of dynamic rock fragmentation in the motion of large landslides. *Engineering Geology*: 10.1016/j.enggeo.2008.11.004.

Deplus, C., Le Friant, A., Boudon, G., Komorowski, J.-C., Villemant, B., Harford, C., Segoufin, J. and Cheminee, J.-L. (2001). Submarine evidence for large-scale debris avalanches in the Lesser Antilles Arc. *Earth and Planetary Science Letters* 192(2), 145-157.

Dufresne, A., Siebert, L., Bernard, B., Sparks, RSJ, Takarada, J., Clavero, J., Belousov, A. and Belousova, M. (2008). Volcanic debris avalanche deposit database – a progress report. *Abstract*. IAVCEI General Assembly, Reykjavik, Iceland.

Dufresne, A. and Davies, T.R. (2009). Longitudinal ridges in mass movement deposits. *Geomorphology* 105: 171-181.

Eglit, M.E. and Demidov, K.S. (2005). Modelling of snow avalanches. In: Shahinpoor, M. (ed) Advances in the mechanics and the flow of granular materials 2. Clausthal-Zellerfeld and Gulf Publ. Co., Houston, Texas: 577-588.

Eisbacher, G.H. (1979). Cliff collapse and rock avalanches (sturzstroms) in the Mackenzie Mountains, northwestern Canada. *Canadian Geotechnical Journal* 16: 309-334.

Eppler, D.B., Fink, J. and Fletcher, R. (1987). Rheological properties and kinematics of emplacement of the Chaos Jumbles rockfall avalanche, Lassen Volcani National Park, California. *Journal of Geophysical Research* 92: 3623-3633.

Erismann, T.H. (1979). Mechanisms of large landslides. *Rock Mechanics* 12(1): 15-46.

Evans, S.G., Aitken, J.D., Wetmiller, R.J. and Horner, R.B. (1987). A rock avalanche triggered by the October 1985 North Nahanni earthquake, District of Mackenzie, N.W.T. *Canadian Journal of Earth Sciences* 24: 176-184.

Evans, S.G., Hungr, O. and Enegren, E.G. (1994). The Avalanche Lake rock avalanche, Mackenzie Mountains, Northwest Territories, Canada; description, dating, and dynamics. *Canadian Geotechnical Journal* 31(5): 749-768.

Evans, S.G. and Clague, J.J. (1988). Catastrophic rock avalanches in glacial environments. *Landslides, Proceedings 5th Symposium, Lausanne* 2: 1153-1158.

Evans, S.G. and Clague, J.J. (1998). Rock avalanche from Mount Munday, Waddington Range, British Columbia, Canada. *Landslide News* 11: 23-25.

Evans S.G., Hungr O. and Clague J.J. (2001). Dynamics of the 1984 rock avalanche and associated distal debris flow on Mount Cayley, British Columbia, Canada; implications for landslide hazard assessment on dissected volcanoes. *Engineering Geology* 61(1): 29-51.

Fairchild, L.H. (1985). Lahars at Mount St. Helens, Washington. University of Washington, Seattle, Washington, PhD thesis: 374.

Fairchild, L.H. (1987). The importance of lahar initiation processes. In: Costa, J.E. and Wieczorek, G.F. (eds) Debris flows/avalanches: processes, recognition, and mitigation. *Geological Society of America Reviews in Engineering Geology* 7: 51-61.

Fleming, R.W., Ellen, S.D. and Algus, M.A. (1989). Transformation of dilative and contractive landslide debris into debris flows: an example from Marin County, Caifornia. *Engineering Geology* 27: 201-223.

Francis, P.W. and Wells, G.L. (1988). Landsat Thematic Mapper observations of debris avalanche deposits in the Central Andes. *Bulletin of Volcanology* 50(4): 258-278.

Francois, B., Lacombe, F. and Herrmann, H.J. (2002). Finite width of shear zones. *Physical Review E - Statistical, Nonlinear, and Soft Matter Physics* 65(3): 031311/1-031311/7.

Friedmann, S.J. (1997). Rock-avalanche elements of the Shadow Valley Basin, eastern Mojave Desert, California: processes and problems. *Journal of Sedimentary Research* 67(5): 792-804.

Fukuoka, H., Sassa, K., Wang, G. and Sasaki, R. (2006). Observation of shear zone development in ring-shear apparatus with a transparent shear box. *Landslides* 3: 239-251.

Galli, P. (2000). New empirical relationships between magnitude and distance for liquefaction. *Tectonophysics* 324: 169-187.

Gauer, P. and Issler, D. (2004). Possible erosion mechanism in snow avalanches. *Annals of Glaciology* 38: 384-392.

Gee, M.J.R., Gawthorpe, R.L. and Friedmann, S.J. (2006). Triggering and evolution of a giant submarine landslide, Offshore Angola, revealed by 3d seismic stratigraphy and geomorphology. *Journal of Sedimentary Research* 76(1): 9-19.

Geertsema, M., Hungr, O., Schwab, J. W. and Evans, S. G. (2006). A large rockslide-debris avalanche in cohesive soil at Pink Mountain, Northeastern British Columbia, Canada. *Engineering Geology* 83: 64-75.

Glicken, H.X., Voight, B. and Janda R.J. (1981). Rockslide-debris avalanche of May 18, 1980, Mount St. Helens volcano. *Abstract*. IAVCEI Symposium on Arc Volcanism: 109-110.

Glicken, H.X. (1986). Rockslide-debris avalanche of May 18, 1980, Mount St. Helens Volcano, Washington. Santa Barbara, University of California at Santa Barbara, 98 pp.

Glicken, H. (1991). Sedimentary architecture of large volcanic debris avalanches. In: Fisher, R.V. and Smith, G.A. (eds.), Sedimentation in Volcanic Settings, 45. SEPM Spec. Publ.: 99–106.

Glicken, H. (1996). Rockslide-Debris Avalanche of May18, 1980, Mount St. Helens, Washington. *USGS Open-file Report* 96-677: 90 pp.

Govi, M. (1989). The 1987 landslide on Mount Zandilla in the Valtellina, northern Italy. *Landslide News* 3: 1-3.

Hancox, G.T. and Perrin, N.D. (1994). Green Lake landslides: a very large ancient rockslide in glaciated terrain, Fiordland, New Zealand. *Institute of Geological and Nuclear Sciences Science Report* 93/18: 50 pp.

Harp, E.L., Jibson, R.W., Kayen, R.E., Keefer, D.K., Sherrod, B.L., Carver, G.A., Collins, B.D., Moss, R.E.S. and Sitar, N. (2003). Landslides and liquefaction triggered by the M 7.9 Denali Fault earthquake of 3 November 2002. *GSA Today* 13(8): 4-10.

Hauser, A. (2002). Rock avalanches and resulting debris flow in Estero Parraguirre and Río Colorado, Región Metropolitana, Chile. In: Evans, S.G. and DeGraff, J.V. (eds) Catastrophic Landslides: Effects, Occurrence and Mechanisms. *Geological Society of America Reviews in Engineering Geology* 15: 135-148.

Hazlett, R.W., Buesch, D., Anderson, J.L., Elan, R. and Scandone, R. (1991). Geology, failure, and implications of seismogenic avalanches of the 1944 eruption at Vesuvius, Italy. *Journal of Volcanology and Geothermal Research* 47(3-4): 249-264.

Heim, A. (1932). Bergsturz und Menschenleben (Landslides and human lives). Vierteljahrsschrift der Naturforschenden Gesellschaft in Zürich, 77, Beer & Co. in Komm., Zürich: 218 p.

Hewitt K. (1988). Catastrophic landslide deposits in the Karakoram Himalaya. *Sciences* 242: 64-67.

Hewitt, K. (2006). Rock avalanches with complex run out and emplacement, Karakoram Himalaya, Inner Asia. In: S. G. Evans, G. Scarascia-Mugnozza, A. L. Strom and R. L. Hermanns (eds) Landslides from Massive Rock Slope Failure. *Nato Science Series. Series IV, Earth and Environmental Sciences* 49: 521-550.

Hewitt, K., Clague, J.J. and Orwin, J.F. (2008). Legacies of catastrophic rock slope failures in mountain landscapes. *Earth-Science Reviews* 87: 1-38.

Hürlimann, M. and Ledesma, A. (2003). Giant mass movements in volcanic islands: the case of Tenerife. Occurence and mechanisms of flow-like landslides in natural slopes and earthfills, Sorrento: 105-115.

Hsü KJ. (1975). Catastrophic debris atreams (Sturzstroms) generated by rockfalls. *Geological Society of America Bulletin* 86(1): 129-140.

Hungr, O. (1990). Mobility of rock avalanches. Tsukuba, Japan, *Reports of the National Research Institute for Earth Science and Disaster Prevention* 46: 11–20.

Hungr, O. (1995). A model for the runout analysis of rapid flow slides, debris flows and avalanches. *Canadian Geotechnical Journal* 32: 610-623.

Hungr, O., Evans, S.G., Bovis, M. and Hutchinson, J.N. (2001). Review of the classification of landslides of the flow type. *Environmental and Engineering Geosciences* 7: 221-238.

Hungr, O. and Evans, S.G. (2004). Entrainment of debris in rock avalanches: an analysis of a long run-out mechanism. *Geological Society of America Bulletin* 116(9/10): 1240-1252.

Hungr, O. (2005). Classification and terminology. In: Jakob, M. and Hungr, O. (eds) Debris Flow Hazards and Related Phenomena. Springer-Verlag: 9-24.

Hungr, O., McDougall, S. and Bovis, M. (2005). Entrainment of material by debris flows. In: Jakob, M. and Hungr, O. (eds) Debris Flow Hazards and Related Phenomena. Springer-Verlag: 135-158.

Hungr, O. (2006). Rock avalanche occurrence, process and modelling. In: Evans, S.G., Mugnozza, G.S. and Strom, A. (eds) Landslides from Massive Rock Slope Failure. Springer Verlag: 243-266.

Hurst, A., Cartwright, J. and Duranti, D. (2003). Fluidization structures produced by upward injection of sand through a sealing lithology. In: van Rensbergen P, Hillis RR, Maltman AJ, Morley, CK (eds) Subsurface Sediment Mobilisation. *Geological Society Special Publications* 216: 123-138.

Hutchinson, J.N. and Bhandari, R.K. (1971). Undrained loading, a fundamental mechanism of mudflows and other mass movements. *Géotechnique* 21: 353-358.

Iverson, R.M. (1997). The physics of debris flows. *Reviews of Geophysics* 35(3): 245-296.

Iverson, R.M., Reid, M.E., Iverson, N.R., LaHusen, R.G., Logan, M., Mann, J.E. and Brien, D.L. (2000). Acute sensitivity of landslide rates to initial soil porosity. *Science* 290(5491): 513-516.

Jibson, R.W., Harp, E.L., Schulz, W. and Keefer, D.K. (2006). Large rock avalanches triggered by the M 7.9 Denali Fault, Alaska, earthquake of 3 November 2002. *Engineering Geology* 83: 144-160.

Johnson, B. (1978). Blackhawk landslide, California, U.S. Rockslides and avalanches 1, Natural phenomena. Elsevier, Amsterdam, pp. 481-504.

Jomelli, V. and Bertran, P. (2001). Wet snow avalanche deposits in the French Alps; structure and sedimentology. *Geografiska Annaler. Series A: Physical Geography* 83(1-2): 15-28.

Keefer, D.K. (1994). The importance of earthquake-induced landslides to long-term slope erosion and slope-failure hazards in seismically active regions. *Geomorphology* 10: 265-284.

Kelfoun, K. and Druitt, T.H. (2005). Numerical modeling of the emplacement of Socompa rock avalanche, Chile. *Journal of Geophysical Research B: Solid Earth* 110(12): 1-13.

Kerle, N. and van Wyk de Vries, B. (2001). The 1998 debris avalanche at Casita volcano, Nicaragua – investigation of structural deformation as the cause of slope instability using remote sensing. *Journal of Volcanology and Geothermal Research* 105: 49-63.

Kobayashi, Y. (1994). Effects of basal guided waves on landslides. *Pure and Applied Geophysics* 142(2): 329-346.

Komorowski, J.C., Glicken, H.X. and Sheridan, M.F. (1991). Secondary electron imagery of microcracks and hackly fracture surfaces in sandstone-sized clasts from the 1980 Mount St. Helens debris avalanche deposits: implications for particle-particle interactions. *Geology* 19(3): 261-264.

Korup O. (2004). Geomorphic implications of fault zone weakening; slope instability along the Alpine Fault, South Westland to Fiordland. *New Zealand Journal of Geology and Geophysics* 47(2): 257-267.

Lajeunesse, E., Malverti, L., Lancien, P., Armstrong, L., Métivier, F., Coleman, S., Smith, C.E., Davies, T., Cantelli, A. and Parker, G. (2009). Fluvial and subaqueous morphodynamics of laminar and near-laminar flows: a synthesis. *Sedimentology* (in review).

Langridge, R.M., Weldon II, R.J., Moya, J.C. and Suárez, G. (2000). Paleoseismology of the 1912 Acambay earthquake and the Acambay-Tixmadejé fault, Trans-Mexican Volcanic Belt. *Journal of Geophysical Research* 105(B2): 3019-3037.

LeCorvec, N. (2005). Socompa Volcano destabilisation (Chile) and fragmentation of debris avalanches. Unpublished M.Sc. thesis. Laboratoire Magma et volcans, Clermont-Ferrand, Universite Blaise Pascal, France: 67 pp.

Legros, F., Cantagrel, J.-M. and Devouard, B. (2000). Pseudotachylyte (frictionite) at the base of the Arequipa volcanic landslide deposit (Peru): implications for emplacement mechanisms. *Journal of Geology* 108: 601-611.

Legros F. (2002). The mobility of long-runout landslides. *Engineering Geology* 63: 301-331.

Lucchitta, B.K. (1978). A large landslide on Mars. *Geological Society of America Bulletin* 89(11): 1601-1609.

Lucchitta, B.K. (1979). Landslides in Valles Marineris, Mars. *Journal of Geophysical Research* 84: 8097-8113.

Ludlow-Wiechers, B., Almeida-Leñero, L. and Islebe, G. (2005). Paleoecological and climatic changes of the Upper Lerma Basin, Central Mexico during the Holocene. *Quaternary Research* 64: 318-332.

Luhr, J.F. (2003). Earth. DK Publishing: 520 pp.

Major, J.J. (1984). Geologic and rheologic characteristics of the May 18, 1980 southwest flank lahars at Mount St. Helens, Washington. Pennsylvania State University, State College, Pennsylvania, M.S. thesis: 225 pp.

Mallogi, F., Lanuza, J., Andreotti, B. and Clement, E. (2008). Erosion waves: transverse instabilities and fingering. *Soft Condensed Matter* (cond-mat.soft) http://arxiv.org/abs/cond-mat/0507163.

Maltman, A.J. and Bolton, A. (2003). How sediments become mobilized. In: van Rensbergen P, Hillis RR, Maltman AJ, Morley, CK (eds) Subsurface Sediment Mobilisation. *Geological Society Special Publications* 216: 9-20.

Manzella, I. and Labiouse, V. (2008). Qualitative analysis of rock avalanches propagation by means of physical modelling of non-constrained gravel flows. *Rock Mechanics and Rock Engineering* 41(1): 133-151.

Masch, L., Wenk, H.R. and Preuss, E. (1985). Electron microscopy study of hyalomylonites: evidence for frictional melting in landslides. *Tectonophysics* 115: 131-160.

Mathews, W.H. and McTaggert, K.C. (1978). The Hope rock slides, British Columbia, Canada. In: Voight B (ed). Rockslides and Avalanches I. Amsterdam: 259-274.

McClay, K., Dooley, T. and Zamora, G. (2003). Analogue models of delta systems above ductile substrates. In: van Rensberger, P., Hillis, R.R., Maltman, A.J. and Morley, C.K. (eds) Subsurface Sediment Mobilization. Geological Society, London, Special Publication 216: 411-428.

McClung, D. and Schaerer, P. A. (2006). The Avalanche Handbook, Seattle, WA: Mountaineers Books.

McDougall, S. and Hungr, O. (2004). A model for the analysis of rapid landslide motion across three-dimensional terrain. *Canadian Geotechnical Journal* 41: 1084-1097.

McDougall, S. and Hungr, O. (2005). Dynamic modelling of entrainment in rapid landslides. *Canadian Geotechnical Journal* 42: 1437-1448.

McDougall, S., Boultbee, N., Hungr, O., Stead, D. and Schwab, J.W. (2006). The Zymoetz River landslide, British Columbia, Canada; description and dynamic analysis of a rock slide-debris flow. *Landslides* 3(3): 195-204.

McSaveney, M.J. (1978). Sherman Glacier rock avalanche, Alaska, U.S.A. Rockslides and Avalanches. Amsterdam, Elsevier: 197-258.

McSaveney, M.J., Davies, T.R. and Hodgson, K.A. (2000). A contrast in deposit style and process between large and small rock avalanches. In: Bromhead E, Dixon N, Ibsen ML (eds) Landslides in Research, Theory and Practice. Thomas Telford, London: 1053-1058.

McSaveney, M.J. (2002). Recent rockfalls and rock avalanches in Mount Cook National Park, New Zealand. In: Evans SG, DeGraff JV (eds). Catastrophic landslides: effects, occurrence, and mechanisms. *Review in Engineering Geology* 14: 35-70.

Mears, A.I. (1980). A fragment-flow model of dry-snow avalanches. *Journal of Glaciology* 26: 153-163.

Mehl, K.M. and Schmincke, H.-U. (1999). Structure and emplacement of the Pliocene Rogue Nublo debris avalanche deposit, Gran Canaria, Spain. *Journal of Volcanology and Geothermal Research* 94: 105-134.

Melosh, H.J. (1979). Acoustic fluidization: a new geologic process? *Journal of Geophysical Research* 84(B13): 7513-7520.

Miyabuchi, Y. (1999). Deposits associated with the 1990-1995 eruption of Unzen Volcano, Japan. *Journal of Volcanology and Geothermal Research* 89: 139-158.

Moore, J.G. and Chadwick, W.W., Jr. (1995). Offshore geology of Mauna Loa and adjacent areas, Hawaii. *Geophysical Monograph* 92: 21-44.

Naranjo, J.A. and Francis, P. (1987). High velocity debris avalanche at Lastarria Volcano in the North Chilean Andes. *Bulletin of Volcanology* 49: 509-514.

Neall, V.E. (1976). Lahars as major geological hazards. *Bulletin of the International Association of Engineering Geology* 13(1): 233-240.

Nicoletti, P.G. and Sorriso-Valvo, M. (1991). Geomorphic controls of the shape and mobility of rock avalanches. *Geological Society of America Bulletin* 103(10): 1365-1373.

Osipov, V.I., Gratchev, I.B. and Sassa, K. (2005). The mechanism of liquefaction of clayey soils (M124). In: Sassa, K., Kukuoka, H., Wang, F. and Wang, G. (eds) Landslides: risk analysis and sustainable disaster management, Springer Verlag: 127-131.

Palmer, B.A., Alloway, B.V., Neall, V.E., Fisher, R.V. and Smith, G.A. (1991). Volcanic-debris-avalanche deposits in New Zealand - lithofacies organization in unconfined, wet-avalanche flows. In: Fisher, R.V. and Smith, G.A. (eds.), Sedimentation in Volcanic Settings 45, *SEPM Special Publication*: 89-98.

Peterson, D.W. and Tilling, R.I. (2000). Lava Flow Hazards. In Sigurdsson, H., Houghton, B.F., McNutt, S.R., Rymer, H. and Stix, J. (eds) Encyclopedia of Volcanoes, Academic Press: 957-971.

Philip, H. and Ritz, J.-F. (1999). Gigantic paleolandslide associated with active faulting along the Bogd fault (Gobi-Altay, Mongolia). *Geology* 27(3): 211-214.

Pierson, T.C. (1985). Initiation and flow behaviour of the 1980 Pine Creek and Muddy River lahars, Mount St. Helens, Washington. *Geological Society of America Bulletin* 96: 1056-1069.

Piotrowski, J.A., Larsen, N.K. and Junge, F.W. (2004). Reflections on soft subglacial beds as a mosaic of deforming and stable spots. *Quaternary Science Reviews* 23: 993-1000.

Plafker, G. and Ericksen, G.E. (1978). Nevados Huascarán avalanches, Peru. In: Voight B (ed). Rockslides and Avalanches I. Amsterdam: 277-314.

Pollet, N. and Schneider, J.-L.M. (2004). Dynamic disintegration processes accompanying transport of the Holocene Flims sturzstrom (Swiss Alps). *Earth and Planetary Science Letters* 221: 433-448.

Ponomareva, V.V., Melekestsev, I.V. and Dirksen, O.V. (2006). Sector collapses and large landslides on late Pleistocene-Holocene volcanoes in Kamchatka, Russia. *Journal of Volcanology and Geothermal Research* 158(1-2): 117-138.

Pouliquen, O., Delour, J. and Savage, S.B. (1997). Fingering in granular flows. *Nature* 386(6627): 816-817.

Pouliquen, O. and Vallance, J.W. (1999). Segregation induced instabilities of granular flows. *Chaos* 9(3): 621-630.

Pralong, A. and Funk, M. (2006). On the instability of avalanching glaciers. *Journal of Glaciology* 52(176): 31-48.

Quantin, C., Allemand, P. and Delacourt, C. (2004). Morphology and geometry of Valles Marineris landslides. *Planetary and Space Science* 52(11): 1011-1022.

Reiche, P. (1937). The toreva-block, a distinctive landslide type. *Journal of Geology* (65): 538-548.

Richards, J.P. and Villeneuve, M. (2001). The Llullaillaco Volcano, Northwest Argentina: construction by Pleistocene volcanism and destruction by sector collapse. *Journal of Volcanology and Geothermal Research* 105(1-2): 77-105.

Robin, C. and Boudal, C. (1987). A gigantic Bezymianny-type event at the beginning of modern Volcan Popocatepetl. *Journal of Volcanology and Geothermal Research* 31(1-2): 115-130.

Sassa, K. (1988). Geotechnical model for the motion of landslides (Special lecture). Proceedings, *5th International Symposium on Landslides* 1: 37-56.

Sassa, K. and Wang, G.H. (2005). Mechanism of landslide-triggered debris flows: liquefaction phenomena due to the undrained loading of torrent deposits. In: Jakob, M. and Hungr, O. (eds) Debris Flow Hazards and Related Phenomena. Springer Verlag: 81-104.

Savage, W. and Baum, R. (2005). Instability of steep slopes. In: Jakob, M. and Hungr, O. (eds) Debris Flow Hazards and Related Phenomena, Springer Verlag: 53-79.

Schneider, J.-L. and Fisher, R.V. (1998). Transport and emplacement mechanisms of large volcanic debris avalanches: evidence from the northwest sector of Cantal Volcano (France). *Journal of Volcanology and Geothermal Research* 83: 141-165.

Schuster, R.L. and Crandell, D.R. (1984). Catastrophic debris avalanches from volcanoes. *IV International Symposium on Landslides --Iv Symposium International Sur Les Glissements De Terrains*. Downsview, Univ. Toronto: 567-572.

Shaller, P.J. (1991). Analysis of a large moist landslide, Lost River Range, Idaho, U.S.A. *Canadian Geotechnical Journal* 28(4): 584-600.

Shea, T., van Wyk de Vries, B. and Pilato, M. (2008). Emplacement mechanisms of contrasting debris avalanches at Volcán Mombacho (Nicaragua), provided by structural and facies analysis. *Bulletin of Volcanology* 70(8): 899-921.

Shreve, R.L. (1968). Leakage and fluidization in air-layer lubricated avalanches. *Geological Society of America Bulletin* 79(5): 653-657.

Sibson, R.H., White, S.H. and Atkinson, B.K. (1979). Fault rock distribution and structure within the Alpine Fault Zone: a preliminary account. In: Walcott RI, Cresswell MM (eds). The origin of the Southern Alps. *The Royal Society of New Zealand Bulletin* 18: 55-65.

Siebe, C., Komorowski, J.C. and Sheridan, M.F. (1992). Morphology and emplacement of an unusual debris-avalanche deposit at Jocotitlán Volcano, Central Mexico. *Bulletin of Volcanology* 54(7): 573-589.

Siebe, C., Abrams, M., Macías, J.L., 1995. Derrumbes gigantes, depósitos de avalancha de escombros y edad del actual cono del Volcán Popocatépetl. In: Comité Científico Asesor UNAM-CENAPRED: Volcán Popocatépetl, estudios realizado drante la crisis 1994-1995. Edición Especial, Secretaría de Gobernación, México, D.F., 195-220.

Siebert, L. (1984). Large volcanic debris avalanches: characteristics of source areas, deposits, and associated eruptions. *Journal of Volcanology and Geothermal Research* 22(3-4): 163-197.

Siebert, L., Beget, J.E. and Glicken, H. (1995). The 1883 and late-Prehistoric eruptions of Augustine Volcano, Alaska. *Journal of Volcanology and Geothermal Research* 66(1-4): 367-395.

Siebert, L. (2002). Landslides Resulting from Structural Failure of Volcanoes. *Reviews in Engineering Geology* 15: 209-235.

Smith, G.A. and Fritz, W.J. (1989). Volcanic influences on terrestrial sedimentation. *Geology* 17(4): 375-376.

Smith, G.A. and Lowe, D.R. (1991). Lahars, volcano-hydrologic events and deposition in the debris flow; hyperconcentrated flow continuum. *Special Publication - Society of Economic Paleontologists and Mineralogists* 45: 59-70.

Smith, G.M., Davies, T.R., McSaveney, M.J. and Bell, D.H. (2006). The Acheron rock avalanche, Canterbury, New Zealand : Morphology and Dynamics. *Landslides* 3(1): 62-72.

Sosio, R., Crosta, G.B. and Hungr, O. (2008). Complete dynamic modeling calibration for the Thurwieser rock avalanche (Italian Central Alps). *Engineering Geology* 100(1-2): 11-26.

Sousa, J. and Voight, B. (1991). Continuum simulation of flow failures. *Geotechnique* 41(4): 515-538.

Sovilla, B., Burlando, P. and Bartelt, P. (2006). Field experiments and numerical modeling of ma entrainment in snow avalanches**.** *Journal of Geophysical Research F: Earth Surface* 111(3): FO30007.

Sparks, R.S.J., Gardeweg, M.C., Calder, E.S. and Matthews, S.J. (1997). Erosion by pyroclastic flows on Lascar volcano, Chile. *Bulletin of Volcanology* 58(7): 557-565.

Spray, J.G. (1995). Pseudotachylyte controversy: fact of friction. *Geology* 25: 1119-1122.

Stadelmann, J. (1983). Zur Dokumentation der Bergsturzereignisse vom Huascaran. In: Patzelt, G. (ed) Die Berg- und Gletscherstürze vom Huascaran, Cordillera Blanca, Peru. Universitätsverlag Wagner, Innsbruck: 51-70.

Stephenson, E.L., Maltman, A.J. and Knipe, R.J. (1994). Dynamic permeability in deforming accretionary prism sediments. In: Parnell (ed) Geofluids 93, fluid evolution, migration, and interaction in rocks. *Geological Society, London, Special Publications* 78: 113-125.

Stewart, B., Zernack, A., Procter, J. (2006). Field Trip Guide, GSNZ-NZGS Joint Conference, Massey University, New Zealand.

Strom, A. (2006). Morphology and internal structure of rockslides and rock avalanches: grounds and constraints for their modelling. In: Evans, S.G. Scarascia-Mugnozza, G., Strom, A.L. and Hermanns R.L. (eds), *Nato Science Series. Series IV, Earth and Environmental Sciences* 49: 305-328.

Suter, M. (1991). State of stress and active deformation in Mexico and western Central America. In: Slemmons, D.B. et al. (eds) Neotectonics of North America. Geological Society of America, Decade of North American Geology, Decade Map Volume 1: 410-421.

Suter, M., Martínez, M.L., Legorreta, O.Q. and Martínez, M.C. (2001). Quaternary intra-arc extensions in the central Trans-Mexican Volcanic Belt. *GSA Bulletin* 113(6): 693-703.

Takahashi, T (2001). Mechanism and simulation of snow avalanches, pyroclastic flows and debris flows. *Special Publication of the International Association of Sedimentology* 31: 11-43.

Takarada, S., Ui, T. and Yamamoto, Y. (1999). Depositional features and transportation mechanism of valley-flling Iwasegawa and Kaida debris avalanches, Japan. *Bulletin of Volcanology* 60(7): 508-522.

Terzaghi, K. (1943). Theoretical Soil Mechanics. Wiley, New York: 510 pp.

Tischer, M., Bursik, M.I. and Pitman, E.B. (2001). Kinematics of sand avalanches using particle-image velocimetry. *Journal of Sedimentary Research* 71(3): 355-364.

Toniolo, H., Harff, P., Marr, J., Paola, C. and Parker, G. (2004). Experiments on reworking by successive unconfined subaqueous and subaerial muddy debris flows. *Journal of Hydraulic Engineering* 130(1): 38-48.

Turnbull, J.M. and Davies, T.R.H. (2006). A mass movement origin for cirques. *Earth Surface Processes and Landforms* 31(9): 1129-1148.

Tuttle, M.P. (2001). The use of liquefaction features in paleoseismology: Lessons learned in the New Madrid seismic zone, central United States. *Journal of Seismology* 5: 361-380.

Ui, T. (1983). Volcanic dry avalanche deposits—identification and comparison with nonvolcanic debris stream deposits. *Journal of Volcanolology and Geothermal Research* 18: 135–150

Ui, T. and Glicken, H. (1986). Internal structural variations in a debris-avalanche deposit from ancestral Mount Shasta, California. *Bulletin of Volcanology* 48: 189–194.

Vaid, Y.P. and Sivathayalan, S. (2000). Fundamental factors affecting liquefaction susceptibility of sands. *Canadian Geotechnical Journal* 37: 592-606.

Vallance, J.W., Siebert, L., Rose Jr, W.I., Girón, J.R. and Banks, N.G. (1995). Edifice collapse and related hazards in Guatemala. *Journal of Volcanology and Geothermal Research* 66(1-4): 337-355.

Vallance, J.W. and Scott, K.M. (1997). The Osceola mudflow from Mount Rainier: sedimentology and hazard implications of a huge clay-rich debris flow. *Geological Society of America Bulletin* 109(2): 143-163.

Vallance, J.W. (2000). Lahars. In Sigurdsson, H., Houghton, B.F., McNutt, S.R., Rymer, H. and Stix, J. (eds) Encyclopedia of Volcanoes, Academic Press: 601-616.

Vallance, J.W. and Ballard, R.D. (2000). Lahars. In: Sigurdsson, H., Houghton, B.F., McNutt, S.R., Rymer, H. and Stix, J. (eds) Encyclopedia of Volcanoes. Academic Press: 601-616.

Vallance, J.W., Siebert, L., Rose Jr, W.I., Girón, J.R. and Banks, N.G. (1995). Edifice collapse and related hazards in Guatemala. *Journal of Volcanology and Geothermal Research* 66: 337-355.

van Gassen, W. and Cruden, D.M. (1989). Momentum transfer and friction in the debris of rock avalanches. *Canadian Geotechnical Journal* 26(4): 623-628.

van Wyk de Vries, B. and Francis, P.W. (1997). Catastrophic collapse at stratovolcanoes induced by gradual volcano spreading. *Nature* 387: 387-390.

van Wyk De Vries, B., Self, S., Francis, P.W. and Keszthelyi, L. (2001). A gravitational spreading origin for the Socompa debris avalanche. *Journal of Volcanology and Geothermal Research* 105(3): 225-247.

Vespermann, D. and Schmincke, H.-U. (2000). Scoria Cones and Tuff Rings. In Sigurdsson, H., Houghton, B.F., McNutt, S.R., Rymer, H. and Stix, J. (eds) Encyclopedia of Volcanoes, Academic Press: 683-694.

Voight, B., Janda, R.J., Glicken, H. and Douglass, P.M.. (1983). Nature and mechanics of the Mount St. Helens rockslide-debris avalanche of 18 May 1980. *Geotechnique* 33(3): 243-273.

Voight, B. and Sousa, J. (1994). Lessons from Ontake-San: a comparative analysis of debris avalanche dynamics. *Engineering Geology* 38(3-4): 261-297.

von Poschinger, A. (1994). Some special aspects of the "impact" of a landslide on the valley floor. *Landslide News* 8: 26-28.

von Poschinger, A., Wassmer, P. and Maisch, M. (2006). The Flims rockslide; history of interpretation and new insights. In: Evans, S.G., Scarascia-Mugnozza, G. Strom, A.L. and Hermanns, R.L. (eds) Landslides from massive rock slope failure. Nato Science Series IV, Earth and Environmental Sciences Vol.49: 329-356.

Walker, G.P. (2000). Basaltic Volcanoes and Volcanic Systems. In Sigurdsson, H., Houghton, B.F., McNutt, S.R., Rymer, H. and Stix, J. (eds) Encyclopedia of Volcanoes, Academic Press: 283-289.

Wang, C.-Y., Wong, A., Dreger, D.S. and Manga, M. (2006). Liquefaction limit during earthquakes and underground explosions: implications on ground-motion attenuation. *Bulletin of the Seismological Society of America* 96(1): 355-363.

Wardle P. (1980). Primary succession in Westland National Park and its vicinity, New Zealand. *New Zealand Journal of Botany* 18:221-232.

Weichert, D., Horner, R.B. and Evans, S.G. (1994). Seismic signatures of landslides: the 1990 Brenda Mine collapse and the 1965 Hope rockslides. *Bulletin of the Seismological Society of America* 84(5): 1523-1532.

Whitehouse, I.E. (1983). Distribution of large rock avalanche deposits in the Central Southern Alps, New Zealand. *New Zealand Journal of Geology and Geophysics* 26(3): 271-279.

Wright, C.A. (1998). The Ad 930 long-runout Round Top debris avalanche, Westland, New Zealand. *New Zealand Journal of Geology and Geophysics* 41(4): 493-497.

Yarnold, J.C. and Lombard, J.P. (1989). Facies model for large rock avalanche deposits formed in dry climates. In: Colburn, I. P., Abbott P. L. and Minch J. (eds) Field Trip Guidebook - Pacific Section, Society of Economic Paleontologists and Mineralogists 62: 9-31.

Yarnold, J.C. (1993). Rock-avalanche characteristics in dry climates and the effect of flow into lakes: insights from mid-Tertiary sedimentary breccias near Artillery Peak, Arizona. *Geological Society of America Bulletin* 105(3): 345-360.